MODEL STUDY OF THE HYDRAULICS RELATED TO FISH PASSAGE THROUGH EMBEDDED CULVERTS

A Thesis Submitted to the College of
Graduate Studies and Research
In Partial Fulfillment of the Requirements
For the Degree of Master of Science
In the Department of Civil and Geological Engineering
University of Saskatchewan
Saskatoon

By

MEGAN E. GARNER

PERMISSION TO USE

In presenting this thesis in partial fulfilment of the requirements for a Postgraduate degree from the University of Saskatchewan, I agree that the Libraries of this University may make it freely available for inspection. I further agree that permission for copying of this thesis in any manner, in whole or in part, for scholarly purposes may be granted by the professor or professors who supervised my thesis work or, in their absence, by the Head of the Department or the Dean of the College in which my thesis work was done. It is understood that any copying or publication or use of this thesis or parts thereof for financial gain shall not be allowed without my written permission. It is also understood that due recognition shall be given to me and to the University of Saskatchewan in any scholarly use which may be made of any material in my thesis.

Requests for permission to copy or to make other use of material in this thesis in whole or part should be addressed to:

Head of the Department of Civil and Geological Engineering
University of Saskatchewan
Saskatoon, Saskatchewan S7N 5A9

ABSTRACT

Corrugated steel pipe (CSP) culverts are widely used as an economical alternative for conveying streams and small rivers through road embankments. While passage of the design flow is generally the primary goal for culvert design, consideration must also be given to maintaining connectivity within the aquatic environment for fish and other aquatic organisms. In Canada, the design criteria for fish passage through culverts are generally specified in terms of a maximum mean flow velocity corresponding to the weakest swimming fish expected to be found at a specific location. Studies have shown, however, that the velocity distribution within a CSP culvert may provide sufficient areas of lower velocity flow near the culvert boundary to allow for fish passage, even when the mean flow velocity may exceed a fish's swimming ability. Improved knowledge of the hydraulic conditions within CSP culverts, combined with research into fish swimming capabilities and preferences, may make it possible to better tailor culvert designs for fish passage while at the same time decreasing construction costs.

To meet the requirements of regulators, various measures may be taken to reduce culvert flow velocities. Embedding, or setting the invert of a culvert below the normal stream bed elevation, is a simple and inexpensive method of increasing the flow area in a culvert flowing partially full, thereby decreasing flow velocity. Fish traversing through an embedded culvert benefit not only in terms of lower mean flow velocities, but also even lower flow velocities in the near boundary region. In the province of Saskatchewan culvert embedment is regularly used as a means to improve fish passage conditions.

In this study, a laboratory scale model was used to study the velocity distribution within a non-embedded and embedded CSP culvert. An acoustic Doppler velocimeter was used to measure point velocities throughout the flow cross section at several longitudinal locations along the culvert. The hydraulic conditions were varied by changing the discharge, culvert slope and depth of embedment. The point velocity data were analyzed to determine patterns of velocity and turbulence intensity at each cross section, as well as along the length of the culvert. The results from the embedded culvert tests were compared with the results from the equivalent non-embedded tests, so that initial conclusions could be made regarding the use of embedment to improve conditions for fish passage.

Analysis of the cross section velocity distributions showed that, even the non-embedded culvert had a significant portion of the flow area with flow velocity less than the mean velocity. The results from the embedded tests confirmed that embedding the culvert reduced the flow velocity throughout each cross section, although the effect was most significant for the cross sections located greater than one culvert diameter downstream from the inlet. This variation in effectiveness of embedment at reducing flow velocities is attributed to the length of the M1 backwater profile relative to the culvert length, and thus the differential increase in flow depth that occurred at each measurement location along the culvert.

For both the non-embedded and embedded culvert the peak point magnitudes of turbulence intensity were found to be located near the culvert inlet where the flow was contracting. In terms of the cross section average turbulence intensity, in the non-embedded culvert turbulence increased with distance downstream from the inlet and was highest at the cross sections located near the culvert outlet. Embedding the culvert was found to either have no impact, or to slightly increase, the cross section average turbulence intensity near the inlet. Again, a result that is attributed to the tapering out of the M1 backwater profile at locations near the inlet under the flow conditions tested. However, beyond eight culvert diameters downstream from the inlet, embedment did result in lower cross section average turbulence intensity when compared to the non-embedded culvert.

The measured velocity profiles for the non-embedded tests were found to compare well to the theoretical log-law velocity distribution using a k_s value of between 0.012 m and 0.022 m, or approximately one to two times the corrugation amplitude, when the datum for analysis was considered to be located at the crest of the pipe corrugation. The cross section velocity distributions for the non-embedded tests compared very well to the model proposed by Ead et al. (2000). Based on this assessment, it appears that the Ead et al. model is potentially suitable for use in predicting the amount of the cross sectional area in a non-embedded culvert with flow velocity less than the design target for culvert fish passage design purposes.

Overall, the results of the study confirm that, embedding a CSP culvert may be an effective way to improve fish passage conditions in terms of both flow velocity and turbulence intensity.

ACKNOWLEDGEMENTS

I would like to thank my supervisor, Dr. Jim Kells, for allowing me the opportunity to come to Saskatchewan to take part in this project, as well as for his continued patience and good humour during completion of this thesis. I would also thank the members of the project advisory committee, Chris Katopodis, Dr. Sumner, Dr. Mazurek and Dr. Feldman, for their participation and input. Special acknowledgment must also go to Brennan Pokoyoway and Dale Pavier for their assistance in setting up and operating the experimental equipment, as well as their much appreciated company in the lab.

Financial assistance for this research was provided by Fisheries and Oceans Canada and the Saskatchewan Ministry of Highways and Infrastructure. Additional support was provided by Fisheries and Oceans Canada through the loan of the ADV, without which the project would not have been possible. Financial and in-kind support for initiating this research project at the University of Saskatchewan was also provided by Manitoba Transportation and Government Services, British Columbia Ministry of Transport and FSI Culvert and Atlantic Industries Limited. I am also grateful for the financial support received through a University of Saskatchewan Graduate Scholarship as well as the 2009 Forsberg Scholarship.

TABLE OF CONTENTS

LIST OF FIGURES

LIST OF TABLES

LIST OF VARIABLES

a	coefficient from Rajaratnam and Katopodis (1990)
C	coefficient from Rajaratnam and Katopodis (1990)
d	depth of streaming flow in the fully developed flow portion of a baffled culvert
D	culvert diameter
g	acceleration due to gravity
h	baffle height
I_{mag}	turbulence intensity
I_{magAve}	average turbulence intensity for cross section based on integration of I_{mag} contour plot
J	ratio of centreline shear velocity to mean cross section shear velocity
k_s	Nikuradse equivalent sand roughness
K	coefficient from Rajaratnam and Katopodis (1990)
L	baffle spacing
Q_{int}	discharge calculated through velocity-area integration of contour plot
Q_*	dimensionless discharge
Q	discharge
r	culvert radius
R	hydraulic radius
S	slope
u_*	shear velocity
U_*	global shear velocity
$\bar{v}$	mean point velocity over measurement interval
v	flow velocity at individual measurement point in streamwise direction

$v_{x,y,z}$ velocity at individual measurement point in x, y or z direction

V_{ave} average cross section longitudinal flow velocity

V_{aveYn} mean flow velocity calculated based on normal depth

V_b barrier velocity - maximum velocity over baffle at culvert centreline

V_{b*} dimensionless barrier velocity

y_d height above datum where velocity dip occurs

y_o depth of flow between two baffles

y_z distance above invert

Y_n normal depth

Y_z depth of flow at location offset from culvert centreline

z horizontal offset from culvert centreline

z_0 half the top width of the flow

α coefficient from Ead et al. (2002)

β coefficient from Ead et al. (2002)

γ specific weight of water

ρ fluid density

τ shear stress

τ_0 cross section average shear stress

1. INTRODUCTION

1.1. Background

Culverts are widely used throughout the world as an economical alternative for crossing streams and small rivers. Of the various culvert materials and shapes available, circular corrugated steel pipe (CSP) culverts are frequently used due to their cost effectiveness, widespread availability, versatility, and ease of installation (Corrugated Steel Pipe Institute, 2007). However, in terms of amenability to fish passage, this type of culvert is generally considered to be the least favourable alternative because, when installed conventionally, they often produce unnatural hydraulic conditions (Chilibeck et al., 1993). To minimize the impact on the aquatic environment, these culverts must be carefully designed, taking into account more than just the conveyance of a design flow.

To sustain healthy populations, fish must be able to move throughout their habitat to spawn, locate food, escape from predators, or to move away from unfavorable conditions such as changes in water temperature or low water levels (Katopodis, 1992). If designed or installed improperly, culverts may fragment aquatic habitat by preventing movement of fish and other aquatic organisms. This fragmentation barrier can be in the form of shallow flow depths, a perched outlet, or velocities and/or turbulence conditions that exceed the swimming ability of the local fish species (Frei, 2006). Taking into account their prevalence, circular CSP culverts may therefore present one of the greatest potential threats to the connectivity and health of aquatic ecosystems.

To address this potential threat, standards have been established with respect to design for fish passage at culvert crossings. For example, the Fisheries and Oceans Canada document titled "Land Development Guidelines for the Protection of Aquatic Habitat" sets out a series of requirements regarding minimum design parameters for culvert installations in fish bearing waterways (Chilibeck et al., 1993). In addition to the requirements of this federal agency, provincial governments may also establish their own requirements with respect to ensuring protection of the aquatic environment (e.g., Fisheries and Oceans Canada and Saskatchewan Environment and Resource Management, 1994; Fisheries and Oceans Canada and Manitoba Natural Resources, 1996).

The key fish passage criterion established by government agencies are generally based on achieving an average cross section velocity (i.e., discharge divided by the flow area) that does not exceed the swimming capabilities of the weakest swimming fish in the local area for a certain design flow event (e.g., Fisheries and Oceans Canada and Saskatchewan Environment and Resource Management, 1994). Designing culverts based on such requirements often results in a large diameter culvert being required in order to generate a sufficiently low average velocity. It is well established, however, that the velocity distribution within the open channel flow occurring in a culvert flowing partially full is not uniform. In fact, the velocity is zero at the boundary (i.e., no-slip boundary condition) and increases through the core of the flow area. A discussion outlining these fundamental concepts can be found in any comprehensive hydraulics textbook (e.g. Chow, 1959; French, 1985).

In addition to considerations of flow velocity, there is also growing awareness that turbulence conditions have a significant influence on fish behaviour and swimming performance (Smith et al., 2006). Although there is still much work to be done in order to fully appreciate the effects of turbulence on fish passage through engineered structures, fish passage design criteria may eventually evolve to incorporate turbulence considerations, in addition to the existing velocity requirements.

Through studies of fish behavior, it has been determined that fish are equipped with advanced sensory systems, which they use to evaluate the hydraulic conditions that surround them (Katopodis, 2005). It has also been determined that fish use their sensory systems to seek out preferential velocity and turbulence conditions through which to travel and rest (Mountjoy, 1986; Behlke et al., 1991). Considering the inherent velocity distribution within a culvert, it has been proposed by some researchers that the low velocity regions produced around the culvert boundary by the roughness of the corrugations on a CSP culvert may be significant enough to allow fish to swim upstream, even when the mean velocity exceeds their swimming ability (e.g. Ead et al., 2000; Magura, 2008). Taking these areas of lower velocity into account in culvert design, along with a fish's natural ability to detect and use these regions, has the potential to reduce the specification and installation of unnecessarily large culverts. Reducing culvert sizes would save transportation agencies and taxpayers from unnecessary costs.

In addition to utilizing the natural velocity variation within the flow area, various mitigation measures can be implemented to improve fish passage conditions through a culvert. One such option is culvert embedment, whereby the culvert invert is set below the streambed elevation without backfilling along the invert (i.e. a plain invert remains). In the case of a culvert flowing partially full, installing the culvert in this way increases the flow area within the culvert, thus reducing the mean flow velocity. This method, documented in Katopodis (1992), has been proposed and is actively being employed by the Saskatchewan Ministry of Highways and Infrastructure as a simple and inexpensive option for improving fish passage conditions.

Another alternative for reducing the flow velocity in a culvert is to install baffles along the culvert invert. Baffles have been designed in various shapes and configurations, but their purpose in all cases is to increase the roughness of the invert, thereby decreasing the flow velocity, while at the same time creating low velocity zones in which fish may rest while traversing through the culvert (Rajaratnam and Katopodis, 1990).

Based on a review of the available literature, no studies of the velocity or turbulence distributions in either embedded plain invert culverts, or embedded and baffled invert culverts, appear to have been documented to date. As such, this report documents a model study of the hydraulics of flow through a non-embedded and embedded circular CSP culvert for various flow conditions and both plain and baffled inverts. The main purpose of this study was to contribute to existing research in order to better understand, quantify, and predict the velocity distribution in such culverts.

1.2. Research Objectives

The specific objectives of this research project were to:

- Measure and analyze the velocity distribution for various configurations of a non-embedded and embedded plain invert CSP culvert, and use the results to draw conclusions about the area of the cross section with flow velocity less than the mean;
- Compare the measured velocity distributions to those obtained from predictive equations found in the literature (specifically Ead et al., 2000), which may be suitable for application to culvert design;

- Undertake a preliminary assessment of the turbulence conditions of the flow within a CSP culvert, with and without embedment;
- Complete a minor investigation into the effect of baffles on the velocity and turbulence conditions of a non-embedded and embedded CSP culvert; and,
- Interpret the results of the model study in terms of fish passage, based on information regarding fish behaviour and preferences available from published research.

1.3. Scope of Work

The scope of this research project was limited to a laboratory study using a 500 mm diameter annular CSP culvert. Testing was completed at culvert slopes of 0.4 percent and 1.0 percent, and discharges of 50 L/s, 70 L/s and 90 L/s. At each slope, the culvert was first set-up in a non-embedded condition and was then subsequently embedded to 0.1 times the culvert diameter and 0.2 times the culvert diameter. Testing with the baffled invert was limited to the 1.0 percent culvert slope and 90 L/s discharge only. The study was limited to hydraulic measurements only and did not include any component involving testing with actual fish.

1.4. Organization of Thesis Document

The material covered in this thesis document is divided into five chapters as follows. Chapter 2 contains a review of pertinent literature regarding culvert hydraulics, fish passage principles, and previous studies regarding engineered fishways. Chapter 3 describes the scope of the work and experimental set-up, including details of the measurement equipment and related background work. Chapter 4 presents an analysis and interpretation of the experimental data. Chapter 5 summarizes the findings of the research and the conclusions of the study in terms of the specific research objectives, as well as providing recommendations for future study in terms of experimental set-up and potential areas for further investigation. Finally, more detailed experimental data, as well as much of the analysis to support the findings reported in Chapter 4, are presented in various appendices where presentation in the main body of the thesis was not practical.

2. LITERATURE REVIEW

2.1. Background to Fish Passage Design

2.1.1. Importance of Maintaining Fish Passage

Maintaining pathways through or around engineered works such as dams, culverts or other water control structures, is critical to sustaining strong fish populations (Katopodis et al., 2001). When barriers to fish passage are present at such structures, fish habitat becomes fragmented, which interferes with many functions requiring mobility such as searching for food, escaping from predators, and responding to changing environmental conditions such as water temperature or low water levels (Katopodis, 1992). Permanent habitat fragmentation divides fish populations into smaller groups. Where survival remains possible, each group becomes more susceptible to localized changes in conditions from which they cannot escape and, over the long term, the population may become weakened due to the loss in genetic diversity (Frei, 2006; MacDonald and Davies, 2007). According to the Saskatchewan Fish Habitat Protection Guidelines, a single barrier, such as may occur at a culvert, can impact the fish stocks of an entire drainage basin (Fisheries and Oceans Canada and Saskatchewan Environment and Resource Management, 1994). Even temporary barriers that occur during a fish's spawning period have the potential to impact short term fish stocks, as fish can tolerate only an approximately three day delay enroute to spawning grounds without serious impacts on reproductive success (Fisheries and Oceans Canada and Saskatchewan Environment and Resource Management, 1994).

2.1.2. Fish Swimming Mechanics

Basic knowledge of fish swimming morphology and performance is key to successful fish passage design. Katopodis (2005) describes three distinct fish swimming modes: anguilliform (eel-like), subcarangiform (trout-like) and escosiform (pike-like). Within each swimming mode, fish swimming speeds are divided into three categories: sustained, prolonged, and burst (Katapodis, 1992). Sustained swimming speeds can be maintained indefinitely, prolonged speeds can be maintained for up to approximately 30 minutes and burst speeds can be performed for less than 20 seconds (Katopodis, 1992). The sustained and prolonged swimming motions are carried out primarily by the red muscle system; in this mode, swimming performance decreases very slowly with time (Behlke et al., 1991). Burst swimming effort is

produced through the white muscle system, which cannot perform for long periods of time (Behlke et al., 1991). Katopodis (2005) notes that, in addition to swimming speed, fish also change their swimming style depending on the hydraulic conditions they encounter. Specifically, Katopodis (2005) describes how in smooth flows fish use a "deliberate undulatory" swimming motion, whereas, when encountering more turbulent flows, fish will change to a more relaxed swimming motion in order to utilize turbulent eddies to reduce their swimming effort.

Most fish species in Saskatchewan are subcarangiform swimmers, except for burbot and northern pike (Fisheries and Oceans Canada and Saskatchewan Environment and Resource Management, 1994). Northern pike are generally considered to be the weakest swimming fish species in Saskatchewan and therefore, where present, they may represent the limiting fish swimming performance for fish passage design purposes. Northern pike are classified as escosiform swimmers and their swimming ability is comparable to anguilliform swimmers (Fisheries and Oceans Canada and Saskatchewan Environment and Resource Management, 1994). Therefore, of particular pertinence to culvert design in Saskatchewan, Figure 2.1 illustrates the distance that various lengths of anguilliform swimming fish (e.g. northern pike) can travel at different swimming speeds under a range of countering flow velocities.

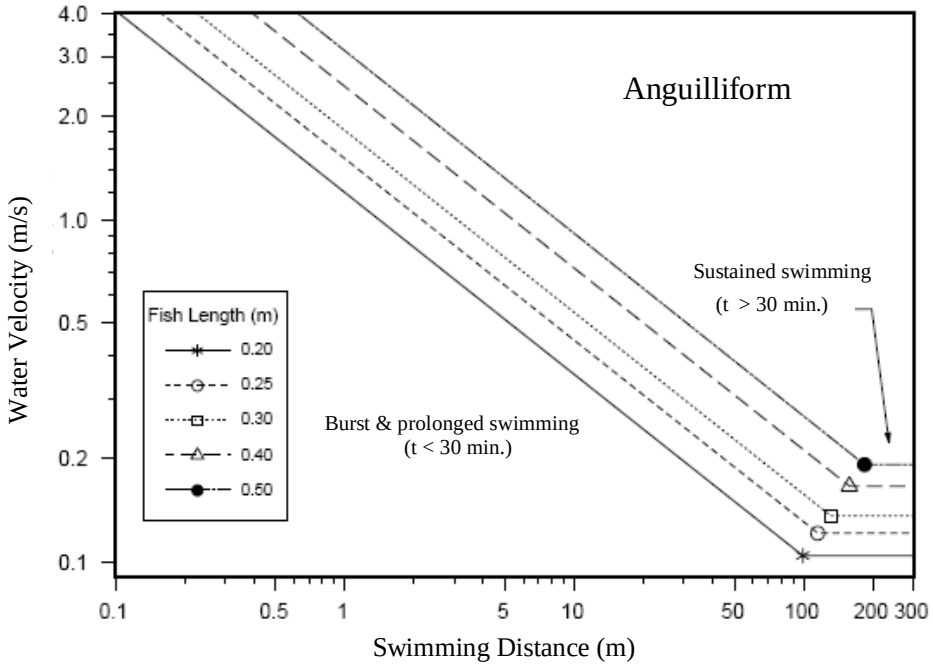

Figure 2.1: Swimming distance curve for anguilliform swimming mode (from Katopodis, 1992).

2.1.3. Studies of Fish Swimming Performance and Preferences

There are many studies reported in the literature regarding the behaviour of fish in response to varying velocity and turbulence conditions. Fish response has been studied in terms of swimming capability and habitat selection preferences, with related studies completed in both laboratory flumes and in the natural environment. Swimming capability can be measured as time to fatigue, where the fish are pushed to exhaustion under a given set of flow conditions, or as critical velocity, where the flow velocity is increased until the fish are unable to swim against the flow (Nikora et al., 2003). The metabolic cost of swimming against various flow conditions can also be measured based on the oxygen requirements of the fish (Enders et al., 2003). Some examples of these various types of studies are presented below.

In terms of documentation of fish swimming performance, Katopodis (1992) describes a compilation of over 500 fish swimming performance references, some of which the information shown in Figure 2.1 is based on. In another example, Barber and Downs (1996) reference results from a number of sources that relate the fork length (length from the tip of the snout to the end of the middle caudal fin rays) of various fish species to their swimming abilities. An example of the type of information presented by Barber and Downs is shown in Figure 2.2. In a more recent example, Haro et al. (2004) reported on a laboratory study in which they developed regression-based models for predicting the maximum travel distance of six fish species for a range of flow velocities within each fish's burst swimming speed range.

Lupandin (2005) reports on a laboratory study of the swimming ability of perch in terms of critical velocity at various levels of turbulence, including comparison of the scale of the turbulence relative to fish body size. From the results of the study, Lupandin concluded that both fish length and turbulence intensity significantly influenced the critical flow velocity that a fish could withstand. Specifically, it was found that the longer the fish, the greater the turbulence intensity that was tolerable and that for each fish length there appeared to be a "critical" turbulence intensity level. When the turbulence intensity exceeded this critical value, the reduction in the swimming ability of the fish increased from that experienced when the turbulence intensity was below the critical value. Lupandin also noted that, when a fish becomes unbalanced due to turbulence, it spreads its pectoral fins in order to stabilize itself, which increases the drag on its body and thus decreases its swimming capability.

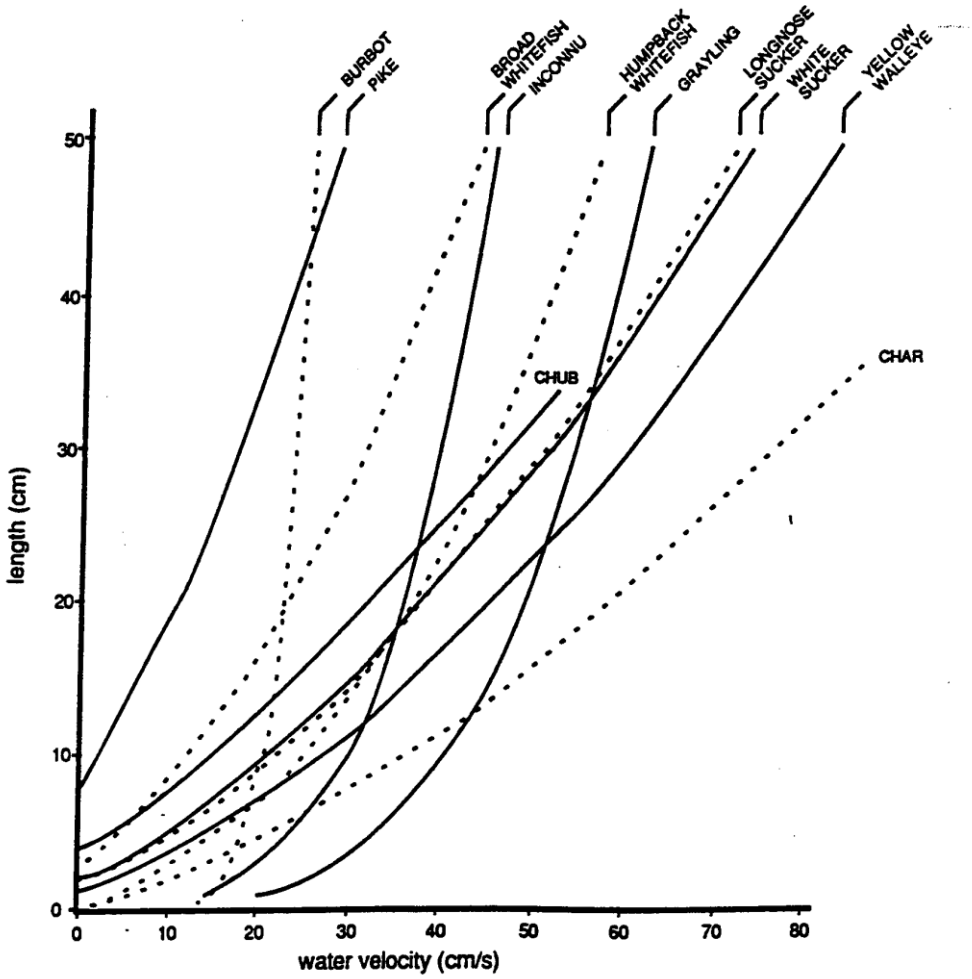

Figure 2.2: Relationship between fork length and ability to move 100 m in 10 minutes for fish from the Mackenzie River (from Barber and Downs, 1996)

Cotel et al. (2006) studied the location preferences of brown trout in a Michigan stream in terms of flow velocity and turbulence intensity. In the study, the positions of brown trout were determined via observations from snorkelers. Velocity measurements were taken at these locations and also at locations where fish were not located, but which had similar conditions to those containing fish. All instances where brown trout were observed occurred in dips in the bed, where the location was shaded, and where large woody debris was present. Thus, although Cotel et al. concluded that these variables clearly drive site selection, they were able to be eliminated from their comparison of conditions that impact a fish's selection of resting location. In all cases, the brown trout were observed within the bottom 15 cm of the flow depth, with 85 percent found in positions within 5 cm of the stream bottom, a position characterized by high turbulence intensity. Comparing the turbulence intensity values of the occupied sites to those of

nearby unoccupied sites, Cotel et al. concluded that under the conditions studied, brown trout were positioned in the locations with relatively lower turbulence intensity.

In contrast to Lupandin (2005) and Cotel et al. (2006), Nikora et al. (2003) found that turbulence had negligible effect on the swimming performance of inanga, a fish native to New Zealand. In the Nikora et al. study, fish were placed in a flume with smooth sides or corrugated sides and the time to fatigue was measured for various discharges. The flow velocity and turbulence were measured at various cross sections within the flume using an acoustic Doppler velocimeter prior to testing with the fish. Measurements indicated that the turbulence intensity was highly variable throughout the cross section, especially in the rough channel where it was significantly greater than in the smooth channel. Despite the differences in turbulence properties between the smooth and rough experimental channels, Nikora et al. found that turbulence had no effect on the time to fatigue of the inanga fish throughout the range of flow velocities tested. They also concluded that turbulence did not affect the paths of fish swimming through the channels, because the fish did not appear to preferentially select the lower turbulence regions.

Enders et al. (2003) studied the effort of juvenile Atlantic salmon in terms of the oxygen consumption of fish swimming against different velocity and turbulence conditions. They found that at a mean flow velocity of 18 cm/s the respiration rate increased by 1.3 times for a 3 cm/s increase in the standard deviation (RMS) of velocity. At a mean flow velocity of 23 cm/s, the respiration rate increased by 1.6 times for the same 3 cm/s increase in standard deviation. These results suggest that turbulence increases the effort expended by fish in swimming upstream and that the effect of a specific turbulence level increases with the mean flow velocity.

Liao (2007) discusses the apparent conflicting findings in published research in terms of whether turbulence has a negligible, positive or negative effect on a fish's swimming ability. Liao states that in some situations fish may be able to use turbulence to their advantage to reduce the effort required to swim, whereas in other situations turbulence is a hindrance, increasing the energy cost of swimming, or discouraging fish from entering areas of higher turbulence altogether. Whether a given turbulence condition is of benefit or detriment to a specific fish is attributed to the fish's body size, swimming strength and ability to stabilize its body, as well as the predictability (i.e., steadiness in magnitude, direction, and scale) of the turbulence.

2.1.4. Principles of Culvert Fish Passage Design

There are several types of fish passage barriers that may be present within a culvert, for example: velocities that exceed swimming ability; a perched invert; lack of resting opportunities; or shallow flow depths (Mountjoy, 1986). In terms of fish passage, bridges are regarded as a superior alternative for facilitating stream crossings as they produce minimal constriction in the flow area, resulting in lower flow velocities and more natural fish passage conditions than culverts (Chilibeck et al., 1993). Therefore, if costs were not a constraint, wherever a crossing of a fish bearing stream or river is necessary a bridge would be installed. In reality, because costs are always a controlling factor, culverts are widely used for water crossings due to their inexpensive material cost and ease of construction. Of the various forms of culverts available, circular culverts are the most widely used shape, unfortunately though such pipes are regarded as the least preferable alternative from a fish passage perspective, as they generally provide the most unnatural channel geometry and flow conditions (Chilibeck et al., 1993).

In the past, culverts were often designed with the only constraint being the passage of a specific design flow without causing upstream flooding (Behlke et al., 1991). It is now widely recognized that culverts designed with only flow conveyance in mind may cause velocity barriers that result in habitat fragmentation (e.g. Katopodis, 2005; Richmond et al., 2007: Hotchkiss and Frei, 2008; Kemp and Williams, 2008). However, designing a culvert to accommodate both a significant peak flow event and fish passage (which may occur under a range of flow conditions) is a complex undertaking, often resulting in large and relatively expensive culvert installations being required. To add further complication, peak flow velocities in culverts generally occur during spring runoff, timing which may coincide with the spring spawning period for fish such as northern pike, arctic grayling, sauger, walleye, and suckers (Fisheries and Oceans Canada and Saskatchewan Environment and Resource Management, 1994).

As mentioned in Chapter 1, culvert design criteria are generally based on achieving a mean flow velocity that does not exceed the swimming capabilities of the local fish species for a specific set of design conditions (i.e., design discharge, culvert slope, etc.). For example, among many criteria, Fisheries and Oceans Canada specifies maximum mean flow velocities for various lengths of culvert, as well as a minimum flow depth, that should be present for successful fish

migration to occur (Chilibeck et al., 1993). The fundamental design condition required by regulatory agencies, is that fish passage through a culvert may be delayed by no more than three days, while a delay of three or more days is tolerable no more frequently than once every ten years (Katopodis, 1992; Chilibeck et al., 1993; Fisheries and Oceans Canada and Saskatchewan Environment and Resource Management, 1994).

Design criteria based on mean flow velocity assume that this velocity represents the typical conditions a fish would encounter inside a culvert. The Saskatchewan Fish Habitat Protection Guidelines note that, because of the variation in velocity within the cross section, the mean flow velocity in a culvert may exceed a fish's swimming ability yet not prevent passage (Fisheries and Oceans Canada and Saskatchewan Environment and Resource Management, 1994). These guidelines note, however, that further research on the velocity distribution within culverts is required before more precise velocity targets can be specified.

Reducing the velocity in a culvert in order to meet fish passage requirements can be accomplished in several ways, including increasing the culvert size, embedding the culvert, creating an artificial backwater condition, or by adding roughness elements such as baffles or large rocks (Abbs et al., 2007). For a pipe flowing partially full embedding a culvert, or setting the invert below the streambed elevation, as illustrated in Figure 2.3, increases the flow area, thereby decreasing the mean velocity. This approach is currently being applied in the province of Saskatchewan as a simple and inexpensive means to improve fish passage conditions. Magura (2008) studied the velocity distribution in an embedded culvert where the invert was backfilled with granular material to the natural streambed elevation, sometimes also referred to as a streambed simulation culvert installation a concept first used on the Liard Highway culverts (Katopodis, 2005). No information appears to have been published regarding the effect of embedment on the hydraulic conditions within a culvert where the invert is left exposed. As such, further research is required on this technique in order to understand and confirm the potential benefit for fish passage.

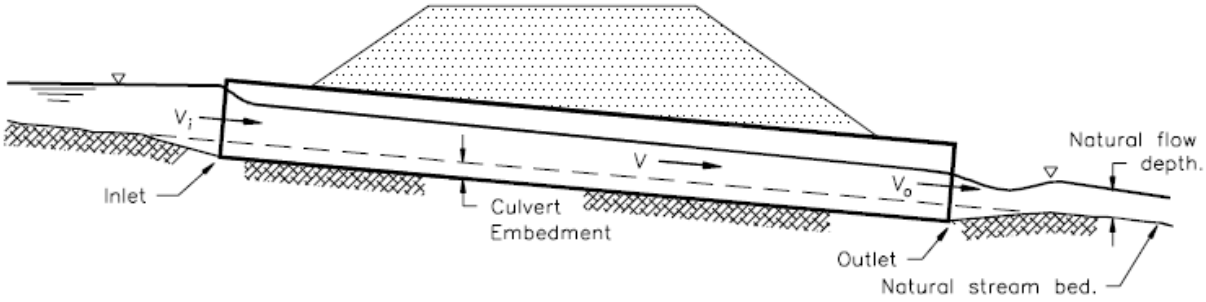

Figure 2.3: Schematic illustration of an embedded culvert (from Katopodis, 1992).

2.2. Culvert Hydraulics

2.2.1. Flow Development in Culverts

The gradual adjustment of flow within a culvert can be described in terms of changes in both flow depth and velocity profiles along the culvert length. Hydraulics textbooks, such as Chow (1959), detail flow depth profile classifications in terms of the channel slope and how the flow depth compares to the normal and critical flow depths. For example, in a mildly sloped (i.e. slope less than critical) embedded culvert the transition from the flow depth just downstream of the inlet, to a tailwater depth which is greater than the normal depth, would be classified as an 'M1' water surface profile. If the tailwater depth at a culvert outlet is known, this gradually varied flow profile may be calculated theoretically moving upstream through the culvert from the outlet to the point at which the flow reaches normal depth.

The layer of water located immediately next to a solid wall is called the boundary layer (Schlichting, 1960). Within this boundary layer the fluid velocity increases from zero against the wall (no slip condition) to some maximum flow velocity. Along the length of the flow path the thickness of the boundary layer increases in the downstream direction. According to Chow (1959), flow is considered to be fully-developed when the thickness of the boundary layer equals the depth of flow, and once fully-developed the velocity profile takes on a consistent shape. Within the boundary layer, the velocity profile can be described by the Prandtl-von Karman velocity distribution law, more commonly referred to as the log-law, which will be discussed in Section 2.2.3 (Chow, 1959). Within a region of fully developed flow, the velocity profile for any experimental conditions can be theoretically calculated based on this law.

The most complex hydraulic conditions within a culvert are generally acknowledged to occur near the inlet. In their discussion of culvert inlet hydraulics, Behlke et al. (1991) described what occurs at the inlet in terms of the conversion of potential energy of the water in the pool upstream of the culvert being converted to kinetic energy as the flow streamlines converge and the flow area contracts through the inlet. According to Behlke et al., the contraction zone is very short and is followed by a slightly longer (several culvert diameters in length) deceleration zone, where the flow streamlines diverge and spread out into the culvert cross section. Behlke et al. suggest that, where the inlet pool is at least two times as wide as the culvert diameter, the contracted flow area at the culvert inlet will be approximately three quarters of the flow area that occurs further downstream in the culvert barrel. The inlet contraction and deceleration zones, as described by Behlke et al., are illustrated in Figure 2.4.

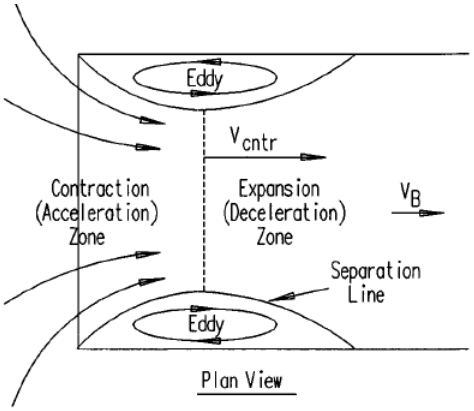

Figure 2.4: Schematic of the contraction and expansion zones near a culvert inlet where V_{cntr} is the average flow velocity in the contracted flow section and V_B is the average flow velocity further downstream from the inlet (from Behlke et al., 1991).

Rajaratnam et al. (1991) investigated the flow characteristics near the inlet of a smooth circular pipe at slopes of 1%, 3%, and 5%, under supercritical flow conditions. Observing the water surface profile, in what they termed the near-field entrance region of the pipe, these authors noted that for all discharges tested above a certain value (specific to each pipe slope), a wave was produced downstream of the inlet and that the amplitude of the wave increased with discharge. Beyond this wave, Rajaratnam et al. determined that the distance downstream from the inlet at which the depth of flow stabilized was approximately 15 times the critical depth of flow and from that point downstream the maximum velocity value along the centreline profile became relatively constant. Through their work, Rajaratnam et al. were also able to develop

equations to predict the location (longitudinally downstream from the inlet) and value of the maximum flow velocity within the entrance region of the pipe.

Magura (2008) evaluated the development of subcritical flow in an embedded and backfilled CSP culvert by estimating the thickness of the boundary layer as the depth at which the measured velocity was 99 percent of the maximum velocity in the profile (this assumption is described in Chow, (1959)). From his results, Magura determined that the flow became fully-developed (i.e., the boundary layer depth was equal to the flow depth) at between 4.4 and 6.1 diameters downstream from the inlet, with the distance increasing with the discharge and culvert slope. In contrast, Ead et al. (2000) found that flow in a non-embedded CSP culvert became fully-developed at a distance of only 1.6 diameters downstream from the inlet (for both sub and supercritical flow). Similarly, Richmond et al. (2007) determined that, based on velocity profile observations, the flow was fully-developed at approximately two diameters downstream from the inlet in a CSP culvert.

2.2.2. Shear Stress Distribution in Culverts

Shear stress is defined as force per unit area that produced by flowing water (Chow, 1959). The distribution of the shear stress across the wetted perimeter is non-uniform, varying with the velocity profile at each horizontal offset (Munson et al., 1998). For a Newtonian fluid the shear stress is equal to the velocity gradient perpendicular to the bed times a proportionality constant equal to the fluid viscosity (Streeter et al., 1998). Chow (1959) shows that

$$\sqrt{\frac{\tau}{\rho}} = u_* \tag{2.1}$$

where τ is the shear stress, ρ is the fluid density and u_* is a quantity with units of velocity and is thus termed shear velocity.

Knight and Sterling (2000) conducted laboratory experiments in a smooth wall pipe to determine the cross sectional velocity and shear stress distributions for both plain invert and embedded (backfilled) invert conditions, and subcritical and supercritical flow regimes. From their results, Knight and Sterling determined that the shear stress around the perimeter of the pipe varied from approximately 0.6 to 1.2 times the mean cross section shear stress ($\tau_o = \gamma RS$, where γ

is the specific weight of water, R is the hydraulic radius and S is the slope) . They found that, for deeper flows, the ratio of the shear stress at the boundary to the mean cross section shear stress was constant across a larger portion of the perimetric distance (defined as the horizontal offset from the pipe wall divided by the cross section wetted perimeter) compared to shallower flows. Therefore, they concluded that the distribution of bed shear stress became more uniform as the depth of flow increased.

Ead et al. (2000) analyzed the horizontal shear stress distribution in their experiment based on the ratio of shear stress at various offsets to the centreline shear stress. They found that the variation could be described by a single curve, which they described with a third order polynomial equation. This equation was then used as one of the building blocks for a two-dimensional velocity distribution model. Based on their data, Ead et al. concluded that, moving from the culvert centreline towards the wall, the shear stress is essentially constant until an offset of approximately 0.6 z/r is reached (where z is the offset from the culvert centreline and r is the culvert radius), at which point the shear stress begins to decrease rapidly.

Magura (2008) calculated the shear velocity around the perimeter of an embedded and backfilled CSP culvert under various flow conditions. Magura's results indicated that the shear velocity reached a maximum value at an offset of between 0.06 m and 0.12 m from the culvert centerline and then sharply decreased to approximately 20-50 percent of the maximum at the culvert wall. Magura confirmed that the magnitude of the shear velocity was heavily influenced by the average cross section velocity, as well as the shape of the velocity contours. These results are similar to Knight and Sterling's (2000) shear stress distribution findings, with the exception that the maximum value was not located at the culvert centreline, an effect that Magura attributed to the presence of the granular backfill through the pipe.

2.2.3. Velocity Distribution in Culverts

The one-dimensional velocity distribution for open channel flow has been the subject of great study and has resulted in the development of various predictive equations, the most well-known of which is the Prandtl-von Karman universal velocity distribution, or log-law, given by Chow (1959) as:

$$v = 2.5u_* \ln\left(\frac{y_z}{y_o}\right) \quad (2.2)$$

where v is the flow velocity at a distance y above the channel bed, u_* is the shear velocity at the specific location in the cross section and y_o is a constant of integration. This equation is valid within the turbulent boundary layer and is therefore suitable to predict the vertical velocity distribution throughout the flow depth when flow is fully-developed (i.e., where the boundary layer extends to the water surface). Equation 2.2 can be further refined for a hydraulically rough boundary, such as a CSP culvert, by relating the y_o term to the roughness height, such that:

$$\frac{v}{u_*} = 2.5 \ln\left(\frac{y_z}{k_s}\right) + 8.5 \quad (2.3)$$

where k_s is the Nikuradse equivalent sand roughness of the boundary surface (French, 1985; Ead et al., 2000).

More recent velocity distribution studies relevant to culvert hydraulics include that of Mountjoy (1986), who carried out a field study involving 49 non-embedded culvert installations in Alaska. At each site, one centreline vertical velocity profile, located at the culvert outlet, was measured. The results were used to develop a predictive equation for calculating the velocity profile, based only on knowledge of the velocity at 0.6 of the flow depth from the water surface. Mountjoy suggested that the velocity at 0.6 of the depth, which would be unknown unless it could be measured, could be assumed to be equal to the average flow velocity (discharge/flow area) based on normal depth.

Barber and Downs (1996) measured the velocity distribution across the complete flow area for 51 cross sections in several different model pipes, for various flow conditions, and compared their measured results to the predictive equation developed by Mountjoy (1986). Barber and Downs completed their analysis based on "effective band widths" of velocity relative to the maximum velocity in the cross section (i.e., v_x/v_{max}). This method involved calculating the area between each v_x/v_{max} contour from the actual measured data plot, translating these areas into perfectly circular contours and then extracting the centreline velocity profile from this theoretical circular velocity contour plot. The authors processed the data this way in order to eliminate

asymmetry that had been observed in the measured velocity contour plots. Based on their findings, Barber and Downs concluded that the Mountjoy method produced a more accurate prediction of the velocity profile than a method documented by Chiu (1993).

Several attempts have been made to develop a relationship to quantitatively predict the two-dimensional velocity distribution of the flow area in culverts. For example, House et al. (2005) completed a field study to produce velocity cross sections for six culvert installations in Oregon. In these culverts, the inverts had been placed below the bed level and backfilled with gravel through the entire culvert length. From their measurements, House et al. developed a model to allow prediction of the percent of the flow area below a specified velocity. House et al. identified that their proposed model had a significant tendency to under-predict the percent of area less than the specified velocity and suggested that testing of a wider range of embedded backfilled culverts is required to improve the accuracy of the model.

Magura (2008) also analyzed the two-dimensional velocity distribution in his model CSP culvert trials for various slopes and flow conditions. Based on his experimental measurements, Magura found a very consistent distribution of v_x/V_{ave} for all his tests, regardless of the variation in depth of flow or velocity range as shown in Figure 2.5. Magura, however; did not attempt to determine a predictive relationship based on his data.

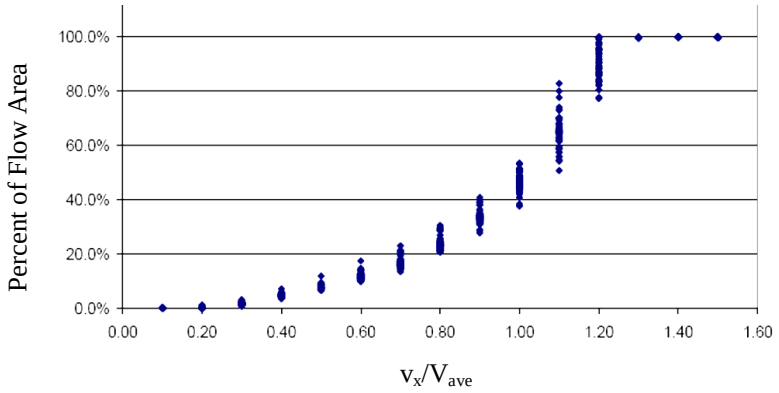

Figure 2.5: Experimentally determined velocity distribution in terms of percent of area less than v_x/V_{ave} for an embedded and backfilled CSP culvert (Magura, 2008).

In addition to attempts to better quantify the velocity distribution, work has also been done to map and then predict the two-dimensional distribution for open channel flow occurring in culverts. Of special relevance to this project is a study completed by Ead et al. (2000), in which point velocity measurements, taken in a non-embedded, plain invert model culvert set a

various slopes, were compared with flow velocities calculated from the log-law velocity equation (Equation 2.2). Noting the presence of the velocity dip near the water surface was causing a discrepancy between the expected and measured results, Ead et al. (2000) proposed a method of calculating point velocities in a corrugated steel pipe anywhere in the cross section, requiring only the location of the desired point relative to the culvert centreline and invert. It was intended that this method would accurately predict the flow velocity through the velocity dip region (i.e. at the surface of the flow area), and would therefore be an improvement on the log-law. The system of equations proposed by Ead et al. is:

$$\frac{v_x}{V_{ave}} = \left[\left(\frac{2.30}{\kappa}\right)\log\left(\frac{y_z}{k_s}\right) + 8.50\right]\sqrt{f_3\left(\frac{z}{z_0}\right)}\left(\frac{J\sqrt{g}n}{R^{1/6}}\right) \tag{2.4}$$

for $\frac{y_z}{k_s} < \frac{y_d}{k_s}$, and

$$\frac{v_x}{V_{ave}} = \left[\left(\frac{2.30}{\kappa}\right)\log\left(\frac{y_z}{k_s}\right) + 8.50 - \frac{\frac{y_z}{k_s} - f_1\left(\frac{z}{z_0}\right)}{\frac{Y_z}{k_s} - f_1\left(\frac{z}{z_0}\right)} \times f_2\left(\frac{z}{z_0}\right)\right]\sqrt{f_3\left(\frac{z}{z_0}\right)}\left(\frac{J\sqrt{g}n}{R^{1/6}}\right) \tag{2.5}$$

for $\frac{y_z}{k_s} > \frac{y_d}{k_s}$

where the f_1, f_2 and f_3 are functions defined as:

$$f_1\left(\frac{z}{z_0}\right) = \frac{y_d}{k_s} = -6.91\left(\frac{z}{z_0}\right)^2 - 2.05\left(\frac{z}{z_0}\right) + 9.00 \tag{2.6}$$

$$f_2\left(\frac{z}{z_0}\right) = 5.98\left(\frac{z}{z_0}\right) + 0.90 \tag{2.7}$$

$$f_3\left(\frac{z}{z_0}\right) = -20.00\left(\frac{z}{z_0} - 0.60\right)^3 + 2.75\left(\frac{z}{z_0} - 0.60\right)^2 - 0.40\left(\frac{z}{z_0} - 0.60\right) + 1.00 \tag{2.8}$$

for $\frac{z}{z_0} \geq 0.6$, or

$$f_3\left(\frac{z}{z_0}\right) = 1.00 \tag{2.9}$$

for $\frac{z}{z_0} < 0.6$.

The variables in the Ead et al. (2000) equations are as follows: v_x is the longitudinal point velocity being calculated; V_{ave} is the average cross section velocity; y_z is the height of the calculation point above the datum; y_d is the height above the datum at which the velocity dip occurs; k_s is the Nikuradse equivalent sand roughness value for the culvert; z is the lateral distance of the desired point from the culvert centerline; z_o is half the top width of the flow; J is the ratio of centerline shear velocity to mean cross section shear velocity (i.e. $\tau_o = \rho g R S$); r is the hydraulic radius; and Y_z is the depth of flow at the specific location (i.e. flow depth at that offset from the culvert centreline). The centreline shear velocity was determined experimentally from measured centreline vertical velocity profiles.

Ead et al. (2000) defined the datum for their model at halfway between the corrugation crest and trough at the culvert invert and determined, based on their experimental results, that the appropriate k_s value for a CSP pipe was equal to the amplitude of the corrugations. Ead et al. proposed that their model was suitable for determining the area of the cross section with flow velocity less than a desired prolonged fish swimming speed, thus predicting the area suitable for fish passage. The Ead et al. model was developed based on cross sections where the flow was fully-developed, thus is applicable to that situation only.

Richmond et al. (2007) reported on a laboratory study of the velocity and turbulence in a non-embedded, plain invert, helical CSP culvert set at a slope of 1.14 percent. The centreline velocity profiles collected in the study were used to determine the shear velocity, which in turn was used to compare the data to the log-law and to fit an experimental value of k_s. Similar to Ead et al. (2000), Richmond et al. concluded that k_s was approximately equal to the corrugation amplitude of the pipe material.

2.2.4. Turbulence in Culverts

Enders et al. (2003) define turbulence as the relatively smaller, three-dimensional fluctuations in flow that occur over time around the larger scale mean flow velocity. In a natural channel, turbulence is generated by shear on the bed and flow separation around bluff bodies such as rocks and large woody debris located in the flow path (Smith et al., 2005).

Although the average cross section velocity is generally used as the design condition for fish passage criteria, there is increasing recognition that turbulence conditions in a culvert may be just as significant for fish passage (Morrison et al., 2009). The impact of turbulence on fish passage through culverts is not well understood; however, research has shown that fish generally prefer to occupy areas of low turbulence. This preference may be due to the fact that turbulence negatively impacts a fish's swimming ability and may make it difficult for them to position themselves in lower velocity zones (Frei, 2006). Frei (2006) also notes that excessive turbulence may prevent a fish from passing through a high velocity zone, even though they may have the necessary burst speed to traverse the velocity barrier. Such isolated velocity barriers may occur within a culvert at the inlet or along a baffled invert.

Turbulence is commonly quantified in terms of turbulence intensity, which is a dimensionless expression of turbulence that is calculated by dividing the standard deviation (RMS), of the instantaneous velocity measurements by the mean velocity of the flow as in:

$$\text{RMS v} = \sqrt{\frac{1}{N}\sum_{i=1}^{N}(v-\bar{v})^2} \tag{2.10}$$

$$\text{Turbulence Intensity} = \frac{\text{RMS v}}{\bar{v}} \tag{2.11}$$

where N is the number of instantaneous velocity measurements within the measurement interval, v is the instantaneous velocity, and $\bar{v}$ is the mean velocity over the measurement interval at the specific measurement location (Odeh et al., 2002). Use of this means of quantifying turbulence is supported by researchers such as Kemp and Williams (2008), who state that turbulence intensity is one of the most ecologically relevant descriptors of flow turbulence. The definition of turbulence intensity, shown in Equation 2.11 which uses the mean point velocity, is supported

by Cotel et al. (2006), who contend that the ability of fish to maintain stability in a turbulent flow condition is dependent not only on the magnitude of the turbulent velocity fluctuations, but also on the mean flow velocity. According to these researchers, as the mean flow velocity increases, the stability of a fish also increases, an effect they compare to the ease of balancing a bicycle at high speed versus low speed. Thus, if turbulence intensity is calculated based on the mean flow velocity at the measurement point, it takes into account the ability of a fish to withstand greater velocity fluctuations at a higher flow velocity.

2.3. Fish Passage Through Culverts

According to Behlke et al. (1991), a fish typically uses its prolonged swimming speed to traverse relatively slowly through a culvert and may only apply its burst swimming speed to negotiate very short difficult conditions, such as may be encountered at the culvert inlet. As a result, barriers to fish movement can be caused by exceeding either a fish's prolonged swimming speed, burst speed, or a combination of the two (Frei, 2006). Such barriers can be complete (i.e., total blockage for a certain fish species under all conditions), temporary (i.e., only present under certain flow conditions), or partial (i.e., affecting only some members within a fish species population) (Frei, 2006).

Although fish passage criteria are calculated based on average velocities, it is well established that the velocity distribution within a flow field is not uniform, with lower velocity zones occurring around the perimeter of the culvert, and higher velocities occurring through the core and at the surface. Fish possess complex sensory systems that enable them to adjust their body orientation, swimming speed, and style to whatever hydraulic conditions they encounter (Katopodis, 2005). Using this sensory system, fish will seek out areas of lower flow velocity or other preferential hydraulic conditions within the cross section through which to travel (Fisheries and Oceans Canada and Saskatchewan Environment and Resource Management, 1994). For example, Lupandin (2005) notes that fish have been shown to be able to recognize and preferentially select different flow turbulence conditions, a choice which depends on the fish species, motivation for movement, and physiological state of each fish. According to Katopodis (2005), fish have been observed to wander across the flow field when they encounter turbulent flow, and it is believed that they do this in order to search for less turbulent flow. Based on observations of arctic grayling, Behlke et al. (1991) found that the velocity in the locations and

paths occupied by fish passing upstream through a culvert were generally from 0.1 to 0.8 times the average velocity in the cross section.

Considering findings such as those of Behlke et al. (1991), Katopodis (2005) and Lupandin (2005), utilizing the mean velocity (as discussed in Section 2.1.4) as the basis for fish passage design may be an overly conservative estimate of the actual conditions that a fish has to contend with when swimming upstream within a culvert. However, without knowledge of the velocity distribution of the flow field within in a culvert, it is difficult to set accurate criteria in terms of fish passage requirements. For example, the Saskatchewan Ministry of Environment Fish Habitat Protection Guidelines state that for adult subcarangiform swimmers, the mean cross sectional water velocity should be less than 0.8 m/s in culverts greater than 25 m in length and less than 1.0 m/s in culverts less than 25 m in length (Fisheries and Oceans Canada and Saskatchewan Environment and Resource Management, 1994). These criteria are based on accommodating the swimming ability of an average length fish and assumes that the fish must swim at that constant velocity for the entire culvert length. If more detailed information regarding the velocity distribution within a culvert was available more definitive design requirements could be set, potentially reducing the cost of culvert installations, while still providing the necessary fish passage conditions.

In terms of where fish choose to swim within a culvert, Behlke et al. (1991) observed that arctic grayling frequently utilize the upper corners of the cross section and swim so their bodies are normal to the culvert boundary (as illustrated in Figure 2.6), instead of aligning themselves vertically. This may be especially true of juvenile fish which, according to Barber and Downs (1996), have been observed to frequently swim near the culvert boundaries.

Prediction of the success of fish passage through culverts and fishways requires consideration of not only the swimming speed and endurance of the fish of interest, but also knowledge of fish behaviour in similar hydraulic conditions (Peake, 2008). Compared to the number of general studies with respect to swimming capabilities and preferences, comparatively little work has been documented in terms of the implications of these responses to fish passage through engineered fishways.

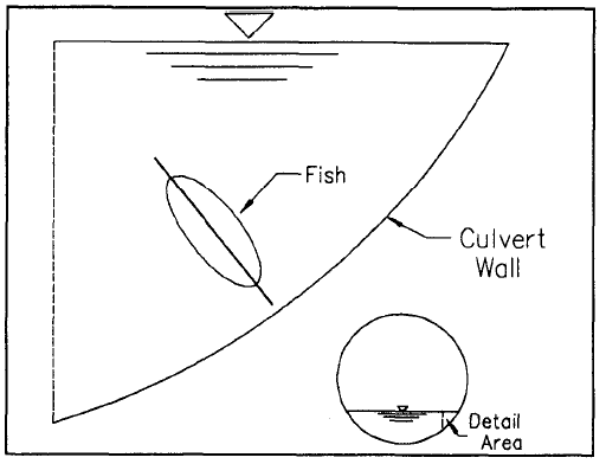

Figure 2.6: Frequent pathway for upstream fish travel as observed by Behlke et al. (1991) (from Behlke et al., 1991).

Engineered hydraulic structures generally have simple shapes and sharp edges, which produce higher turbulence levels than natural objects (Smith et al., 2005). Therefore, Smith et al. suggest that any positive correlation between turbulence and fish habitat that occurs due to natural cover can not necessarily be extended to the case of manmade structures. Hotchkiss and Frei (2007) suggest that culvert retrofits that are intended to reduce flow velocity (e.g., baffles), thereby enabling fish passage, may have the side effect of increasing turbulence, thus discouraging fish from entering or completing the passage through the structure.

In terms of velocity barriers to fish passage within a culvert, Behlke et al. (1991) found that conditions in the flow contraction region near the inlet may present the most significant barrier to upstream-swimming fish. However, they note that the re-circulating eddies at the sides of the flow may provide locations for fish refuge, while gathering strength to combat the high velocities in the flow acceleration zone located immediately at the inlet. Based on their observations of arctic grayling, Behlke et al. determined that, when conditions at the inlet were not challenging, fish would choose to swim along the culvert invert. Under more difficult conditions, they found that fish would rest in the eddies and then attempt to pass through the culvert inlet immediately adjacent to the culvert walls, obviously attempting to avoid the central portion of the acceleration zone flow region.

Peake (2008) studied the reaction of northern pike, walleye, and white suckers to various culvert outlet conditions. The results indicated that, for northern pike and white suckers, whether the fish would enter the culvert to attempt upstream passage did not vary with the velocity of flow in the culvert. Peake, however; did find that the volume of the pool downstream of the culvert outlet appeared to be a consistent factor in determining the entrance probability of all three species. Specifically, when the volume of water in the pool was small the fish were much more likely to enter the culvert than for the same discharge with a larger pool. Peake suggests that this effect may have been due to higher turbulence in the smaller pool, which encouraged the fish to move out of this area.

Analyzing velocity measurements taken at locations offset from the centerline of a large CSP culvert, Richmond et al. (2007) identified the presence of a reduced velocity and turbulence (measured in terms of the RMS of the time series of velocity measurements) zone in one corner of the flow area, which they attributed to secondary currents produced by the helical corrugations. The Richmond et al. study was unique in that the authors attempted to directly relate hydraulic measurements to actual biological observations. To do this, in addition to taking velocity measurements for hydraulic analysis, the study also included observations of fish passage through the culvert. The authors observed that fish passed upstream through the upper right corner of the flow, in the area they had identified as the reduced velocity and turbulence zone. These results appear to confirm that where lower velocity and/or turbulence areas exist within a flow cross section, fish may be able detect these areas and use them to their advantage.

Smith et al. (2005) tested the selection preference of juvenile rainbow trout of either low or relatively higher turbulence channels at various discharge levels. Fish in the test were categorized as either large or small, the behaviour of the fish was observed as they selected one of the channels, and the final position of each fish was recorded. It was found that generally both the large and small fish sizes preferentially selected the lower turbulence channel. As the discharge increased, however; a point was reached where fish preferred the higher turbulence channel. This point occurred at a lower discharge for small size fish compared to the larger sized fish.

Kemp and Williams (2008) assessed the impact of turbulence on downstream salmon smolt migration in culvert fishways. Specifically, they attempted to determine whether measures taken to introduce more complex flow patterns in culverts to improve upstream migration conditions for adult salmon were detrimental to smolts making the journey downstream. In order to test this hypothesis, a flume was divided into two channels, a control channel with smooth walls and a modified channel with more complex flow patterns created by various roughness elements. Through their results, Kemp and Williams confirmed previous research that showed that downstream migrating smolts do not move passively with the velocity of flow through culverts, but rather actively seek out preferential conditions. In light conditions, Kemp and Williams found the fish avoided entry to the more complex passage, while in dark conditions as soon as fish encountered the more complex hydraulic conditions they frequently tried to escape them by swimming upstream. While Kemp and Williams cite previous research in which it was suggested that fish that had evolved to live in turbulent rivers would likely use turbulent kinetic energy to reduce the effort required for swimming, their study showed that downstream migrating salmon preferentially selected the route that had the least turbulence.

To further complicate the relationship between fish swimming abilities and preferences to culvert hydraulics, Katopodis (2005) notes that fish swimming speed, endurance, agility and other performance characteristics vary not only with fish species but also fish length, water temperature and the specific morphology of each fish, in addition to many other variables. Additionally, as noted by Peake (2008), whether a fish enters and successfully passes through a hydraulic barrier depends not only on whether the fish is physically able, but also on the motivation and willingness of the fish to do so. For example, fish that are hungry are more likely to enter turbulent conditions in search of more efficient feeding conditions than fish that are satiated (Lupandin, 2005). Therefore, designing for fish passage based on matching hydraulic conditions to discrete values of a certain fish species swimming capabilities and turbulence thresholds may not always be adequate.

2.4. Baffled Invert Culverts

2.4.1. Purpose of Installing Weir Baffles along Invert

As mentioned in Section 2.1.4, installing baffles is one alternative that has been proposed for improving fish passage conditions in a new or existing culvert. The baffles are fixed along

the culvert invert and essentially divide the bottom portion of the flow area into a series of cells (Rajaratnam and Katopodis, 1990). Baffles may improve fish passage conditions by both providing resting areas for fish and by reducing the overall velocity of the flow through the culvert (MacDonald and Davies, 2007). To traverse the length of the culvert, a fish may either use its prolonged or sustained swimming speed to move continuously through the culvert, or rest between the baffles and use its burst speed to pass over one or more baffles before resting again in an upstream cell (Ead et al., 2002).

An extensive model study of various baffle configurations, within a non-embedded smooth-walled circular pipe, was completed at the University of Alberta and reported in a series of papers, the results of which are summarized in Ead et al. (2002). Based on the results of these studies, Ead et al. concluded that weir and slotted weir baffle systems were as effective as more complex baffle designs (e.g., offset baffle, spoiler baffle, etc.) with respect to improving fish passage conditions. In consideration of this, as well as their simpler design and construction requirements, Ead et al. proposed the weir baffle as being one of the best choices for culvert fishways. Figure 2.7 illustrates the weir baffle design.

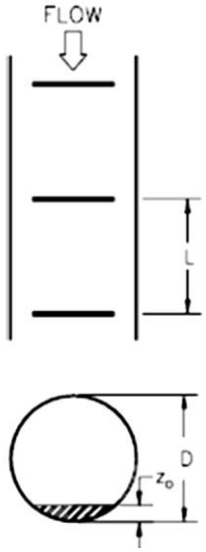

Figure 2.7: Weir baffle configuration (from Katopodis, 1992).

2.4.2. Related Studies of the Hydraulics of Baffled Invert Culverts

The weir baffle system is essentially similar to a pool and weir fishway, which is the earliest type of fishway that was built (Rajaratnam et al., 1988). Rajarantnam et al. (1988) identified two distinct modes of operation for pool and weir fishways: plunging mode, where the

water level in the pool is below the upstream weir crest, and streaming mode, where the water surface is continuous over the weirs. In streaming mode, Rajaratnam et al. described a stream of constant thickness and width, and a slope equal to the fishway slope, flowing over the weirs and the cell of water contained between the weirs. The streaming mode flow pattern is shown in Figure 2.8. Based on experimental results, Rajaratnam et al. determined that the dimensionless discharge in a pool and weir fishway of 2% to 15% slope is related to the depth of flow over the weir such that:

$$Q_* = 1.5\sqrt{\frac{L}{d}} \tag{2.12}$$

where Q_* is the dimensionless discharge, L is the baffle spacing and d is the depth of the streaming flow in the fully-developed flow portion of the fishway, measured relative to the top of the weirs.

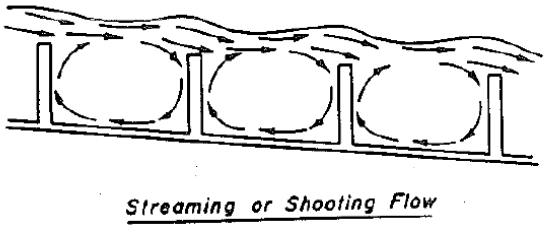

Figure 2.8: Illustration of streaming flow in a pool and weir fishway (from Rajaratnam et al., 1988).

Rajaratnam and Katopodis (1990) reported on the results of a laboratory study that dealt specifically with the weir baffle culvert fishway. Rajaratnam and Katopodis postulated that, as the streaming flow moved across the pool of water held between the baffles, it created significant turbulent shear. This shear in turn induced the re-circulating flow that was observed to occur in each pool between the weirs. Through their experimental measurements, Rajaratnam and Katopodis found that the maximum negative velocity at the bottom of the pool between the baffles was more than one-third of the maximum forward velocity.

Rajaranam and Katopodis (1990) termed the depth of flow between two baffles located within the region of fully-developed flow as the characteristic depth. The authors proposed a

relationship between dimensionless discharge and the ratio of the characteristic depth to the culvert diameter as follows:

$$Q_* = C\left(\frac{\text{characteristic depth}}{D}\right)^a \tag{2.13}$$

where C and 'a' were experimentally determined for various baffle height and spacing combinations and D is the culvert diameter.

In Rajaratnam and Katopodis' (1990) weir baffle study, the depth of flow was measured along the culvert centreline and a Pitot tube was used to measure point velocities at various locations between one set of baffles. The results from these experiments were used to develop equations to predict the flow depth and barrier velocity for the weir baffle installation. Based on velocity profiles measured at the baffle location, both at the culvert centerline and at various horizontal offsets, Rajaratnam and Katopodis observed that there was little difference in velocity across the baffle width and therefore termed the peak velocity occurring over the baffle at the culvert centerline as the barrier velocity (V_b) for a given flow condition. Rajaratnam and Katopodis identified that the dimensionless barrier velocity ($V_{b*} = \frac{V_b}{\sqrt{gSD}}$) was related to the characteristic flow depth such that:

$$V_{b*} = K\left(\frac{\text{characteristic depth}}{D}\right) \tag{2.14}$$

where K is a coefficient that varies with baffle spacing and height. Based on the results of their experimental tests and related analysis, Rajaratnam and Katopodis were able to determine that; for a weir baffle culvert fishway with baffles that are between 0.15D and 0.1D in height, a baffle spacing of 0.6D was "very effective" and that a baffle spacing of 1.2D was "somewhat too large".

Based on the results of numerous studies involving six types of baffles (including Rajaratnam et al. (1988) and Rajaratnam and Katopodis (1990)), Ead et al. (2002) determined for all types of culvert fishways that:

$$Q_* = \alpha \left(\frac{y_0}{D}\right)^2 + \beta \left(\frac{y_0}{D}\right) \quad (2.15)$$

where α and β are coefficients that vary with h/D and y_0 is the depth of flow between baffles and h is the baffle height. Analyzing the various velocity profiles, Ead et al. also concluded that for all culvert fishways:

$$\frac{V_b}{\sqrt{gDS}} = 10 \left(\frac{y_0}{D}\right) \quad (2.16)$$

where V_b is the maximum velocity at the barrier, S is the culvert slope and g is acceleration due to gravity.

In a field study involving several species of fish native to Australia, MacDonald and Davies (2007) found that installing baffles (in this case spoiler baffles) in a culvert increased fish passage success by at least 10 times that for the plain invert control test. MacDonald and Davies also concluded that fish passage success (defined as a completed passage upstream through the test culvert) increased as the complexity and density of the baffle configuration, and resulting increase in flow heterogeneity, was increased. This finding is somewhat contrary to the conclusion of Rajaratnam et al. (1988) who, for various reasons, advocated the use of less complex baffle styles and configurations.

In terms of studying the turbulence field in a baffled invert culvert, Morrison et al. (2009) conducted experiments for sloped-weir and slotted-weir baffle configurations. In their experiment, Morrison et al. used an acoustic Doppler velocimeter to measure point velocities throughout the flow area at several locations relative to each baffle configuration. Their results showed that, downstream of the baffle, the two baffle types produced turbulence distributions that could be directly related to the flow structure created by each baffle. However, they found that the effect of the baffles on the turbulence distributions had disappeared by 4.32 m downstream from the baffle (in a baffle spacing of 4.62 m), at which point the turbulence distribution was similar to that of the plain invert condition. Morrison et al. attempted to use their data to draw comparisons with some previous observations regarding fish passage past

baffles. These observations had found that, for a specific baffle set-up, juvenile fish had adjusted their location of passage over the baffle (i.e., centre or side of baffle) in accordance with various flow conditions. Morrison et al., however; were not able to find any relationships between these observations and the turbulence data collected in their study.

2.5. Summary

Maintaining fish passage at culverts is key to protecting fish populations from the adverse effects of development. Within a culvert, fish passage may be impeded by many factors, two of which are flow velocity or turbulence conditions which exceed the swimming capability of local fish species.

There has been considerable study of fish swimming style, performance, and preferences in terms of hydraulic conditions. In Saskatchewan, the weakest swimming fish species in an area is frequently the northern pike and, as such, design flow velocities must accommodate the swimming ability of this species. Culvert fish passage design standards are typically based on achieving a mean flow velocity through the culvert under a specific design flow condition that does not exceed these documented swimming capabilities. However, such fish passage criteria do not account for the ability of fish to choose their swimming path based on the velocity distribution that exists within the flow cross section. In Saskatchewan, as in many other jurisdictions, turbulence conditions are not routinely addressed by fish passage standards, although it is acknowledged that turbulence may also be a factor in fish passage.

Several models have been proposed for predicting the velocity distribution for flow through culverts, however, it would appear none has been developed or tested to the point where it is being widely applied in the context of more accurate fish passage design. Ideally, culvert design may eventually become further refined to take this knowledge into consideration; however, further research is required before this can take place.

Installing culverts with the invert below the streambed grade, in order to increase the flow area and thereby reduce the flow velocity, is frequent practice in the province of Saskatchewan and is recommended by the province's Environment Ministry to improve fish passage conditions. The effect of embedding a culvert in this way on the velocity and turbulence conditions within a culvert has not been the subject of any documented study to date.

In the past, baffles placed along the invert, have also been utilized as a means to improve fish passage conditions within culverts by providing resting areas, increased flow depth and reduced flow velocity. Although such installations have been the focus of extensive study, especially in Alberta, the complete cross sectional velocity and turbulence distribution in culverts equipped with baffles has not been previously documented.

As outlined in Chapter 1, the purpose of this research project is to investigate some of these issues and contribute to the body of knowledge regarding the hydraulic conditions within CSP culverts in the context of fish passage.

3. EXPERIMENTAL METHODS

3.1. Introduction

The experimental work was conducted at the University of Saskatchewan Hydrotechnical Lab from June to August 2008 and January to May 2009. In the experiments, flow through a model CSP culvert was examined under various conditions. Extensive measurements, including flow depths, centreline velocity profiles and velocity cross sections, were taken at various longitudinal locations inside the culvert. An acoustic Doppler velocimeter was used to conduct the velocity measurements. This chapter describes the experimental set-up and equipment used, and provides the details of the experimental program.

3.2. Experimental Set-Up

3.2.1. Model Culvert

The model culvert used to conduct this research was a 500 mm diameter, 8.0 m long, 68 mm x 13 mm corrugated steel plate pipe. The culvert was set up in a 20 m long 1.2 m wide, 0.63 m deep rectangular re-circulating flume equipped with an in-line magnetic flow meter. The experimental set-up is shown in Figure 3.1. A culvert with annular corrugations was selected in order to prevent the development of asymmetric flow that is known to occur in helical corrugated pipe. In addition to this, at a larger scale, helical corrugations become almost annular (i.e., the helix angle approaches 90°), and therefore it was determined that using an annular corrugated pipe for a scale model was a better representation of flow conditions in a large prototype culvert (Abbs et al., 2007).

Flow in the flume was directed through the culvert by means of headwalls cut from PVC sheets, which were fitted around the outside of the culvert and installed in the flume near the culvert inlet and outlet. Along the barrel of the culvert, plywood gussets mounted on steel angles were used to support the culvert at six locations. Each piece of steel angle was mounted on two vertical half-inch threaded stainless steel rods as shown in Figure 3.2. To adjust the slope of the culvert, the supports were raised and lowered by turning nuts above and below the steel angle. The slope of the culvert was initially set using a point gauge and then confirmed using a survey level.

a)  b) 

Figure 3.1: Photographs of model set-up showing: a) Culvert being set-up in flume, and b) culvert installed and flume filled with water for testing.

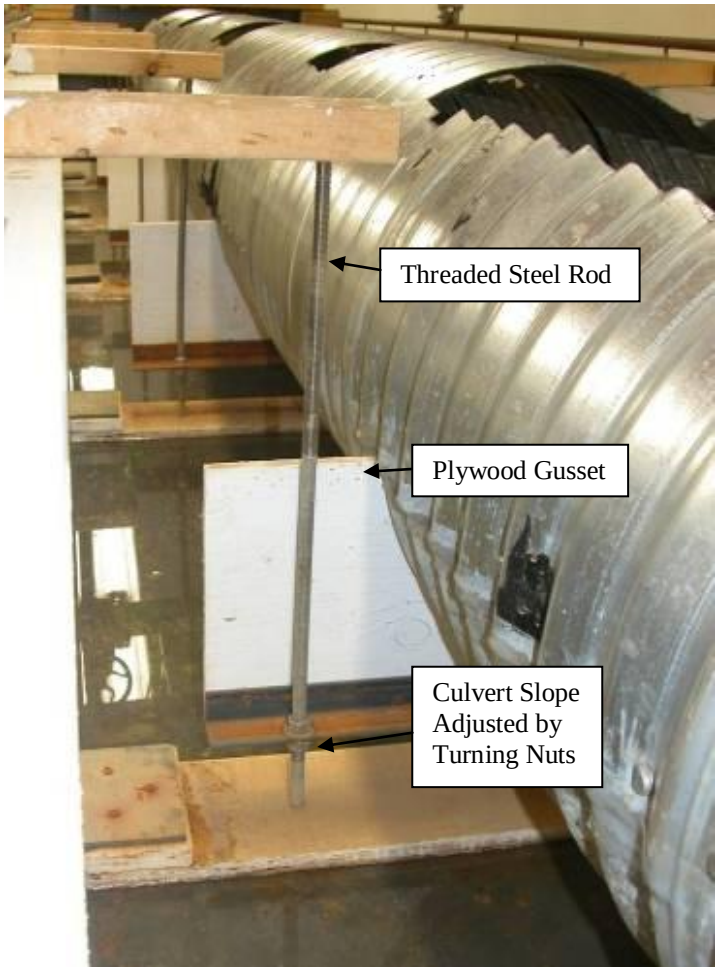

Figure 3.2: Close-up view of the culvert support system.

In order to access the interior of the culvert for flow measurements, fifteen access holes had previously been cut into the crown of the pipe. The locations of these access holes are shown in Figure 3.3 and listed in Table 3.1

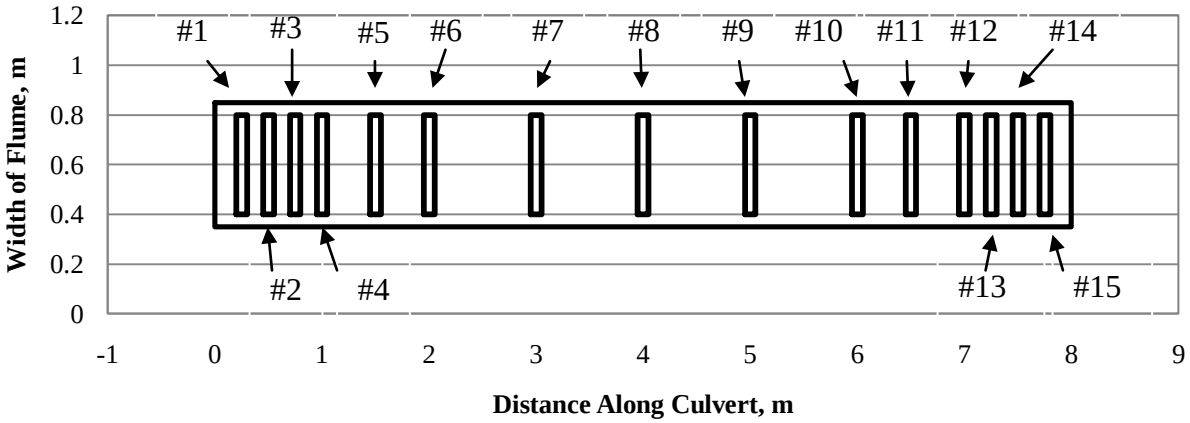

Figure 3.3: Plan view of culvert showing locations of measurement access holes.

Table 3.1: Sample locations used in experimental study.

Access Hole #	Distance from Inlet, m	Distance from Inlet, x Culvert Diameter
1	0.25	0.5D
2	0.50	1.0D
3	0.75	1.5D
4	1.00	2.0D
5	1.50	3.0D
6	2.00	4.0D
7	3.00	6.0D
8	4.00	8.0D
9	5.00	10.0D
10	6.00	12.0D
11	6.50	13.0 D
12	7.00	14.0D
13	7.25	14.5D
14	7.50	15.0 D
15	7.75	15.5D

Granular material consisting of crushed stone with a median diameter of 38 mm was placed at the inlet and outlet of the culvert as shown in Figure 3.4. The granular material was graded at the culvert invert elevation for a distance of 1.0D upstream of the inlet and 3.0D downstream of the outlet. Further upstream and downstream of those points, the granular

material was graded to what would, in a prototype culvert installation, be the natural channel bed at the desired embedment depth (an embedded culvert is illustrated in Figure 2.3).

Figure 3.4: Looking downstream through the culvert. Granular material was placed at the inlet and outlet to represent a streambed.

In the final phase of the project, weir baffles were installed along the culvert invert. In their review of various baffle configurations, Ead et al. (2002) found that the weir baffle system provided equivalent results to more complex baffle arrangements, while being much simpler to install. As per the recommendations given in Rajaratnam and Katopodis (1990), a baffle height of 0.1D was used for this experiment. A baffle spacing of 476 mm, or just less than 1.0D, was selected to coincide with the corrugation interval, allowing the baffles to be placed in every seventh corrugation trough. Figure 3.5 shows the culvert with the baffles installed.

Figure 3.5: Baffles installed in the culvert.

3.2.2. ADV Operation

Velocity measurements were made using a SonTek 16 MHz 3-D acoustic Doppler velocimeter with a 50 Hz maximum sampling rate equipped with down-looking and up-looking probe heads. The ADV operates on the Doppler shift principle. As illustrated in Figure 3.6, pings of sound are emitted at the end of the probe stem which upon hitting particles in the flow are scattered or reflected back towards the probe. The inherent assumption in the operation of the ADV is that the velocity of the scattering particles is equal to the velocity of the fluid in which they are suspended. In order for this to be true the particles in the flow must have specific characteristics in terms of size, specific gravity and shape. Frequently, commercially prepared seeding material is used in studies involving acoustic Doppler velocimetry in order to ensure that the particles accurately represent the flow.

Data was collected using Horizon ADV, a software package supplied by SonTek with the ADV unit. At each measurement interval, the ADV records the velocity, signal strength (signal to noise ratio, or SNR), and the consistency of the measured velocity during the sampling period (correlation score, or COR) for each velocity component (x, y, z). This information is reported in real-time on the Horizon ADV output screen. For this experiment, the 50 Hz sampling rate, the highest possible for the ADV system being used, was selected.

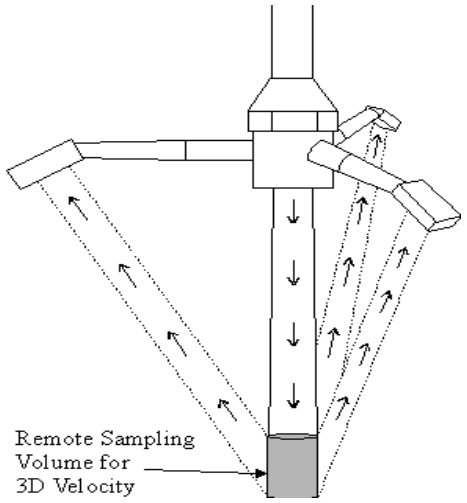

Figure 3.6: ADV sample point location with respect to probe (from http://www.SonTek.com\product\advm\advmxdsc.htm)

In order for the SonTek software to accurately calculate velocity, the speed of sound in the fluid must be known. This calculation relies on user-entered values of water temperature and salinity. For example, a five-degree temperature change, or 12 ppt change in salinity, would cause a one percent change in the speed of sound (SonTek, 2002). At the start of the experiment, the salinity of the water coming into the lab was measured using a HACH Sension 156 probe (pH, Conductivity, DO). The measured value of 0.2 ppt was considered to be typical of City of Saskatoon treated drinking water (confirmed by email to the City of Saskatoon utility department). At such low levels, even a doubling of salinity would not make a significant difference in the speed of sound. At the start of each day, or any time water was added to the flume, the temperature of the water was measured using a standard mercury lab thermometer (0.5°C measurement precision). When new water was added, the flume was allowed to run for at least 10 minutes to allow for mixing prior to taking the temperature or starting measurements. Additionally, when new water was added, the temperature was monitored as it would gradually increase with time until it attained room temperature.

The ADV is factory calibrated and requires no further lab calibration. It is accurate to +/-1% of the measured velocity, unless the probe is damaged. The system is equipped with a beam check operation, which allows the user to detect problems with the probe based on the return signal strength measured by the three receivers. Over the course of the experiment, the beam check was completed on approximately a weekly basis in order to confirm that the ADV was working properly.

One of the primary sources of error for both the ADV and the Pitot-static tube is likely the ability to accurately align the device with the direction of flow. In this case, a similar technique was used to align both instruments with the direction of flow. Textbook values for the maximum acceptable yaw angle for a Pitot-static tube are 12 to 20 degrees, which would produce errors of less than +/- 1.0% (Munson, Young, Okiishi, 1998). A similar value for the effect of yaw on ADV measured velocities was not found. As previously noted, the accuracy of the ADV measurements is considered to be +/- 1.0% of the measured velocity (SonTek, 2002).

The ADV sample volume is located 5 cm below the probe head and has a height of 5.6 mm. Since the probe head must be submerged during operation, the down-looking probe is

not capable of taking measurements within the top 5 cm of the flow (SonTek, 2002). At higher flow velocities, the inaccessible area near the water surface was found to be slightly greater than 5 cm due to the disturbance caused by the probe head. Within the upper portion of the flow area, the up-looking probe was utilized, which requires positioning the probe head 5 cm or more below the sample point location. In the case of some of the shallow flow depths, an area within the middle of the flow existed where measurements could not be taken with either probe (i.e., it was too shallow to position the down-looking probe 5 cm above, or the up-looking probe 5 cm below). The proximity of the sampling volume to the culvert boundary near the culvert sides and upper corners of the flow area was limited by the span of the ADV probe head (i.e., to avoid contact of the arms with the culvert wall), and the size of the opening in the culvert crown which constrained the maximum rotation angle of the ADV probe.

3.2.3. ADV Traverse System

The ADV probe was mounted on a traverse system consisting of two motors, one that adjusted the vertical position of the ADV and one that rotated it about a central pivot point. The traverse motors were controlled by LabVIEW software. By adjusting the vertical offset (mm from starting position) and rotation position (+/- degrees from vertical), the probe could be positioned throughout the majority of the flow cross section. Figure 3.7 illustrates the concept of this traverse system, with the dashed lines illustrating the type of measurement transects possible through the combination of rotation and vertical adjustment of the probe.

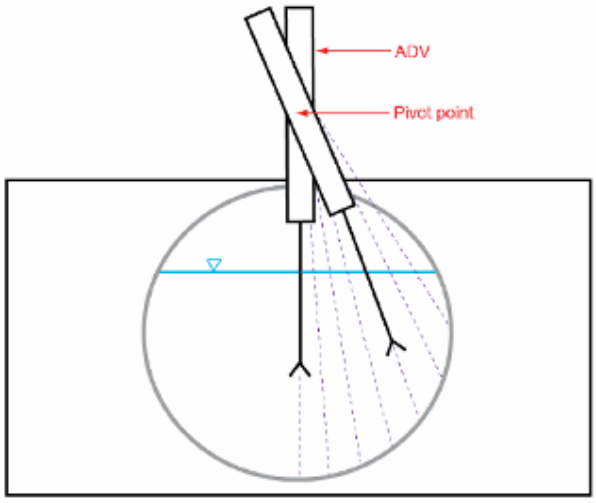

Figure 3.7: Schematic illustration of the ADV positioning system (T. Abbs, personal communication, 7 Feb. 2008).

The motorized traverse system was mounted on a trolley running on the flume rails, allowing it to be manually positioned at any longitudinal location along the length of the culvert. The trolley position was set using a tape measure fixed to the flume wall. A photograph of the traverse system and trolley is shown in Figure 3.8. The slope of the trolley was adjusted to correspond with the slope of the culvert using metal shims placed under the rear trolley supports. This adjustment ensured that the ADV probe was oriented perpendicular to the direction of flow for each culvert slope. In addition to longitudinal position, the trolley system also facilitated manual vertical and horizontal adjustments to the starting location of the motorized traverse system. Once the initial position was set, LabVIEW software was used to control the traverse motors to position the probe at the desired vertical position and rotation angle.

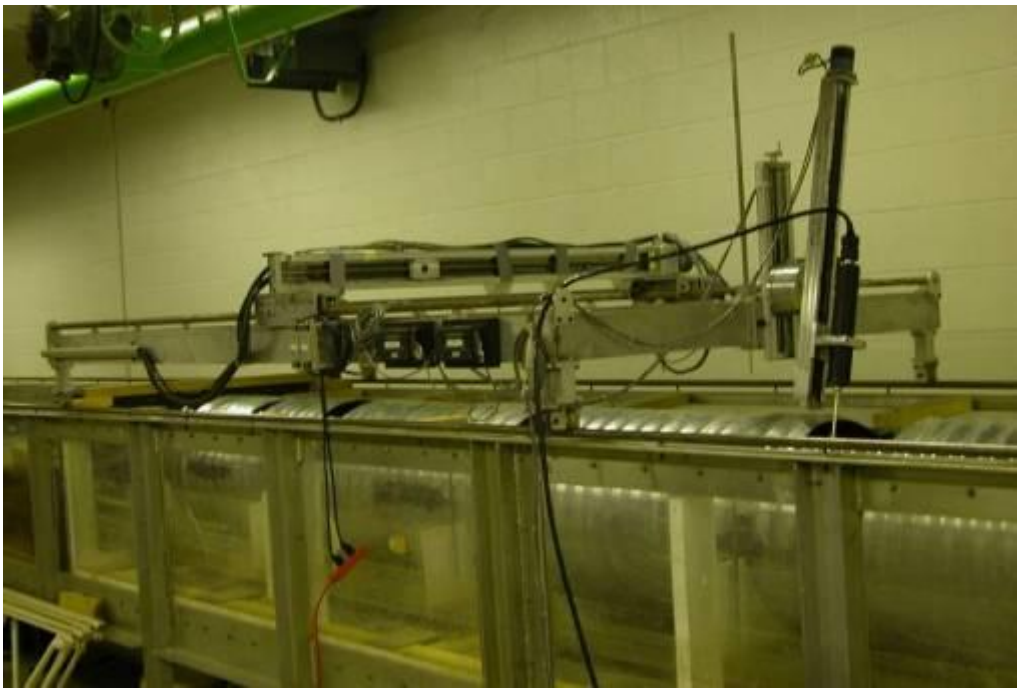

Figure 3.8: Photograph of the ADV positioning system mounted on the trolley.

3.3. Experiment Preparations

3.3.1. Magnetic Flow Meter Calibration

Flow through the flume used in this experimental program is measured with an in-line magnetic flow meter, which is located just downstream of the pump. The flow meter reports to a precision of 0.01 Volts, which translates to approximately the nearest 1.3 L/s (the relationship between flow and voltage is: $Q\ (m^3/s) = 0.0397\ V + 0.0009$). However, the meter fluctuates constantly and can be realistically only set to +/- 0.02 Volts, or +/-1.7 L/s.

Before starting the experimental program, the calibration of the magnetic flow meter was confirmed against the results of the last calibration which was completed in 2006. This was done by measuring the head over a rectangular sharp-crested weir installed in the flume as shown in Figure 3.9, over a range of discharges. The results of the testing correlated well with the results from the 2006 calibration and the established relationship between the voltage output from the magnetic flow meter and the pumping rate was used to calculate the discharge for this experimental program.

Figure 3.9: Photograph of flume calibration check using a rectangular weir installed in the flume just downstream from the culvert outlet.

3.3.2. Stillwater Profile

Water surface levels were measured at each access hole for each test condition. This measurement was taken using a manual point gauge (precision 0.2 mm) mounted on the flume rails. Prior to commencing the experimental program, a stillwater profile was measured over the

length of the culvert to locate any discrepancies in the point gauge measurements due to variability in the elevation of the trolley rails. The results, shown in Figure 3.10, indicated a variation of less than +/- 1.5 mm at all access hole locations. The results of the stillwater profile were used to adjust all measurements where rail height was a factor.

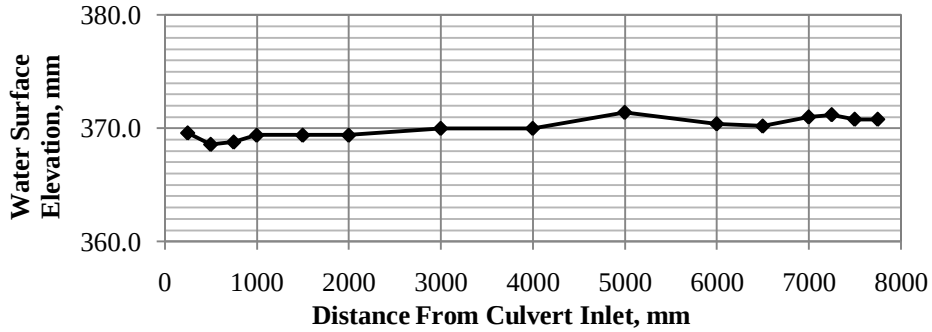

Figure 3.10: Stillwater profile measured to check the elevation of the flume rails.

3.3.3. ADV Calibration Confirmation

As a check on the ADV accuracy, comparison testing was carried out between velocities measured along the culvert centreline at Hole 9 (see Figure 3.3), with the down-looking ADV probe versus velocities measured with a Pitot-static tube connected to a manometer board. To do this, the Pitot-static tube was mounted on the ADV traverse and positioned at the same locations as the ADV probe head. For each test, the flow depth and discharge were adjusted and then the measurements were taken, first with the ADV and then the Pitot-static tube. The testing was conducted under various flow conditions at the 1% culvert slope producing point velocities of between 15 and 120 cm/s. In this research, the flow velocities measured with the ADV ranged from approximately 20 to 130 cm/s, approximately spanning the range of velocities tested against the Pitot-static tube.

The results of this comparison testing are shown in Figure 3.11 to Figure 3.14. On each figure, the Pitot-static tube velocity measurements are represented by a point and the ADV measurements are represented by two lines indicating the upper and lower confidence limits of the measurement series. Good correlation was found between the measured values for velocities up to approximately 90 to 100 cm/s. At higher velocities, there appeared to be a trend of the ADV reporting slightly lower velocities than measured with the Pitot-static tube. These results are similar to the findings reported by Gautam (2008) who, through similar experiments also

carried out at the University of Saskatchewan, found that at velocities greater than 60 cm/s point velocity measurements taken with a 3-D ADV were slightly less than the velocities measured with a Pitot-static tube in the upper part of the flow region. Gautam's experiment utilized a completely different 3-D SonTek ADV system, but the same Pitot-static tube as used in this experiment.

Collectively, when the ADV measured velocities are compared with those measured using the Pitot-static tube, a mean difference of -1.22 cm/s and a median difference of -1.10 cm/s is found. Of the 52 point velocities measured, the differences ranged from approximately -9 cm/s to +5 cm/s, with 20 points having a higher velocity when measured with the ADV and 32 points having a lower velocity when measured with the ADV. Based on these results, for the purposes of this research project the effect of any discrepancy is considered to be negligible.

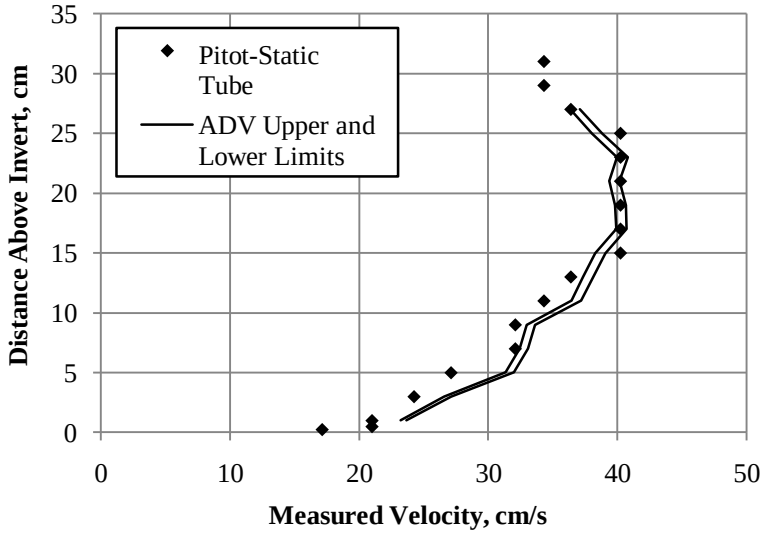

Figure 3.11: Correlation between velocity measurements taken with Pitot-static tube vs. the ADV for velocity range of approximately 25 to 40 cm/s.

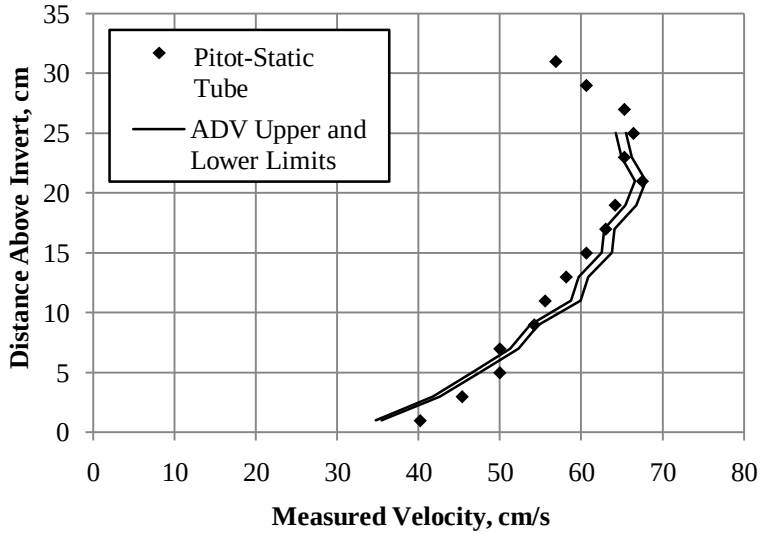

Figure 3.12: Correlation between velocity measurements taken with Pitot-static tube vs. the ADV for velocity range of approximately 40 to 65 cm/s.

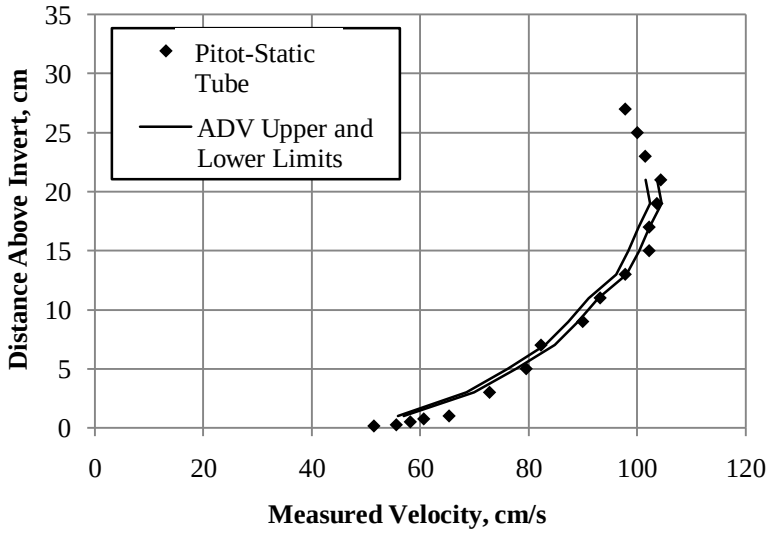

Figure 3.13: Correlation between velocity measurements taken with Pitot-static tube vs. the ADV for velocity range of approximately 50 to 100 cm/s.

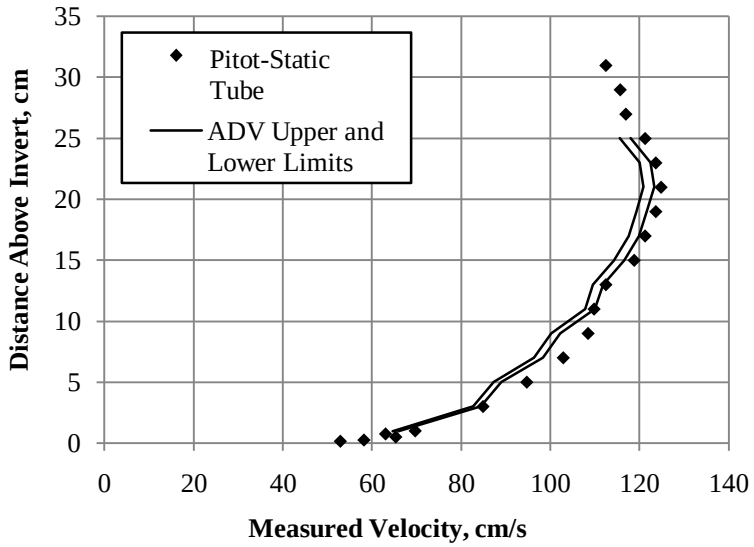

Figure 3.14: Correlation between velocity measurements taken with Pitot-static tube vs. the ADV for velocity range of approximately 60 to 120 cm/s.

3.3.4. Comparison between Up- and Down-Looking Probes

In addition to the Pitot-static tube testing, the up-looking and down-looking probes were tested to check for any discrepancy between the two probes. Similar to the Pitot-static tube tests, vertical profiles at the culvert centreline were completed under a variety of flow conditions to the limits of both the up- and down-looking probes (i.e., the top and bottom 5 cm were inaccessible to the down- and up-looking probes, respectively) at Hole 9. The results are shown in Figure 3.15 to Figure 3.18. The data from the up- and down-looking probes were collected at slightly offset vertical locations, so direct comparison between individual data points is not possible. However, the velocity profile plots show that the data between the two probes correlates well. Based on this information the data obtained with the two probes were considered to be equivalent.

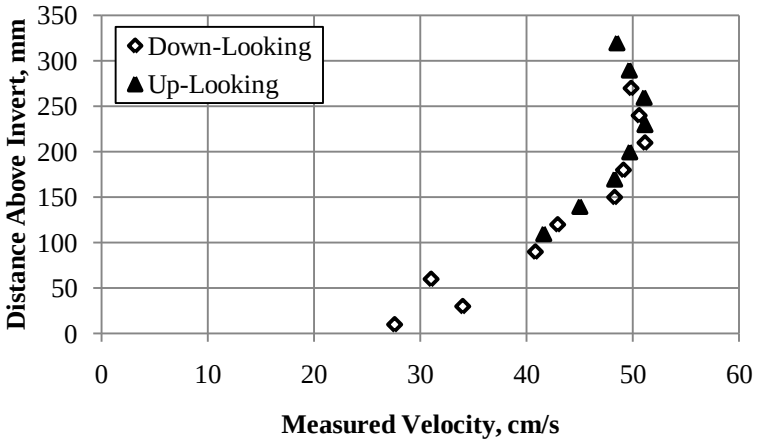

Figure 3.15: Correlation between velocity measurements taken with down and up-looking ADV probes for velocity range of approximately 40 to 50 cm/s.

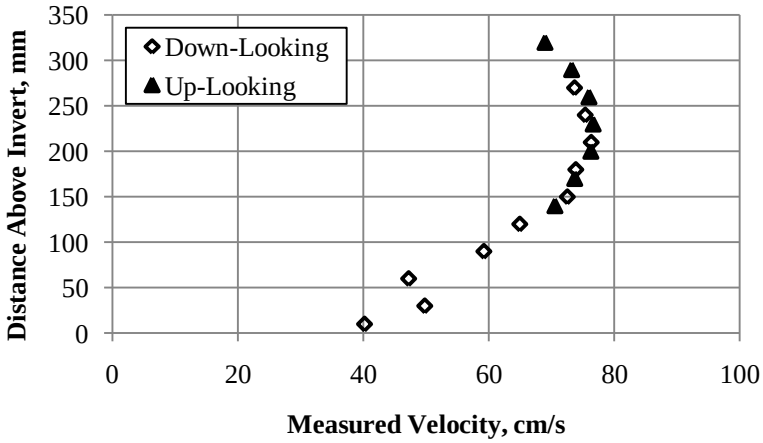

Figure 3.16: Correlation between velocity measurements taken with down and up-looking ADV probes for velocity range of approximately 70 to 80 cm/s.

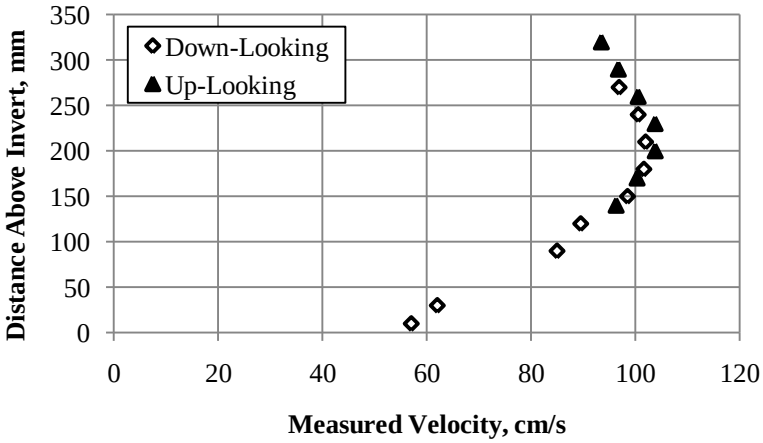

Figure 3.17: Correlation between velocity measurements taken with down and up-looking ADV probes for velocity range of approximately 90 to 105 cm/s.

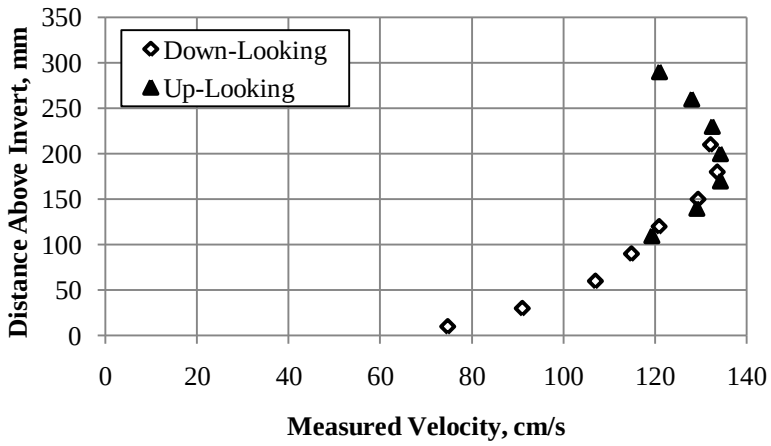

Figure 3.18: Correlation between velocity measurements taken with down and up-looking ADV probes for velocity range of approximately 120 to 135 cm/s.

3.3.5. Up-Looking Probe Orientation

The assignment of the x, y, and z axes to the receiver arms of the ADV is part of the factory calibration and cannot be adjusted. The up-looking probe head is oriented such that, to obtain a positive x-direction velocity, the probe stem must be located directly upstream of the receiver. Obviously, the probe cannot be operated this way because the sample volume is heavily disrupted by the upstream interference from the probe stem. In order to work around this, for the testing at the 0.4% slope, which was the first slope tested, the up-looking probe was oriented with the probe stem downstream of the receiver head resulting in negative x-velocities (these were then converted to positive numbers during data processing).

Subsequent to the completion of the 0.4% slope testing, it was discovered through consultation with SonTek that the manufacturer recommends that the up-looking probe be oriented sideways in the flow, such that the stem is located off to the side of the probe head. In this configuration, the x- and y-direction velocities are interchanged. Although not noted in the ADV operating manual, this configuration is recommended to avoid any backwatering effect from the stem that may alter the flow velocity at the measurement point.

In order to test for any discrepancy caused by the streamwise probe orientation used for the 0.4% culvert slope data collection, the up-looking probe was tested in both orientations over the range of velocities that had been measured. The position of the sideways oriented probe was adjusted such that the measurement location was the same as when the probe was in the

streamwise orientation. The results, shown in Figure 3.19 and Figure 3.20, showed little deviation between the two orientations, with differences ranging from +1.8 cm/s to -1.7 cm/s with a mean difference of 0.6 cm/s. Nevertheless, for the testing conducted at the 1.0% culvert slope, the sideways orientation for the up-looking probe was adopted based on the manufacturer's recommendation.

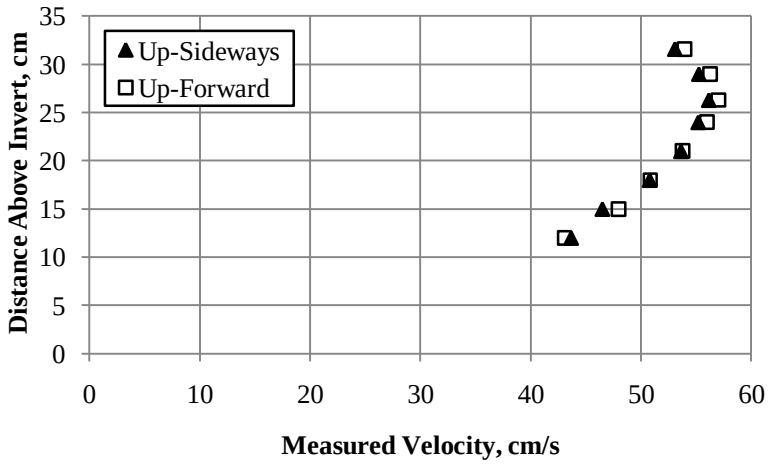

Figure 3.19: Correlation between velocity measurements taken with up-looking ADV probe oriented sideways to the flow and streamwise to the flow, for velocity range of approximately 40 to 60 cm/s.

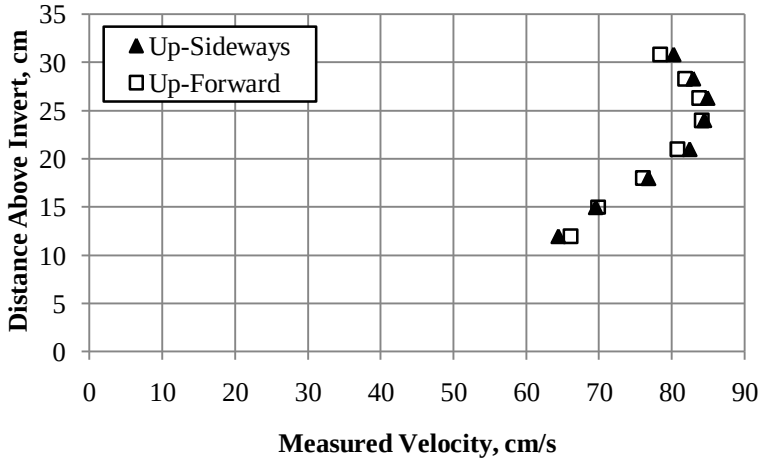

Figure 3.20: Correlation between velocity measurements taken with up-looking ADV probe oriented sideways to the flow and streamwise to the flow, for velocity range of approximately 60 to 85 cm/s.

3.4. Data Collection

3.4.1. Locations for Data Collection

For each configuration of the plain invert culvert, four centreline vertical velocity profiles and five velocity cross sections were collected at locations along the pipe length as indicated in Table 3.2. Measurements of the water surface elevation were taken at all access holes.

Table 3.2: Types and locations of experimental measurements.

Access Hole #	Location (metres D/S from inlet)	Measurements
1, 2, 4, 8, 14	0.25, 0.5, 1.0, 4.0, 7.5	Cross section, Flow depth
6, 7, 9, 11	2.0, 3.0, 5.0 6.5	C/L profile, Flow depth
3, 5, 10, 12, 13, 15	0.75, 1.5, 6.0, 7.0, 7.25, 7.75	Flow depth

For the testing with the baffled invert, velocity data were collected over one baffle spacing through the access hole located 10D (5 m) downstream from the culvert inlet (hole #9). This location was selected based on the assumption that it would be in the region of fully-developed flow. Cross sections were collected at 0.25L upstream of the baffle, at the baffle, and at 0.25L and 0.50L downstream of the baffle, where L is the baffle spacing, in this case 476 mm.

For each cross section, the ADV traverse was used to rotate the probe between 0° and 21° (in both positive and negative directions) and point velocity measurements were taken at various vertical locations at selected rotations (e.g. at a 5° rotation velocity measurements were located at: 18 mm, 33 mm, 58 mm, 88 mm… etc. offsets from the culvert wall). At the centreline, the lowest measurement point was located 10 mm above the culvert invert. Although the ADV operation manual suggests that velocity can be measured as close as 1 mm from a solid boundary, 10 mm was selected as a practical limit in order to help ensure that the ADV probe was not damaged from any inadvertent contact with the culvert wall. Once the probe was rotated out of the vertical position, the proximity of the lowest measurement point became limited by the probe arms, which had to be kept a safe distance from the culvert wall in order to prevent damage from accidental impact.

Figure 3.21 illustrates the layout of the velocity measurement sampling grid for a theoretical maximum flow area. The density of the sample points near the culvert boundary was

slightly greater than the density through the core of the flow area, in order to better capture the steeper velocity gradient that occurs in the near-boundary region. The exact locations of the sample points nearest the water surface were adjusted slightly to suit each specific cross section so that the entire depth of flow was covered. The total number of sample points for each cross section varied from 46 to 167 depending on the depth of flow. For smaller flow areas, the grid shown in Figure 3.21 was truncated to encompass only the actual flow area.

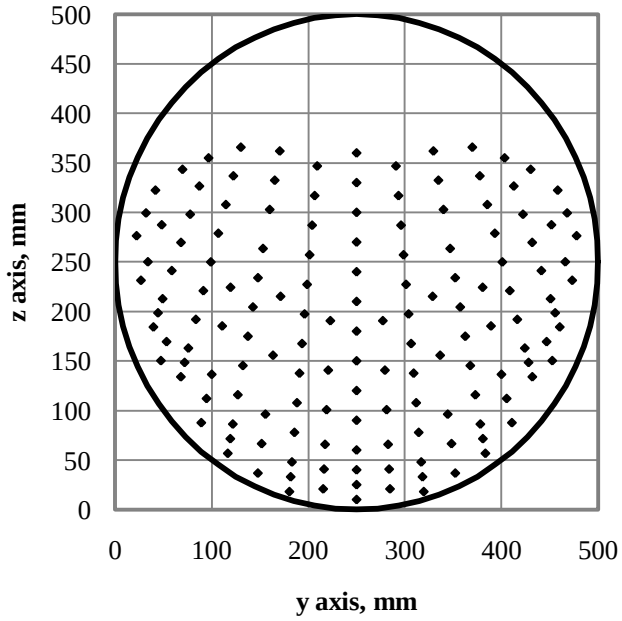

Figure 3.21: ADV sample point grid for velocity cross sections.

In the first part of the study, where the model culvert was set at a slope of 0.4%, velocity measurements were taken throughout the entire cross section (i.e., at as many of the points shown in Figure 3.21 as would fit within the flow area). Using this approach it was found that the data collection requirements of the project were very time consuming due to the large number of samples required for each cross section. In analyzing the 0.4% slope data set, a high degree of symmetry was observed in the results. Therefore, it was decided to investigate what the impact of sampling only half (i.e., one side plus the points on the centreline) of each cross section would have been. A data subset, consisting of nine cross sections, was selected as indicated in Table 3.3. For each of the cross-sections, the side of the cross section (RS or LS) used for the symmetry analysis was alternated. The data set used for this analysis did not include the data from the up-looking probe, as those data were not available at the time.

Table 3.3: Summary of locations and sides used for cross section symmetry check.

Cross Section #	Discharge (L/s)	Embedment	Access Hole #	Location (m D/S from Inlet)	Side Used for Symmetry
1	50	0D	1	0.25	RS
2			8	4.00	LS
3			14	7.50	RS
4	70	0.1D	1	0.25	LS
5			8	4.00	RS
6			14	7.50	LS
7	90	0.2D	1	0.25	RS
8			8	4.00	LS
9			14	7.50	RS

The effect of using only half of the data set was analyzed by comparing the discharge calculated through velocity-area integration of contour plots of the measured velocity data to the measured discharge from the magnetic flow meter. The details of the procedures used to complete the velocity area integration are discussed in detail in Section 3.5. While the velocity-area integration was intended to provide a quantitative comparison of the results, a visual assessment of the contour plots was also conducted as a qualitative evaluation of the symmetry of the plots in terms of contour shape and size.

For each cross section, the discharge calculated based on velocity-area integration using half the data set, as well as the complete data set, were compared in terms of the percent error from the discharge measured using the magnetic flow meter. The two error values for each cross section were then compared to determine if the results based on using only half the data set had improved or worsened the result. The results of this comparison are shown in Figure 3.22. In this figure a positive number indicates the error decreased and a negative number indicates the error increased. Four of the cross-sections created using half of the data set improved the results of the velocity-area integration, while five caused a decrease in accuracy. The maximum improvement in accuracy was 1.9% and the maximum decrease in accuracy was 1.4%. Two of the five cross sections created using the right hand side of the data set, and two of the four cross sections created using the left hand side of the data set, resulted in increased accuracy. Therefore, there was no clear trend of one side producing more accurate results than the other.

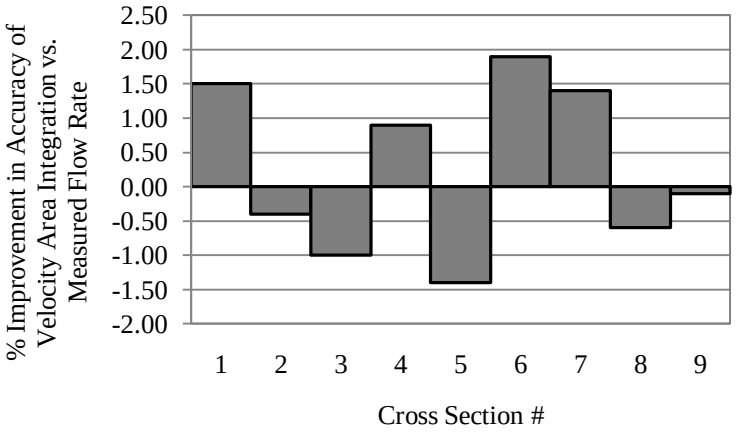

Figure 3.22: Bar chart showing the percent improvement in the accuracy of the velocity-area integration results (vs. measured discharge) based on using data from half the cross section, compared to the results based on data from entire cross section. Cross section numbers refer to listing in Table 3.3.

In terms of the visual symmetry assessment, some examples of the contour plots produced using the complete data sets are shown in Figure 3.23 and Figure 3.24. All of the plots showed similar patterns of velocity and turbulence intensity on either side of centreline. Figure 3.23(a) shows the velocity contour cross section plot that had the highest level of symmetry, while Figure 3.23(b) shows the velocity contour cross section plot that had the lowest level of symmetry. Similarly, Figure 3.24(a) and (b) show the turbulence intensity contour plots that were found to have the highest and lowest levels of symmetry, respectively. As can be seen here, the general finding of the visual assessment was that even the most asymmetrical contour plots have a relatively high degree of symmetry.

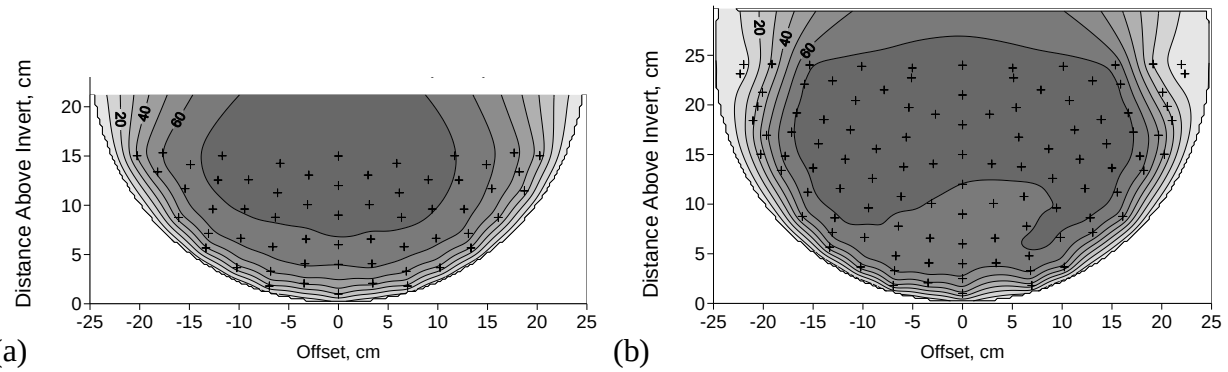

Figure 3.23: (a) Velocity cross section that showed the greatest symmetry, (b) velocity cross section that showed the least symmetry (based on data available when symmetry analysis was undertaken). Contours are in units of cm/s.

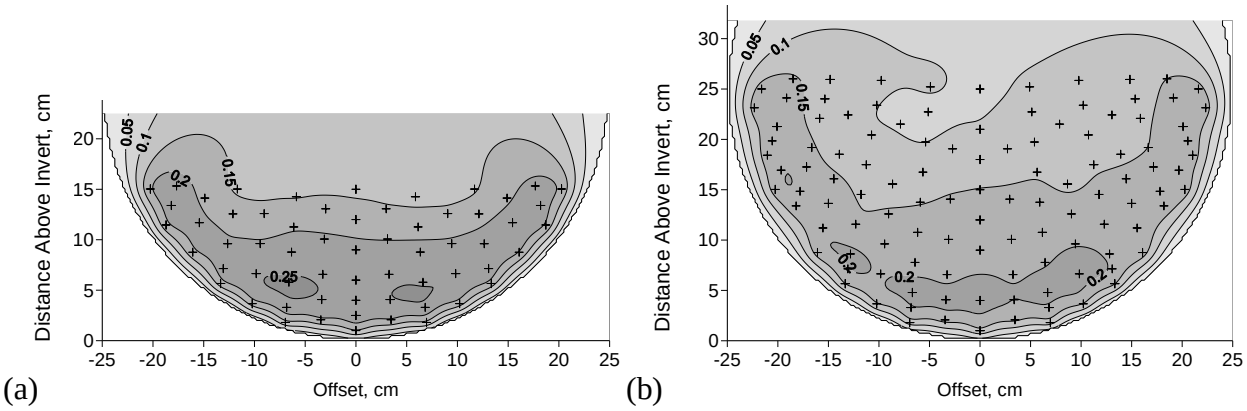

Figure 3.24: (a) Turbulence intensity cross section that showed the greatest symmetry, (b) turbulence intensity cross section that showed the least symmetry (based on data available when symmetry analysis was undertaken).

Based on this assessment, the effect of sampling only along the centreline plus one side of the cross section, and assuming symmetry, was not expected to be significant. However, the time savings afforded by the reduced sampling were considerable. Therefore, for the components of the model study completed at a 1.0% culvert slope, as well as with the baffled invert, data was only collected along the centreline and one side of the cross section. In terms of which side of the cross section to sample, the results of the symmetry analysis showed no clear trend that favoured one side over the other. It was decided, based on ease of operation of the equipment, to collect data on the right hand side of the cross section.

3.4.2. Sample Time

The duration of point velocity sampling with an ADV is key to ensuring the collection of sufficient data to accurately determine the mean point velocity and turbulence level. Where data quality (defined by the signal to noise ratio and correlation score of each sample) is weak, a longer sampling duration is advantageous, as it increases the number of data points that may meet whatever filter criteria are being used and therefore be available for use in calculating the mean velocity and variation in instantaneous velocity. In previous research completed with ADVs at the University of Saskatchewan, the data quality was noted to diminish significantly near the culvert boundary, while during the same testing session, much better data quality was generally found at sample point locations closer to the core of the flow area. In the study outlined by Abbs et al. (2007), a consistent ADV sample time of 10 minutes was used for all sample points, regardless of data quality. In comparison, for very similar research projects, Magura (2008) and Richmond et al. (2007) used consistent ADV sample times of just 40 s and 80 s, respectively.

Prior to commencing data collection, the use of a variable sampling duration, to account for the variability in data quality through the cross section, was explored. Data were collected at various distances above the culvert invert at the centreline. The data were filtered (using WinADV software) based on criteria of signal to noise ratio (SNR) greater than 15 and correlation score (COR) greater than 70 (data analysis is more thoroughly discussed in Section 3.5). The data set was then truncated at various lengths of time and the statistics for each data sub-set were calculated. The resulting velocity analysis, shown in Table 3.4, confirmed that the mean streamwise velocity takes slightly longer to stabilize at locations closer to the boundary.

A similar analyisis, using the same data set as the velocity analysis, was conducted to investigate the effect of sample time on the root mean square (RMS) of the series of instantaneous velocity measurements and therefore on the calculated turbulence intensity values. These results, shown in Table 3.5, are less clear than those for velocity, but appear to indicate that at points closer to the invert, the RMS (and therefore the calculated turbulence intensity) is slightly reduced with longer sampling times. For the sample points located greater than 15 cm away from the invert, the longer sampling time appears to slightly increase the RMS value.

However, for sample times greater than two minutes, the change in RMS compared to the results obtained after 10 minutes of sampling was less than 0.3 cm/s for all measurements.

Table 3.4: Summary of impact of sample time on streamwise velocity measurements.

Distance Above Culvert Invert, cm	Variation from 10 Minute Result, cm/s				Velocity at 10 minutes, cm/s	ADV Accuracy*, cm/s
	Sample Time, min					
	1	2	5	8		
1	-1.0	0.6	0.5	0.3	35.5	+/- 0.4
3	0.4	-0.7	-0.5	0.0	41.4	+/- 0.4
6	2.3	0.9	0.2	0.4	46.4	+/- 0.5
8	1.2	0.9	0.1	0.1	58.0	+/- 0.6
11	0.1	0.2	-0.1	0.0	71.4	+/- 0.7
15	0.0	0.3	0.1	0.0	80.7	+/- 0.8
19	0.7	-0.2	0.0	0.0	87.0	+/- 0.9
23	0.2	-0.3	-0.1	0.0	85.0	+/- 0.9

*Based on SonTek's stated accuracy of 1% of the measured velocity.

Note: Shaded squares indicate measurements that were within the accuracy range of the ADV when compared to the mean velocity measured after 10 minutes.

Table 3.5: Summary of impact of ADV sample time on RMS velocity values.

Distance Above Culvert Invert, cm	Sample Time, min				
	1	2	5	8	10
	RMS, cm/s				
1	11.7	11.9	11.5	11.6	11.6
3	12.4	12.1	12.2	11.9	11.9
6	11.1	11.2	11.1	11.1	11.1
8	10.4	10.7	10.6	10.6	10.4
11	9.0	8.7	8.7	8.7	8.6
15	6.0	6.0	6.1	6.2	6.3
19	3.8	4.1	4.1	4.2	4.2
23	3.8	4.2	4.3	4.3	4.3

Based on the above analyses, a variable sample time of 2, 5, or 10 minutes was used for this research. Generally, samples within the core of the flow area exhibited good signal to noise ratios and correlation scores, and stable velocities. At these points, data was collected for two minutes. A maximum sample time of 10 minutes was used for sample points near the culvert boundary, and for those that exhibited weak SNR and COR scores. A five-minute sampling

duration was used for intermediate quality points. As the data collection system was not automated, the decision on sample time was made during data collection based on real-time observation of the data quality in terms of SNR and COR.

3.5. Data Analysis

3.5.1. Data Processing

Once the ADV data was collected the raw ADV output files were processed using WinADV, a program developed and maintained by the United States Bureau of Reclamation for manipulating and analyzing ADV data. WinADV allows the user to view, filter and transform data contained in the .ADV files created by SonTek's Horizon ADV data collection software. The output produced by WinADV contains the summary statistics and pertinent information calculated from the filtered data set. Examples of the information output from WinADV include the sample time, number of samples that passed the user-specified filter criteria, mean value and RMS of the velocity components (x,y,z), average SNR/COR values over the sample period, as well as information pertaining to the ADV settings during data collection. For this project, WinADV was used to filter the instantaneous velocity data, extracting only measurements with a signal to noise ratio and correlation score greater than a specified value, and to eliminate velocity spikes. For data collected with the probe positioned on an angle, WinADV was also used to rotate the data to align it with the centreline coordinate system.

The signal to noise ratio is used to assess the strength of the received acoustic signal versus the ambient electronic noise level of the ADV instrument (SonTek, 2002). Where the water is very clear and there is little signal scattering, the return signal received by the ADV is very weak and the SNR is low. Where there is considerable particulate matter in the flow, the resulting signal strength, and therefore SNR, is high. Wahl (2000) recommends a minimum SNR of 15 for instantaneous velocity measurements and turbulence analysis and SonTek (2002) recommends a minimum SNR of 15 when sampling at 25 Hz or faster.

The correlation score is used to assess the consistency of the series of velocity measurements that are contained within each sampling interval (Wahl, 2000). For this experiment the ADV was set to record data at 50 Hz (the maximum frequency for the instrument used), however the ADV actually sends and receives acoustic "pings" at a faster rate (SonTek,

2002). As such, each 50 Hz velocity measurement is actually an average of a larger data set which the operator does not see and which is not recorded. The correlation score is reported as a percentage, with 100% indicating a completely consistent signal (SonTek, 2002). SonTek guidelines suggest that COR values should ideally be greater than 70%, however values as low as 30% can be used in some circumstances where the SNR is high and the flow is turbulent (Wahl, 2000; SonTek, 2002).

For this project, filter criteria consisting of a signal to noise ratio greater than 15 and correlation score greater than 70% were applied to all of the data collected. These values are noted by the software developer as being benchmarks for good data (Wahl, 2000) and are in keeping with previous work completed at the U of S (Abbs et al. 2007). These filter criteria have also been used by other researchers who have published work involving data collected with an ADV (e.g. Smith et al., 2005; and Smith et al., 2006).

In conducting these experiments, it was found that as long as the SNR was above 15 the COR was always above 70%. Fresh water from the city water supply has insufficient scattering material in the flow to achieve a SNR greater than 15. Because the experimental set-up included gravel that contained clay/silt residue, some particulate matter was introduced into the flow. By periodically stirring the gravel and sweeping along the bottom of the flume it was possible to keep enough particles in suspension to maintain the SNR above the minimum value. Towards the end of the experiment, when the flume had been drained and re-filled several times, washing away the majority of this fine sediment, a small amount of bentonite clay was added to the flume to improve the signal quality when required.

Inherent in the use of the ADV is the assumption that the scattering particles are moving at the same speed as the fluid which is carrying them. According to Agelinchaab and Tachie (2006), assuming a particle moves exactly with the flow is a sound assumption where the settling velocity of the particles is small compared to the measured velocity and sampling rate. Although Agelinchaab and Tachie's reference pertains to a study completed using particle image velocimetry, it stands to reason that the same concept applies to work utilizing acoustic Doppler velocimetry. Ideally the reflecting particles in an acoustic Doppler velocimetry study should be spherical, have a small diameter and have a specific gravity close to one. As this was not the

case for the particles in this study (i.e. silt/clay) this may have introduced some error into the flow measurements obtained.

The third WinADV filter criteria which was used was the spike detection filter. As mentioned previously, the ADV measures the velocity of the flow based on the phase difference between emitted and received acoustic signals. In situations where the flow velocity is close to the upper limit of the user-specified velocity range, the probe will occasionally report erroneous negative velocities (Wahl, 2000). The velocity is incorrectly interpreted by the ADV because when the phase difference is greater than 180° the probe cannot distinguish between positive and negative velocities (Wahl, 2000). WinADV uses a velocity spike filter based on work done by Goring and Nikora (2002), which is recommended for removing the negative velocities produced by short-duration velocity spikes.

3.5.2. Calculation of Turbulence Intensity

The WinADV program outputs RMS velocity values for each direction of flow (x, y and z) as well as two RMS values for the combined x, y and z axis velocity data. The first combined value is the vector sum of the magnitudes of the RMS of each of the individual velocity components (i.e., $\sqrt{RMSv_x^2+RMSv_y^2+RMSv_z^2}$). The second value is the RMS of the series of instantaneous combined velocity magnitudes (i.e., RMS (v_1, v_2, v_3...v_n)). For this study the first RMS value has been used.

In this research, the velocity fluctuations have been expressed in terms of turbulence intensity, which is generally defined as the RMS of the instantaneous velocity measurements at a point in the flow divided by the mean velocity over the measurement period at the same measurement point (e.g. Enders et al., 2003), as described in Section 2.2.4. However, for the purposes of this study, turbulence intensity has been computed as:

$$I_{mag}=\frac{RMSv_xv_yv_z}{V_{aveYn}}, \tag{3.1}$$

where I_{mag} is the calculated turbulence intensity and V_{aveYn} is the mean velocity of the flow based on normal depth for each combination of culvert slope and discharge. The same divisor (i.e. V_{aveYn}) was used to calculated turbulence intensity for both embedded and non-embedded

tests. This approach allows for direct comparison of the turbulence levels between points, as well as between different cross sections and for various embedment conditions.

3.5.3. Data Plotting and Analysis

The resulting velocity and turbulence intensity data was input into a program called Surfer 8 (Golden Software) to create contour plots and conduct data analysis on the aggregate data set for each cross section.

To produce the contour plots Sufer 8 creates a grid of evenly spaced interpolated data points throughout the cross section area based on the measured data. For this study, the multiquadric radial basis interpolation function was selected in Surfer 8 to produce the data grid. Radial basis functions are exact interpolators, that is, the interpolated surface honours all data points (Palaseanu and Pearlstine, 2008). The multiquadric method was developed to interpolate between measured elevations to produce topographic maps (Carlson and Foley, 1991). Franke (1982) documented a comprehensive review of available methods for scattered data interpolation. Franke compared the results of the various methods based on factors such as: accuracy in producing a known surface, visual appearance, sensitivity and computational effort. Based on his testing, Franke concluded that the multiquadric radial basis interpolation method provided consistent and often the most accurate results of all the methods tested. Likely in light of findings such as these, the multiquadric method is recommended by the creators of the Surfer 8 program as possibly the best choice of the radial basis methods available in the program (Golden Software Inc., 2002). Carlson and Foley (1992) included the multiquadric method in their assessment of radial basis methods used to specifically interpolate between track data (i.e., data that has been collected along tracks as opposed to scattered data points). Carlson and Foley (1992) concluded that the multiquadric method is effective in interpolating track data and generally resulted in smaller RMS errors than other methods tested.

Beyond the work of Franke (1982), the literature reflects many subsequent studies into various applications of the multiquadric function, as well as much consideration of the best method of selecting the smoothing parameter, called R^2 (not related to the statistical R^2), which is a required input for the calculation. In terms of visual effect, the sharpness of the contours increases as the R^2 parameter is decreased, whereas they become flatter as the R^2 parameter is

increased (Palaseanu and Pearlstine, 2008). Although there has never been any agreement on the best method of determining R^2, traditionally it has been calculated based on a combination of the number of data points, data point spacing, or the size and dimensions of the data set (Carlson and Foley, 1991).

Surfer 8 calculates a default value of R^2 via:

$$R^2 = \frac{(\text{length of the diagonal of the data extent}) \times 2}{(25 \times \#\text{ of Data Points})}, \tag{3.2}$$

which the program uses in the calculation of the interpolated data grid (Golden Software Inc., 2002). Other values of R^2 were tested (the user has the option to manually enter an R^2 value for the cross section), but it was found that the default R^2 value calculated by Surfer 8 produced acceptable results. Smaller R^2 values produced little change in the appearance of the plots and no advantage was found to using a larger R^2 value (i.e., processing times were acceptable). Therefore, it was decided to utilize the Surfer 8 calculated value.

In addition to producing the contour plots, Surfer 8 also allows the user to conduct queries to determine the portion of the mapped area less than or greater than a specified contour value. Using this function, quantitative information on the velocity and turbulence intensity was extracted from the contour plots.

In addition to the plotting and analysis completed with the Surfer 8 software, water surface profiles and centreline velocity and turbulence intensity profiles were plotted in Excel for each test.

3.5.4. Assumption Regarding Conditions at the Culvert Boundary

The point velocity measurements nearest the culvert boundary were located approximately 1 cm from the boundary. Initially, it was planned to add artificial data points at the culvert boundary with a zero velocity value in order to reflect the no-slip boundary condition. However, observing the plots produced by Surfer 8 when these artificial data points were included, it was apparent that the software was not able to correctly interpolate between the zero velocity boundary condition and the nearest measured data points, producing wider contour spacing than actually exists in this area and under-estimating the velocity gradient in the

near-boundary region. Conversely, when these zero velocity points were not included, Surfer 8 predicts near boundary values similar to the closest data point. The overall effect is that these plots produce an overestimate of the discharge calculated through velocity-area integration, because the very low velocities near the culvert wall are not accounted for.

Theoretically, with zero velocity at the boundary there is also zero turbulence intensity, and the same procedure (i.e., an inferred zero boundary condition) could also be applied to the analysis of turbulence intensity. However, in many cross sections, the measurement points near the boundary showed the highest turbulence intensities in the entire cross section. With the inclusion of a zero boundary condition, Surfer 8 indicated a swath of low turbulence intensity adjacent to the culvert boundary. Therefore, using a zero boundary condition resulted in a misleading representation of the true turbulence intensity conditions in the near boundary region.

Considering these findings, a zero velocity and zero turbulence intensity boundary were not applied and only the measured data points were used in generating the contour plots. In the context of fish passage, the results presented are therefore a slightly conservative estimate of the actual velocity and turbulence conditions very near the culvert boundary, as they are higher than the values that theoretically exist in that region.

4. PRESENTATION, ANALYSIS AND DISCUSSION OF RESULTS

4.1. Introduction

This Chapter begins with analysis and discussion of the quality of the data set collected for this research project. The presentation and discussion of the results are then separated into analysis and discussion of the plain invert and baffled invert data sets. Each of these components of the study are discussed in terms of the longitudinal water surface profiles, centreline vertical velocity profiles and velocity cross sections for both the non-embedded and embedded conditions, followed by a discussion of the results of the turbulence analysis. Additionally a brief interpretation of the results in the context of fish passage, based on information on fish behaviour and preferences found in the published literature, has been included where possible.

4.2. Data Quality

In order to establish confidence in the data collected with the ADV, and to provide a foundation for further analysis, it was decided that an evaluation of the data quality was required. In order to do this a comparison was made between the discharge measured with the magnetic flow meter (Q) and the discharge calculated through velocity-area integration (Q_{int}) of the contour plot for each cross section viz:

$$\% \text{ Error } Q_{int} = \frac{(Q_{int} - Q)}{Q} \times 100 \tag{4.1}$$

Each cross section area was integrated at a 0.05 m/s interval. Tables containing a summary of the cross section details, as well as the corresponding value of Q_{int} and the percent error of Q_{int}, are located in Appendix B. For the 0.4% slope, the percent error of Q_{int} ranged from +0.5% to +10.5% with an average value of +5.3%. For the 1.0% slope, the percent error of Q_{int} ranged from -11.2% to +7.8% with an average value of -0.9%. For the 1.0% slope with baffled invert, the percent error of Q_{int} ranged from -5.0% to 0.8% with an average value of -3.1%. Figure 4.1 illustrates the breakdown of the error analysis for all 102 cross sections that were included in the experimental program (both culvert slopes, non-embedded, 0.1 and 0.2D embedments and both the plain and baffled invert). Overall, the results are distributed between +/-10%, with 69 cross sections having a positive value of percent error of Q_{int} and 33 cross sections having a negative value. The overall average error in all the cross sections is +1.7%.

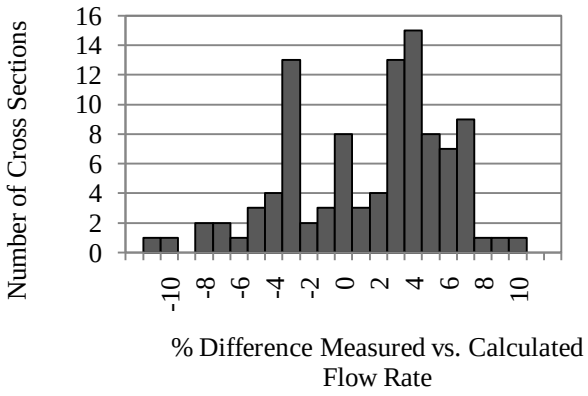

Figure 4.1: Breakdown of the percent error in Q_{int} relative to the discharge measured with the magnetic flow meter for the complete set of 102 cross sections that were sampled.

A complete set of streamwise velocity contour plots is contained in Appendix A. All plots are displayed with a contour interval of 0.1 m/s and have been left unshaded for visual clarity. Point velocity measurement locations are indicated on each cross section with '+' symbols.

The velocity-area integration results found in this study are similar to those obtained by other researchers. For example, in a very similar experiment Magura (2008) reported an error range of -10.2% to 2.8% with an average of 4.1%. Of Magura's 78 cross sections, 76 yielded velocity-area integration results that were less than the laboratory measured discharge (i.e., had negative values of % Error Q_{int}). Also reporting on a similar style of experiment, Barber and Downs (1996) experienced a range of errors between calculated and measured discharge from -9% to +22% for 51 cross sections, with the results being approximately evenly split between positive and negative values. Therefore, for the purposes of this research, an overall accuracy range of approximately +/-10% is considered reasonable.

4.3. Water Surface Profiles

The depth of flow in the model culvert was measured at 17 locations for each test: at the inlet, at each of the 15 access holes identified in Table 3.1, and at the outlet. At the culvert outlet the depth of flow was set to equal the normal depth in the culvert for that particular scenario (or, for the embedded tests, the normal depth plus the embedment depth). A complete set of water surface profiles can be found in Appendix C. The focus of this section is the interpretation of these water surface profiles in order to make some basic observations on the development of

flow through the culvert, as well as the effect of embedment on the flow conditions through comparison with the profiles generated in the non-embedded tests.

For all tests, a noticeable flow contraction and subsequent expansion and fluctuation of the water surface was observed for some distance downstream from the culvert inlet. An example of the typical inlet contraction observed is shown in Figure 4.2. Rajaratnam et al. (1991) termed the section of culvert near the inlet, where the contraction and expansion occurs, the "near-field entrance region" and analyzed flow development in this area for supercritical flow in a circular pipe flowing partially full, both in terms of flow depth and centreline velocity profiles as described in Section 2.2.1.

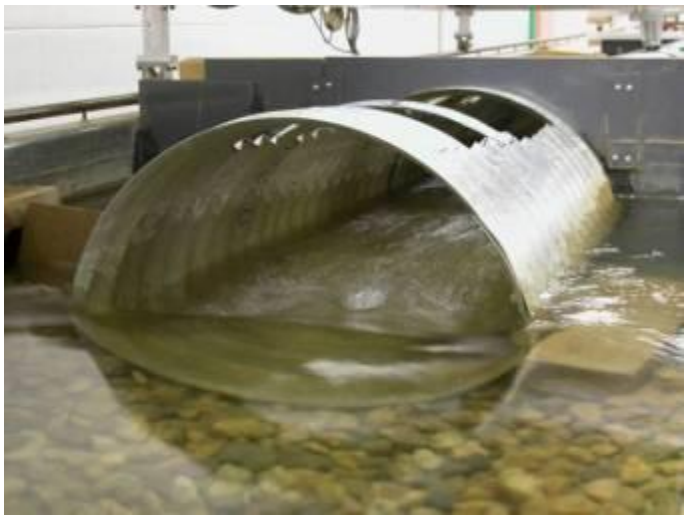

Figure 4.2: Example of typical flow contraction that occurred at the culvert inlet.

The water surface profiles from the inlet to the longitudinal mid-point of the culvert for the non-embedded tests at the 0.4% and 1.0% culvert slopes are shown in Figure 4.3 and Figure 4.4, respectively. All profiles show the characteristic wave produced downstream from the contraction, with the amplitude of the wave increasing with discharge and culvert slope, as described by Rajaratnam et al. (1991). Because the flow depth measurements in this experiment were limited to relatively long intervals in this region of quickly changing flow conditions, the measurements may not have captured the absolute crest and peak of the near-field wave described by Rajaratnam et al. (1991). As such, the true wavelength and amplitude could not be accurately determined.

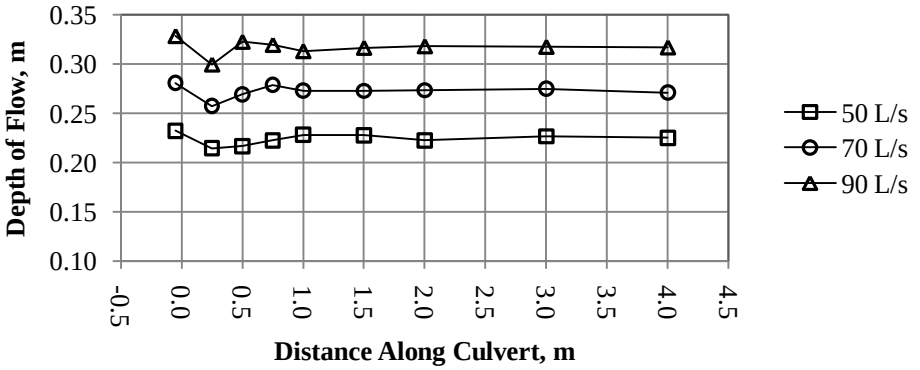

Figure 4.3: Near-field entrance region for 0.4% culvert slope, non-embedded tests.

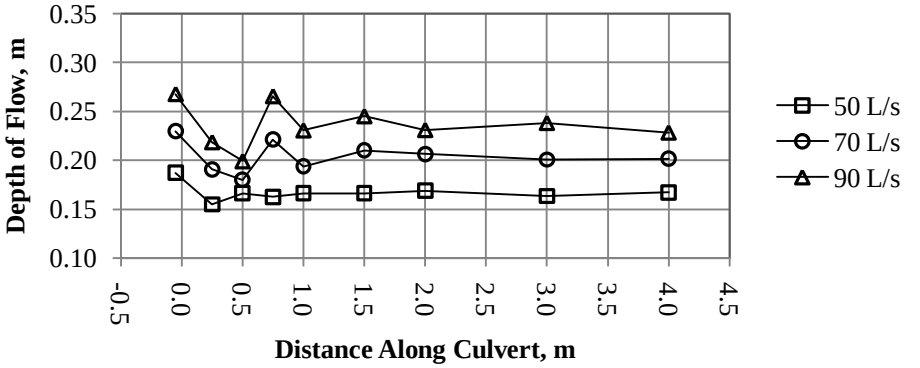

Figure 4.4: Near-field entrance region for 1.0% culvert slope, non-embedded tests.

Observing the flow development along the culvert length, it was found that the non-embedded tests generally stabilized at or slightly above normal depth, within a distance of approximately 4D to 8D (2 to 4 m) downstream from the inlet. This suggests that the flow was approaching a fully-developed condition at this point, which is in general agreement with the findings of Magura (2008). Figure 4.5 shows the water surface profiles for the non-embedded 0.4% culvert slope tests, illustrating the typical flow depth evolution that occurred through the non-embedded culvert. For the purposes of further analysis of the non-embedded scenarios tested in this research, the flow has conservatively been considered to be fully-developed beyond Hole 8, or 8D downstream from the inlet (the mid-point of the total culvert length).

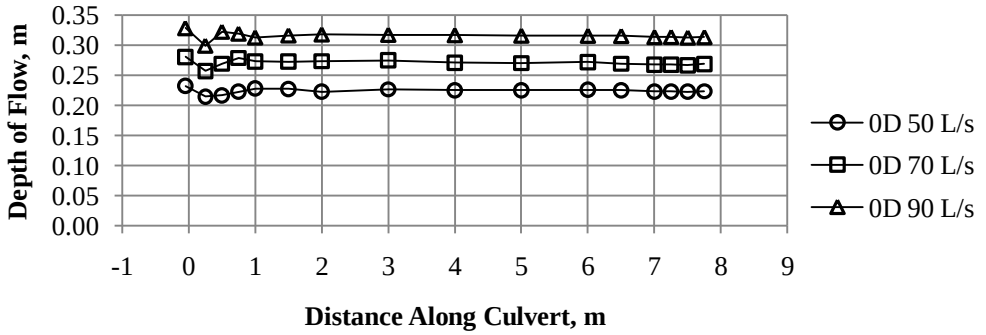

Figure 4.5: Water Surface Profiles for non-embedded culvert for 0.4% culvert slope.

The water surface profile through an embedded culvert at a subcritical slope would be classed as an M1 gradually varied flow profile. At the inlet, the flow contracts from the headwater depth to between critical and normal depth just inside the culvert inlet. Progressing downstream from the point where the water reaches its minimum depth, the flow gradually expands towards its normal depth. In a non-embedded subcritically sloped culvert, the flow expansion would be limited to this depth (depending on the culvert length and tailwater it may not reach normal depth). However, in an embedded culvert, due to the higher tailwater, the flow continues to expand, finally reaching the tailwater depth at the culvert outlet (which, in the case of this experiment was set at the normal depth plus the embedment depth).

The theoretical M1 backwater profile was calculated for each of the embedment conditions tested, an example profile is shown in Figure 4.6. For these experiments it was found that the M1 profile extended upstream beyond the culvert inlet in all cases. A comparison between the calculated depth of the M1 profile at the culvert inlet and the normal depth for each test condition are shown in Table 4.1. This illustrates how the length of the profile changes with culvert slope, discharge and embedment.

The longitudinal extent of the M1 profile relative to the culvert length, dictates whether embedment will have an impact on the conditions at the culvert inlet. If the profile has not attained normal depth by the time the inlet is reached, the M1 backwater will interfere with (partially or completely drown out) the inlet contraction and embedment will be effective at changing the flow conditions at the inlet. If the profile is mature at some distance downstream of the inlet area, embedment will presumably have little or no impact on the flow conditions at the

inlet. For the conditions tested in this project, the test case where the M1 profile produced by embedment affected inlet conditions the least, is for the 1.0% culvert slope, 50 L/s discharge and 0.1D embedment. In contrast, the test condition where the effect is greatest is for the 0.4% culvert slope, 90 L/s discharge and 0.2D embedment. The measured flow depth profiles for each of these cases, plotted with the calculated M1 backwater profiles are shown in Figure 4.7 and Figure 4.8, respectively.

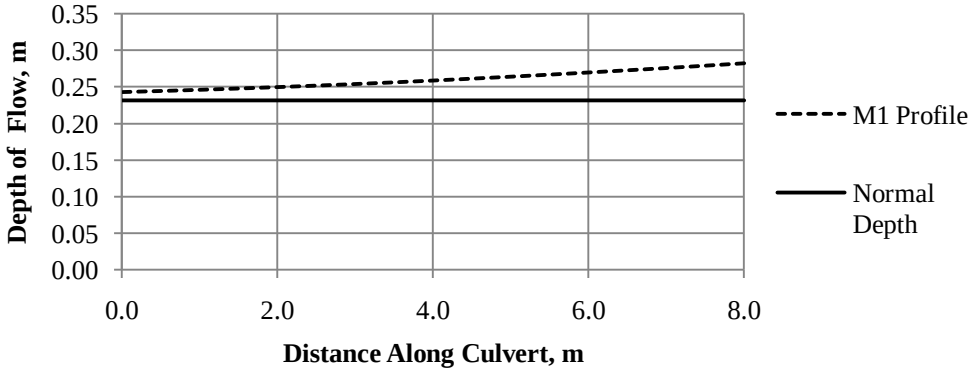

Figure 4.6: Calculated M1 water surface profile for 1.0% culvert slope, 90 L/s discharge, 0.1D embedment.

Table 4.1: Comparison between M1 profile depth at culvert inlet and normal depth for each test condition.

Culvert Slope	Embedment	Flow Rate, L/s	Normal Depth, m	M1 Depth at Inlet, m	Difference, m	Difference, %
0.40%	0.1D	50	0.216	0.249	0.033	15
		70	0.262	0.298	0.036	14
		90	0.307	0.346	0.039	13
	0.2D	50	0.216	0.293	0.077	36
		70	0.262	0.342	0.080	31
		90	0.307	0.390	0.083	27
1.0%	0.1D	50	0.168	0.173	0.005	3
		70	0.202	0.210	0.008	4
		90	0.232	0.243	0.011	5
	0.2D	50	0.168	0.202	0.034	20
		70	0.202	0.240	0.038	19
		90	0.232	0.274	0.042	18

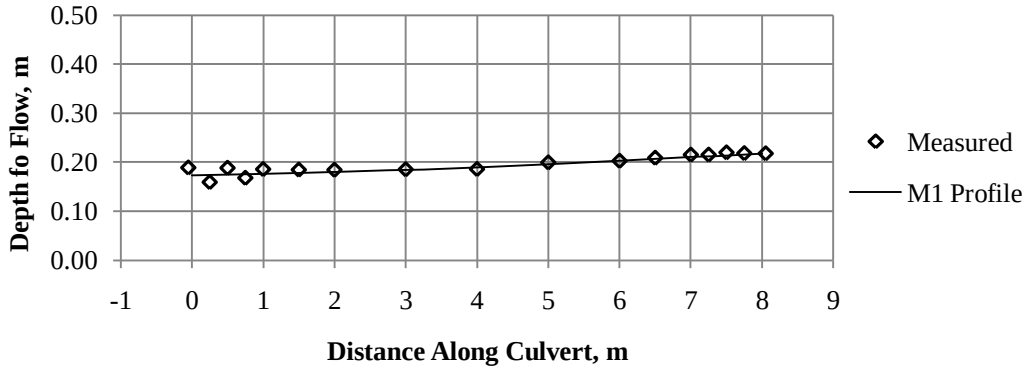

Figure 4.7: Measured flow depth profile plotted with calculated M1 backwater profile for 1.0% culvert slope, 50 L/s discharge and 0.1D embedment. M1 profile almost reaches normal depth near inlet, thus embedment interferes minimally with inlet conditions.

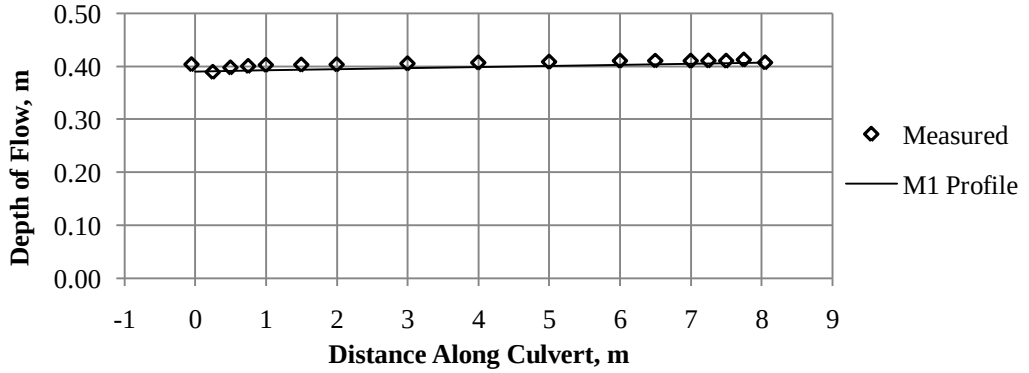

Figure 4.8: Measured flow depth profile plotted with calculated M1 backwater profile for 0.4% culvert slope, 90 L/s discharge and 0.2D embedment. M1 profile would extend well beyond the inlet, thus backwater profile produced by embedment affects inlet conditions.

Figure 4.9 illustrates an example of three near-field entrance region (as defined by Rajaratnam et al. (1991)) water surface profiles measured in this study. In this case for the 1.0% culvert slope and 90 L/s discharge for each of the embedment depths. Comparing the flow depth in the near-field entrance region for the embedded tests to the non-embedded tests, it is apparent that embedment reduces the amplitude of the wave downstream from the flow contraction because the M1 backwater profile extends to the inlet in both cases (0.1D and 0.2D).

Figure 4.10 and Figure 4.11 illustrate the effect of embedment on the water surface profiles over the entire culvert length for the 70 L/s discharge, 0.4% and 1.0% culvert slopes, respectively. For all discharges at both the culvert slopes, the effect of embedment on the water surface profiles was similar. As the embedment was increased from non-embedded, to 0.1D, and then to 0.2D embedment, the difference between the flow depth just downstream of the inlet (i.e.,

the contracted flow section) and the tailwater depth increased. In other words, the variation in the depth of flow along the culvert increased with increasing embedment. The effect of embedment was more noticeable at the 1.0% culvert slope than the 0.4% culvert slope.

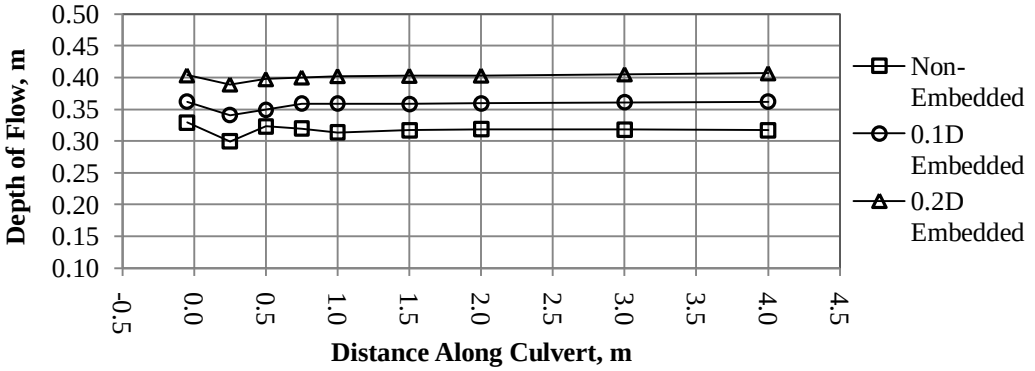

Figure 4.9: Effect of embedment on flow depth in near-field entrance region for 90 L/s at 1.0% culvert slope.

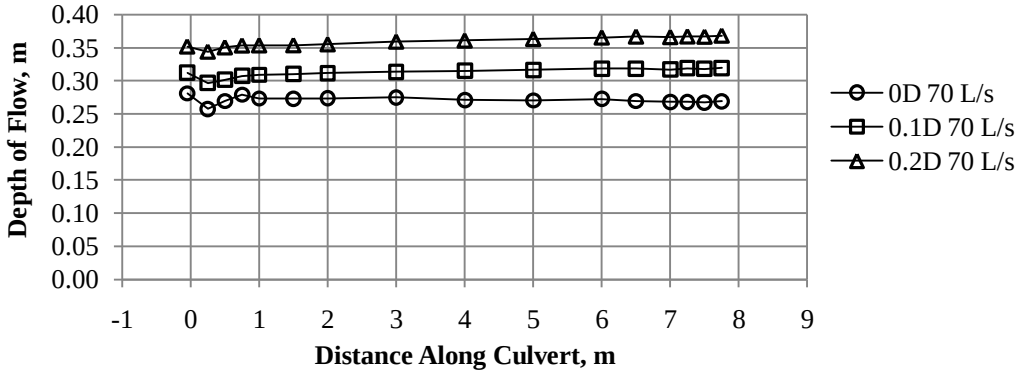

Figure 4.10: Depth profiles for the 0.4% culvert slope for non-embedded and embedded tests for the 70 L/s discharge.

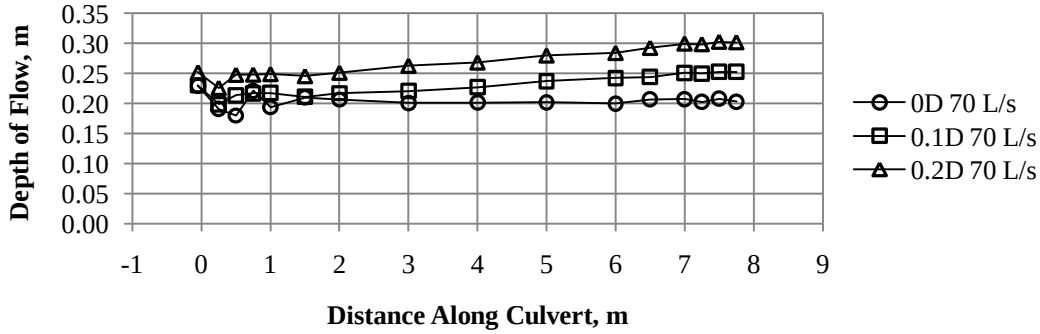

Figure 4.11: Depth profiles for the 1.0% culvert slope for non-embedded and embedded tests for the 70 L/s discharge.

The limitation of embedment for improving fish passage conditions is dependent on the length of the M1 profile relative to the total culvert length. In the case of the conditions tested in this experimental program, the M1 profile (and corresponding increase in flow area) extends through the entire culvert length. Therefore, flow conditions for fish passage in terms of flow velocity are improved throughout the culvert. If the M1 profile had been shorter than the culvert length this would not be the case.

In terms of culvert fish passage, inlet conditions have been acknowledged as one of the key potential barriers to upstream swimming fish due to the significant forces generated by the flow contraction and expansion (Behlke et al., 1991). In this context, the more stable conditions near the inlet produced by embedment (when the M1 profile extends the entire length of the culvert) may translate to improved fish passage conditions in the inlet region. In terms of the conditions along the barrel, if it is assumed that fish prefer consistent, stable flow conditions, the greater the length of the culvert for which stable flow conditions exist (i.e. consistent flow depth and therefore consistent velocity conditions) could be interpreted as advantageous for fish passage. This may mean that the variable longitudinal flow conditions produced by embedment along the culvert barrel may not be completely positive from a fish passage perspective.

This analysis points to the fact that when considering using embedment to promote fish passage, careful consideration must be given to the length of the culvert installation and the selection of an embedment depth that will produce the desired results through a significant portion (if not all) of the culvert length.

4.4. Velocity Profile Analysis

4.4.1. Flow Development

Vertical velocity profiles at the culvert centreline were collected at Holes 1, 2, 4, 6, 7, 8, 9, 11 and 14 for each combination of slope, discharge and embedment. Figure 4.12 shows the velocity profiles for the 0.4% culvert slope, 70 L/s discharge (non-embedded) and illustrates the typical velocity profile evolution along the culvert length that was observed. The profiles were grouped into two plots for ease of viewing and to highlight the change in the velocity profile along the culvert.

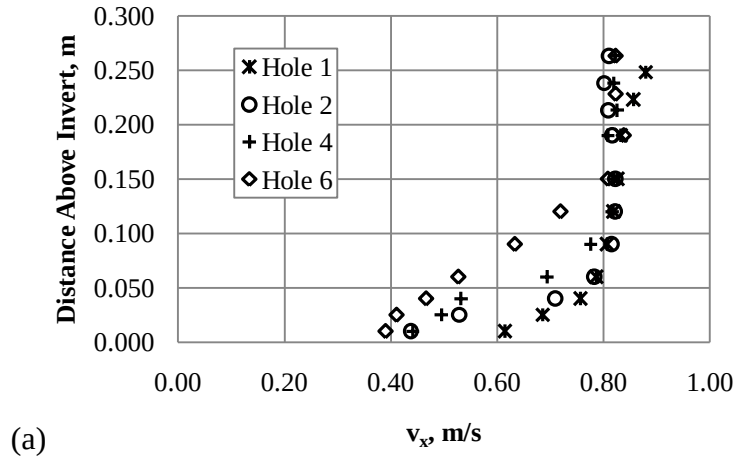

(a)

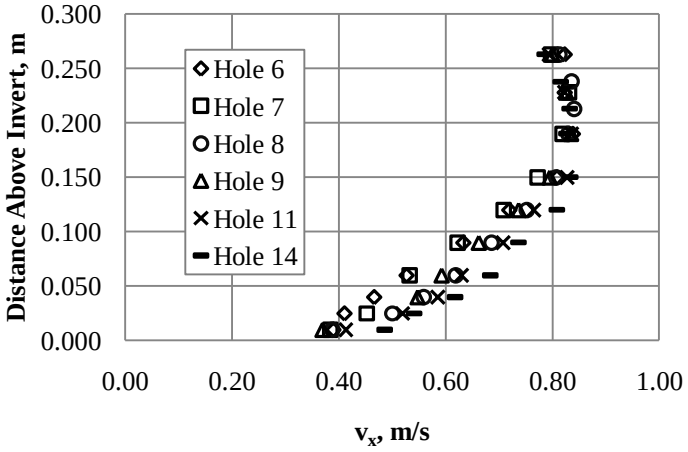

(b)

Figure 4.12: Velocity profiles for 0.4% culvert slope, 70 L/s discharge, non-embedded for (a) from the 0.25 m to 2.0 m downstream from the inlet and (b) from 2.0 m to 7.5 m downstream from the inlet.

For Holes 1 to 6, the profiles are quite variable, changing significantly from one location to another even though the distance between each profile is relatively small (e.g. only 0.25 m from Hole 1 to Hole 2). Between Holes 6 and 8 the profiles begin to collapse to a common curve, confirming the approach to a fully-developed flow condition through this portion of the culvert. Beyond Hole 8 the profiles are relatively similar, although in some cases the profile at Hole 14 shows a slight acceleration in the lower to mid-depth portion of the profile, likely related to the close proximity of the outlet. A complete set of velocity profiles can be found in Appendix D.

Figure 4.13 to Figure 4.18 break out the profiles for all the non-embedded tests by measurement location along the culvert. At all locations for each slope, the profiles are

frequently very similar for the lower portion regardless of the discharge, indicating that, for a specific culvert slope, most of the increase or decrease in discharge occurs in the upper portion of the flow area. This appears to be especially true for the portion of the culvert downstream of Hole 6.

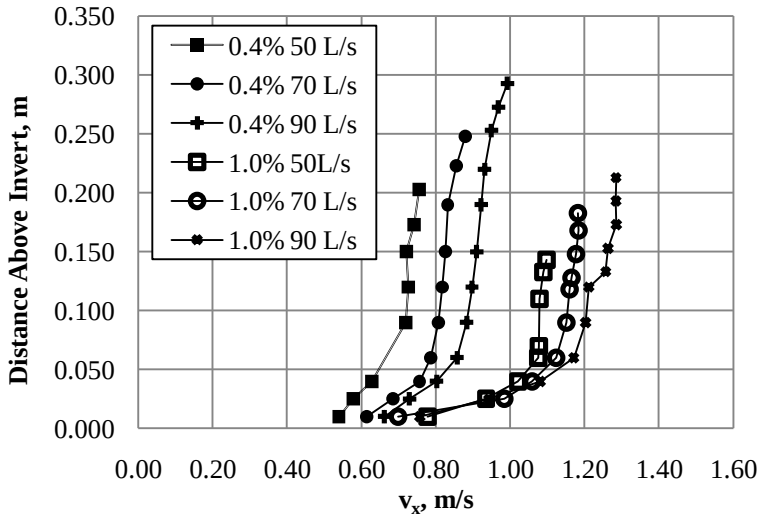

Figure 4.13: Velocity profiles at Hole 1 for all non-embedded tests. The legend indicates the culvert slope (%) and discharge (L/s) corresponding to each profile.

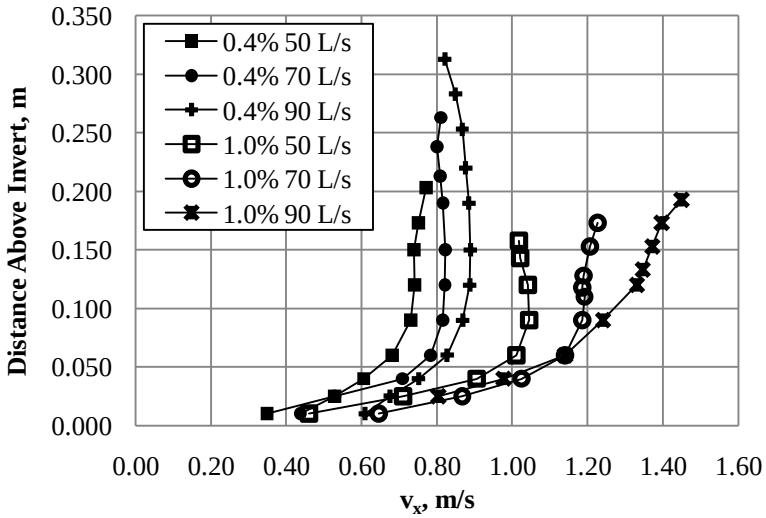

Figure 4.14: Velocity profiles at Hole 2 for all non-embedded tests. The legend indicates the culvert slope (%) and discharge (L/s) corresponding to each profile.

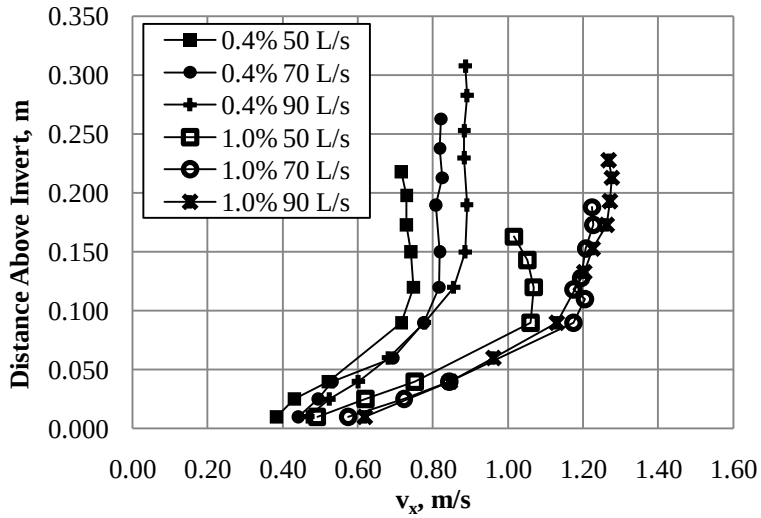

Figure 4.15: Velocity profiles at Hole 4 for all non-embedded tests. The legend indicates the culvert slope (%) and discharge (L/s) corresponding to each profile.

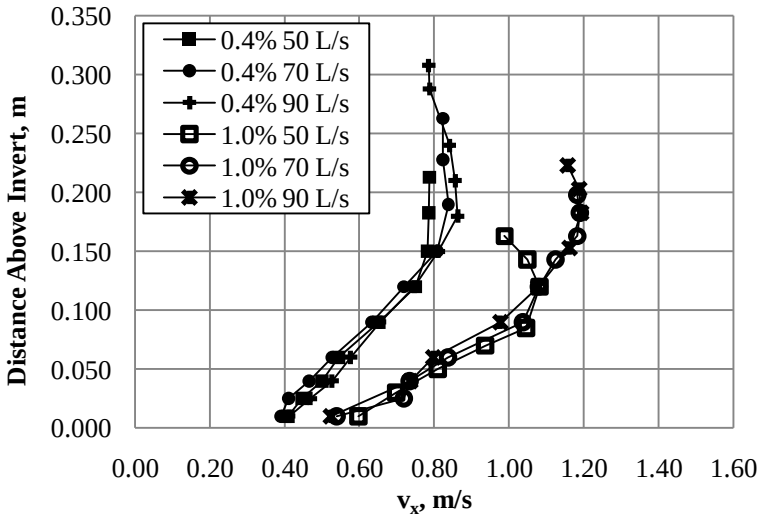

Figure 4.16: Velocity profiles at Hole 6 for all non-embedded tests. The legend indicates the culvert slope (%) and discharge (L/s) corresponding to each profile.

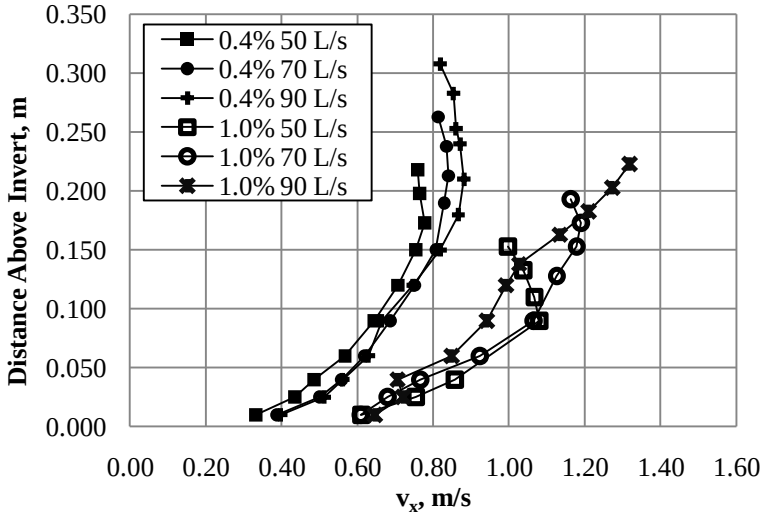

Figure 4.17: Velocity profiles at Hole 8 for all non-embedded tests. The legend indicates the culvert slope (%) and discharge (L/s) corresponding to each profile.

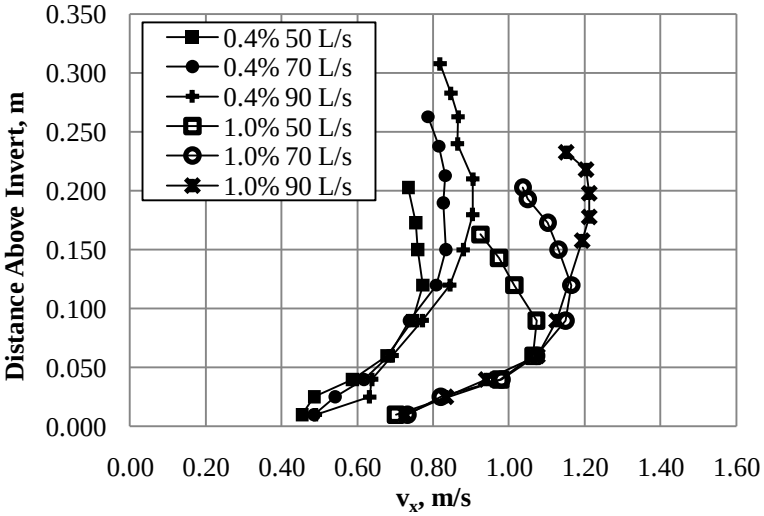

Figure 4.18: Velocity profiles at Hole 14 for all non-embedded tests. The legend indicates the culvert slope (%) and discharge (L/s) corresponding to each profile.

At Hole 1, the velocities measured at the point closest to the invert are slightly greater than the velocities measured at the same depth further downstream. For example, for the 0.4% culvert slope, the velocities near the invert at Hole 1 are in the range of 0.6 m/s, whereas at Hole 2 and beyond they are closer to 0.4 m/s. Near the inlet, where the flow is in the most undeveloped state, the profiles exhibit a steeper velocity gradient close to the invert followed by a relatively vertical profile compared to the profiles from locations further downstream. Of note at Holes 1 and 2 (Figure 4.13 and Figure 4.14) is that the maximum point velocity in each profile generally occurs either at or very close to the water surface. As the flow begins to develop the

arc shape of the velocity profile becomes more noticeable. Around Hole 6 and 8 (Figure 4.16 and Figure 4.17), the location of maximum velocity drops below the water surface (i.e., the surface velocity dip as described by Ead et al. (2000) appears) and remains below the surface at Hole 14.

At Hole 8 (Figure 4.17), the profile for the 1.0% culvert slope and 90 L/s discharge is anomalous in that while it should appear to the right of the 50 and 70 L/s profiles (i.e., having slightly higher velocities), it does not. This finding is believed to be attributed to some error in the experimental set-up, possibly related to the discharge or depth not being set properly, or the ADV not being positioned in the exact centre of the culvert. The result of the velocity-area integration for the cross section measured at Hole 8 indicates an error of -4.3%, which is consistent with the position of the velocity profile.

From the perspective of a fish travelling upstream through the culvert, these profiles show that velocity conditions near the invert are relatively consistent for each culvert slope. For example, for the 0.4% culvert slope the velocity at the one or two measurement points closest to the invert fall roughly between 0.4 and 0.5 m/s for all discharges and longitudinal positions along the culvert. The vertical velocity gradient varies with both slope and longitudinal position along the culvert, with the profile being steeper at the locations closest to the inlet and for the 1.0% versus 0.4% culvert slope. Therefore, the usefulness of the invert region for fish passage based on velocity is tempered by the fact that the shear velocity in the invert region is high. If however, as observed by Behlke et al. (1991), fish prefer to swim closer to the sides and in the upper area of the flow as opposed to near the invert, velocity profiles at the culvert centreline may be of little relevance for fish passage consideration. The horizontal shear velocity distribution and its potential effect on fish passage are discussed in the following section.

4.4.2. Horizontal Distribution of Shear Velocity

This section describes the procedures used to calculate the shear velocity at the culvert boundary from the experimental velocity measurements and compares the results, in terms of the magnitude and horizontal distribution of the shear velocity, to the findings of studies described in Section 2.2.2. The shear velocity distribution is important because, like velocity, it also may be a factor in determining the path that a fish selects to travel through a culvert.

In order to investigate the distribution of the shear velocity (u_*) at locations around the culvert, the Surfer 8 software was used to extract vertical velocity profiles at 0.05 m, 0.1 m, 0.15 m and, in some of the deeper cross sections, 0.2 m horizontal offsets from the culvert centreline, for the non-embedded cross sections within the region of fully-developed flow (i.e. at Hole 8 and 14). Surfer 8 sampled the gridded data and output a point velocity value at 0.01 m intervals along each vertical profile. This data could not be obtained directly from measured data as point measurements were made with the ADV rotated at various angles away from the centreline and not along vertical transects. For the data collected at the 0.4% culvert slope, profiles were extracted on both sides of the centreline and the velocity values were averaged. For the 1.0% data set, profiles were only taken on one side as symmetry had been assumed for the cross sections. Figure 4.19 shows an example of the velocity profile data extracted from the Surfer 8 cross section plots.

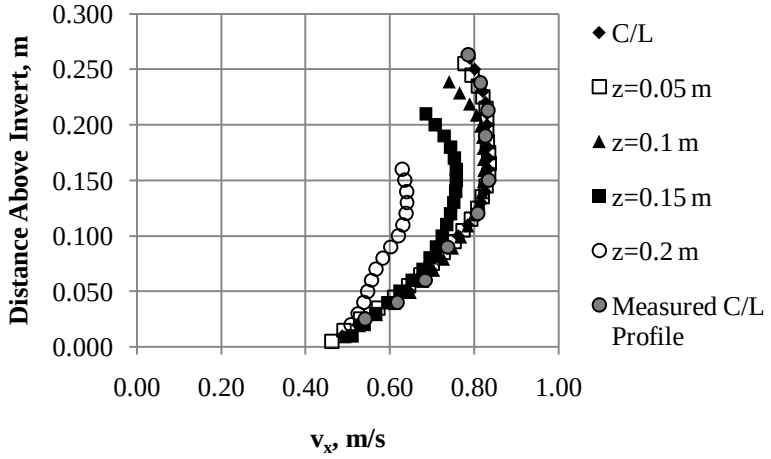

Figure 4.19: Example of the velocity profiles extracted from Surfer 8 at various offsets from the culvert centreline, in this case for 0.4% culvert slope, 70 L/s discharge from the cross section at Hole 14 (non-embedded).

The procedure used to calculate u_* for each profile was identical to that used by Ead et al. (2000) and Magura (2008). This method, based on Equation 2.2, involves plotting the point velocity data versus the distance above the culvert invert (datum) on a semilog scale. From this plot, the slope of the line through the linear portion of the data, divided by 2.5, gives the experimental value of u_*. For this analysis Excel was used to plot and fit the line to the data.

The calculation of shear velocity was found to depend significantly on the selection of the datum for the velocity profiles. When the datum is considered to be the corrugation crest, which is generally the case for hydraulic calculations involving corrugated culverts (e.g. the culvert diameter is measured from inside crest to inside crest), the lower portion of the velocity profile maintains somewhat of an arc shape. An example of this is shown in Figure 4.20.

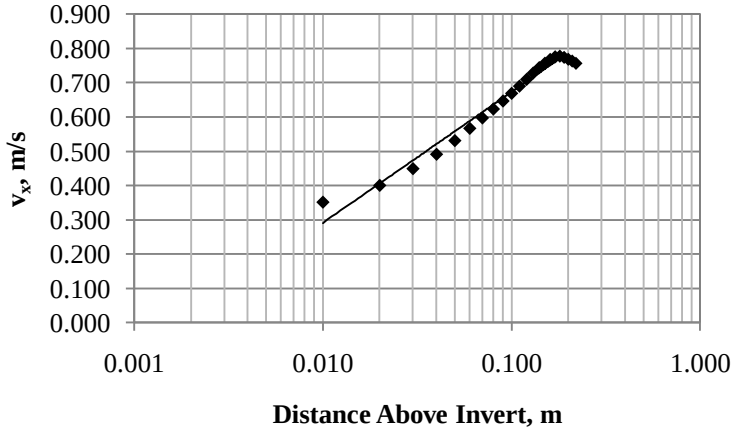

Figure 4.20: Example of determination of shear velocity with the vertical datum located at the corrugation crest. Data is from 0.4% culvert slope, 50L/s discharge at centreline of Hole 8.

Alternatively, the datum can be set at the corrugation trough whereby the corrugations would then be interpreted as a series of equally spaced roughness elements projecting into the flow area. When the data is plotted using the trough as datum, the lowest point in the velocity profile aligns better with the data set than it does if the datum is set at the corrugation crest. An example of this is shown in Figure 4.21, using the same data set as that used to produce Figure 4.26. Noting the desire to produce a linear profile, Ead et al. (2000) took a position somewhere between these two options, selecting a location mid-way between the corrugation crest and trough as the datum for shear velocity analysis. This version of the datum, using the same data set as in the previous two figures, is shown in Figure 4.22.

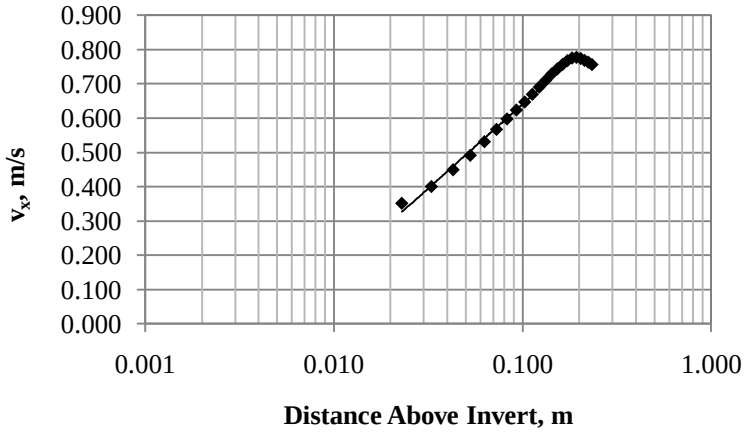

Figure 4.21: Example of determination of shear velocity with the vertical datum located at the corrugation trough. Data is from 0.4% culvert slope, 50L/s discharge at centreline of Hole 8.

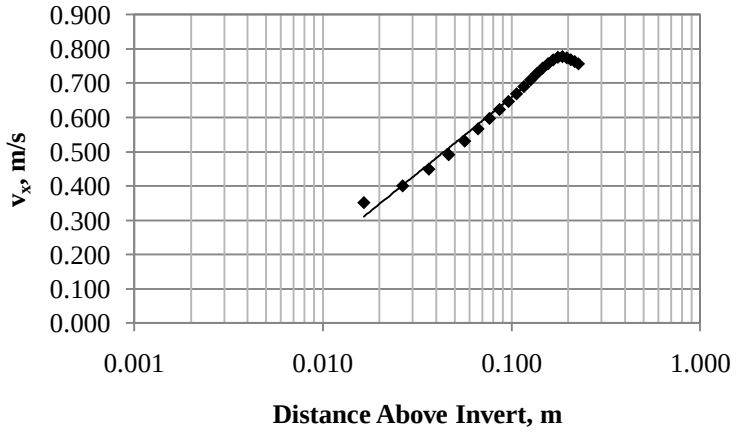

Figure 4.22: Example of determination of shear velocity with the vertical datum located mid-way between the corrugation crest and trough, as in Ead et. al (2000). Data is from 0.4% culvert slope, 50L/s discharge at centreline of Hole 8.

In order to determine the impact of the selection of datum location, the shear velocity was calculated at the various offsets from the culvert centreline (i.e., 0.05, 0.1, 0.15 and 0.2 m) using each of the three datums (crest, trough and mid-point). Each calculation was based on the same set of data points, which included all values extracted from the Surfer 8 cross section up to and including the maximum point velocity value; no discretion was applied in the selection of data points to provide the best fit line. The results, expressed non-dimensionally as the horizontal offset (z) divided by the culvert radius (r) (0.25 m) and the shear velocity for each vertical divided by the global shear velocity (U_*) calculated based on normal depth determined from:

$$U_* = \sqrt{gRS} \tag{4.2}$$

where g is gravitational acceleration, R is the hydraulic radius and S is the culvert slope, are shown in tabular form in Appendix E. A selection of these results, for the data collected at 0.4% culvert slope, 50L/s discharge at Hole 8 (i.e., corresponding to the examples shown in the previous three figures), is shown in Table 4.2. As the data in Table 4.2 shows, with the datum at the corrugation crest, the values of u_*/U_* were consistently below one, while with the datum at the trough u_*/U_* values at the centreline were consistently greater than one. Using the mid-point datum (i.e., the Ead et al. (2000) preferred datum) the values fell between the two. The results make it apparent that, when calculating the shear velocity in this manner, the selection of datum will influence the results.

Table 4.2: Calculated shear velocities at culvert boundary based on various datums for data collected at 0.4% culvert slope, 50L/s discharge at Hole 8.

	Offset (z/r)	u_*/U^*		
		Datum		
		Corrugation Trough	Corrugation Midpoint	Corrugation Crest
0D 50 Hole 8	0.0	1.28	1.16	0.99
	0.2	1.21	1.05	0.83
	0.4	1.22	1.08	0.90
	0.6	0.94	0.89	0.67
	0.8	0.53	0.47	0.41

Theoretically, it is known that the value of u_*/U_* at the culvert centreline must be greater than unity because shear velocity is greatest at that location (i.e. because flow depth is greatest at the centreline). Therefore, these results also suggest that setting the datum at the corrugation trough, or mid-point between the trough and crest, provides a better assessment of shear velocity than utilizing the corrugation crest as the datum.

For each of the datums, the pattern of shear velocity across the width of the culvert varied as expected, with the highest value occurring at or near the culvert centreline and decreasing with increasing offset. Figure 4.23 shows the results of the shear velocity analysis when the datum is set at the corrugation mid-point. For both the 0.4% and 1.0% slope data sets, the rate of change

of shear velocity with distance from the centerline appears to increase beyond z/r of approximately 0.4.

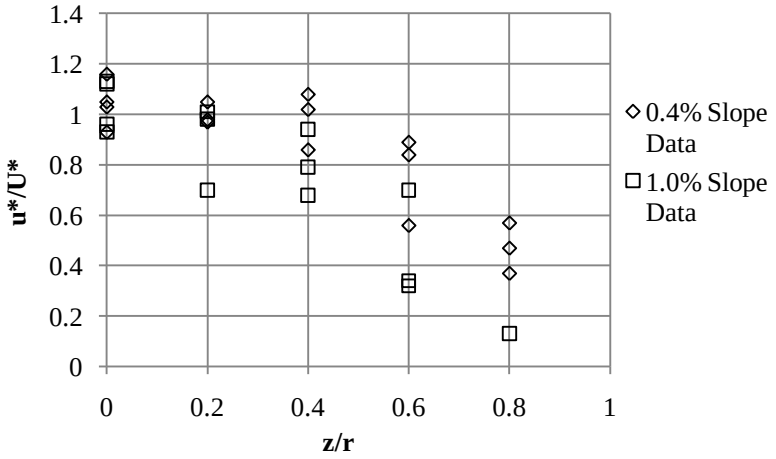

Figure 4.23: Non-dimensionalized shear velocity distribution for data collected under the non-embedded condition at Holes 8 and 14 for all discharge rates with the datum set at the mid-point of the corrugation.

The shear velocity distribution shown in Figure 4.23 is similar to that observed by Magura (2008) who found the value of u_*/U_* varied from approximately 1.4 at the culvert centreline to 0.5 near the culvert wall, for experimental results obtained in a backfilled embedded corrugated pipe. In Magura's work, the issue of the datum selection was not relevant because the corrugations on the bottom of the pipe were covered by a layer of gravel and as such the datum was set at a value representing the average surface elevation of the gravel bed. In his results, Magura observed that the greatest shear velocities occurred some distance offset from the culvert centreline, an effect that he attributed to the presence of the backfilled invert.

The shear velocity distribution found through these experiments can also be compared to the shear stress distribution described by Ead et al. (2000). In the case of this experiment, the shear velocity was found to vary little from the centreline to a horizontal offset of 0.4 z/r, whereas Ead et al. found that the shear stress varied negligibly from the centreline to an offset of 0.6 z/r. Both experimental results showed that beyond these offsets the shear velocity (or shear stress as expressed by Ead et al.), decreased rapidly with increasing offset towards the culvert wall.

The shear velocity results produced in this study also bear resemblance to the shear stress distributions for circular pipes developed by Knight and Sterling (2000). Knight and Sterling observed that the shear stress was relatively constant for the central portion of the flow width and only began to decrease at a point offset from the culvert centreline, as was found to be the case for the shear velocity results presented here. Knight and Sterling also found that the uniformity of the shear stress distribution across the flow width increased with the flow depth. As can be seen in Figure 4.29, the shear velocity for the 0.4% culvert slope (for which flow depths were greater than the 1.0% culvert slope), was slightly more uniform than for the 1.0% culvert slope. This is in agreement with the findings of Knight and Sterling.

If, as suggested by Papanicolaou and Talebbeydokhti (2000), fish prefer to travel through areas of low shear stress, and therefore by extension low shear velocity, the results presented here support the fact that fish would likely prefer the conditions near the sides of the culvert, as opposed to the conditions near the invert where the shear velocity is at its peak within the cross section.

4.4.3. Comparison to Theoretical Velocity Distribution

As described in Section 4.3 and 4.4.1, for the non-embedded experiments documented here, the flow appears to be fully-developed downstream from the mid-point of the culvert (Hole 8). For comparative purposes, the velocity profiles from the fully-developed flow region for the non-embedded tests were analyzed in terms of their fit to the Prandtl von Karman velocity distribution law (Equation 2.2).

For each discharge, the velocity data collected at the culvert centreline at Holes 8, 9, 11 and 14 was plotted together semi-logarithmically as described in Section 4.4.2 in order to determine a shear velocity (u_*) value specific to that discharge/culvert slope combination. This procedure was applied to the measured velocity profiles for both the 0.4% and 1.0% slopes and for all discharges. For the calculation of u_*, all data points were used for the trendline except those close to the water surface that were not part of the linear portion of the velocity profile. Following the example of Ead et al. (2000), the datum was set halfway between the corrugation crest and trough (i.e., 0.0065 m below the crest). As shown in Section 4.4.2, the selection of datum impacts the determination of shear velocity, and the analysis completed using the

experimental data from this study suggests that placing the datum at the mid-point between the corrugation crest and trough is a reasonable assumption based on the u_*/U_* ratios. A summary of the results for u_*/U_* for the velocity profile analysis is shown in Table 4.4.

The ratio of the centerline shear velocity to the global shear velocity would be expected to be greater than 1.0, as this is the location of maximum flow depth. As can be seen in Table 4.3, however, several of the experimentally determined centreline shear velocities are less than the calculated global shear velocities. These results for u_*/U_* are similar to those found by Ead et al. (2000), whose results from a similar experimental program showed ratios of centerline to global shear velocity varying from approximately 0.7 to just less than 1.2 (cf. Figure 10 in Ead et al.). Of the 15 experiments by Ead et al., 11 (73%) had a u_*/U_* ratio less than 1.0, 10 (67%) had a ratio of less than 0.9 and 4 (0.27%) had a ratio less than 0.8. Ead et al. attributed this discrepancy to the "difficulty in determining the shear velocity from the velocity profiles".

Table 4.3: Summary of global shear velocities and centreline shear velocities determined based on measured velocity profiles with datum set between the crest and trough of the corrugation.

Culvert Slope	Discharge, L/s	U_*, m/s	u_*, m/s	u_*/U_*
0.4%	50	0.067	0.072	1.08
	70	0.071	0.072	1.01
	90	0.074	0.074	0.99
1.0%	50	0.096	0.010	1.08
	70	0.103	0.080	0.78
	90	0.108	0.093	0.86

Proceeding with the values of u_* given in Table 4.4, the measured velocity profiles for Holes 8, 9, 11 and 14 for the non-embedded case for each culvert slope were plotted together as v_x/u_* versus y/k_s, where y is the distance above the assumed datum and k_s is the Nikuradse equivalent sand roughness of the boundary. Because the value of k_s for a CSP pipe is not a well-established parameter (although it is generally assumed to be associated with the corrugation height), similar to the work of Magura (2008) and Ead et al. (2000), the value of k_s was adjusted until a good fit (based on visual assessment) between the data and the theoretical log law was found. The results are shown in Figure 4.24 and Figure 4.25. When fitting the regression line to the data set, only the data points used in the calculation of u_* were utilised (i.e., points near the

water surface were not included). The value of k_s that provided the best fit was found to be 0.057 m for the 0.4% culvert slope and 0.030 m for the 1.0% culvert slope.

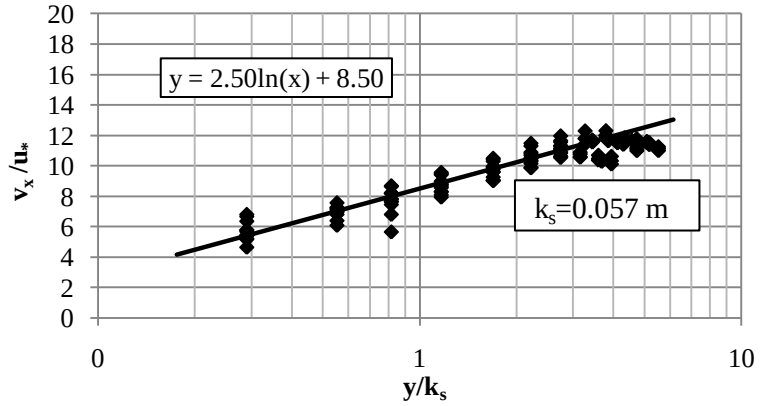

Figure 4.24: Comparison of measured centreline velocity profile data vs. log law for 0.4% culvert slope, all discharges, data collected at Holes 8, 9, 11, and 14. The equation shown on the graph is the fitted equation calculated in Excel while the line represents the theoretical log law. In this case, the line fitted to the data through regression is a perfect match to the log-law when k_s is assumed to be 0.057 m.

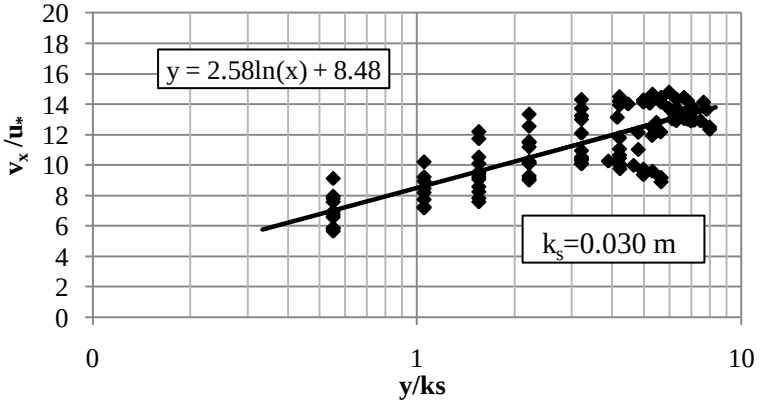

Figure 4.25: Comparison of measured centreline velocity profile data vs. log law for 1.0% culvert slope, all discharges, data collected at Holes 8, 9, 11, and 14. The equation shown on the graph is the fitted equation calculated in Excel, while the line represents the theoretical log law.

In order to demonstrate the sensitivity of the log law comparison to the calculation of u_* and the range of potential k_s values, the centerline shear velocities were re-calculated using the same procedure described above with the datum set at the crest of the invert corrugation. Defining the datum in this way is more typical of traditional culvert hydraulic calculations, where the discontinuous flow area within the corrugations is not considered as part of the useful flow area. Table 4.4 shows the complete set of shear velocity data, obtained using this datum and corresponds to Table 4.3. As can be seen from this data, these results for u_* are less than

those calculated based on the mid-point datum, producing u_*/U_* values which are all less than one (where, as mentioned previously, theoretically these values should be greater than one).

Table 4.4: Summary of global shear velocities and centerline shear velocities determined based on measured velocity profiles with datum set at the corrugation crest.

Culvert Slope	Discharge, L/s	U_*, m/s	u_*, m/s	u_*/U_*
0.4%	50	0.067	0.059	0.89
	70	0.071	0.057	0.80
	90	0.074	0.061	0.83
1.0%	50	0.096	0.083	0.86
	70	0.103	0.080	0.78
	90	0.108	0.069	0.64

Similar to the procedure already described, the measured velocity profiles for Holes 8, 9, 11, and 14 for each culvert slope, and for each of the non-embedded tests, were plotted together as v_x/u_* versus y/k_s using the revised u_* values (based on the placing the datum at the corrugation crest). Again, the value of k_s was adjusted until the best fit between the data and the theoretical log law was found. The results for the 0.4% and 1.0% culvert slopes are shown in Figure 4.26 and Figure 4.27, respectively. The value of k_s that provided the best fit was found to be 0.022 m for the 0.4% culvert slope and 0.012 m for the 1.0% culvert slope.

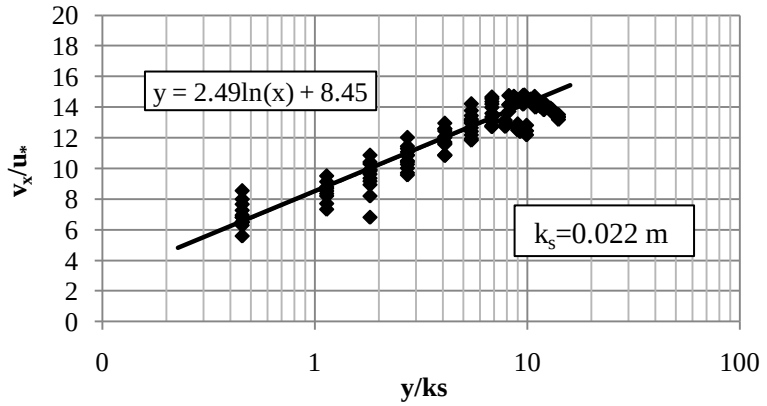

Figure 4.26: Comparison of measured centreline velocity profile data vs. log law for 0.4% culvert slope, all discharges, data collected at Holes 8, 9, 11, and 14. The equation shown on the graph is the fitted equation calculated in Excel while the line represents the theoretical log law.

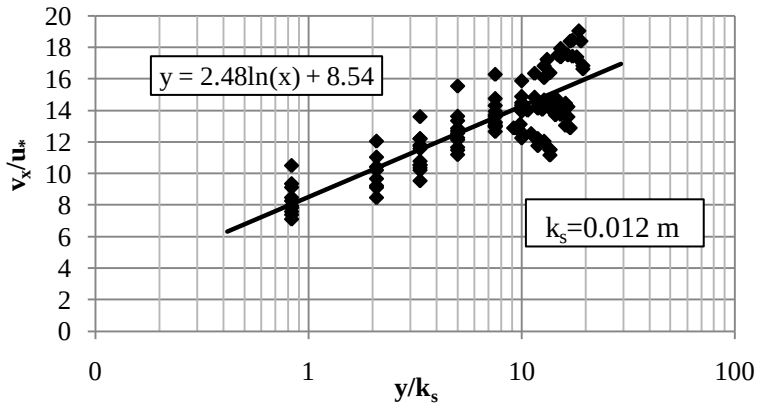

Figure 4.27: Comparison of measured centreline velocity profile data vs. log law for 1.0% culvert slope, all discharges, data collected at Holes 8, 9, 11, and 14. The equation shown on the graph is the fitted equation calculated in Excel while the line represents the theoretical log law.

The k_s values required to fit the log law velocity distribution when the datum was set at the crest of the corrugation are closer to the corrugation height of 0.013 m than the k_s values required when the Ead et al. (2000) datum was used, which were in the order of two to four times the corrugation amplitude. In both cases, the fit of the 0.4% culvert slope data set to the log law was closer than for the 1.0% culvert slope data set and the 0.4% culvert slope also produced slightly larger k_s values. In contrast, Ead et al. determined that the k_s value based on their experiments was exactly equal to the corrugation height, in their case 12 mm.

It should be noted that the value of k_s has a somewhat loose association with physical measurement of the channel substrate roughness dimension. For example, French (1985) states that equating k_s to the roughness height is not an exact relationship. French notes that, in addition to describing the vertical dimension of the boundary roughness, it also relates to their geometric arrangement and spacing, and that in French's opinion k_s can only rarely be expected to correspond to the height of the roughness elements. French does not elaborate on whether perfect dimension and amplitude boundary roughness elements, such as of a CSP pipe, would be expected to have a stronger or weaker relationship between k_s and roughness height.

Relating the k_s value to the corrugation amplitude is similar in theory to relationships that have been proposed between k_s and the particle diameter of channel bed material. For example Chang (1988) provides relationships between k_s and bed material diameter (d) varying from $k_s=1.25d_{35}$ to $k_s=3.0d_{90}$, where d_{35} and d_{90} are the 35 and 90 percent passing sieve sizes of the bed material, respectively. Taking this wide range of k_s to bed roughness relationships into

consideration, it can be concluded that the experimental data produced a reasonable fit to the theoretical log law distribution, and that the k_s value for the model culvert is between one and four times the corrugation amplitude.

4.4.4. Effect of Embedment on Vertical Velocity Profiles

As expected, embedding the culvert reduced the streamwise flow velocities throughout the depth of flow. An example of the typical change in the velocity profile resulting from embedment is shown in Figure 4.28. Comparing the profiles, it can be seen that the effect of embedment is to both reduce velocities as well as to produce a more uniform profile over the entire depth. This increase in the linearity of the profiles is due to the fact that the velocities near the culvert invert are reduced less by embedment than are the velocities closer to the water surface. The complete set of velocity profiles for both the 0.1D and 0.2D embedments, plotted for each slope and discharge combination, can be found in Appendix D.

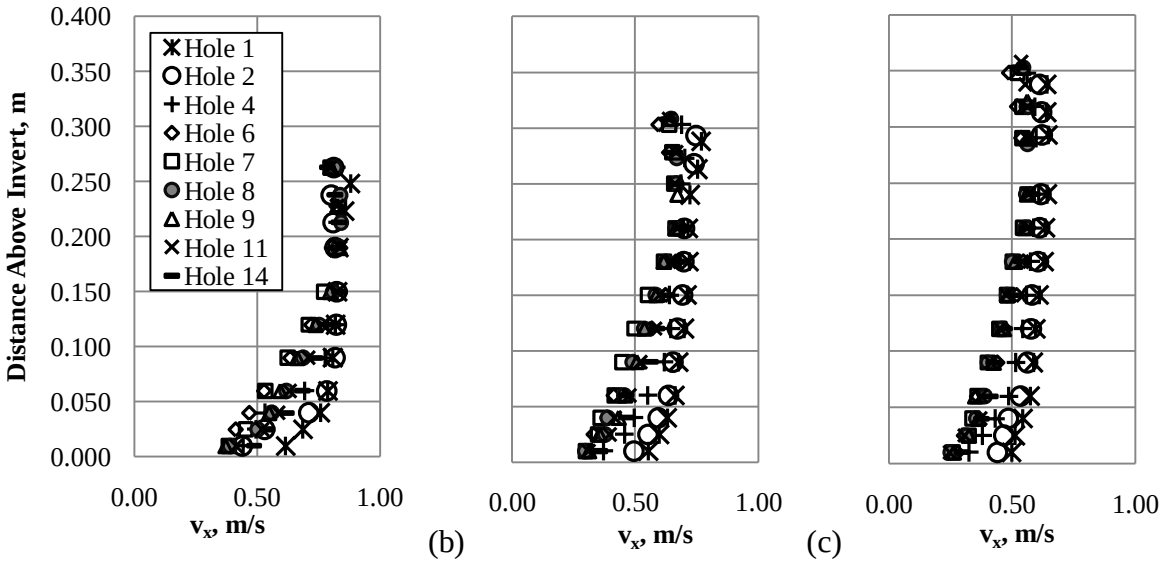

Figure 4.28: Centreline vertical velocity profiles for the 0.4% culvert slope and 70 L/s discharge for (a) non-embedded, (b) 0.1D embedded and (c) 0.2D embedded tests.

Interpreting these results in terms of fish passage, it has been shown that embedment produces lower flow velocities (both in terms of overall mean velocity as well as point velocities throughout the profile), which suggests that the embedded culvert may provide more amenable conditions for fish than the same non-embedded culvert. As in the case of the non-embedded culvert, conditions at the invert for each culvert slope do not change significantly with either

discharge or longitudinal position. However, as shown in Figure 4.28, the effect of the successive embedment levels is to produce a steeper, more uniform velocity profile than found in the same non-embedded culvert. As noted previously, fish are thought to be averse to swimming in areas with high velocity gradients. Therefore, in terms of the velocity conditions at the culvert centreline, these results confirm that embedment likely does improve fish passage conditions.

4.5. Velocity Cross Section Analysis

4.5.1. Non-Embedded Velocity Cross Sections

As described in Chapter 3, in addition to the velocity profiles, point velocity data was collected throughout the flow area at five locations along the culvert length. This data was used to produce contour plots of streamwise velocity, a complete set of which can be found in Appendix A. When viewing the plots, it should be remembered that, as described in Chapter 3, based on the symmetry of the contour plots of the 0.4% culvert slope data, data for the 1.0% culvert slope tests was only collected on one side of the cross section and symmetry for these contour plots has been assumed.

Comparing the contour plots for the non-embedded tests, similar patterns are evident in the velocity distribution progressing downstream from the inlet. Figure 4.29 illustrates this development of the velocity contours for the example of the 50 L/s discharge for each of the two culvert slopes studied. At Hole 1, the cross sections show the highest velocity contour occupying a very large portion of the flow area. Considering the law of continuity, this is required due to the relatively smaller cross sectional flow area compared to the downstream conditions (due to the contraction that occurs as flow passes through the culvert inlet), as well as the presence of the negative velocities in the upper corners of the flow area as discussed in Section 4.2.1. At Holes 2 and 4, the size of the core high velocity flow area begins to decrease, contracting inwards towards the centre of the cross section. Near the water surface, the edges of this core flow area also begin to draw in towards the culvert centreline giving the central flow core more of an oblong shape. At Holes 8 and 14, the relative percentage of the flow area occupied by the highest velocity contour decreases further, in many cases dropping below the water surface (i.e., the velocity dip is large enough to be captured by the 0.1 m/s contour interval). In all cases, the lower velocity contours surrounding the core contour follow the same pattern (shape) as the internal contour. Of note is that there is a significant area around the

perimeter where flow velocities are significantly less than the core flow velocity, which confirms the results of Magura (2008). The prevalence of these low velocity areas is greatest in the cross sections from Hole 4 downstream, however even at Holes 1 and 2 the lower velocity areas around the invert and walls are still significant.

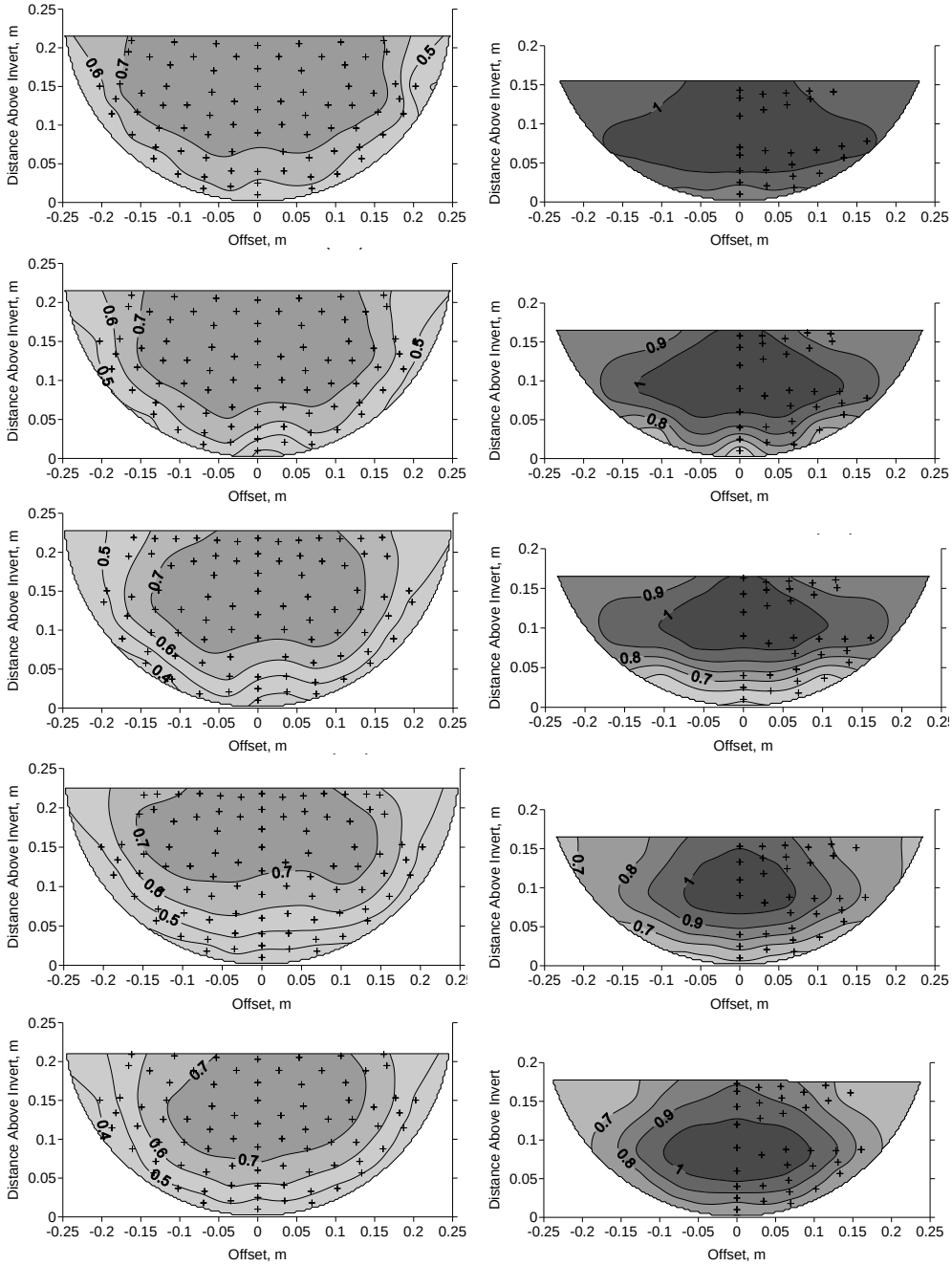

Figure 4.29: Contour plots of v_x (m/s) for 0.4% culvert slope (left column) and 1.0% culvert slope (right column) for 50 L/s discharge (non-embedded). Plots from top to bottom correspond to Holes 1, 2, 4, 8 and 14, respectively.

Although in almost all cases the lowest velocity contours are located at the culvert invert, the upper corners of the flow area also have relatively low velocities. The lower velocity areas in these cross sections correspond well with the areas proposed by Behlke et al. (1991) (shown in Figure 2.6), as being preferential pathways for fish travelling upstream. In some cases, the lack of measured data in the cross section corners (restricted by the physical limitations of the ADV and the positioning traverse), may have caused a slight overestimation of the velocity in these areas through the Surfer 8 interpolation procedure. It can be concluded from the velocity contour plots that the significant cross section area with velocity less than the average velocity may be suitable for fish passage. Further analysis to quantify this area is provided in the following sections.

4.5.2. Effect of Embedment on Velocity Cross Sections

The streamwise velocity plots for the embedded culvert tests (which can be found in Appendix A) exposed similar trends and patterns in velocity contours as in the non-embedded tests. For example, Figure 4.30 shows the contour plots for the data collected at Hole 4 for the 0.4% culvert slope and 90 L/s discharge for each of the embedment levels and illustrates the highly consistent contour shapes, evident in many of the contour plots. In terms of the effect of embedment on the velocity cross section, the central (i.e. highest) velocity contour is reduced by 0.1 m/s for each successive embedment depth. For each increase in embedment, the amount of the cross section area covered by the lowest velocity (in this case 0.5 m/s) contour increases, to the point where a 0.4 m/s velocity contour appears at the 0.2D embedment. This magnitude of reduction was typical for both culvert slopes and all three discharges.

The velocity data collected with the ADV was also used to create plots of streamwise velocity non-dimensionalized by the normal depth average velocity (V_{aveYn}) for each flow condition. Examples of these plots are shown in Figure 4.31 and a complete set is included in Appendix G. For each combination of discharge and slope, the same value of V_{aveYn} was used for all cross sections, including both the non-embedded and embedded tests. Using this standard non-dimensionalizing value provided a consistent basis for comparison between results at different locations along the pipe, as well as for the different embedment levels. It should be remembered when looking at the plots that, because of the standard non-dimensionalizing value, the distribution of velocity above and below the normal depth velocity is not equal for many of

the plots. Additionally, the lack of data in the upper corners of the flow area skew the results in some cases. For example, the non-embedded plot in Figure 4.31(b) shows a large portion of the flow area with a velocity greater than 1.2 V_{aveYn}, because the depth of flow at this location is less than normal depth and the negative velocities in the corners of the flow area could not be captured.

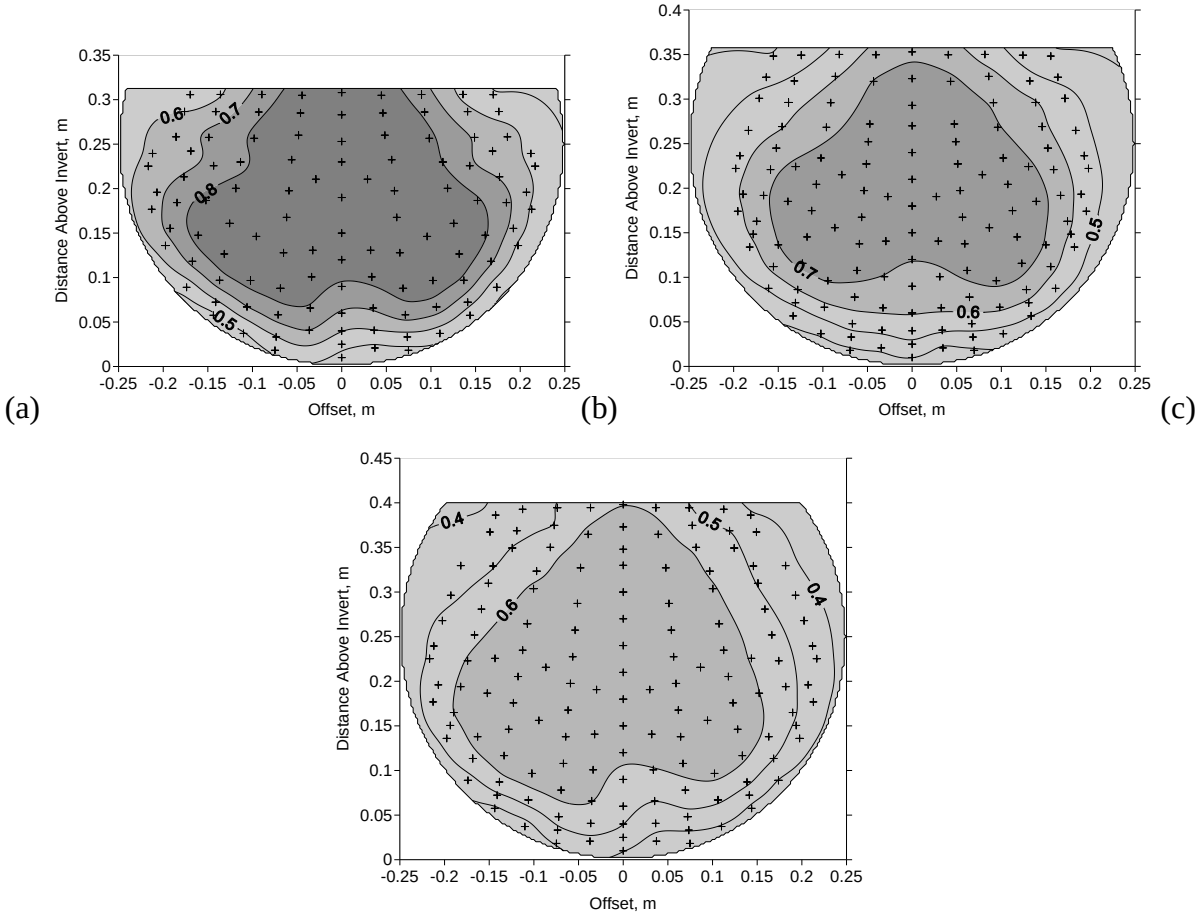

Figure 4.30: Streamwise velocity contour plots in units of m/s for 0.4% culvert slope, 90L/s discharge for a) non-embedded, b) 0.1D embedded and c) 0.2D embedded culvert at Hole 4.

In all cases, the results of the embedded tests were successful in demonstrating the reduction in flow velocities dictated by continuity. Figure 4.31(a) illustrates the change in the contour plots of v_x/V_{aveYn} at Hole 8 for the 0.4% culvert slope and 50 L/s discharge. In this case, the highest velocity contour changes from 1.2 V_{aveYn} for the non-embedded culvert to 1.0 V_{aveYn} and 0.8 V_{aveYn} for the 0.1D and 0.2D embedments, respectively.

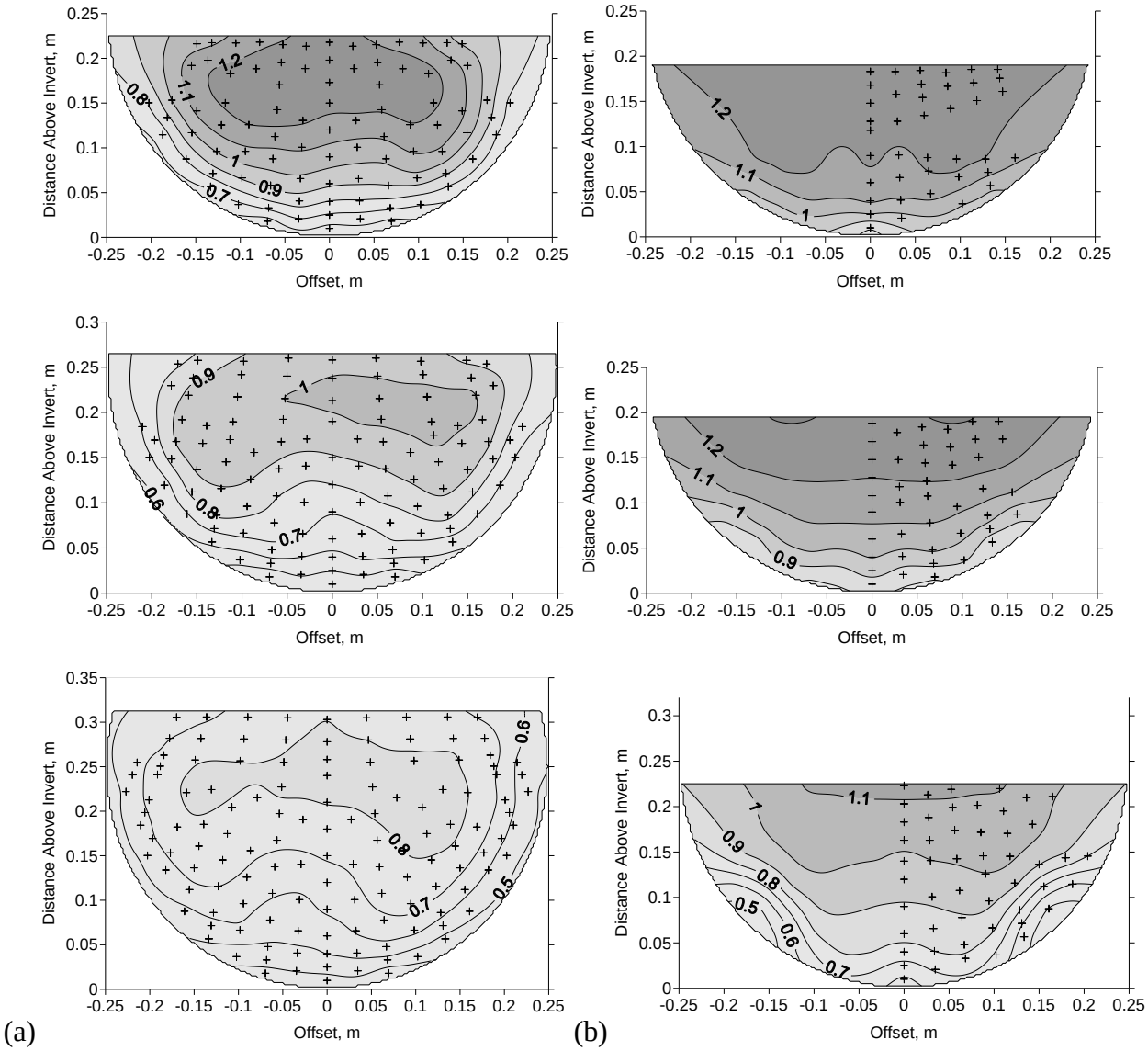

Figure 4.31: Contour plots of v_x/V_{aveYn} for a) 0.4% culvert slope, 50 L/s discharge at Hole 8; and b) 1.0% culvert slope, 70 L/s discharge at Hole 1. From top to bottom plots are for non-embedded, 0.1D embedded and 0.2D embedded tests.

The case where embedment was of least value in reducing velocities was at the cross sections immediately downstream of the inlet at the 1.0% culvert slope. At these locations, the increase in flow area due to M1 backwater profile produced by embedment was the lowest (as discussed in Section 4.3). Because the increase in flow area due to embedment was minimal, so too the reduction in velocities was less at these locations than for cross sections further downstream. Figure 4.31(b) shows the reduced effect of embedment at Hole 1 for the 1.0% slope and 70 L/s discharge, where embedding the culvert by 0.1D only slightly reduces the flow

area within the 1.2 V_{aveYn} velocity contour and the 0.2D embedment reduces the highest contour to 1.1 V_{aveYn}.

In order to quantitatively evaluate the effect of embedment on the velocity cross sections, the results were analyzed in terms of the percent of the cross section area less than V_{aveYn}. For example, Figure 4.32(a) and (b) illustrate the results for the 0.4% culvert slope, 50 and 90 L/s discharges, respectively. Figure 4.33 shows the same information for the 1.0% culvert slope. Comparing the results from parts (a) and (b) of each figure a general decrease in the percent of the cross section area with velocity less than V_{aveYn} with increasing discharge is apparent. There are some deviations from this trend, which may occur because of fluctuations in the flow area near the inlet (i.e., affecting locations within 2D downstream from the inlet) that are noted in Section 4.2, or be related to the experimental error discussed in Section 4.1. Regardless, both Figure 4.32 and Figure 4.33 illustrate that, even for the non-embedded test conditions, up to 50% of the cross sectional area has velocity less than V_{aveYn} for these examples. A complete set of similar figures for all slopes and discharges are located in Appendix F. Based on this analysis it may be concluded that, for a given slope, the effectiveness of a specific embedment depth at increasing the percent of the cross section area with velocity less than the average decreases with increasing discharge at locations along the culvert that are influenced by the M1 backwater profile.

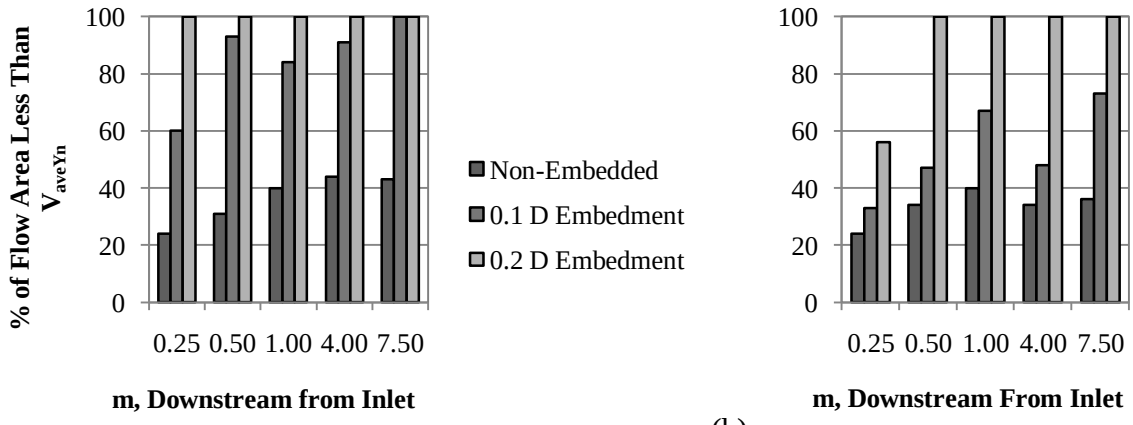

(a) (b)

Figure 4.32: Variation in the percent of flow area less than V_{aveYn} for 0.4% culvert slope for (a) 50 L/s discharge and (b) 90 L/s discharge.

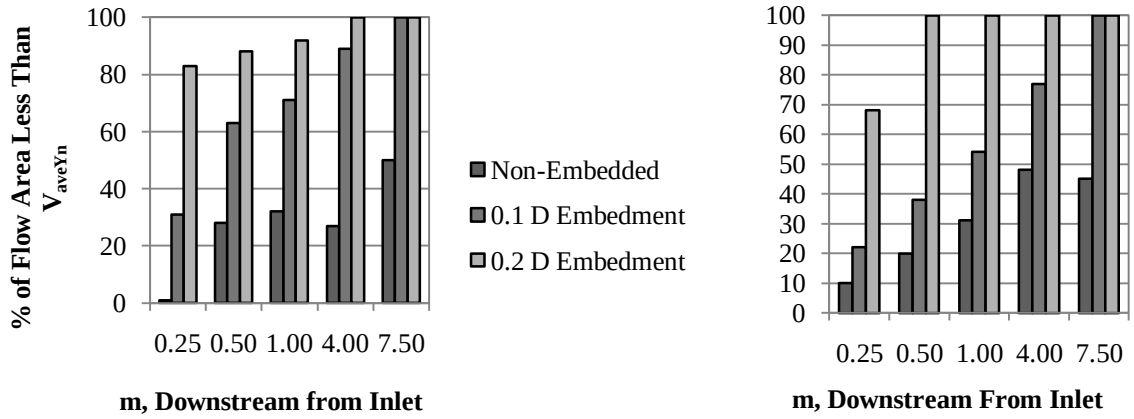

(a) (b)

Figure 4.33: Variation in the percent of flow area less than V_{aveYn} for 1.0% culvert slope for (a) 50 L/s discharge and (b) 90 L/s discharge.

Analyzing the velocity data in terms of a common average velocity value for each discharge and slope (as in Figure 4.32 and Figure 4.33 and Appendix F), confirms that, in terms of velocity, the conditions near the inlet may represent the greatest barrier to fish passage as they have the least amount of cross section area with velocity less than V_{aveYn}. These figures also confirm the effectiveness of embedment at increasing the amount of area with velocity less than V_{aveYn}, which may produce improved fish passage results. For example, if to satisfy the needs of the local fish species of concern it was determined that 50% of the flow area must be less than the V_{aveYn} for the design conditions (i.e., culvert slope and discharge) which were similar to these experiments, then it would appear that an embedment of 0.2D would be successful at providing that area. The results also suggest that the level of embedment must be increased relative to culvert slope and design discharge (i.e., that the embedment depth should be greater for a steeper culvert or a culvert with a higher design discharge, relative to the embedment depth for another culvert installation with a flatter slope and/or lower design discharge, in order to produce equally effective results). As discussed in Section 4.3, the effectiveness of embedment at improving fish passage conditions along the entire culvert length (i.e. up to and including the inlet), depends on the length of the culvert relative to the length of the M1 backwater profile produced by embedment. Therefore, the level of embedment must also take into account the culvert length if the benefit from embedment is to be maximized.

4.5.3. Velocity-Area Distribution

As discussed in Chapter 2, several researchers have explored the cross sectional velocity distribution in terms of the percent of the flow area less than a specified velocity (e.g. House et al., 2005 and Magura, 2008). In order to assess the relationship in the data set collected for this study, each measured point velocity (v_x) was divided by the average velocity (V_{ave}) for that cross section (i.e., the discharge measured at the magnetic flow meter divided by the flow area at that particular cross section calculated on the basis of the measured flow depth). Surfer 8 was then used to create contour plots for each cross section based on the v_x/V_{ave} data and to extract the percent of the area less than various values of v_x/V_{ave} at intervals of 0.1.

Figure 4.34 shows the results of this analysis for the entire data set from this study, including all cross sections, all discharges, and both non-embedded and embedded tests. As previously mentioned, the corners of the flow area were generally not accessible for the cross sections at the 1.0% culvert slope due to the lower depth of flow. The effect of this is evident in Figure 4.46 in the long tail of data points at low v_x/V_{ave} values for the 0.4% slope data. Had these areas been accessible at the 1.0% slope, it would be expected that the 1.0% slope data set would have had a similar tail.

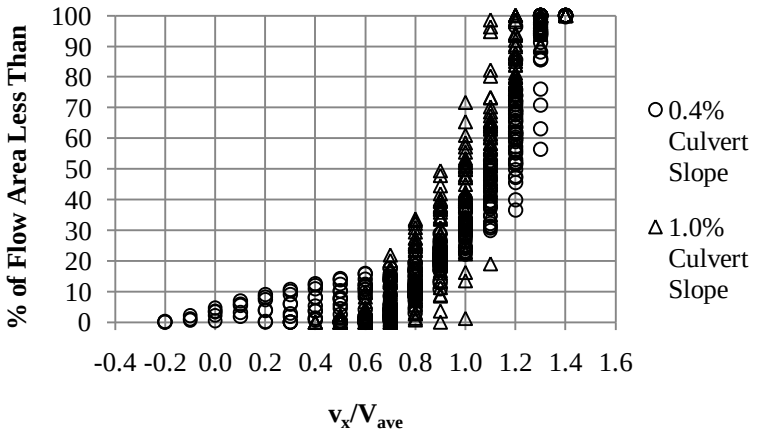

Figure 4.34: Percent area less than v_x/V_{ave} for all cross-sections including both non-embedded and embedded tests.

Figure 4.35 is similar to Figure 4.46, except that the data from Holes 1 and 2 have been removed. As such, the effect of the contraction and negative/low velocity areas in the upper corners near the culvert entrance have been eliminated. As shown in this figure, for this data subset, all cross sections had velocity distributions that fell within the range of 0.4 V_{ave} to

1.4 V_{ave}. This compares to the results obtained by Magura (2008) who, using a similar data set which excluded cross sections affected by the inlet flow contraction, obtained a velocity distribution which fell within the range of 0.1 V_{ave} to 1.4 V_{ave} (a similar figure illustrating Magura's results is shown in Figure 2.5).

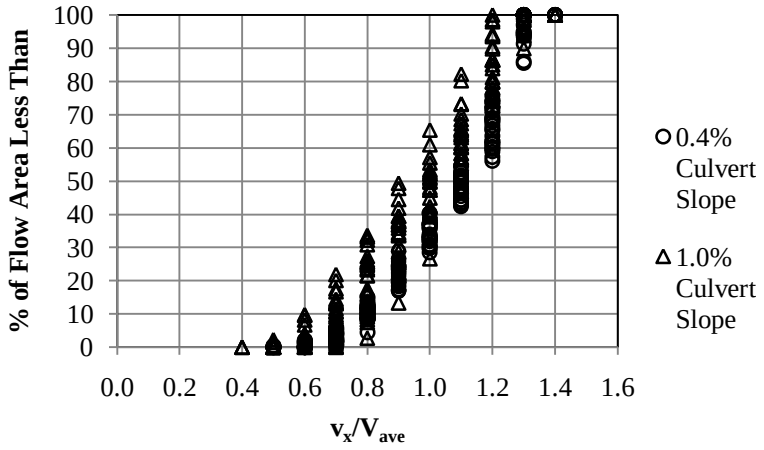

Figure 4.35: Percent of area less than v_x/V_{ave} for cross sections at Holes 4, 8 and 14 including both embedded and non-embedded tests.

Figure 4.36 shows the same data as Figure 4.47, except with the data separated on the basis of the two test slopes. As these two plots illustrate, the distribution of the relative velocity data for the 0.4% culvert slope is more tightly clustered than that of the 1.0% slope data set. This may be due to the fact that the flow conditions for the 0.4% slope, represented in Figure 4.48(a), were much more consistent, whereas the flow depth, and consequently V_{ave}, for the 1.0% culvert slope varied significantly along the length of the culvert as discussed in Section 4.3.

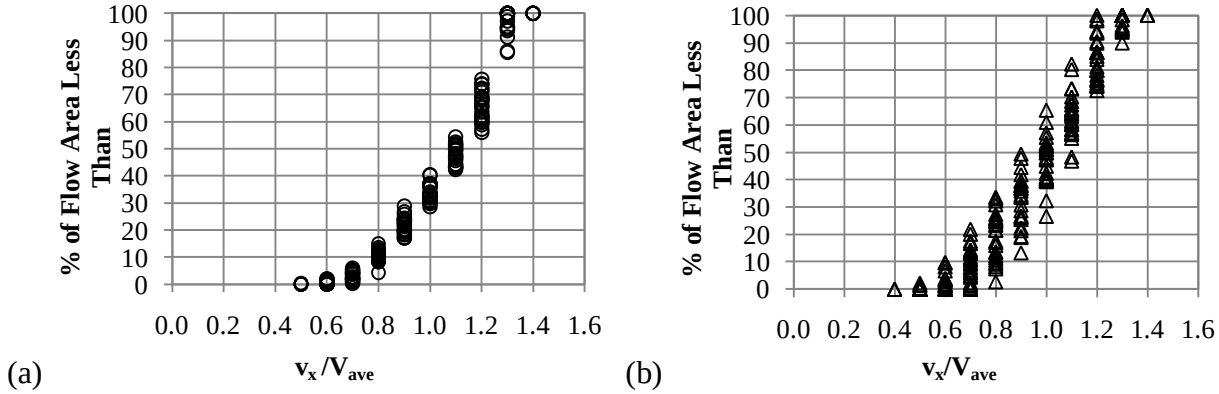

Figure 4.36: Percent of cross section area less than v_x/V_{ave} for (a) 0.4% culvert slope and (b) 1.0% culvert slope for Holes 4, 8 and 14 including both embedded and non-embedded tests.

For each cross section (i.e., for each of Holes 1, 2, 4, 8 and 14), the percent of the flow area less than V_{ave} was determined with Surfer 8; these values are shown in Appendix H. For each test, an average value of the percent of area less than V_{ave} for all the cross sections was calculated so that there was a single value representing the flow conditions over the entire culvert length. These results are summarized in Table 4.5. For the 0.4% culvert slope, the overall average percent of the flow area less than V_{ave} is 31.3% +/-1.2% and for the 1.0% culvert slope it is 42.2% +/- 11.3%. Both averages are for all of the tests completed, including both non-embedded and embedded. The average percent of the area less than V_{ave} for the combined data set is 36.7% +/-16.8%.

Table 4.5: Summary of the percent of flow area less than V_{ave}.

Embedment		0D			0.1D			0.2D			Average
Discharge (L/s)		50	70	90	50	70	90	50	70	90	
Culvert Slope	0.4%	31.1	30.1	30.3	31.5	32.5	32.5	30.4	31.5	31.9	31.3
	1.0%	38.9	33.5	40.6	53.5	40.2	37.5	52.0	40.9	42.2	42.2

For a data set collected at culvert slopes of 0%, 0.5% and 1.0%, Magura (2008) found an average percent area less than V_{ave} of 46% +/- 3.2% using similar data averaging to that used here (i.e., a single representative value was calculated for all cross sections for each trial and these values were then averaged). Magura, however, limited his data set to include only those cross sections where fully-developed flow was observed. For the experiments described here, using only cross sections 4, 8 and 14 for the non-embedded tests (approximately the limits of fully-developed flow), the average percent of the flow area less than V_{ave} is 36.8% +/-8.1%, which is somewhat comparable to the results Magura obtained for his backfilled culvert.

The results presented in this section suggest, similar to Magura (2008), that it may be possible to accurately describe the velocity distribution in a CSP culvert in terms of the percent of flow area less than v_x/V_{ave}. Further research, with more varied flow conditions, is needed to confirm this and to determine what the relationship is. It is important to remember that the velocity distribution presented in this manner does not account for the areal distribution of the velocity contours. Specifically, it does not describe the size and shape of the lower velocity regions, and hence whether these areas may be useful for fish. For example, if 20% of the flow

area has a velocity less than the swimming capability of a specific fish species, that area might be clustered together such that a fish would be able to effectively fit within the area to swim. Alternatively, the area might be distributed in a thin band such that its size at any location is dwarfed by the physical size of the fish, rendering it useless to the fish. This limitation must be kept in mind when considering applications for this type of velocity distribution analysis.

4.5.4. Comparison to Ead et al. (2000) Velocity Distribution Model

Ead et al. (2000) proposed an empirical method for calculating the two-dimensional velocity distribution for fully-developed flow in a CSP culvert (as described in Section 2.2.3). In order to test this method, the Ead et al. procedure was followed to calculate the velocity contours for the fully-developed flow condition for each scenario that was studied (i.e., the non-embedded tests for each culvert slope and discharge). As described by Ead et al., the datum was located at the mid-point between the invert corrugation crest and trough and the k_s value was considered to be 0.013 m, equal to the corrugation amplitude of the model culvert. For each scenario, the Ead et al. method was used to calculate point velocities at the same set of data collection points as used in this study. The point velocities (as v_x/V_{ave}) produced by the Ead et al. method were then input into Surfer 8 and plotted using the same interpolation and data extraction techniques used to plot and analyze the experimentally collected data in terms of the cross section area falling between various v_x/V_{ave} contour values. An example of the calculations implementing the Ead et al. method is included in Appendix I.

The Ead et al. (2000) model requires input of the ratio of the centreline shear velocity to the global shear velocity. The value of the centreline shear velocity to be used in the calculation was determined from the measured velocity profiles for each slope and discharge for Holes 8, 9, 11 and 14 (i.e., those profiles considered to most closely represent the fully-developed flow condition), as described previously in Section 4.4.2. This value was then used to calculate the value of J (the ratio of centreline shear velocity to global shear velocity), as described in Ead et al. The resulting values are shown in Figure 4.37.

Theoretically, the value of J should be greater than one, as the shear velocity would be expected to be greatest at the culvert centreline (where flow is deepest) and decrease towards the sides of the flow area. However, as mentioned by Ead et al. (2000), the values of J that the Ead

et al. model were based on were almost all less than one, as shown in Figure 4.37. In their paper, Ead et al. did not specify how they anticipated the J value would be calculated (i.e., in the absence of experimental data to determine the centreline shear velocity), or if their intention was that an assumed value of J would be used.

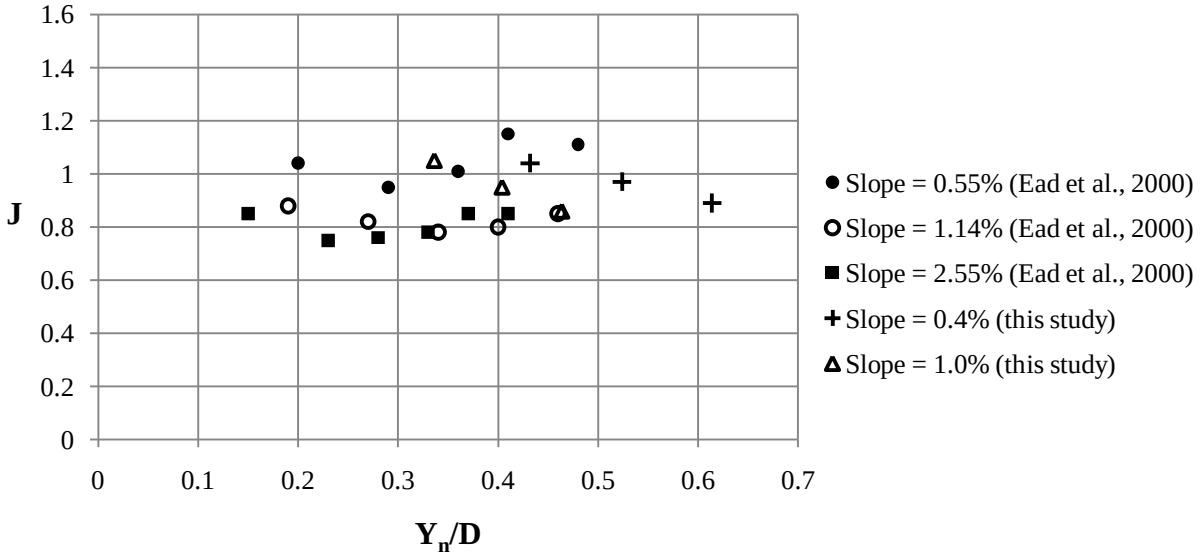

Figure 4.37: Experimental values of J and J values from Ead et al. (2000) (adapted from Ead et al. (2000)).

In order to analyze the deviation of the Ead et al. (2000) model from the experimental velocity data, each calculated point velocity was compared with the corresponding measured point velocity (based on average value obtained at Holes 8 and 14) and the percent error of the Ead et al. model value was determined. For the 0.4% slope, where velocity data was collected for both sides of the cross section, the data for both sides at each measurement point was averaged to determine a single experimental velocity measurement for each point location. For the 1.0% culvert slope, this procedure was not necessary as the data was collected for only one side of the cross section, so each individual velocity measurement could be compared directly to the Ead et al. model value. The results produced by the Ead et al. model were compared to the experimental data in terms of the average percent error for each cross section and the velocity distribution in terms of v_x/V_{ave} for each cross section. For illustrative purposes, contour plots of the point values of percent error in v_x/V_{ave} were also produced to indicate which portions of the flow area were subject to higher/lower degrees of error. These plots can be found in Appendix J and are discussed later in this section.

It was found that the velocity contour plots produced using the Ead et al. (2000) method based on the experimentally derived value of J (the centreline shear velocity as determined from the measured velocity profiles divided by the calculated global shear velocity), almost always significantly over-predicted the flow velocity. When the experimentally derived value of J was relatively close to 0.80 (within the range of the J values used by Ead et al.), the deviation was reasonably low, however, when the value of J approached or exceeded one the deviation was significant. These results are summarized in Table 4.6. In order to improve the results, instead of using experimentally derived J values, the Ead et al. (2000) model was used as described above, but with an assumed J value of 0.80. In all cases this resulted in a reduced average percent error in the point velocities, as shown in Table 4.7.

Table 4.6: Experimentally derived values of centreline shear velocity, corresponding J value and the average percent error in the point velocities calculated with the Ead et al. (2000) model compared to the average experimentally measured value from Holes 8 and 14.

Culvert Slope	Discharge, L/s	U_*, m/s	Centreline Shear Velocity, m/s	J	Average % Error in Point Velocity
0.4%	50	0.067	0.070	1.04	37%
	70	0.071	0.069	0.97	22%
	90	0.074	0.067	0.89	12%
1.0%	50	0.096	0.101	1.05	39%
	70	0.103	0.098	0.95	20%
	90	0.108	0.093	0.86	16%

Table 4.7: J values and resulting average percent error in point velocities for Ead et al. (2000) method using standard value of J of 0.80.

Culvert Slope	Discharge, L/s	J	Average % Error in Point Velocity
0.4%	50	0.80	5.3
	70	0.80	1.0
	90	0.80	0.6
1.0%	50	0.80	5.7
	70	0.80	0.9
	90	0.80	8.0

Figure 4.38 and Figure 4.39 show the comparison between two contour plots based on the velocity values produced by the Ead et al. (2000) model (using the J value of 0.80), versus the

plots produced using the experimental data collected at Hole 8. A complete set of contour plots produced with the Ead et al. model can be found in Appendix J. Figure 4.50 is visually the best match from the six comparison pairs that were produced (i.e., one pair for each combination of slope and discharge), in terms of the shape of the contours. The comparison shown in Figure 4.39 was more typical of the other results, where the contours are of the right magnitudes and appear to be of roughly the correct area, however, the shape, and specifically the orientation, of the Ead et al. produced contours, do not match the experimentally produced plots. The shape of the contours is not affected by the value of J.

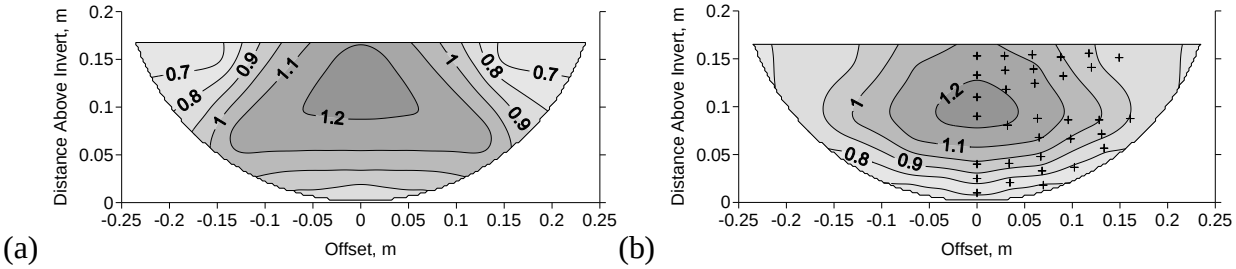

Figure 4.38: Contour plots of dimensionless streamwise velocity for the 1.0% culvert slope and 50 L/s discharge (a) produced from Ead et al. (2000) model to represent fully-developed flow condition and (b) from experimental data collected at Hole 8.

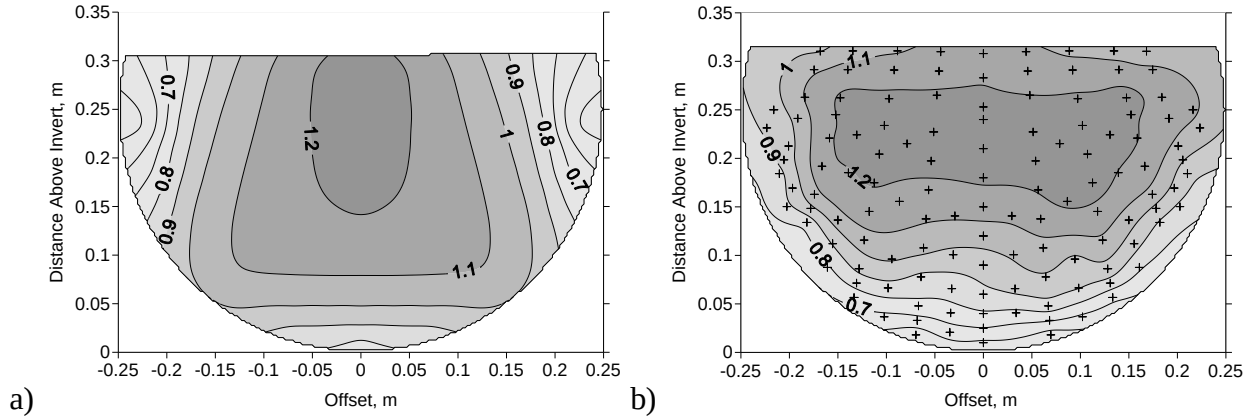

Figure 4.39: Contour plots of dimensionless streamwise velocity for the 0.4% culvert slope and 90 L/s discharge (a) produced from Ead et al. (2000) model to represent fully-developed flow condition and (b) from experimental data collected at Hole 8.

Comparing both sets of plots (i.e. Figure 4.38 and Figure 4.39), it can be seen that the Ead et al. (2000) model correctly predicts the area of highest velocity occurring within the central area of the flow. The Ead et al. plots indicate, however, that the regions of lowest velocity would occur primarily in the upper corners of the flow area. In comparison the

experimental results showed the lowest velocities occurring more continuously over the entire culvert boundary and, perhaps to a greater extent, at the culvert invert. The Ead et al. contour plots indicate that the low velocity areas around that perimeter (potential fish passage routes) are more fragmented, and therefore perhaps of more limited use, than those shown in the measured velocity contour plots. As both contour plots were built using the same data points, the results should not be influenced by the lack of data in the upper corners of the flow area, as this was the same in both cases. Overall, in terms of the shape of the contours, the Ead et al. model plots show a more vertical orientation, whereas the plots produced with the measured data generally show a horizontal orientation. Further, the measured plots from Hole 8 downstream generally reflect the depression of the maximum velocity below the water surface across the entire width of flow, whereas the Ead et al. plots do so to a lesser degree.

Figure 4.40 shows contour plots of the percent of error for the point velocities produced with the Ead et al. (2000) model compared to the measured point velocities for the cross sections shown in Figure 4.38 and Figure 4.39. Similar error plots for the other Ead et al. cross sections are contained in Appendix J. These plots confirm that the Ead et al. model is successful in correctly predicting velocities within the central part of the flow area (as evidenced by regions of 0% error), but underestimates velocities in the upper corners by up to -30% and overestimates velocities near the invert by up to +40%, when compared to the measured velocity data.

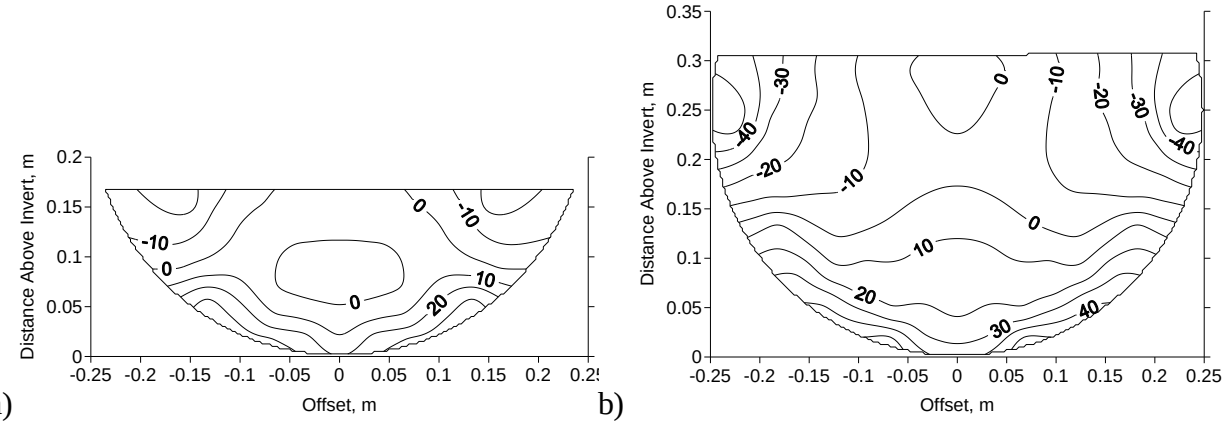

Figure 4.40: Contour plots of percent error in Ead et al. (2000) point velocities compared to measured point velocities for a) 1.0% culvert slope, 50 L/s discharge and b) 0.4% culvert slope, 90 L/s discharge.

Figure 4.41 and Figure 4.42 show the velocity distribution for the contour plots shown in Figure 4.38 and Figure 4.39, respectively. In both cases, the results are very close to that of the measured data (in this case an average of the data obtained at Holes 8 and 14). A complete set of similar velocity distribution plots for all the Ead et al. (2000) produced cross sections can be found in Appendix K. Based on these results, it is clear that in terms of the velocity distribution and amount of the cross section area falling within a specific velocity range the Ead et al. model appears to be accurate. However, this type of analysis does not assess the performance of the Ead et al. model in describing the spatial distribution of the velocity distribution in terms of the size, shape and continuity of the potential fish passage routes through the lower velocity regions.

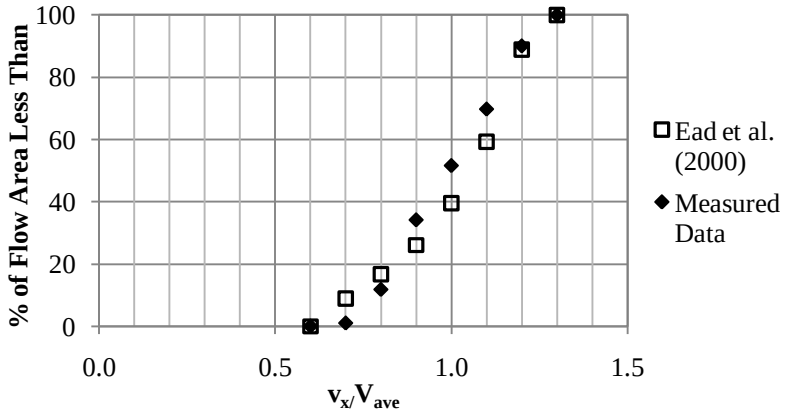

Figure 4.41: Velocity distribution for 1.0% culvert slope and 50 L/s for Ead et al. (2000) and experimental data shown in Figure 4.49.

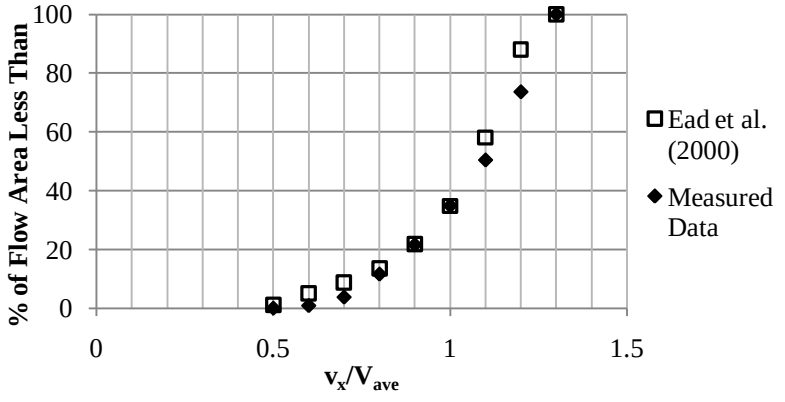

Figure 4.42: Velocity distribution for 0.4% culvert slope, 90 L/s for Ead et al. (2000) and experimental data shown in Figure 4.50.

Ead et al. (2000) recommend that their model is suitable to use for delineation of the areas available for upstream fish passage based on a fish's prolonged swimming speed

capability. Considering the results of this assessment, the Ead et al. model does appear to be suitable for such application, especially if the model is used to determine the velocity distribution and not necessarily the size or location of the lower velocity areas.

4.6. Turbulence Intensity Analysis

In addition to an assessment of the velocity conditions in a CSP culvert, a secondary objective of this study was to complete a preliminary assessment of the turbulence conditions. While the data set may be suitable for use in a more detailed turbulence study, this is beyond the scope of this immediate work. Instead, the focus of the following sections is to provide a high level assessment of the results in terms of general turbulence patterns and to attempt to provide some interpretation of the results in terms of fish passage.

4.6.1. Turbulence Intensity Profiles

As described in Chapter 3, for the purposes of this research turbulence has been assessed in terms of turbulence intensity (I_{mag}), or the root mean square of the instantaneous velocity series divided by the average velocity. Specifically, for this project the average velocity that has been used is based on the normal depth for each culvert slope and discharge combination (V_{aveYn}), as described in Section 4.5.2. As in the case of the velocity analysis, the turbulence intensity analysis was done in this manner to permit direct comparison of turbulence levels throughout the cross section, along the culvert length and between non-embedded and embedded tests. Using the more conventional method of calculating I_{mag}, based on the average velocity for each individual measurement point, would not have facilitated such direct comparison. The downfall of calculating I_{mag} based on V_{aveYn}, however, is that it does not account for the effect of the local velocity on a fish's perception of the turbulence and the impact on swimming effort, as described by Cotel et al. (2006) or Enders et al. (2003). At all locations where point velocities were measured, turbulence intensity was calculated and plotted in the same manner as the velocity data. A complete set of vertical turbulence intensity profiles can be found in Appendix L.

The turbulence intensity profiles exhibited consistent trends for both culvert slopes and all discharges. Generally, the turbulence profiles behave in an opposite manner to the velocity profiles, with the highest turbulence intensities located adjacent to the culvert invert and

decreasing towards the core of the flow area. Figure 4.43 illustrates the typical change in the centreline vertical turbulence intensity profiles along the length of the culvert, in this case for the 1.0% culvert slope and 70 L/s discharges.

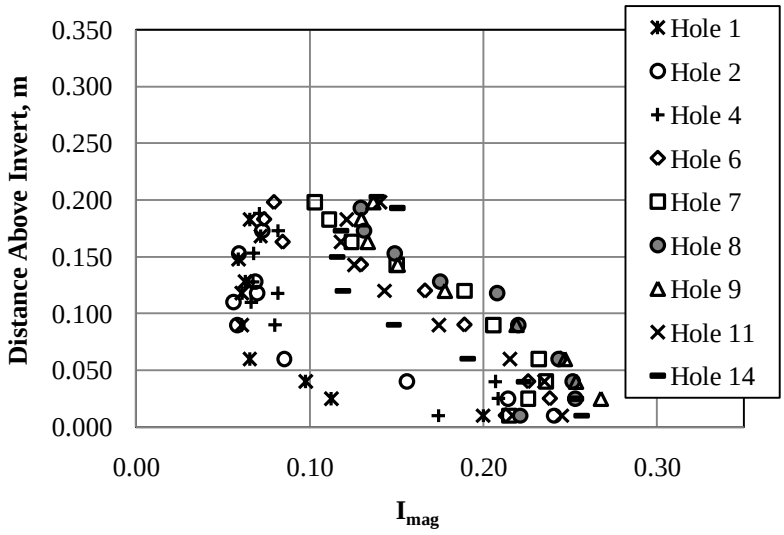

Figure 4.43: Centreline turbulence intensity profiles for the 1.0% culvert slope, 70 L/s discharge.

Examining Figure 4.43 and the figures in Appendix L more closely, it can be seen that for the holes nearest the inlet, the highest turbulence intensities occur nearest the invert and decrease with distance above the invert to some minimum value, which is then relatively constant through the remainder of the profile. At Hole 1 there was typically no increase, or even a slight decrease, in turbulence intensity at the water surface, reflecting the presence of the smooth flow observed at the water surface as the flow accelerated into the culvert. In contrast, the profiles from Hole 6 (4D from the culvert inlet) downstream show a consistent 'S' shaped pattern, achieving their maximum values near, but not immediately adjacent to, the culvert invert, then decreasing steadily before increasing again near the water surface.

4.6.2. Effect of Embedment on Turbulence Intensity Profiles

Figure 4.44(a) and (b) are examples of the turbulence intensity profiles generated by the 0.1D and 0.2D embedments and correspond to the non-embedded profile shown in Figure 4.43. The profiles for the embedded culvert indicate that, in terms of the location of peak values within the flow depth and change in magnitude with distance above the invert, the patterns remain unchanged from the non-embedded condition. However, the turbulence intensities downstream

from Hole 4 decrease throughout the profile, while those nearer to the inlet remained relatively unchanged. As such, the spread in the profiles (over the x-axis of the figures) decreases as a result of embedment.

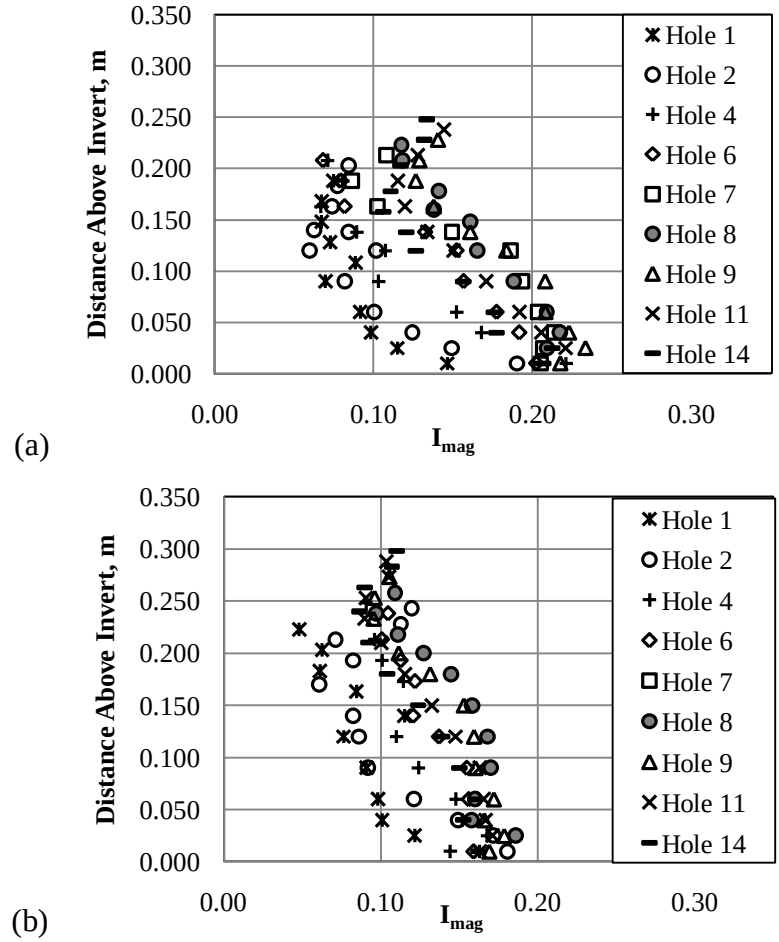

Figure 4.44: Centreline turbulence intensity profiles for the a) 0.1D embedded and b) 0.2D embedded for the 1.0% culvert slope and 70 L/s discharge.

Figure 4.45 shows the complete turbulence intensity profile data set for the 0.4% culvert slope testing, for all discharges and both the non-embedded and embedded tests. A set of similar plots for the 1.0% culvert slope can be found in Appendix L. Comparing the various plots, the effect of embedment on the holes near the inlet versus those further downstream can readily be identified. These plots confirm that embedment has relatively little effect on the profiles at Holes 1 and 2, aside from a slight reduction in peak value at the invert and a subtle change in the shape of the profiles. This even though, as shown in Section 4.3, the M1 backwater profile created by embedment extends to the inlet in all cases, especially for the 0.4% culvert slope. In

contrast, the plots showing the profiles for Holes 8-14 indicate that embedment is effective at reducing the magnitude of turbulence intensity throughout the profile. The turbulence intensity appears to decrease slightly more near the invert which also causes the profile to become more uniform though the flow depth.

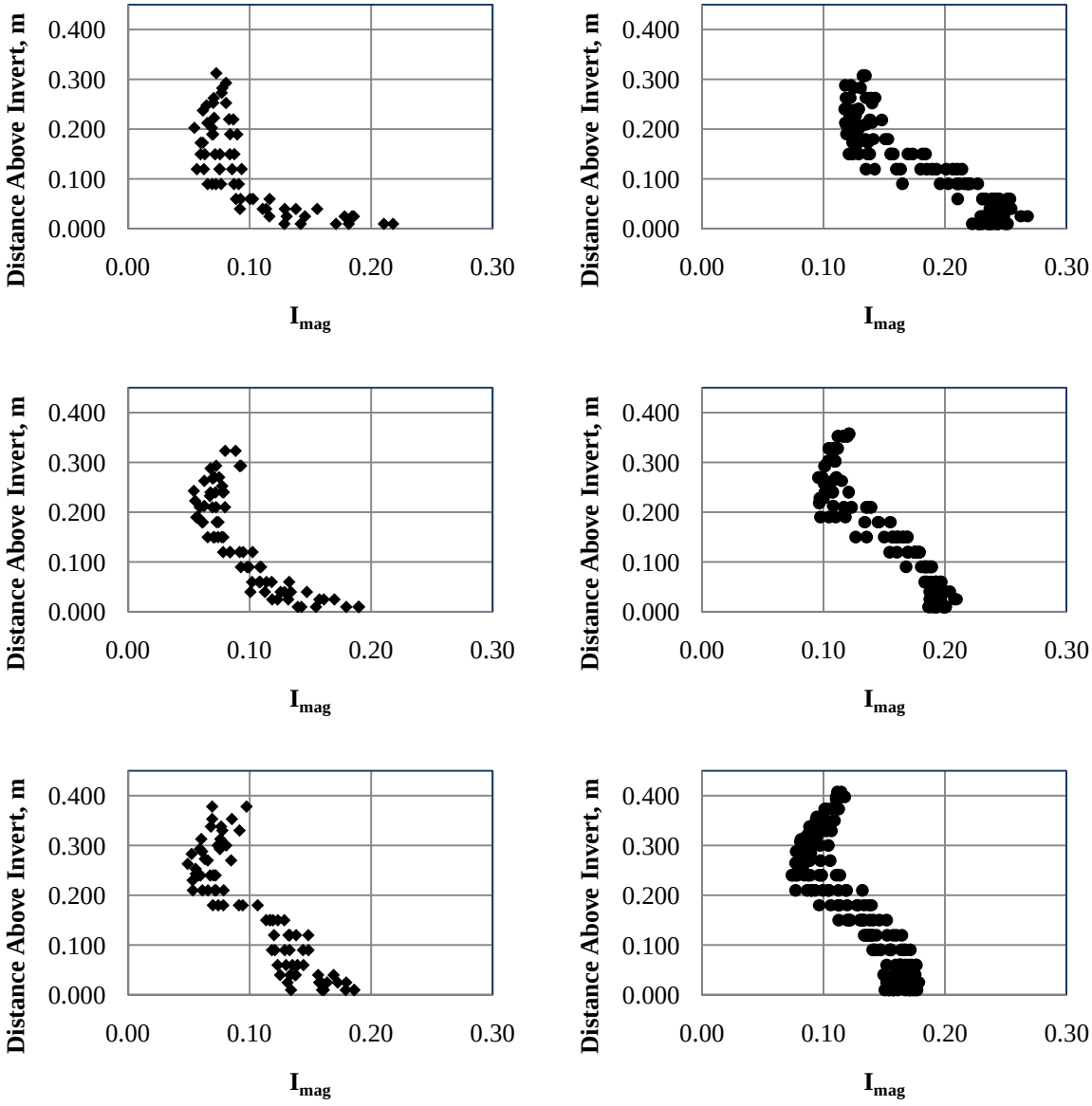

Figure 4.45: Centreline turbulence intensity profiles for the 0.4% culvert slope (50, 70, 90 L/s discharges) for Holes 1 and 2 (left column) and Holes 8-14 (right column). Top, middle and bottom rows are non-embedded, 0.1D embedded and 0.2D embedded test data, respectively.

4.6.3. Turbulence Intensity Cross Sections

This section explores the general patterns of turbulence intensity within the measured cross sections, both at the various cross section locations (e.g. near the inlet vs. further downstream, etc.), as well as changes in the turbulence intensity longitudinally along the culvert under the various test conditions.

The results of the cross sectional turbulence intensity analysis for Holes 1 and 2 were dependent on the ability to access the upper corners of the flow area with the ADV, which in turn depended on the flow depth as previously described. Additionally, at Hole 1, the water surface was not constant across the flow width, but was deeper at the centre of the cross section and slightly shallower in the separation region at the culvert sides. Thus, there was slightly less depth at the sides of the cross section to allow operation of the ADV probe. As a result, the presence of the higher turbulence regions at Holes 1 and 2, which were visually apparent (an example of which is shown in Figure 4.46), were not always able to be captured with the ADV. This was problematic for one or two of the shallower tests for the 0.4% culvert slope, but was a more significant factor for the 1.0% culvert slope tests, where measurements relatively close to the corner areas were only possible for one or two of the cross sections at Holes 1 and 2.

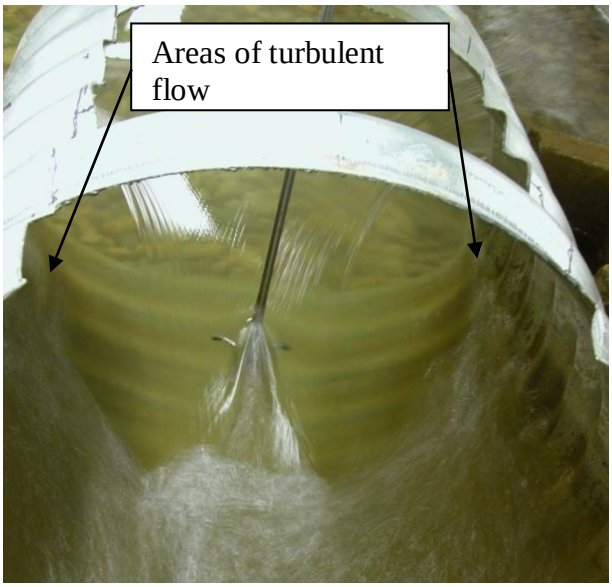

Figure 4.46: Typical conditions near the culvert inlet (looking upstream). Note the turbulence at the water surface at the sides of the flow area and the tongue of low turbulence flow at the centre of the flow area.

Bearing in mind the limitations described above, the model study results did show consistent patterns in the turbulence intensity contour plots along the length of the culvert. Figure 4.47 shows the typical change in the turbulence intensity distributions that was found to occur over the length of the culvert. A complete set of these contour plots can be found in the Appendix M. In all cases, the highest turbulence intensity magnitudes were located at Holes 1 and 2 in the upper corners and along the sides of the flow area, reflecting the effects of flow separation at the culvert inlet. Progressing downstream from the inlet, the magnitude of the peak turbulence intensity was found to decrease and the location of the regions of highest turbulence intensity migrated to the lower portions of the cross section. However, the percent of the cross sectional flow area with larger values of turbulence intensity was found to increase in the downstream half of the culvert. For example, in Figure 4.47(a) (Hole 1) there is a large central core of the flow area where the turbulence intensity is less than 0.1 (which can also be seen in Figure 4.46). In contrast, in Figure 4.47(b) (Hole 8) no portion of the flow area has a turbulence intensity less than 0.1, however, a large portion of the area has turbulence intensity greater than 0.2.

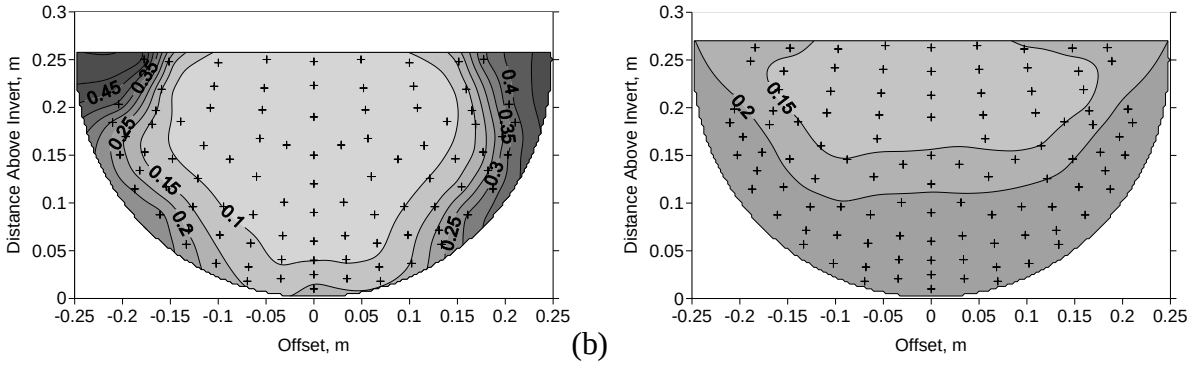

(a) (b)

Figure 4.47: Cross sections of turbulence intensity for the 0.4% culvert slope and 70 L/s discharge for the non-embedded culvert at (a) Hole 1 and (b) Hole 8.

In order to quantify the overall turbulence intensity conditions within the flow area, an average turbulence intensity value was calculated for each cross section. To do this, Surfer 8 was used to determine the area within each turbulence intensity contour interval, from which intensity-area integration was used to calculate a single turbulence intensity value (I_{magAve}), that represents the average conditions for each cross section. The results of this analysis, for each individual cross section and discharge, can be found in Appendix N.

Figure 4.48 and Figure 4.49 show the I_{magAve} results for the non-embedded tests for the 0.4% and 1.0% culvert slopes, respectively, and illustrate the change in turbulence conditions along the culvert length for each discharge. Generally, the average turbulence intensity of the cross section increases with distance downstream from the culvert inlet. The results for all discharges for the 0.4% culvert slope tests show a levelling off of the average turbulence intensity from Hole 8 to Hole 14 (8D to 15D downstream from the inlet). In contrast, the results for all discharges for the 1.0% culvert slope tests consistently indicate a peaking of turbulence intensity conditions at Hole 8 and a slight decrease at Hole 14. No consistent trend appeared to confirm that the average turbulence intensity increased with the discharge, although at many of the cross sections this was found to be the case.

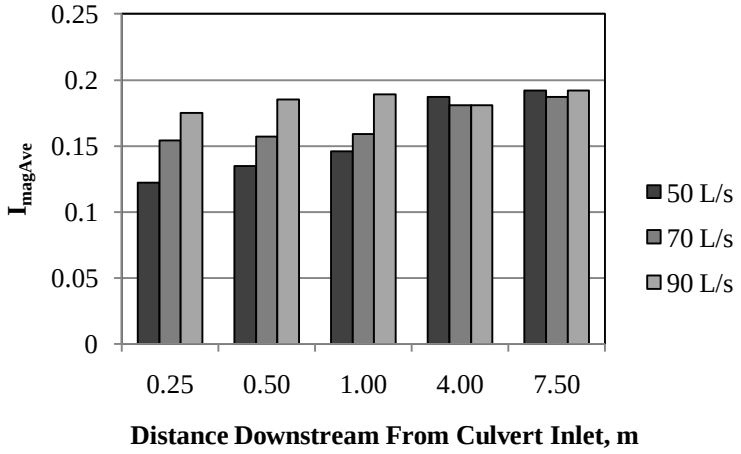

Figure 4.48: Average turbulence intensity for non-embedded 0.4% culvert slope.

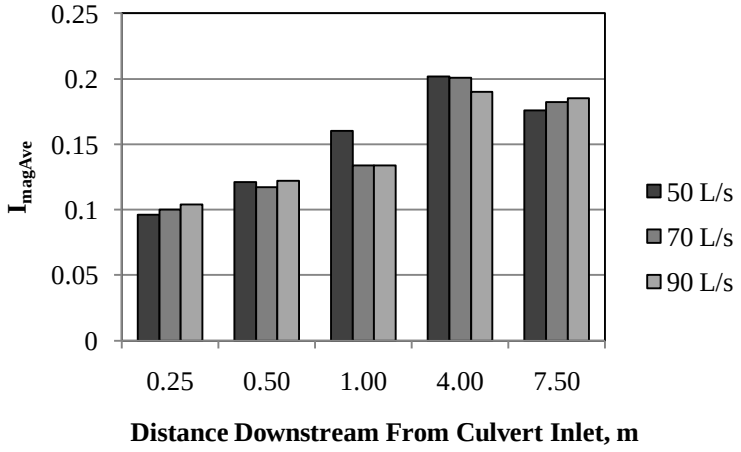

Figure 4.49: Average turbulence intensity for non-embedded 1.0% culvert slope.

Based on the literature review summarized in Chapter 2, it is clear there is some uncertainty regarding the influence of turbulence on fish, as well as a lack of information specific to the impact of turbulence on fish passage through culvert fishways. Additionally, any specific conclusions regarding fish passage require consideration of a specific fish species with known or assumed swimming abilities and preferences. In terms of this research, some general conclusions can be drawn from the results based on the assumption that high turbulence intensity levels detract from the likelihood of successful fish passage and are a potential barrier to fish attempting to traverse through a culvert.

In this discussion, it is important to remember that, for the purposes of this study, turbulence intensity has been defined with respect to the mean velocity calculated for normal flow conditions. In this way, each turbulence intensity value can be compared relative to other values produced in this study, irrespective of local velocities. The values cannot, however, be compared to values outside of this study.

While the local magnitudes of turbulence intensity in the corners at Hole 1 and 2 are high, there is a large central core of low turbulence intensity flow generated as the flow accelerates into the culvert. In fact, the cross section area of the low turbulence intensity core is larger near the inlet than at any other cross section along the culvert length. Therefore, assuming a fish would preferentially elect to swim through the low turbulence core, whether this area presents a potential barrier to fish passage would depend on the velocity that a specific species or individual can accommodate with its burst swimming speed.

At the downstream end of the culvert, the higher turbulence intensity regions occur in the vicinity of the culvert invert and cover a larger area of the flow cross section. Therefore, depending on the preferences and swimming abilities of a specific fish, these turbulence conditions may also force a fish to swim in the higher velocity flow within the central core of the cross section.

In general, it is obvious that the areas of higher turbulence intensity around the culvert margin are also the areas of lowest velocity that were identified in Section 4.5. It is therefore interesting to note that if I_{mag} were calculated based on point velocities, the differences in turbulence intensity across the cross section would have been amplified (e.g. high RMS values

divided by low velocity values would have resulted in larger values of I_{mag} than when divided by the average velocity and vice versa for low RMS values).

These reverse patterns of turbulence and velocity just described mean that the areas that would be assumed to be the best for fish passage in terms of velocity are the least favourable in terms of turbulence intensity. Based on this, it is clear that the route selection of a fish attempting to travel upstream through a CSP culvert would be a balance between their preferences for velocity and relative swimming capabilities as well as their tolerance for turbulence and the impact that turbulent flow conditions have on their swimming ability.

4.6.4. Effect of Embedment on Turbulence Intensity Cross Sections

Figure 4.50 and Figure 4.51 illustrate the effect of embedment on the I_{magAve} results, in this case showing the average value for all discharges at each cross section location. The I_{magAve} results for each individual discharge and embedment combination are provided in Appendix N. As can be seen in Figure 4.50 and Figure 4.51, the effect of embedment varies with the distance downstream from the inlet. At Holes 1 and 2 (0.5 and 1.0D downstream from the inlet), embedment either makes virtually no difference in the average turbulence intensity, or, in most cases, increases the average turbulence intensity. This can partially be attributed to the fact that the flow area near the inlet did not increase with embedment as much as it did further downstream, as discussed in Section 4.3 (i.e. M1 profile effect). The only example in the results where embedment caused a decrease in turbulence intensity at Holes 1 and 2 is for the 0.4% culvert slope, 90 L/s discharge, which is shown in Figure P3 in the appendix. This is also one of the tests for which embedment produced the greatest increase in flow depth near the inlet.

In contrast to the results at Holes 1 and 2, at Holes 8 and 14 (8 and 15D downstream from the inlet), in all cases embedment reduces the average turbulence intensity, with the magnitude of the decrease proportional to the depth of embedment. At Hole 4 (2D downstream from the inlet) the results are mixed, with some cases showing a decrease, while others showed an increase in I_{magAve}. In either case, the magnitude of the change in I_{magAve} resulting from the embedment at Hole 4 is much less than what occurs further downstream.

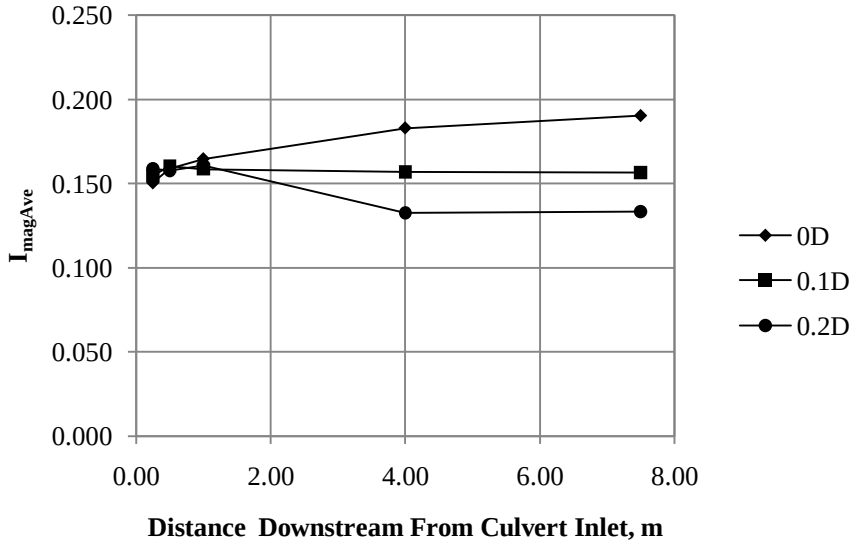

Figure 4.50: Variation of average turbulence intensity along the culvert for 0.4% culvert slope (average of all discharges).

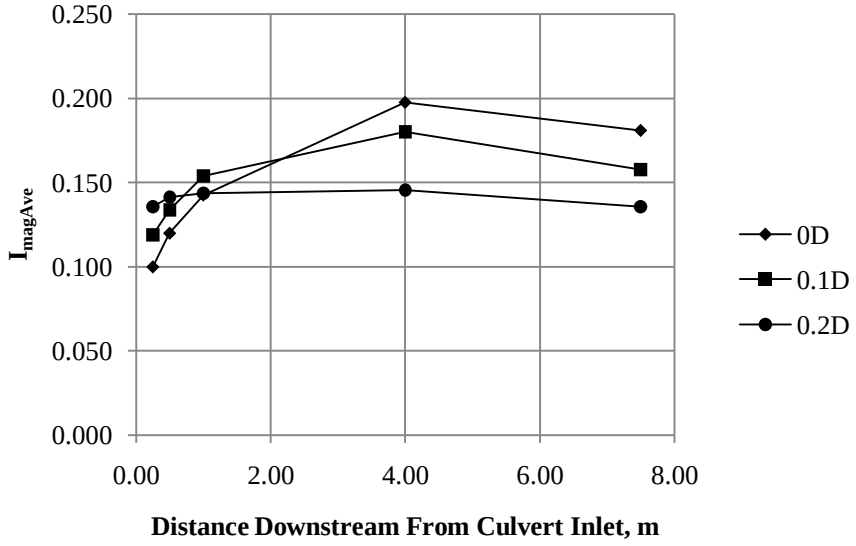

Figure 4.51: Variation of average turbulence intensity along the culvert for 1.0% culvert slope (average of all discharges).

Assuming that a reduction in turbulence intensity is beneficial to fish passage, these results indicate that for the conditions tested, the effect of embedment on the turbulence intensity contour plots is negligible or detrimental at Holes 1 and 2 (i.e., closest to the inlet), but favourable in all cases at Holes 8 and 14 while the results at Hole 4 are mixed. If conditions at the inlet are assumed to be the primary barrier to successful fish passage, it may be concluded

that for these experiments, embedment of a culvert does not provide an improvement for culvert fish passage in terms of turbulence intensity. However, the results appear to confirm that the effectiveness of embedment for reducing turbulence intensity at the inlet is linked to the depth of the backwater profile at the inlet. Although in this case the M1 profile did extend to the inlet for all of the tests completed, there appears to be a minimum depth increase at the inlet required to effectively drown out the flow contraction sufficiently to reduce the turbulence intensity. As the case for reducing the flow velocity, this analysis suggests that when selecting an embedment depth for a specific culvert installation, special consideration must be made regarding the length of the culvert compared to the length of the M1 profile.

4.7. Baffled Invert

At the completion of the plain invert testing, weir baffles were installed in the culvert as described in Chapter 3. The baffled invert condition was tested for the non-embedded, 0.1D and 0.2D embedments, at the 1.0% culvert slope and 90 L/s discharge. Velocity measurements were taken at four locations within one baffle spacing: at 0.25L upstream of the baffle, at the baffle and at 0.25L and 0.5L downstream of the baffle (where L is the baffle spacing, in this case 0.476 m or approximately 1D).

4.7.1. Non-Embedded Flow Depth and Velocity Analysis

For the flow conditions tested, the baffles operated in the streaming mode, as defined by Rajaratnam et al. (1988), with the water surface in the downstream pool always greater than the baffle height. Rajaratnam et al. describe the mechanics of the streaming flow regime as being a stream of approximately constant thickness that flows over the weirs and over the surface of the water contained within the pools between the weirs, as illustrated in Figure 2.8. In this experiment, the depth of flow varied along the culvert, with slight but visible increases in the water surface in the area of each baffle, as can be seen in Figure 4.52. The fluctuation in water surface was greatest at the culvert centreline and minimal near the sides.

Rajaratnam et al. (1988) determined that the dimensionless discharge in a pool and weir fishway of between 2% and 15% slope is related to the depth of flow over the weir as indicated in Equation 2.12. For this experiment, the streaming flow depth is 0.230 m (depth over the weir

crest). Applying Equation 2.12 and the baffle spacing of 0.476 m gives a dimensionless discharge of 2.16. The actual value of dimensionless discharge, viz.

$$Q_* = \frac{Q}{\sqrt{gSD^5}} \text{ (Rajaratnam and Katopodis, 1990)} \qquad (4.3)$$

is 1.63, therefore the conditions in this experiment do not appear to be well represented by the Rajaratnam et al. (1988) relationship.

Figure 4.52: Photograph of the inlet with plain invert (top) and the baffled invert (bottom). The fluctuating water surface resulting from the baffles is visible in the bottom photo.

Ead et al. (2002) also proposed a relationship between dimensionless discharge and the ratio of the characteristic depth to the culvert diameter as shown in Equation 2.15. The characteristic flow depth for a baffled invert culvert was defined by Ead et al. as the depth of flow occurring at the mid-point between two baffles, within the region of fully-developed flow. As the baffle spacing tested was located downstream of Hole 8, it would fall within the fully-developed flow region and therefore the characteristic depth was measured to be 0.272 m (measured from the culvert invert). For a baffle height of 0.1 times the culvert diameter, the values of coefficients α and β proposed by Ead et al. for Equation 2.15 were $\alpha = 9.39$ and $\beta = -1.18$. Applying Equation 2.15 to the measured characteristic depth, along with these values for α and β, results in a dimensionless discharge of 2.14. Similar to the results produced by equation 2.12, it appears that the conditions studied here produced slightly different results than those represented by the equation in Ead et al. (2002). The work of Rajaratnam and Katopodis (1988) and Ead et al. were both based on large data sets, whereas the baffled invert component of the research documented here was limited to only one set of fully developed flow conditions. Therefore, the strength of the comparisons to Equations 2.12 and 2.15 is very limited.

Figure 4.53 shows the centreline vertical velocity profiles for the non-embedded baffled invert culvert at the various sampling locations. The results show that the velocity conditions above the baffle height vary little with position relative to the baffle. Similar to the results of Rajaratnam and Katopodis (1990), the profiles located both upstream and downstream from the baffle show a discontinuity in the profile at approximately the height of the baffle crest (0.05 m above the invert). The velocity measurements at locations 0.25L and 0.5L downstream from the baffle confirm the presence of a re-circulating zone in the pool. Comparing the velocities measured for the profiles at these two locations, a maximum negative velocity of approximately 0.2 times the maximum forward velocity was found to occur. The negative flow velocities were not present at the sampling location located 0.25L upstream of the baffle, indicating that the re-circulating zone did not occupy the entire baffle spacing.

Rajaratnam and Katopodis (1990) found that the maximum, or barrier, velocity ($V_{b)}$ in the culvert centreplane occurred at the baffle. The results in Figure 4.53 indicate that in this experiment the overall maximum velocity at the centreline occurs either at the baffle, or at one of the locations downstream from the baffle, with the results being very similar between locations.

However, at the elevation of the baffle crest, where there is slightly more spread in the data points from each cross section, the maximum velocity is located at the baffle cross section. Applying Equation 2.14 with the measured characteristic depth gives a theoretical barrier velocity of 1.2 m/s. This compares reasonably well with the measured barrier velocity of 1.13 m/s.

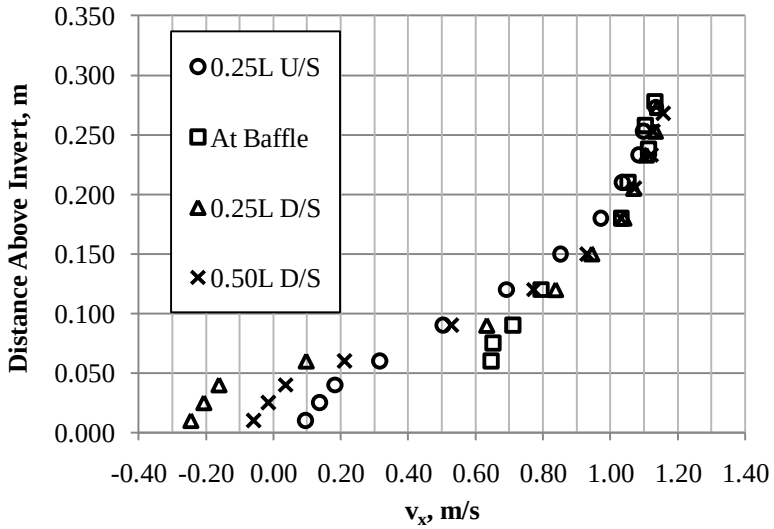

Figure 4.53: Centreline velocity profiles for non-embedded baffled invert culvert. The top of the baffle is located at 0.05 m above the invert. Test conditions were 1.0% culvert slope and 90 L/s discharge.

Figure 4.54 shows the velocity profiles above the baffle at various transverse offsets from the culvert centreline. These profiles were extracted from the velocity cross sections using Surfer 8 to slice the contour plot at the desired offsets as described in Section 4.4.2. This plot illustrates that, although the peak velocity magnitude is located at the culvert centreline near the water surface, nearer to the baffle crest where fish are most likely to be located, the greatest velocity is actually located somewhere between the centreline and the culvert wall and not in the centre of the culvert barrel. Therefore, in terms of velocity, for a fish passing directly over the baffle, the easiest path would actually be directly at the culvert centreline, which is not the intuitive conclusion.

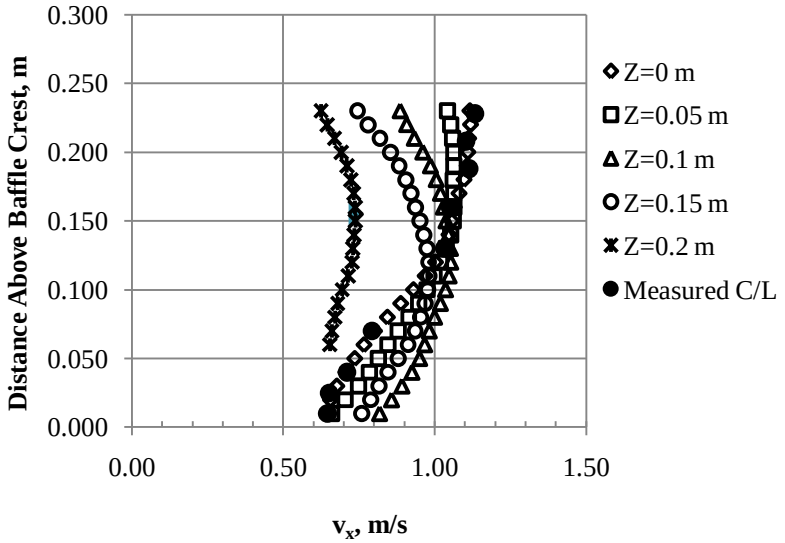

Figure 4.54: Velocity profiles at baffle for various transverse offsets from culvert centreline. Test conditions were 1.0% culvert slope and 90 L/s discharge.

The velocity contour plots from the non-embedded test are shown in Figure 4.55. For the purposes of plotting the cross sections, an average depth (measured mid-way between the centreline and the culvert wall) was used, as the depth at the centreline was not always representative of the entire flow width. Negative velocity zones are indicated as white areas within the cross section. The contour plots show consistent patterns between the measurement locations, clearly indicating the presence of a lobe of higher velocity flow extending down towards the side of the culvert. At the baffle, lower velocities occur at the centre of the baffle as opposed to closer to the sides, as noted with the offset velocity profiles in Figure 4.54.

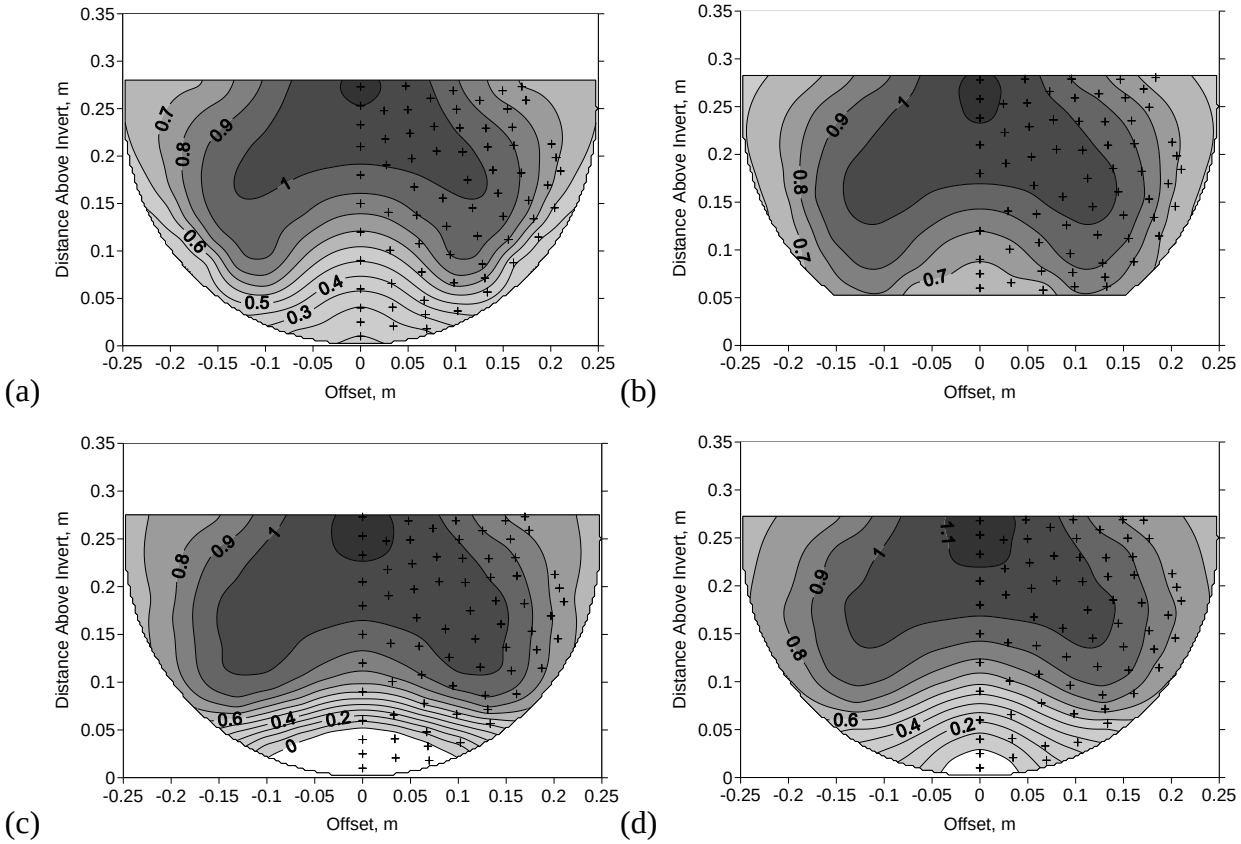

Figure 4.55: Streamwise velocity contour plots in units of m/s, for non-embedded baffled invert trial (a) 0.25L upstream of baffle, (b) at baffle, (c) 0.25L downstream from baffle, and (d) 0.5L downstream from baffle. Negative velocity regions in (c) and (d) are shown as white. Test conditions were 1.0% culvert slope and 90 L/s discharge.

4.7.2. Non-Embedded Turbulence Intensity Analysis

The velocity cross sections collected for the baffled invert condition were also analyzed in terms of turbulence intensity using the same method described in Section 4.6. The results for the non-embedded test case are shown in Figure 4.56. Rajaratnam and Katopodis (1990) describe a turbulent shear layer caused by the streaming flow skimming over the water in the pool below the baffle. This was confirmed in this experiment by the presence of a zone of peak turbulence intensity located at the elevation of the baffle crest at all sampling locations as can be seen in Figure 4.56. At the cross section located 0.25L downstream from the baffle, the shape of the higher turbulence intensity zone was wider than at the other sampling locations, extending almost the full width of the baffle crest as can be seen in Figure 4.56 (c).

Values of average turbulence intensity were calculated for each of the cross sections in the same way as the plain invert tests (Section 4.6.3). For the non-embedded baffled invert,

I_{magAve} values for the four cross sections vary little, ranging from 0.215 to 0.223. In contrast, for the 1.0% culvert slope, non-embedded, 90L/s discharge, plain invert cross sections, the average turbulence intensity ranged from 0.104 to 0.190. The value of 0.190 is located at Hole 8 which is in approximately the same portion of the culvert as the baffle spacing that was studied. Comparing these results, the presence of the baffles, although they may create low velocity zones, also increases the overall turbulence conditions in the culvert.

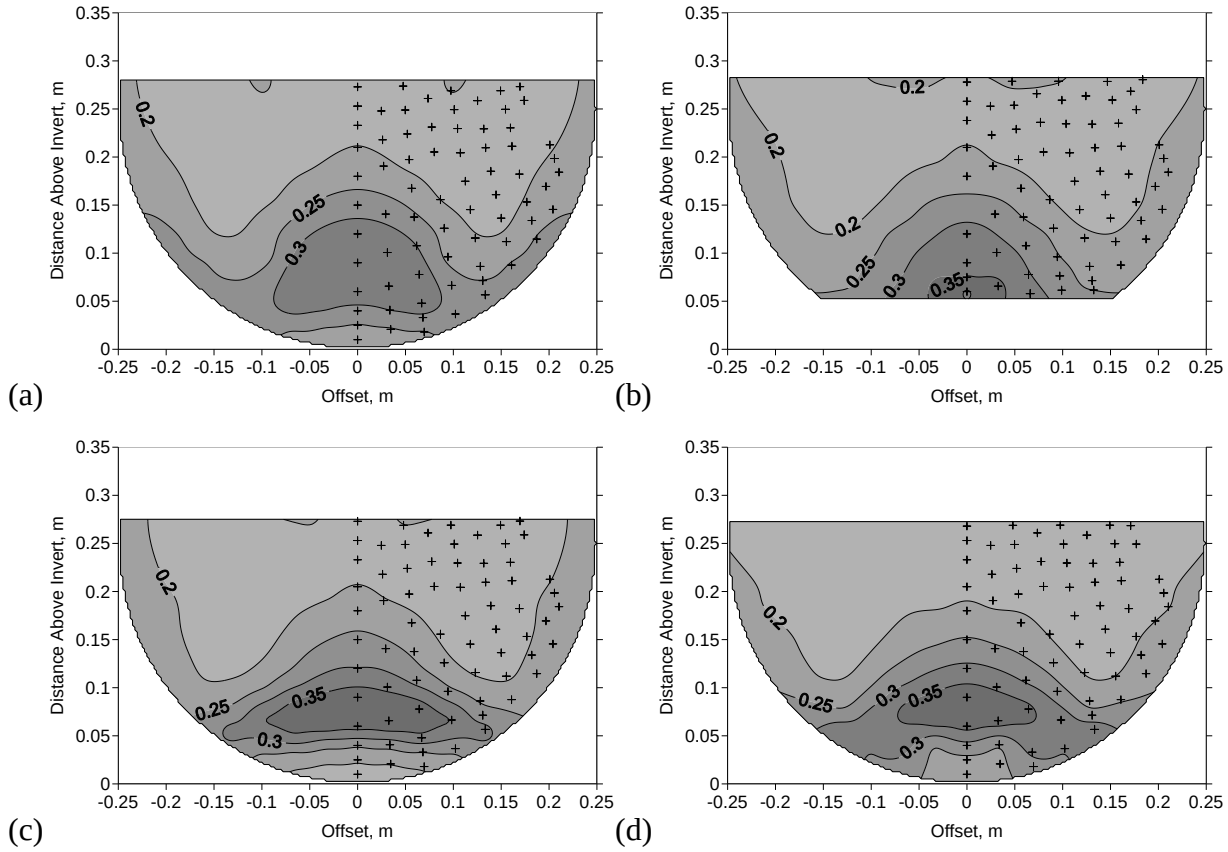

Figure 4.56: Turbulence intensity contour plots for non-embedded baffled invert culvert (a) 0.25L upstream of baffle, (b) at baffle, (c) 0.25L downstream from baffle, and (d) 0.5L downstream from baffle. Test conditions were 1.0% culvert slope and 90 L/s discharge.

4.7.3. Effect of Embedment on Velocity Distribution

In the embedded tests, the effect of the baffles on the depth of flow became less noticeable with increasing embedment. That is, the fluctuations in the water surface were reduced in relation to the embedment depth, as the baffles became less obtrusive to the flow and acted more like roughness elements instead of weirs. This effect was also noted by Rajaratnam and Katopodis (1990).

The impact of embedment on the velocity profiles at 0.2D embedment is shown in Figure 4.57 (a similar plot for 0.1D embedment is contained in Appendix O). Comparing these results to those of the non-embedded culvert (Figure 4.65), it can be seen that the barrier velocity at the baffle is reduced to 0.93 m/s from 1.13 m/s (the value is 1.11 m/s for the 0.1D embedment level). The shape of the profile also changes slightly, exhibiting the velocity dip near the water surface not present in the non-embedded or 0.1D embedded tests, but as seen in many of the velocity profiles for the plain invert tests, especially for the deeper flow conditions.

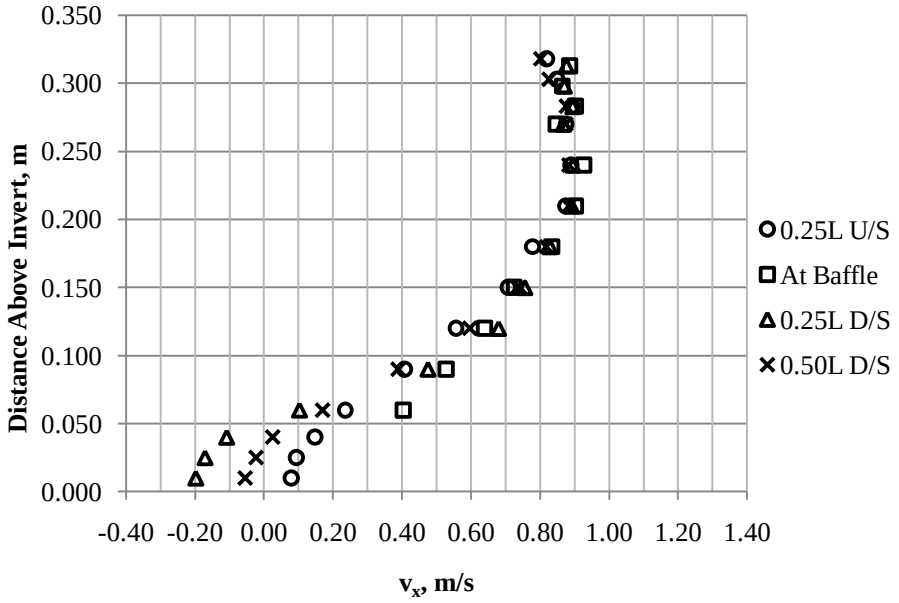

Figure 4.57: Centreline velocity profiles for 0.2D embedded baffled invert. Test conditions were 1.0% culvert slope and 90 L/s discharge.

In the case of the 0.2D embedment, the maximum negative streamwise velocity is -0.20 m/s, or 0.22 times the barrier velocity, similar to the ratio for the non-embedded case. Because both the above-baffle velocities and the negative velocities in the re-circulating zone decrease with embedment, the velocity profiles for the 0.1 and 0.2D embedded tests show a reduced discontinuity at the baffle when compared to the non-embedded profiles.

Similar to Figure 4.54 for the non-embedded test, Figure 4.58 shows velocity profiles above the baffle at various offsets for the 0.2D embedment (see Appendix O for the 0.1D embedded plot). As was the case for the non-embedded trial, the results indicate that directly above the baffle the velocity is at its peak at an offset of approximately 0.1 m from the culvert centreline, and that the lowest velocity area, where a fish may be most likely to pass, is located at

the centre of the baffle. Comparing the plots for the embedded tests to the non-embedded test, it is apparent that embedment does somewhat reduce the variability in the velocity directly above the baffle (the offset profiles become more tightly clustered).

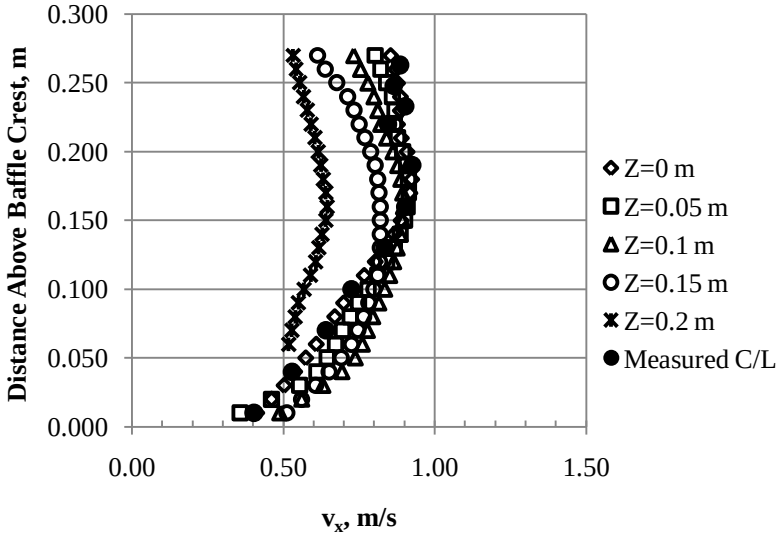

Figure 4.58: Velocity profiles at the baffle for various transverse offsets from the culvert centreline for the 0.2D embedded test. Test conditions were 1.0% culvert slope and 90 L/s discharge.

The velocity contour plots for the cross section locations at the baffle and at 0.25L downstream from the baffle for the 0.2D embedded baffled invert test, are shown in Figure 4.59 (remaining contour plots for the 0.2D embedded test, as well as the 0.1D embedded test, are located in Appendix O). Comparing this figure to Figure 4.55, it can be seen that the highest velocity contour has been reduced from 1.1 m/s for the non-embedded culvert to 0.9 m/s for the 0.2D embedded culvert, but that the lobed shape of the contours remain. Also of note is that the position of the highest velocity area remained at approximately the centre of the culvert (i.e., at about 0.25 m above the invert), regardless of the embedment. Embedment appears to have relatively little effect on the negative velocity region downstream of the baffle, with the size and shape of the area remaining relatively consistent.

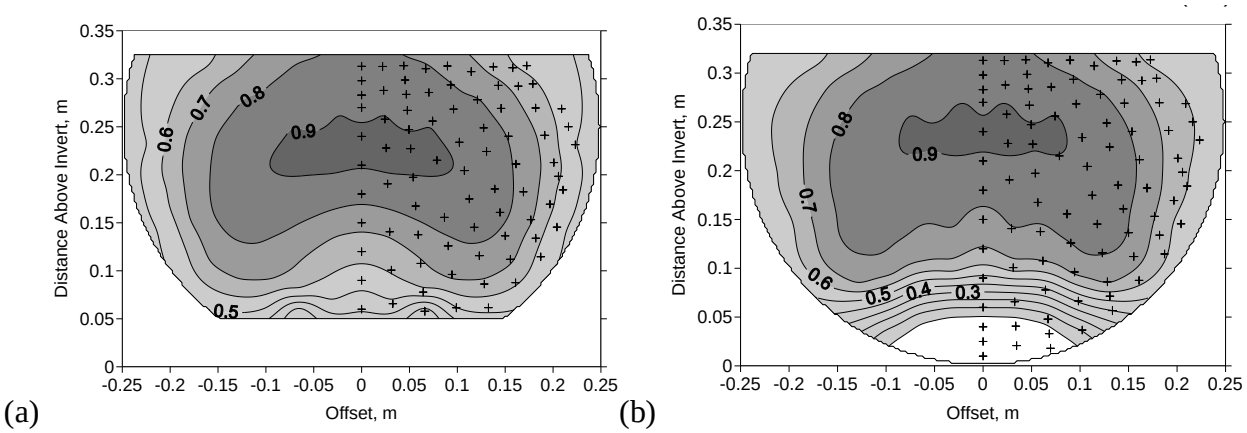

Figure 4.59: Velocity contour plots for 0.2D embedded baffled invert in units of m/s, for (a) at baffle and (b) 0.25L downstream from baffle. Negative velocity regions are shown as white. Test conditions were 1.0% culvert slope and 90 L/s discharge.

4.7.4. Effect of Embedment on Turbulence Intensity Distribution

In terms of turbulence intensity, embedment reduced both the peak values as well as overall turbulence at all of the cross sections sampled. Figure 4.60 shows the turbulence intensity contour plots for the 0.2D embedded culvert for the cross section locations at the baffle and 0.25L downstream from the baffle (remaining plots for 0.2D and 0.1D embedment are located in Appendix O). Comparing this to Figure 4.56, it is clear that the pattern of the contours is similar and that the shear between the streaming flow and the re-circulating flow between the baffles is still clearly evident. Figure 4.61 illustrates the change in average turbulence intensity for each cross section between the non-embedded and embedded tests and confirms the fact that embedment reduces the turbulence generated by the baffled invert in all cases.

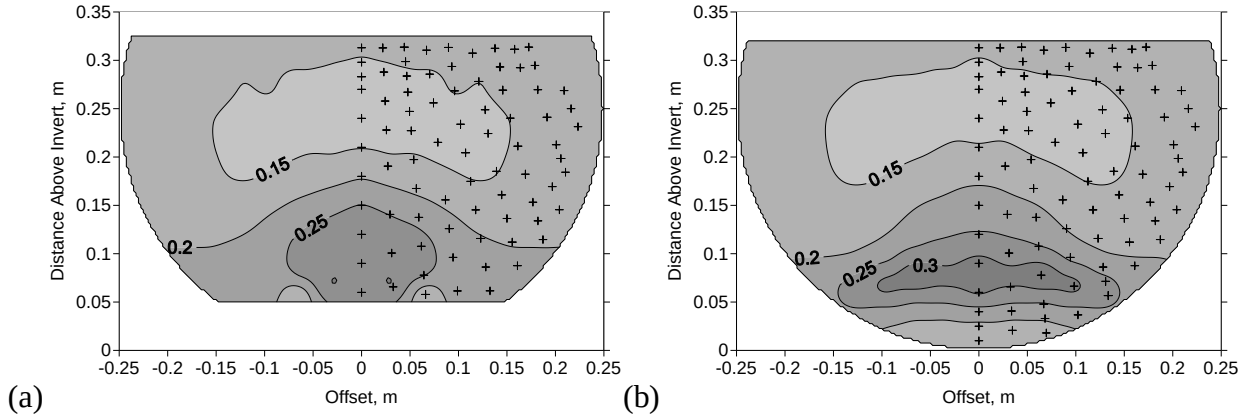

Figure 4.60: Turbulence intensity contour plots for 0.2D embedded baffled invert for (a) at baffle and (b) 0.25L downstream from baffle. Test conditions were 1.0% culvert slope and 90 L/s discharge.

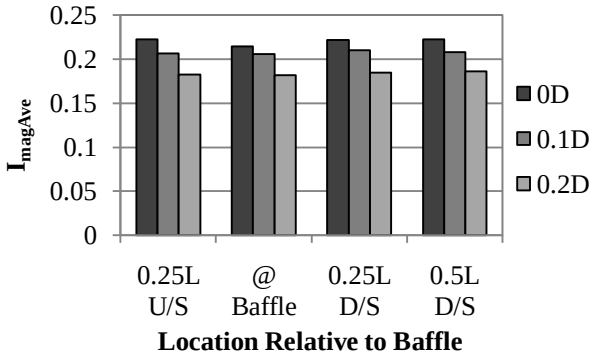

Figure 4.61: Average turbulence intensity values calculated for the baffled invert cross sections.

5. SUMMARY, CONCLUSIONS AND RECOMMENDATIONS

5.1. Summary of Experimental Findings

The purpose of this study was to gain insight into the characteristics of flow through a non-embedded and embedded CSP culvert in terms of both velocity and turbulence conditions. This section summarizes the findings presented in Chapter 4, organized into the three categories of data quality, the plain invert culvert and the baffled invert culvert. In the following section, the pertinent results are then presented to address each one of the research objectives set-out in Chapter 1.

Quality of Experimental Results

The percent error of the discharge calculated from velocity-area integration of the contour plots created with the measured data, compared with the discharge measured with the magnetic flow meter, are between +/- 10% for the 102 cross sections sampled. This is comparable to published results from similar research programs. Therefore, it is concluded that the data set on which the study's results are based is of good quality.

Plain-Invert Culvert

- All water surface profiles through the culvert show a region just downstream from the culvert inlet where the flow area exhibits a contraction followed by a gradual expansion.
- For the non-embedded culvert, the depth of flow stabilizes at approximately normal depth (for these experiments this was also the tailwater depth) at between four and eight culvert diameters downstream from the inlet.
- The water surface profiles for the embedded culvert tests show the magnitude of the inlet contraction is reduced with embedment in proportion to the depth of the backwater profile at the inlet.
- For the non-embedded culvert tests, the velocity profiles measured along the culvert centreline show a gradual transformation progressing downstream from the inlet, until a point is reached where the profiles become relatively invariant with further distance. Observation of these velocity profiles confirm that flow in the non-embedded culvert is fully-developed at approximately four to eight diameters downstream from the inlet. For the purposes of further

analysis, the flow is therefore considered to have achieved full development by eight diameters downstream (in this case the mid-point of the culvert length).

- A dip in the streamwise flow velocity at the water surface is not observed to occur in the non-embedded culvert until approximately 2.0 m (4D) downstream from the inlet. Upstream from that point, the maximum velocity in the profile occurrs at the water surface.
- The shear velocity distribution in the fully-developed flow region in the non-embedded culvert test shows that the shear velocity is greatest near the culvert centreline and decreases towards the culvert sides. The rate of decrease is relatively low from the culvert centreline to an offset of 0.4 of the culvert radius, but is significantly greater from that point to the culvert wall.
- The calculation of shear velocity was found to be dependent on the selection of datum within the culvert (i.e., corrugation crest, trough, or some point in between).
- When the centreline velocity profiles for the portion of the non-embedded culvert where the flow was fully-developed are compared to the log-law velocity distribution, the results indicate that the equivalent roughness of the corrugations (k_s) is between approximately 0.012 m and 0.022 m, or from approximately one to two times the corrugation amplitude of 0.013 m, when the analysis datum is set at the corrugation crest.
- Embedding the culvert reduces the flow velocity throughout the flow depth, however, the effect increases approaching the water surface. As a result, more uniform vertical velocity profiles are produced by embedding the culvert.
- The velocity contour plots for the non-embedded culvert confirm that at all discharges and locations along the culvert there is a significant portion of the cross section area with velocity less than the normal depth average velocity. This area is smaller for the locations near the culvert inlet, due to the contracted flow area, but increases significantly approximately 2D downstream from the inlet.
- The effectiveness of an embedment depth (e.g. 0.1D or 0.2D) at increasing the amount of the cross section area less than the average velocity calculated based on normal depth decreases with increasing discharge.
- The effectiveness of embedment along the culvert is related to the length of the M1 backwater profile relative to the culvert length. In the case of the tests conducted as part of this study the profile extended the entire length of the culvert.

- The percent of the flow area less than the actual average velocity (V_{ave}) for each cross section (calculated based on measured flow depth) varies from approximately 0.4 V_{ave} to 1.4 V_{ave} for both non-embedded and embedded test conditions. Plotted together, the data from all experimental runs clusters approximately along a representative curve regardless of discharge or embedment.
- The measured velocity cross sections for the fully-developed flow region in the non-embedded culvert tests compare well with representative cross sections produced using the Ead et al. (2000) model, especially when a consistent value of 0.8 for the J parameter is applied. This confirms that the Ead et al. model may be suitable for predicting the velocity distribution in a non-embedded CSP culvert.
- Vertical profiles of turbulence intensity at the culvert centreline generally behave in a reverse manner to the velocity profiles, with the turbulence intensities being highest near the invert and decreasing towards the core of the flow area.
- The turbulence intensity profiles beyond approximately 2D downstream of the inlet show a distinct and consistent 'S' shaped configuration.
- The average cross section turbulence intensity is lowest for cross sections near the inlet and increase with distance downstream from the inlet.
- The highest magnitudes of turbulence intensity occur in the upper corners of the flow area just downstream from the inlet, due to the flow separation at the water surface. Further downstream, the areas of higher turbulence intensity in each cross section occupy the lower portion of the cross section area, near the culvert invert.
- The effect of embedment on the turbulence intensity distribution varies with distance downstream from the inlet. At the locations measured near the inlet, embedment makes either no difference in the value of average turbulence intensity for the cross section, or, in many cases, increases the average turbulence intensity. Beyond 8D downstream from the inlet, embedment reduces the average cross section turbulence intensity in all cases.

Baffled-Invert Culvert

- For the non-embedded culvert, the weir baffles created flow conditions similar to those described by Rajaratnam et al. (1988) and Rajaratnam and Katopodis (1990).
- The velocity contour plots at the baffle location show a consistent lobed shape, with the maximum velocity at the baffle crest occurring at an offset position from the culvert centreline and the minimum velocity occurring near the centreline.
- Contour plots of turbulence intensity show a central core of high turbulence at approximately the baffle crest height which extended over the entire length of the baffle spacing. Unlike velocity, at the baffle crest the maximum turbulence intensity occurs near the centreline and decreases outwards towards the culvert wall.
- Embedding the baffled invert culvert causes a smoothing of the water surface as the roughness created by the baffles becomes drowned out. The distinctive lobed shape of the velocity contours remain with embedment, although both the positive and negative streamwise velocities are reduced throughout the flow cross sections, including a reduction in the barrier velocity at the baffle.
- In terms of turbulence intensity, embedment reduces both the peak values of turbulence intensity, as well as the cross section average turbulence intensity, at all sample locations. The position and size of the pocket of higher turbulence intensity located at the baffle crest height remains unchanged with embedment.

5.2. Conclusions

In terms of addressing the specific objectives of this study as identified in Chapter 1, the following conclusions are reported.

Measure and analyze the velocity distribution for various configurations of a non-embedded and embedded plain invert CSP culvert and use the results to draw conclusions about the area of the cross section with flow velocity less than the mean.

The velocity distribution in a non-embedded and embedded plain invert CSP culvert was measured at various discharges for two culvert slopes. For the non-embedded culvert, the flow depth and centreline velocity profiles stabilized at approximately 4D to 8D, indicating that the flow is fully-developed at this point.

As anticipated, embedment reduces the streamwise flow velocity throughout the flow area. Comparing the vertical velocity profiles, the embedded culvert profiles are found to be more uniform over the flow depth, as flow velocities in the upper portion of the flow area are reduced to a greater extent than velocities near the culvert invert.

Analysis of the cross section velocity distributions shows that, even for the non-embedded culvert, there is a significant portion of the cross section area around the culvert boundary that has a streamwise flow velocity less than the mean velocity. For both the non-embedded and embedded tests the velocity distribution varies between 0.4 and 1.4 times the average velocity (based on the measured flow depth at each cross section). The lower velocity zone was found to be located in a continuous band around the culvert boundary.

Embedment of the culvert, and the corresponding increase in flow depth, increases the amount of the flow area with velocity less than the mean along the entire culvert length, although the impact is less significant within approximately one diameter downstream from the inlet. In all the tests conducted for this study, the M1 backwater profile extends to the culvert inlet, however, the increase in flow depth at the upstream end of the culvert was less than at the outlet as the profile tapered out, explaining the variation in results along the culvert length. The effectiveness of a specific embedment depth at reducing the flow velocity decreases with increasing discharge and increasing culvert slope. This effect can also be related to length and relative increase in flow depth produced by the M1 backwater profile for each combination of discharge and culvert slope.

Compare the measured velocity cross sections to those obtained from predictive equations found in the literature (specifically Ead et al., 2000), which may be suitable for application to culvert design.

The measured velocity profiles and cross sections were compared to the theoretical velocity distribution (log-law) and the model developed by Ead et al. (2000), respectively. In both cases, the measured results compare well with the calculated velocity values. In the case of fitting the vertical velocity profiles to the log-law, a value of k_s of between 0.012 m to 0.022 m was found to be appropriate to represent the corrugation roughness of the CSP model, when the

datum for analysis was set at the crest of the corrugation. Strong results for the comparison to the cross section velocity distribution produced using the Ead et al. model confirm that, as proposed by Ead et al., this model is suitable for use in predicting the cross section velocity distribution in a CSP culvert for design purposes.

Undertake a preliminary assessment of the turbulence conditions within a CSP culvert, with and without embedment.

The turbulence conditions were evaluated in terms of turbulence intensity, which was calculated at each sampling point based on the combined magnitude of the variation (RMS) in instantaneous x,y,z direction velocities over the sample time for each sample point and the normal depth average velocity corresponding to the slope and discharge that was being tested.

The turbulence intensity conditions exhibit a reverse pattern to that of the velocity distribution, with higher magnitudes of turbulence intensity generally occurring near the culvert boundary and lower values in the centre of the flow. In terms of the longitudinal variation in turbulence intensity, the peak point magnitudes are located in the upper corners of the flow area, in the cross sections located just downstream from the inlet. However, the cross section average turbulence intensity increases with distance downstream from the inlet and is highest in the cross sections located near the culvert outlet.

The effect of culvert embedment on the turbulence intensity distribution varies along the length of the culvert. Near the inlet, the turbulence intensity profiles and cross sections show little change and in many cases embedment causes increased local turbulence intensity values and an increase in cross section average turbulence intensity. However, beyond 8D downstream, embedment was found to reduce the cross section average turbulence intensity values and cause no localized increases in turbulence intensity. These effects are related to the length and depth of the M1 backwater profile created by embedment relative to the flow conditions of each test and at each longitudinal location. In all tests conducted as part of this study, the M1 profile extended the entire culvert length, however, it appears from the results that the turbulence intensity conditions at the inlet may only be improved for fish passage when the M1 profile exceeds the length of the culvert and produces some minimum flow depth increase at the inlet.

Complete a minor investigation into the effect of baffles on the velocity and turbulence structure of a non-embedded and embedded CSP culvert.

As expected, the installation of baffles along the culvert invert increases the flow depth and decreases the streamwise flow velocities throughout the cross section, when compared to the corresponding plain invert testing. However, in terms of turbulence intensity, the baffled invert produces both higher peak magnitudes, as well as higher cross section average turbulence intensities, when compared to the plain invert. The zone of highest turbulence intensity occurs in the central portion of the flow area, at approximately the height of the baffle crest and is sustained throughout the baffle spacing length.

Embedding the baffled invert culvert produced decreased streamwise flow velocities throughout the flow area, as well as decreased negative velocities between the baffles. Embedment also slightly reduces the turbulence intensity values throughout the cross section, resulting in lower cross section average turbulence intensity values for each successive embedment depth.

Interpret the results of the model study in terms of fish passage, based on information regarding fish behaviour and preferences available from published research.

Attempting to interpret the results of the study in terms of fish passage, the following general conclusions can be inferred:

- There are significant zones near the culvert walls where the velocity is less than the average velocity and which may be of a suitable size for some fish to utilize for migration.
- The locations of lowest velocity are frequently the areas of highest turbulence intensity. The path a fish selects to travel through a culvert is therefore likely to be a trade-off between higher velocity and lower turbulence, or higher turbulence and lower velocity. The selected path, and whether conditions in the culvert are a barrier to fish passage, will depend on a fish's tolerance to turbulence in combination with their swimming ability in terms of velocity.
- In order to avoid areas of relatively high shear stress, a fish may prefer to swim in the lower velocity areas near the sides of a culvert, as opposed to along the invert.

- An important consideration in looking at the areal velocity distribution in terms of fish passage is the size and continuity of the lower velocity areas and whether these areas are suitably sized for a fish to make use of.
- In the experiments conducted for this study, embedment was found to improve fish passage conditions from approximately the mid-point of the culvert length to the outlet, by producing both reduced velocities and turbulence intensities.
- In the area just downstream from the culvert inlet, embedment also reduced velocities by increasing the flow area, although in some cases (especially at the steeper culvert slope) the velocity reduction in this area was significantly less than occurred further downstream. However, embedment did not reduce turbulence intensities near the inlet, and in some cases produced higher peak values and cross section averages. These findings are attributed to the length of the M1 backwater profile produced by embedment relative to the culvert length. Therefore, if conditions near the inlet are considered the most likely barrier to fish passage, careful consideration must be given to the length of a culvert installation relative to the M1 profile when considering embedment as a means to improve fish passage.
- When swimming upstream in a baffled invert culvert, fish must choose between traversing over the baffle crest either in the centre of the baffle, where velocities are lowest but turbulence intensity is highest, or closer to the sides of the baffle, where velocities are higher but turbulence intensity is lower.

5.3. Recommendations for Future Study

The following points outline recommendations for future studies with similar experimental set-ups and/or objectives.

Experimental Set-Up and Data Collection

- The variable ADV sampling time used in this experiment was found to work well and saved a considerable amount of time in the data collection phase, as opposed to implementing one standard longer duration sample time. In future studies using an ADV, consideration should be given to reducing the maximum sample time to no longer than five minutes and the shortest sample time to one minute or less.
- For a study with the ADV involving a limited number of sample points, variable filter criteria could be implemented to ensure that sufficient data pass the filter to make all data points

useable. This could be done in combination with implementing shorter sample times. However, for studies with a large amount of ADV data, such as this one, the use of consistent filter criteria is the only realistic alternative for processing data and in the case of this project did not cause a significant amount of data loss due to filtering.

- For projects requiring extensive data collection with the ADV an automated sampling system would be beneficial.
- The use of fabricated seeding material (glass beads) with the ADV may be advisable to ensure that the scattering particles are perfectly representative of the flow velocity and that the measured velocities are therefore as accurate as possible.
- When measuring velocity cross sections near the inlet of a culvert, use of a side-looking ADV probe would be useful to collect data in the upper corners of the flow area and may improve the quality of the results.

Items for Further Investigation

- A large amount of velocity data was collected in this study that could be utilized to complete further analysis of the turbulence and velocity distributions. A few potential areas for exploration include:
    - Assess the size, shape and continuity of the lower velocity regions in relation to their practical usability by mature or juvenile fish.
    - Examine the horizontal and vertical velocity and turbulence fields. For example, Papanicolaou and Talebbeydokhti (2000) suggest that transverse and vertical velocity distributions are just as important as streamwise velocity in studying the potential for fish passage through a culvert.
- Additional studies regarding the velocity distribution in a CSP culvert under various flow conditions could be used to further develop the plots shown in Section 4.5.3 and in Magura (2008). This could potentially lead to the development of one or more velocity distribution curves that could be applied to culvert fish passage design.
- A study specifically relating to the inlet area of embedded CSP culverts may be able to ascertain what depth of flow increase is required to reliably decrease the turbulence intensities measured in that area (i.e. at what point must the M1 backwater profile intersect

with the inlet end of the culvert). Such information might be useful in deciding on what depth of embedment is required for a specific length of culvert.

- Another area pertaining to fish passage through culverts requiring further investigation is the scale of the turbulent eddies in each plane. As appreciation of how fish utilize eddy structures to reduce their energy expenditure for swimming has increased, it has been suggested by several researchers that the size and frequency of turbulent eddies are possibly as influential to fish passage as velocity conditions. For example, fish may not feel turbulent eddies that are smaller in dimension than their body length, whereas eddies larger than the fish's body length are thought to have a significant effect on fish. Similarly, fish are thought to be less sensitive to eddies in the horizontal plane because they can flex their body to respond, whereas they cannot respond as well to eddies in the vertical plane. Some examples of researchers that have made these observations include Nikora et al. (2003), Lupandin (2005), Smith et al. (2005), and Papanicolaou and Talebbeydokhti (2000).
- Attempting to infer the behaviour of fish based on a purely hydraulic study points out the need for studies of culvert fish passage to be conducted by interdisciplinary teams of engineers and biologists and include actual observation of fish behaviour.
- Although such studies are generally expensive and difficult to carry out, there is no substitute for observation of actual fish behaviour under field conditions. In the future, as fish telemetry studies become less expensive, actual field studies of fish passage through culverts, for which there seem to be few documented cases, may become a more realistic endeavour and would be highly valuable.

REFERENCES

Abbs, T.J., Kells, J.A. and Katopodis, C. 2007. A Model Study of the Hydraulics Related to Fish Passage Through Backwatered Culverts. 18th Canadian Hydrotechnical Conference, CSCE, Winnipeg MB, Canada, August 22-24, 13 p.

Agelinchaab, M, Tachie, M.F. 2006. Open Channel Flow Over Hemispherical Ribs. International Journal of Heat and Fluid Flow, Elsevier, 27: 1010-1027.

Barber, M.E. and Downs, R.C. 1996. Investigation of Culvert Hydraulics Related to Juvenile Fish Passage. Washington State Department of Transportation Report, WA-RD 388.2, 172 p.

Behlke, C.E., Kane, D.L., McLean, R.F. and Travis, M.D. 1991. Fundamentals of Culvert Design for Passage of Weak-Swimming Fish. United States Department of Transportation, Report No. FHWA-AK-RD-90-10, 153 p.

Carlson R.E. and Foley, T.A. 1991. The Parameter R^2 in Multiquadric Interpolation. Computers and Mathematics with Applications, Pergamon Press, 21(9): 29-42.

Carlson, R.E. and Foley, T.A. 1992. Interpolation of Track Data with Radial Basis Methods. Computers and Mathematics with Applications, Pergamon Press, 24(12): 27-34.

Chang, H.C. 1988. Fluvial Processes in River Engineering. Krieger Publishing Company, Florida, 432 p.

Chilibeck, B., Chislett, G. and Norris, G. 1993. Land Development Guidelines for the Protection of Aquatic Habitat. Fisheries and Oceans Canada, accessed on November 2, 2008, URL: http://www.dfo-mpo.gc.ca/Library/165353.pdf, 128 p.

Chiu, C.L. 1993. Application of Probability and Entropy Concepts in Pipe-Flow Study. Journal of Hydraulic Engineering, ASCE, 119(6): 742-755.

Chow, V.T. 1959. Open-Channel Hydraulics. McGraw-Hill Book Company, Toronto, 680 p.

Corrugated Steel Pipe Institute. 2007. Handbook of Steel Drainage and Highway Construction Products. Corrugated Steel Pipe Institute, Cambridge, 470 p.

Cotel, A.J., Webb, P.W. and Tritico, H. 2006. Do Brown Trout Choose Locations with Reduced Turbulence? Transactions of the American Fisheries Society, American Fisheries Society, 135: 310-619.

Ead, S.A., Rajaratnam, N., Katopodis, C. 2002. Generalized Study of Hydraulics of Culvert Fishways. Journal of Hydraulic Engineering, ASCE, 128(11): 1018-1022.

Ead, S.A., Rajaratnam, N., Katopodis, C. and Ade, F. 2000. Turbulent Open-Channel Flow in Circular Corrugated Culverts. Journal of Hydraulic Engineering, ASCE, 126(10): 750-757.

Enders, E.C., Boisclair, D. and Roy, A.G. 2003. The Effect of Turbulence on the Cost of Swimming for Juvenile Atlantic Salmon. Canadian Journal of Fisheries and Aquatic Sciences, NRC Canada, 60: 1149-1160.

Fisheries and Oceans Canada and Manitoba Natural Resources. 1996. Manitoba Stream Crossings Guidelines for the Protection of Fish and Fish Habitat, 48 p.

Fisheries and Oceans Canada and Saskatchewan Environment and Resource Management. 1994. Fish Habitat Protection Guidelines: Road Construction and Stream Crossings, 31 p.

Franke, R. 1982. Scattered Data Interpolation: Tests of Some Methods. Mathematics of Computation, American Mathematical Society, 38(157): 181-200.

Frei, M. 2006. Design of Fish Passage at Bridges and Culvert. M.Sc. Thesis, Washington State University, accessed on November 2, 2008, URL: https://research.wsulibs.wsu.edu:8443/dspace/bitstream/2376/573/1/c _frei_082506.pdf, 208 p.

French, R.H. 1985. Open-Channel Hydraulics. McGraw-Hill Book Company, Toronto, 705 p.

Gautam, B.P. 2008. Submergence Effects on Jet Behaviour in Scour by a Plane Wall Jet. M.Sc. Thesis, University of Saskatchewan, Department of Civil and Geological Engineering, 192 p.

Golden Software Inc. 2002. Surfer 8 User's Guide: Contouring and 3D Surface Mapping for Scientists and Engineers. Golden Software Inc., Golden, CO, 640 p.

Goring, D.G., and Nikora, V.I. 2002. Despiking Acoustic Doppler Velocimeter Data. Journal of Hydraulic Engineering, 128(1): 117-126.

Haro, A., Castor-Santos, T., Noreika, J. and Odeh, M. 2004. Swimming Performance of Upstream Migrant Fishes in Open-Channel Flow: A New Approach to Predicting Passage Through Velocity Barriers. Canadian Journal of Fisheries and Aquatic Sciences, NRC Canada, 61: 1590-1601.

Hotchkiss, R.H. and Frei, C.M. 2007. Design for Fish Passage at Roadway–Stream Crossings: Synthesis Report. accessed on December 27, 2008, URL: http://www.fhwa.dot.gov/engineering/hydraulics/pubs/07033/07033.pdf, 280 p.

House, M.R., Pyles, M.R. and White, D. 2005. Velocity Distributions in Streambed Simulation Culverts Used for Fish Passage. Journal of the American Water Resources Association, Blackwell Publishing, 41(1): 209-217.

Katopodis, C. 1992. Introduction to Fishway Design. Freshwater Institute, Central and Arctic Region, Winnipeg, Manitoba, Canada, 70 p.

Katopodis, C. 2005. Developing a Toolkit for Fish Passage, Ecological Flow Management and Fish Habitat Works. Journal of Hydraulic Research, IAHR, 45(5): 451-467.

Katopodis, C., Kells, J.A. and Acharya, M. 2001. Nature-Like and Conventional Fishways: Alternative Concepts? Canadian Water Resources Journal, Canadian Water Resources Association, 26(2): 211-232.

Kemp, P.S. and Williams, J.G. 2008. Response of Migrating Chinook Salmon Smolts to In-Stream Structure Associated with Culverts. River Research and Applications, Wiley Interscience, 24: 571-579.

Knight, D.W., and Sterling, M. 2000. Boundary Shear in Circular Pipes Running Partially Full. Journal of Hydraulic Engineering, ASCE, 126(4): 263-275.

Liao, J.C. 2007. A Review of Fish Swimming Mechanics and Behaviour in Altered Flows. Philosophical Transactions of the Royal Society B, Royal Society, 362: 1973-1993.

Lupandin, A.J. 2005. Effect of Flow Turbulence on Swimming Speed of Fish. Biology Bulletin, Pleiades Publishing Ltd., 32(5): 461-466.

MacDondald, J.I. and Davies, P.E. 2007. Improving the Upstream Passage of Two Galaxid Fish Species Through a Pipe Culvert. Fisheries Managment and Ecology, Blackwell Publishing, 14: 221-230.

Magura, C. 2008. Hydraulic Characteristics of Embedded Circular Culverts. M.Sc. Thesis, University of Manitoba, Winnipeg, MB, 278 p.

Morrison, R.R., Hotchkiss, R.H., Stone, M., Thurman, D. and Horner-Devine, A.R. 2009. Turbulence Characteristics of Flow in a Spiral Corrugated Culvert Fitted with Baffles and Implications for Fish Passage. Ecological Engineering, Elsevier, 35: 381-392.

Mountjoy, P.K. 1986. Velocity Profile Prediction in Culverts for Fish Passage Design Consideration. M.Sc. Thesis, University of Alaska, Fairbanks, AK, 86 p.

Munson, B.R., Young, D.F. and Okiishi, T.H. 1998. Fundamentals of Fluid Mechanics, 3rd Edition, John Wiley and Sons, USA, 691 p.

Nikora, V.I., Aberele, J., Biggs, B.J.F. and Jowett, I. 2003. Effects of Fish Size, Time-to-Fatigue and Turbulence on Swimming Performance: A Case Study of Galaxias Maculatus. Journal of Fish Biology, Blackwell, 63: 1365-1382.

Odeh, M., Noreika, J.F., Haro, A., Mynard, A., Castor-Santos, T. and Cada, G.F. 2002. Evaluation of the Effects of Turbulence on the Behaviour of Migratory Fish. Report to the Bonneville Power Administration (Final Report 2002), accessed on September 12, 2008, URL: http://pisces.bpa.gov/release/documents/documentviewer.aspx?doc=00000022-1, 46 p.

Palaseanu, M. and Pearlstine, L. 2008. Estimation of Water Surface Elevations for the Everglades, Florida. Computers and Geosciences, Elsevier, 34: 815-827.

Papanicolaou, F. And Talebbeydokhti, N. 2000. Discussion of "Turbulent Open-Channel Flow in Circular Corrugated Culverts". Journal of Hydraulic Engineering, 126(10): 547-548.

Peake, S.J. 2008. Behaviour and Passage Performance of Northern Pike, Walleye and White Suckers in an Experimental Raceway. North American Journal of Fisheries Management, American Fisheries Society, 28: 321-327.

Rajaratnam, N. and Katopodis, C. 1990. Hydraulics of Culvert Fishways III: Weir Baffle Culvert Fishways. Canadian Journal of Civil Engineering, NRC Research Press, 17: 558-568.

Rajaratnam, N., Katopodis, C. and Mainali, A. 1988. Plunging and Streaming Flows in Pool and Weir Fishways. Journal of Hydraulic Engineering, ASCE, 114(8): 939-944.

Rajaratnam, N., Katopodis, C. and Sabur, M.A. 1991. Entrance Region of Circular Pipes Flowing Partly Full. Journal of Hydraulic Research, IAHR, 29(5): 685-698.

Richmond, M.C., Shiqun, D., Guensch, G.R., Tritico, H. And Pearson, W.H. 2007. Mean Flow and Turbulence Characteristics of a Full Scale Spiral Corrugated Culvert with Implications for Fish Passage. Ecological Engineering, Elsevier, 30: 333-340.

Schlichting, H. 1960. Boundary Layer Theory. McGraw-Hill Book Company, Toronto, 647 p.

Smith, D.L., Brannon, E.L. and Odeh, M. 2005. Response of Juvenile Rainbow Trout to Turbulence Produced by Prismatoidal Shapes. Transactions of the American Fisheries Society, American Fisheries Society, 134: 741-753.

Smith, D.L., Brannon, E.L., Shaffi, B. and Odeh, M. 2006. Use of the Average and Fluctuating Velocity Components for Estimation of Volitional Trout Density. Transactions of the American Fisheries Society, American Fisheries Society, 135: 431-444.

SonTek. 2002. SonTek/YSI ADVField Software Manual. SonTEK/YSI Inc., SanDiego, CA, 69 p.

Streeter, V.L., Wylie, E.B. and Bedford, K.W. 1998. Fluid Mechanics. WCB McGraw-Hill, New York, 740 p.

Wahl, T.L. 2000. Analyzing ADV Data Using WinADV. ASCE 2000 Joint Conference on Water Resources Engineering and Water Resources Planning and Management, Minneapolis, Minnesota, USA, July 30-August 2, accessed on June 16, 2008, URL: http://www.usbr.gov/pmts/hydraulicslab/pubs/PAP/PAP-0840.pdf, 10 p.

APPENDICES

Appendix A: Velocity Contour Plots

Naming convention for contour plots

The title in each contour plot conveys the following information (in order):

- Culvert Slope (%)
- Embedment Depth (0D (non-embedded), 0.1D or 0.2D, where D=culvert diameter)
- Discharge (L/s)
- Cross Section Location (H1=hole 1, H2=hole 2, etc.)
- Measurement (and units if appropriate) that is being represented by the contours.

For example: 0.4% 0D 50 L/s H1 vx (m/s) indicates that the cross section is for the 0.4% culvert slope, non-embedded trial, at the 50 L/s discharge, the location is hole 1 and the contour plot is of the streamwise (x) direction velocity in units of m/s.

0.4% Culvert Slope Non-Embedded Cross Sections

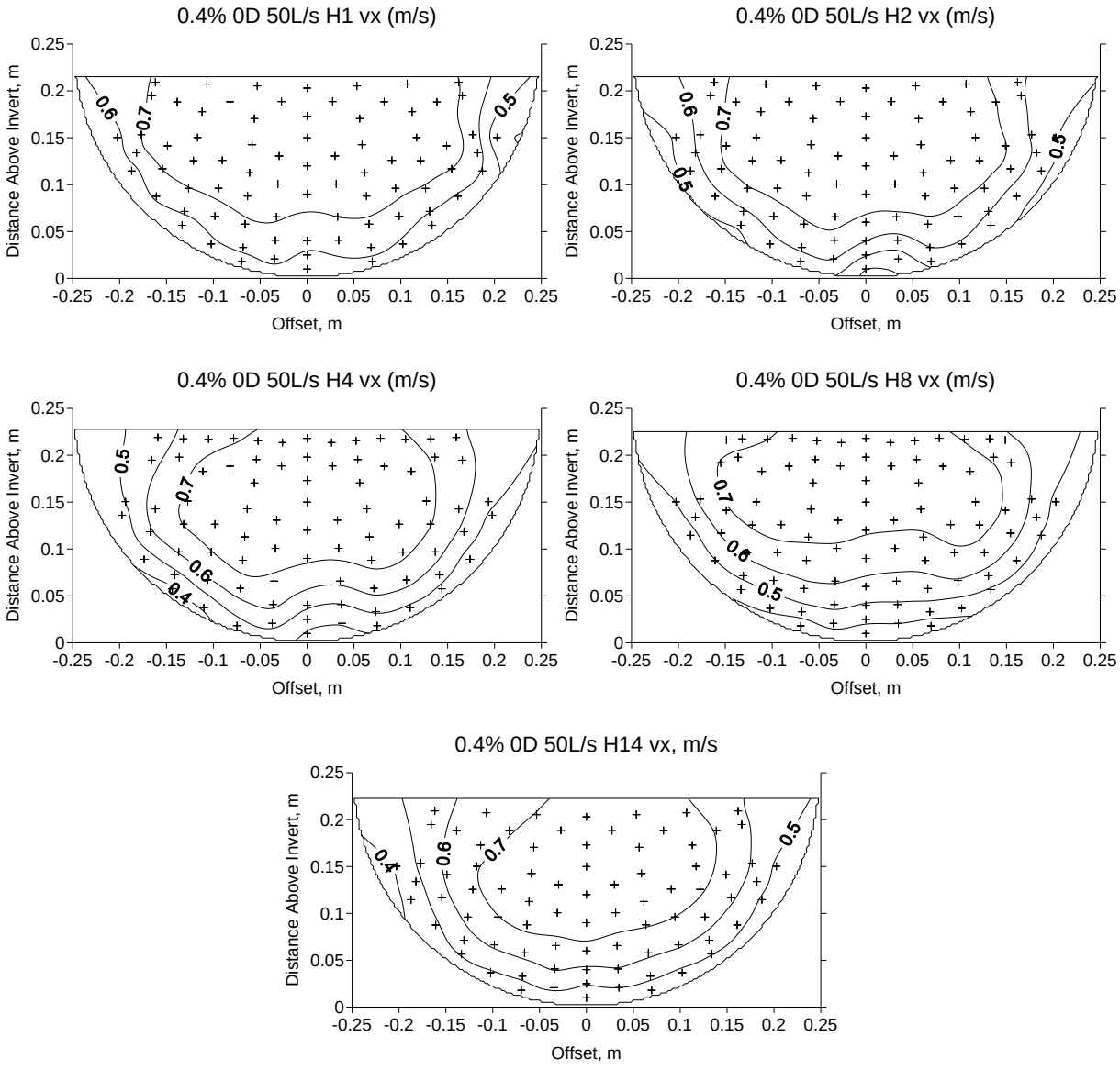

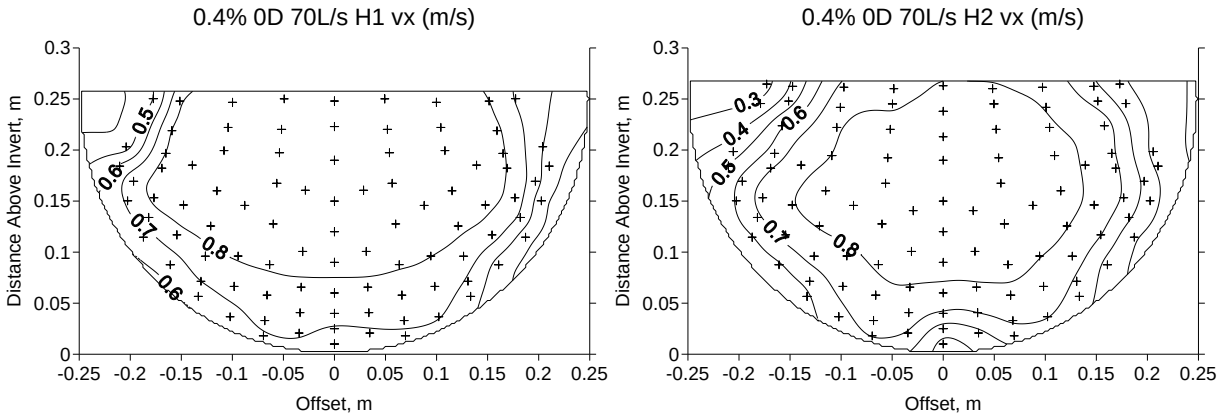
0.4% 0D 70L/s H1 vx (m/s)
Distance Above Invert, m
Offset, m
0.5
0.6
0.7
0.8
0.6

0.4% 0D 70L/s H2 vx (m/s)
Distance Above Invert, m
Offset, m
0.3
0.4
0.5
0.6
0.7
0.8

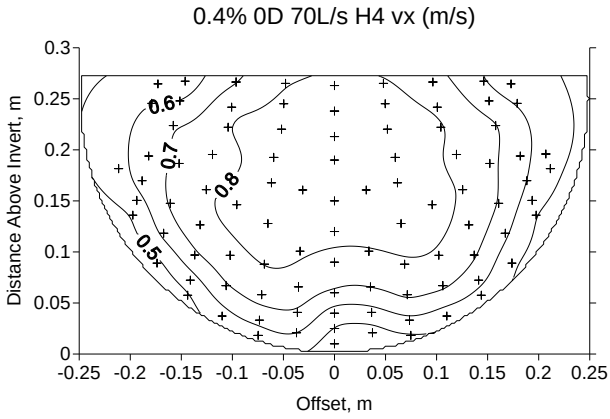
0.4% 0D 70L/s H4 vx (m/s)
Distance Above Invert, m
Offset, m
0.5
0.6
0.7
0.8

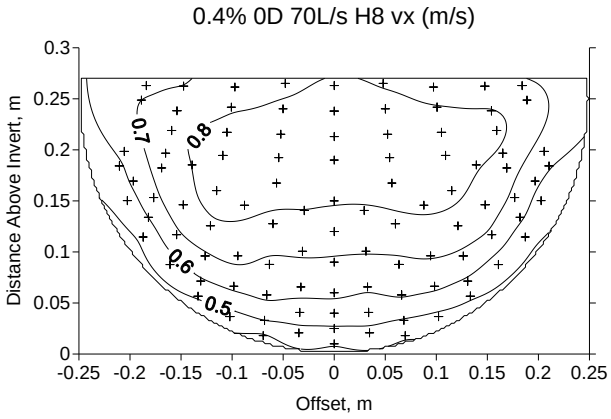
0.4% 0D 70L/s H8 vx (m/s)
Distance Above Invert, m
Offset, m
0.5
0.6
0.7
0.8

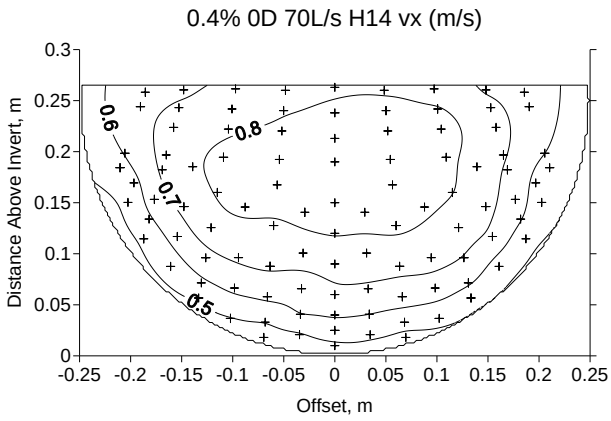
0.4% 0D 70L/s H14 vx (m/s)
Distance Above Invert, m
Offset, m
0.5
0.6
0.7
0.8

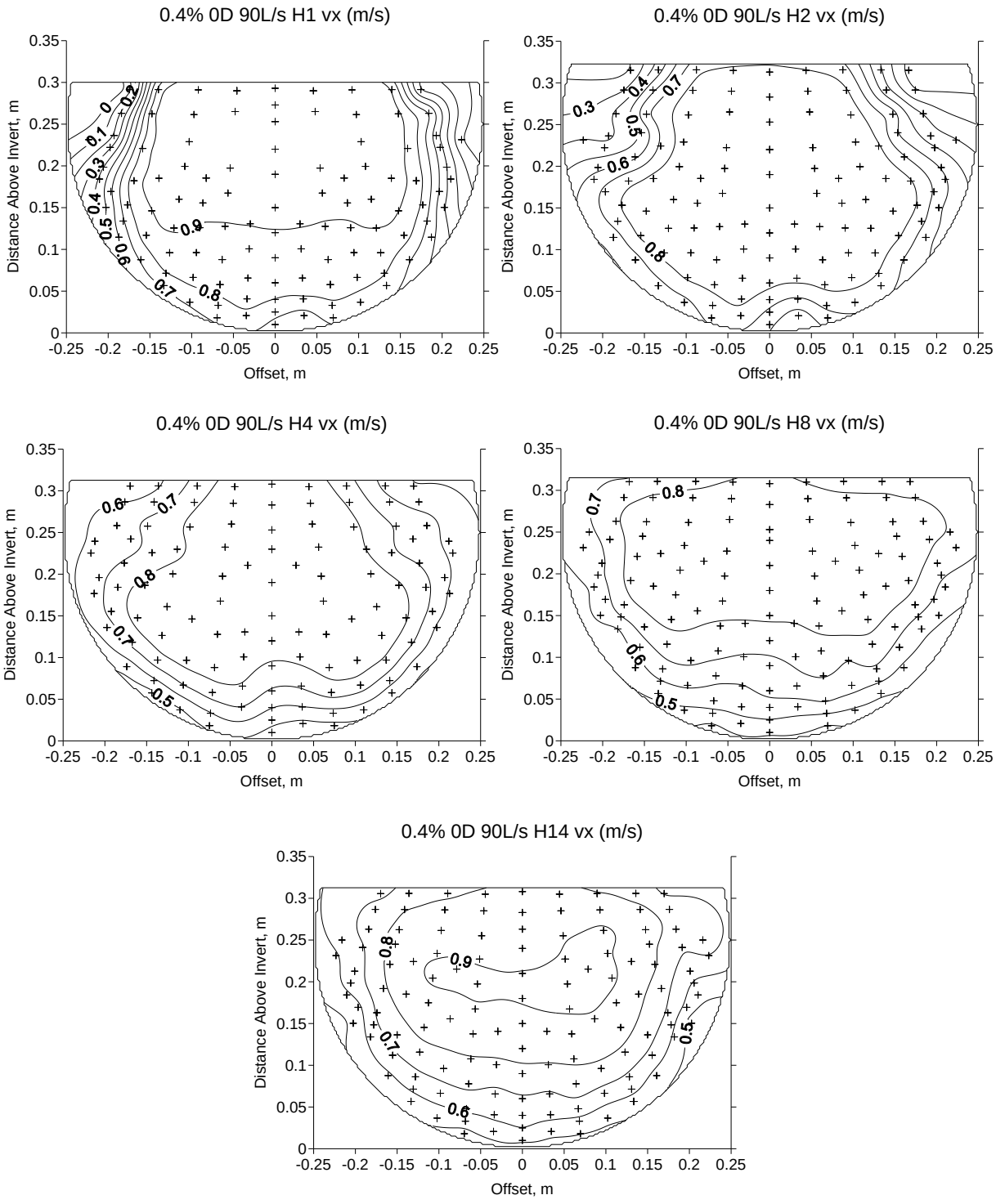
0.4% 0D 90L/s H1 vx (m/s)
0.4% 0D 90L/s H2 vx (m/s)
0.4% 0D 90L/s H4 vx (m/s)
0.4% 0D 90L/s H8 vx (m/s)
0.4% 0D 90L/s H14 vx (m/s)
Distance Above Invert, m
Offset, m

1.0% Culvert Slope Non-Embedded Cross Sections

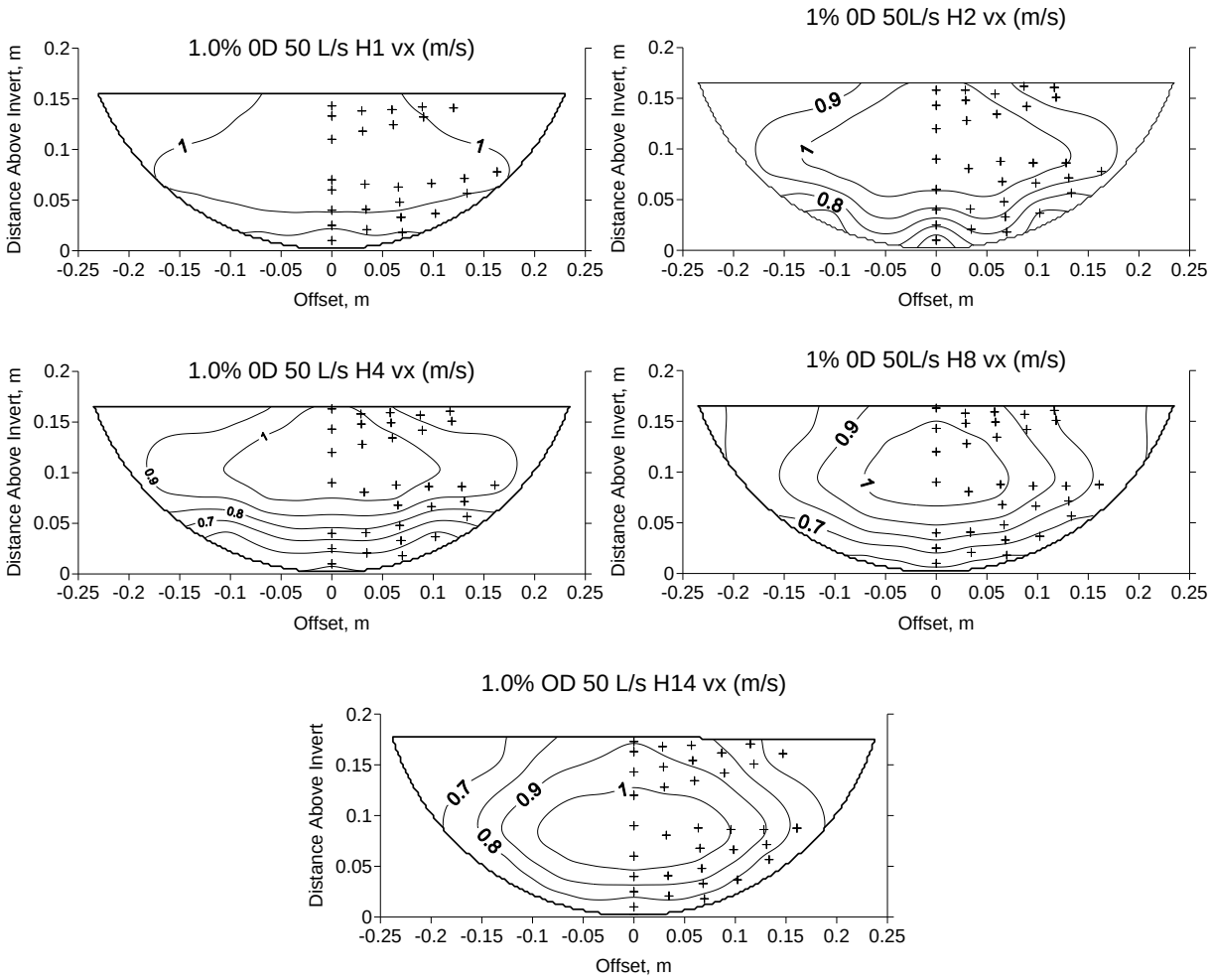

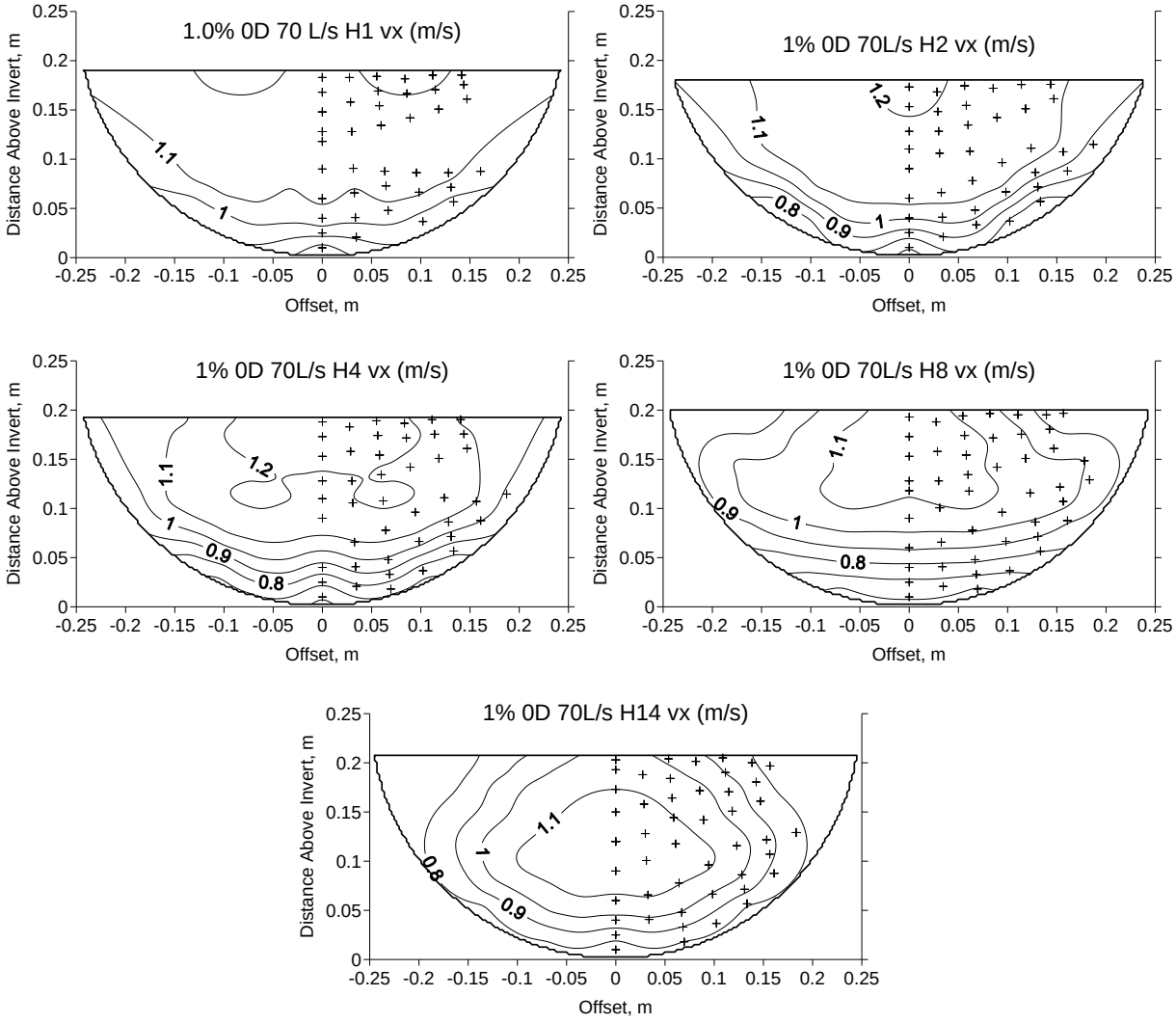
1.0% 0D 70 L/s H1 vx (m/s)
1% 0D 70L/s H2 vx (m/s)
1% 0D 70L/s H4 vx (m/s)
1% 0D 70L/s H8 vx (m/s)
1% 0D 70L/s H14 vx (m/s)
Distance Above Invert, m
Offset, m
0.25
0.2
0.15
0.1
0.05
0
-0.25 -0.2 -0.15 -0.1 -0.05 0 0.05 0.1 0.15 0.2 0.25
1.1
1
1.2
0.8
0.9

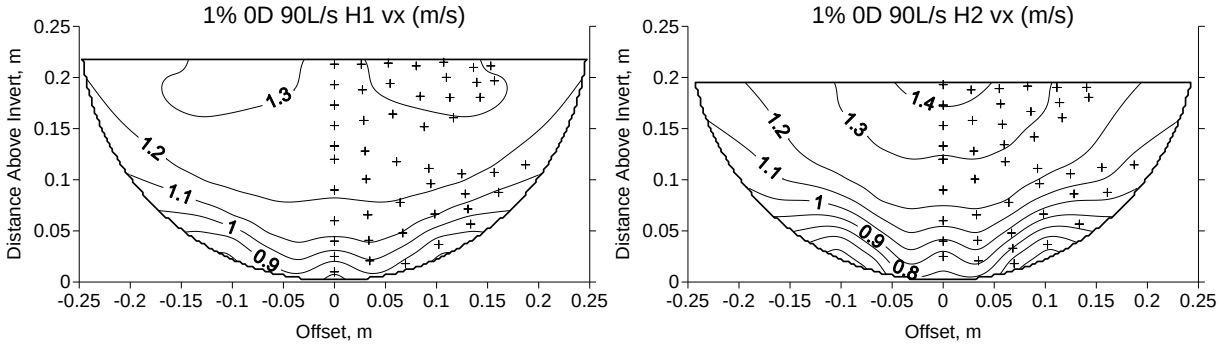
1% 0D 90L/s H1 vx (m/s)
Distance Above Invert, m
Offset, m
1.3
1.2
1.1
1
0.9

1% 0D 90L/s H2 vx (m/s)
Distance Above Invert, m
Offset, m
1.4
1.3
1.2
1.1
1
0.9
0.8

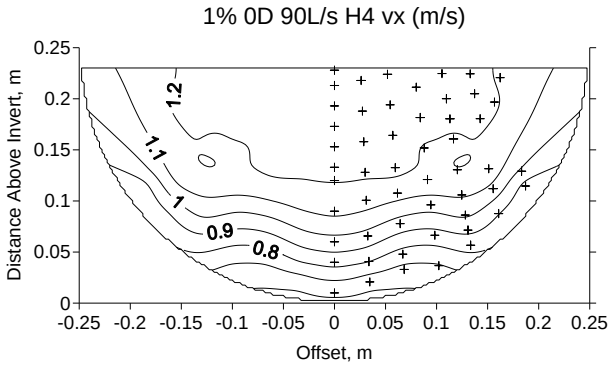
1% 0D 90L/s H4 vx (m/s)
Distance Above Invert, m
Offset, m
1.2
1.1
1
0.9
0.8

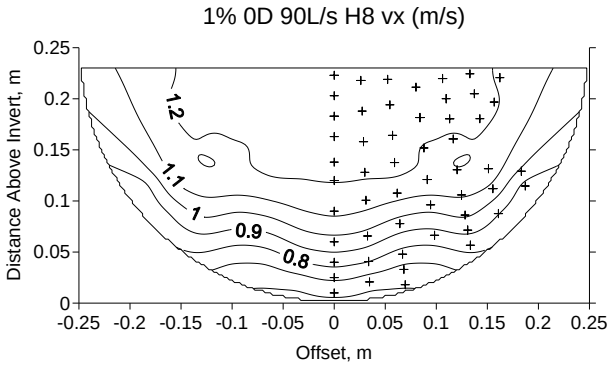
1% 0D 90L/s H8 vx (m/s)
Distance Above Invert, m
Offset, m
1.2
1.1
1
0.9
0.8

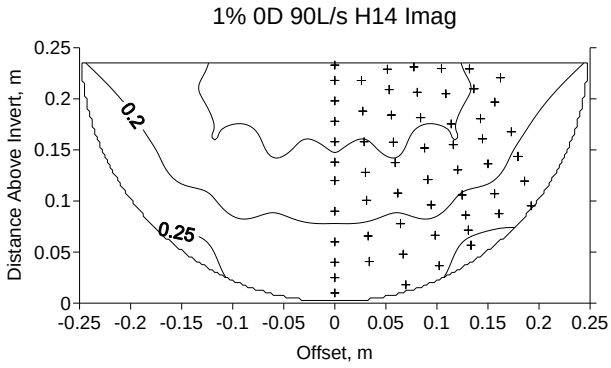
1% 0D 90L/s H14 Imag
Distance Above Invert, m
Offset, m
0.2
0.25

0.4% Culvert Slope 0.1D Embedded Cross Sections

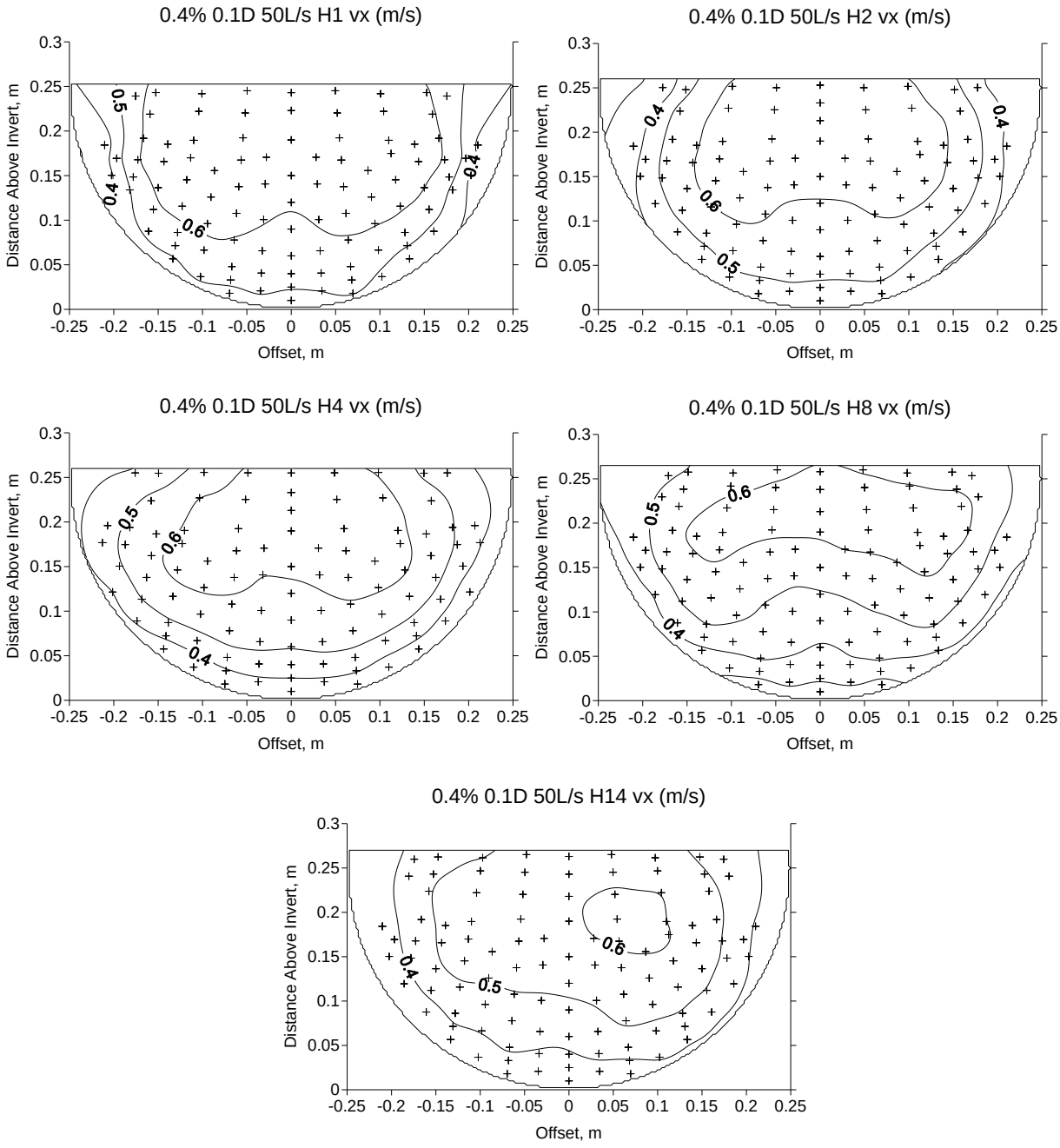

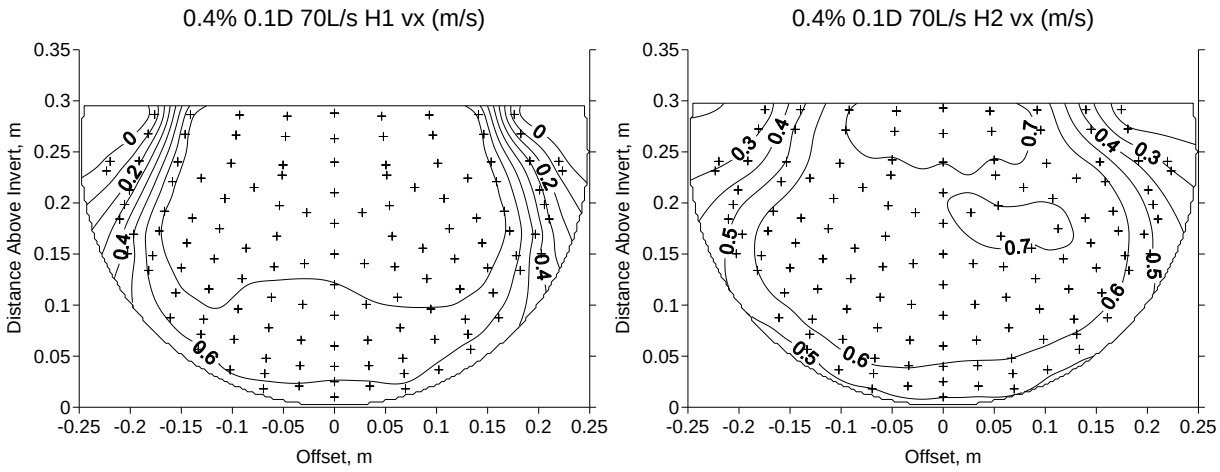
0.4% 0.1D 70L/s H1 vx (m/s)
Distance Above Invert, m
Offset, m

0.4% 0.1D 70L/s H2 vx (m/s)
Distance Above Invert, m
Offset, m

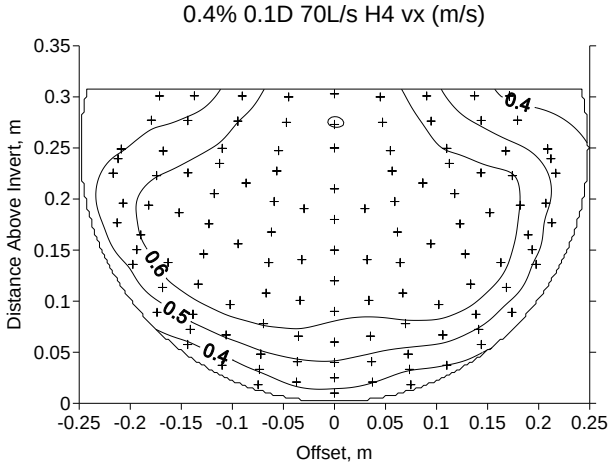
0.4% 0.1D 70L/s H4 vx (m/s)
Distance Above Invert, m
Offset, m

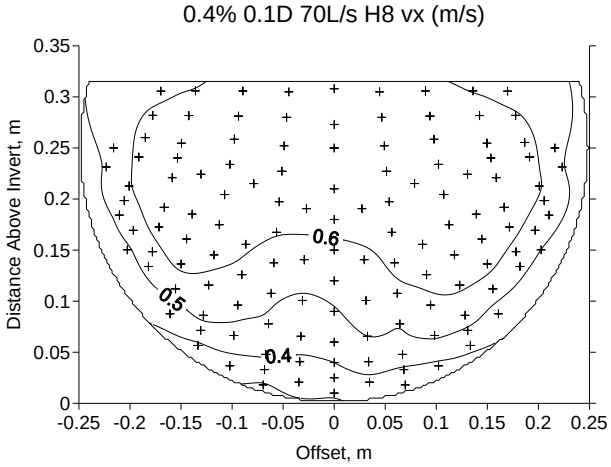
0.4% 0.1D 70L/s H8 vx (m/s)
Distance Above Invert, m
Offset, m

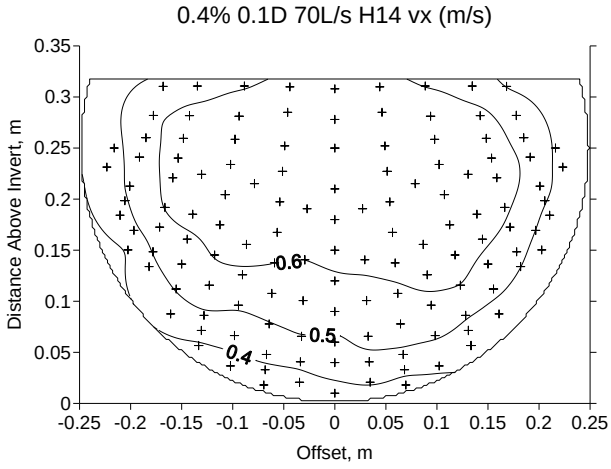
0.4% 0.1D 70L/s H14 vx (m/s)
Distance Above Invert, m
Offset, m

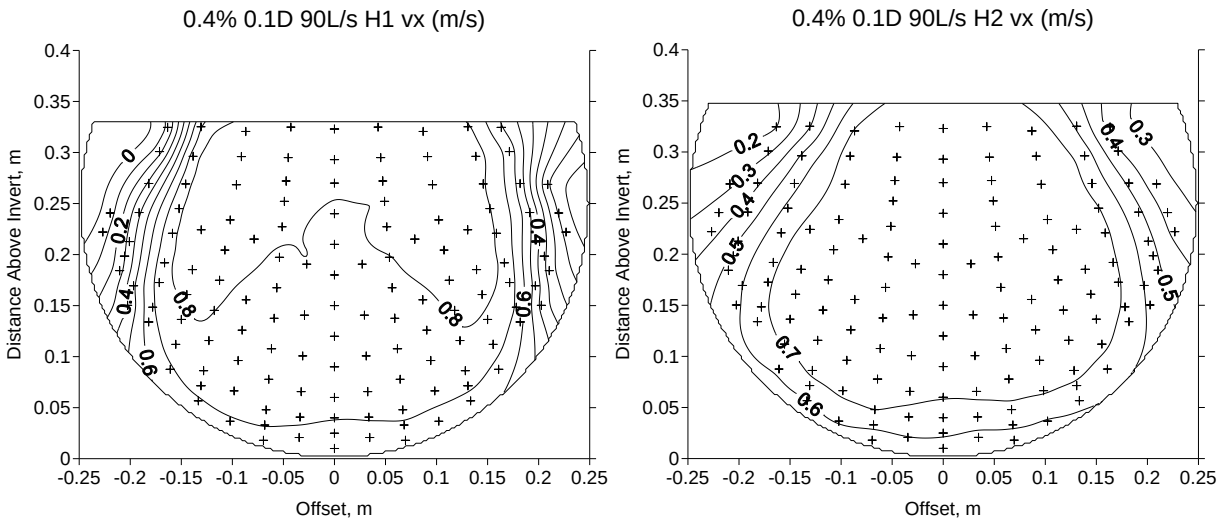
0.4% 0.1D 90L/s H1 vx (m/s)
Distance Above Invert, m
Offset, m
0
0.2
0.4
0.6
0.8
0.8
0.6
0.4

0.4% 0.1D 90L/s H2 vx (m/s)
Distance Above Invert, m
Offset, m
0.2
0.3
0.4
0.5
0.7
0.6
0.4
0.3
0.5

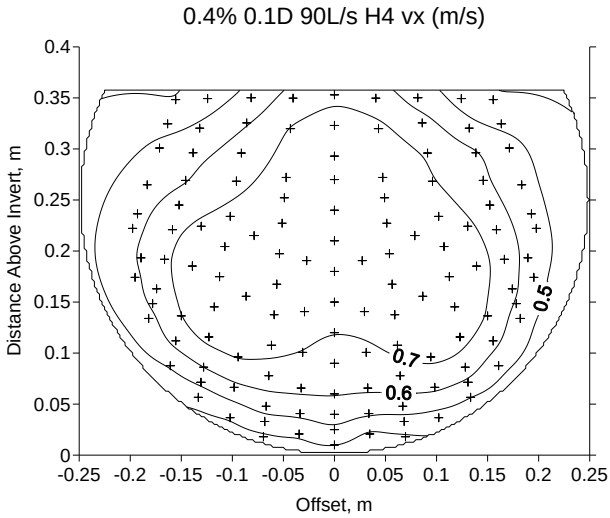
0.4% 0.1D 90L/s H4 vx (m/s)
Distance Above Invert, m
Offset, m
0.7
0.6
0.5

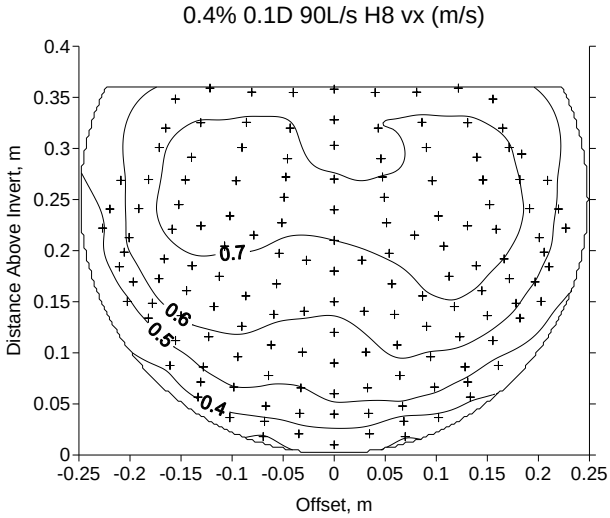
0.4% 0.1D 90L/s H8 vx (m/s)
Distance Above Invert, m
Offset, m
0.7
0.6
0.5
0.4

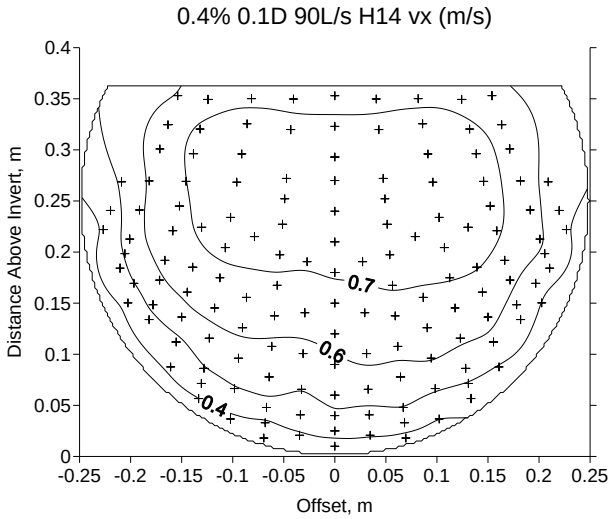
0.4% 0.1D 90L/s H14 vx (m/s)
Distance Above Invert, m
Offset, m
0.7
0.6
0.4

1.0% Culvert Slope 0.1D Embedded Cross Sections

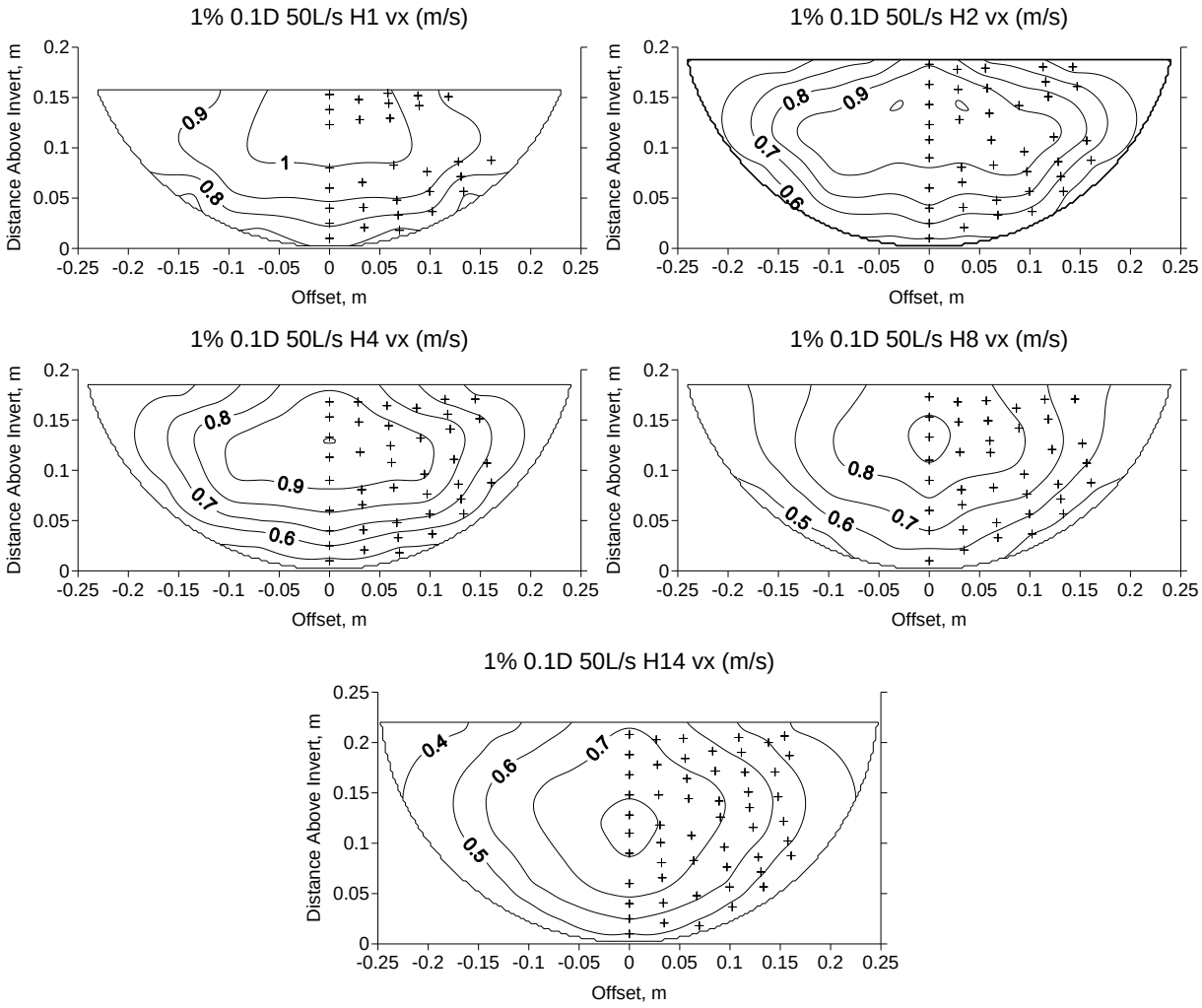

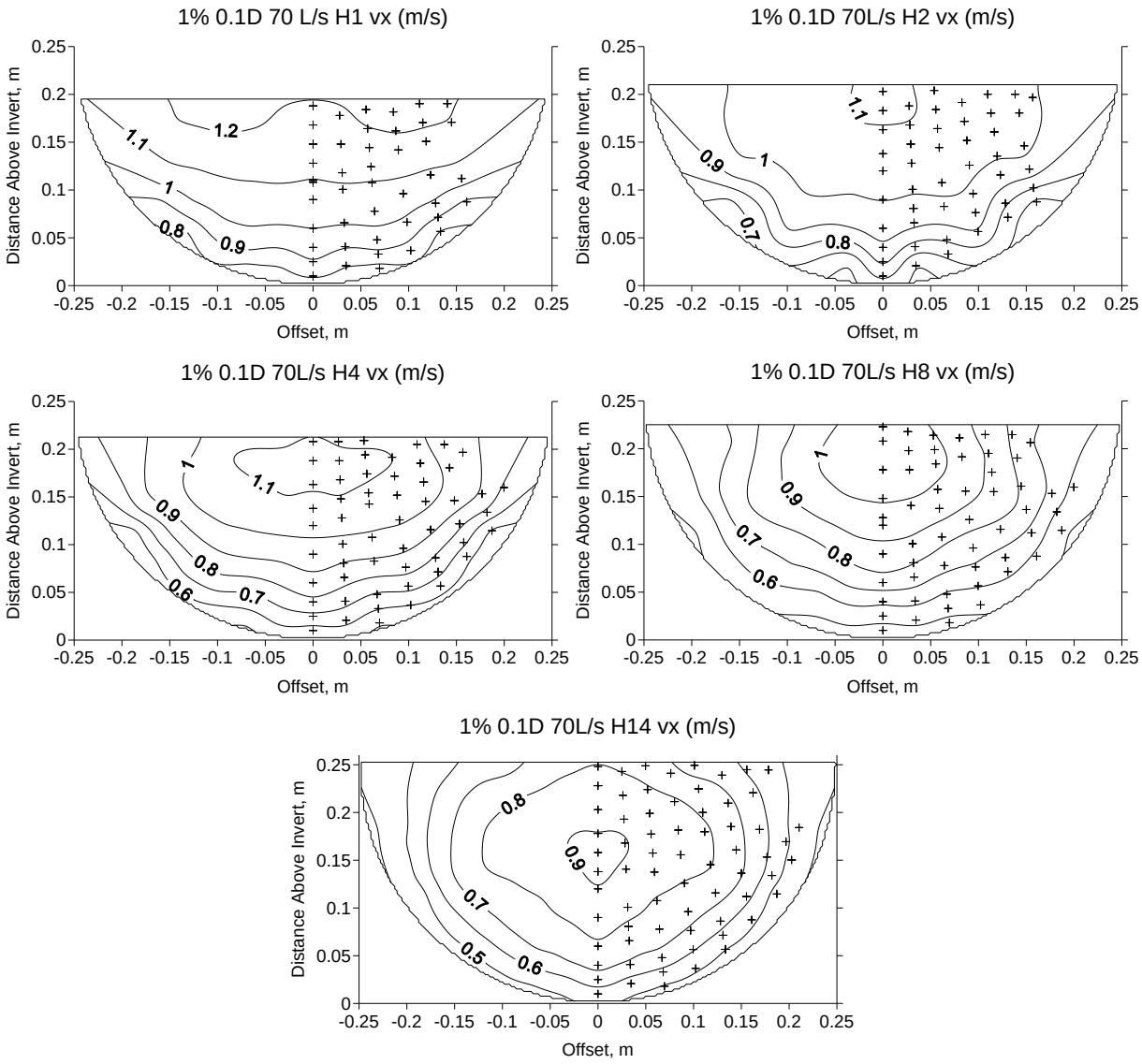
1% 0.1D 70 L/s H1 vx (m/s)
1% 0.1D 70L/s H2 vx (m/s)
1% 0.1D 70L/s H4 vx (m/s)
1% 0.1D 70L/s H8 vx (m/s)
1% 0.1D 70L/s H14 vx (m/s)
Distance Above Invert, m
Offset, m
0.25
0.2
0.15
0.1
0.05
0
-0.25 -0.2 -0.15 -0.1 -0.05 0 0.05 0.1 0.15 0.2 0.25
1.2
1.1
1
0.9
0.8
0.7
0.6
0.5

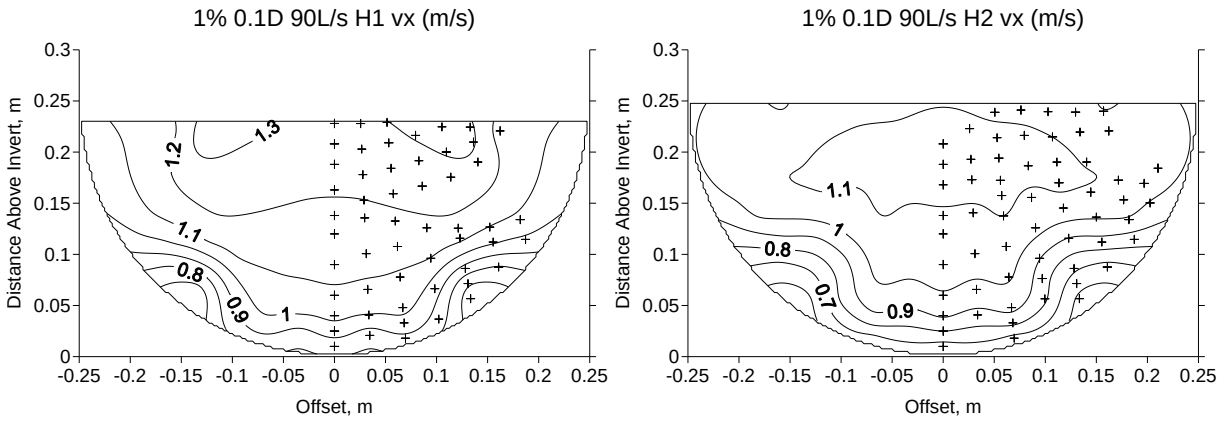
1% 0.1D 90L/s H1 vx (m/s)
Distance Above Invert, m
Offset, m
1.3
1.2
1.1
0.8
0.9
1

1% 0.1D 90L/s H2 vx (m/s)
Distance Above Invert, m
Offset, m
1.1
1
0.8
0.7
0.9

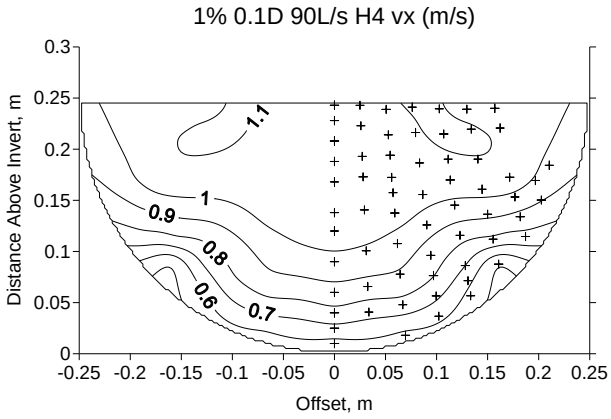
1% 0.1D 90L/s H4 vx (m/s)
Distance Above Invert, m
Offset, m
1.1
1
0.9
0.8
0.6
0.7

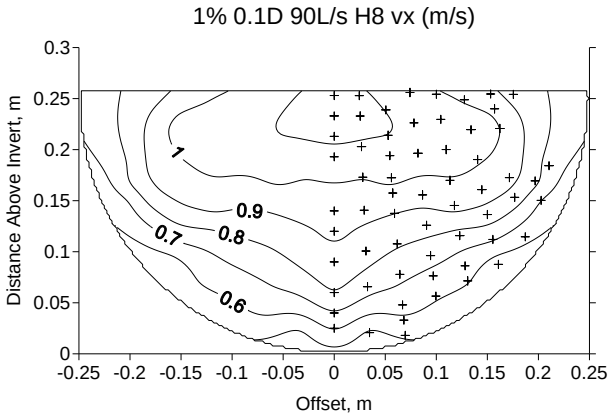
1% 0.1D 90L/s H8 vx (m/s)
Distance Above Invert, m
Offset, m
1
0.9
0.7
0.8
0.6

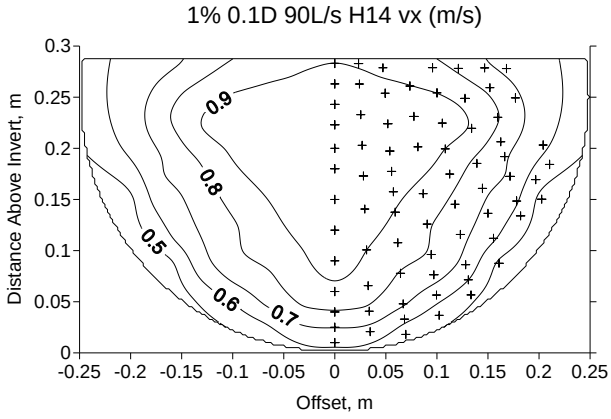
1% 0.1D 90L/s H14 vx (m/s)
Distance Above Invert, m
Offset, m
0.9
0.8
0.5
0.6
0.7

0.4% Culvert Slope 0.2D Embedded Cross Sections

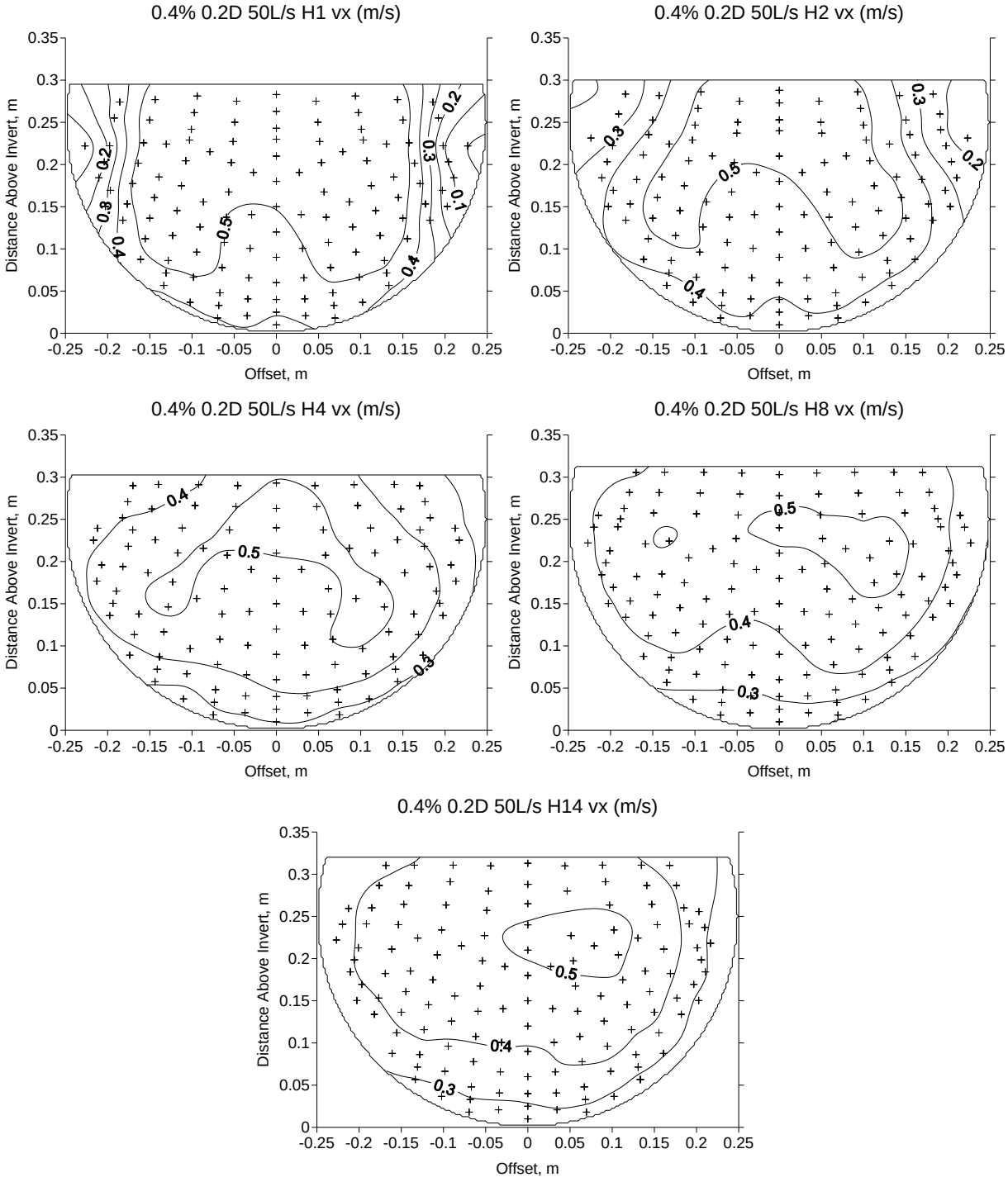

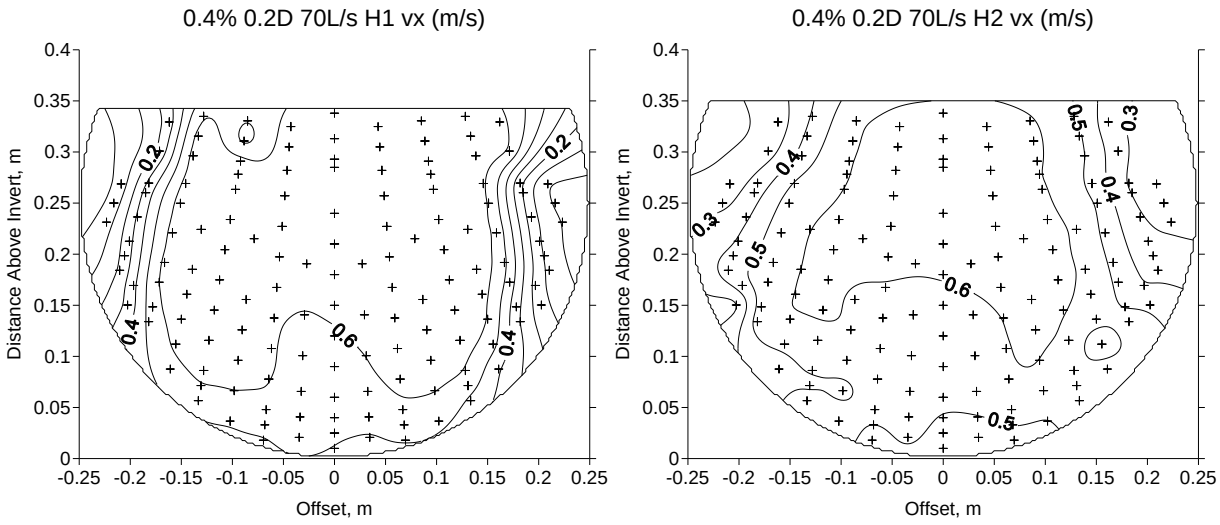
0.4% 0.2D 70L/s H1 vx (m/s)
Distance Above Invert, m
Offset, m
0.2
0.4
0.6

0.4% 0.2D 70L/s H2 vx (m/s)
Distance Above Invert, m
Offset, m
0.3
0.4
0.5
0.6

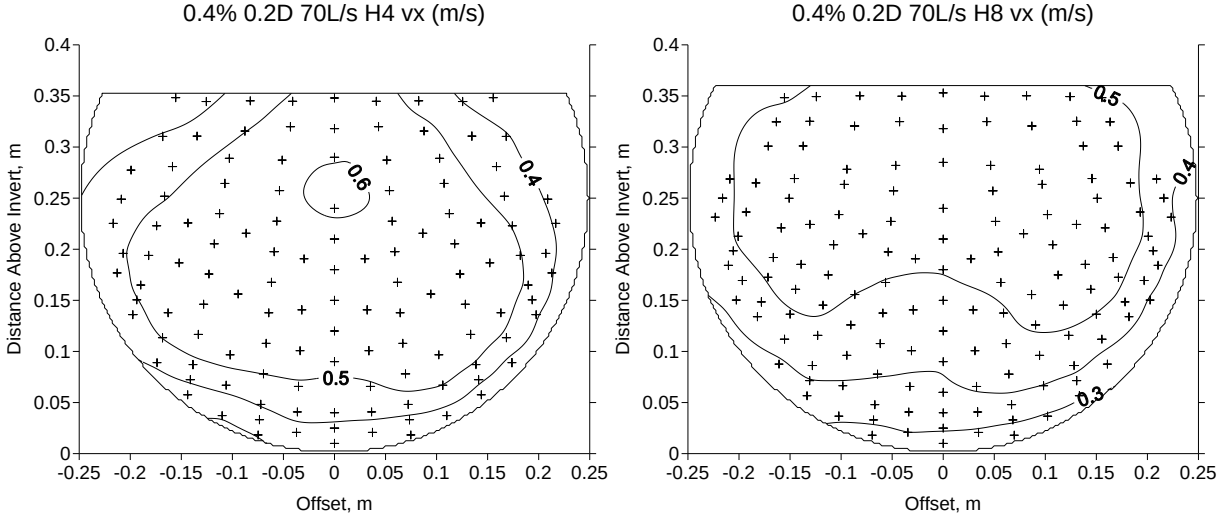
0.4% 0.2D 70L/s H4 vx (m/s)
Distance Above Invert, m
Offset, m
0.4
0.5
0.6

0.4% 0.2D 70L/s H8 vx (m/s)
Distance Above Invert, m
Offset, m
0.3
0.4
0.5

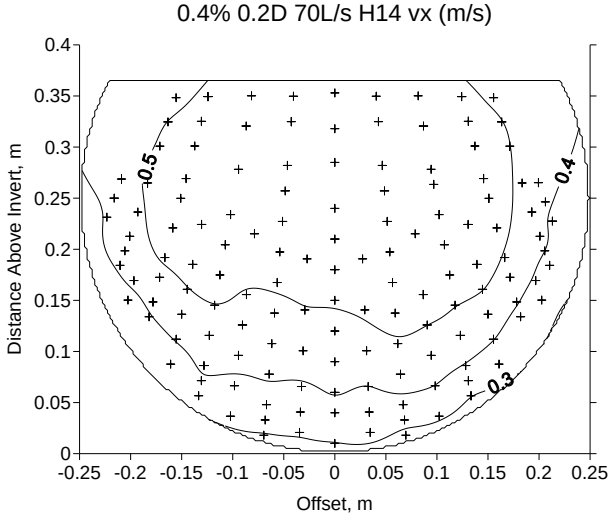
0.4% 0.2D 70L/s H14 vx (m/s)
Distance Above Invert, m
Offset, m
0.3
0.4
0.5

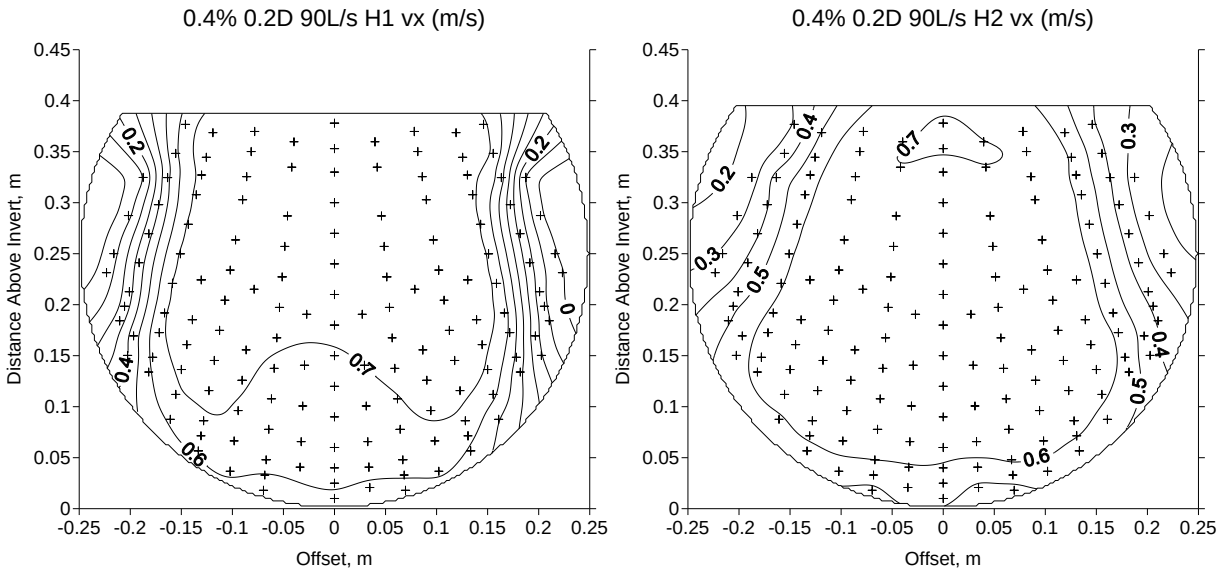
0.4% 0.2D 90L/s H1 vx (m/s)
Distance Above Invert, m
Offset, m
0.4% 0.2D 90L/s H2 vx (m/s)
Distance Above Invert, m
Offset, m

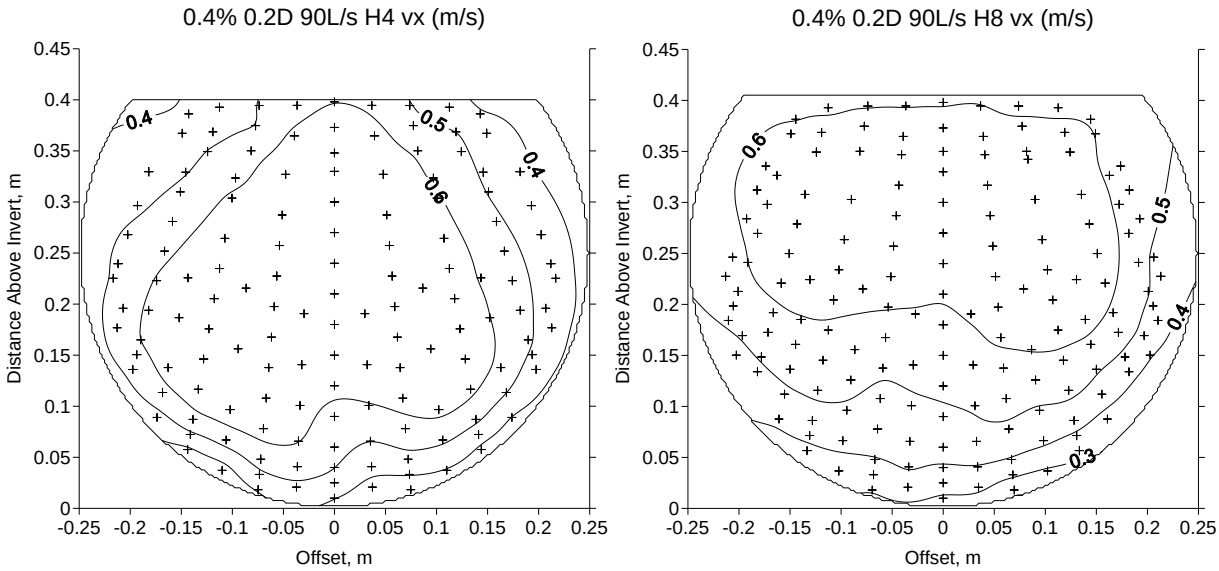
0.4% 0.2D 90L/s H4 vx (m/s)
Distance Above Invert, m
Offset, m
0.4% 0.2D 90L/s H8 vx (m/s)
Distance Above Invert, m
Offset, m

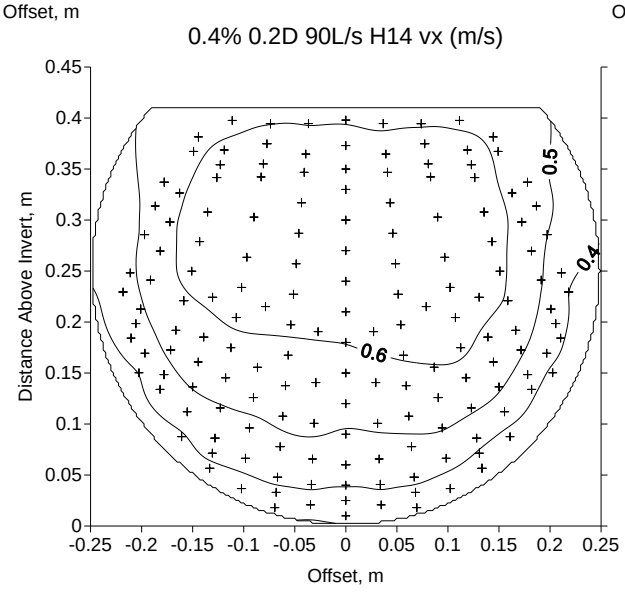
0.4% 0.2D 90L/s H14 vx (m/s)
Distance Above Invert, m
Offset, m

1.0% Culvert Slope 0.2D Embedded Cross Sections

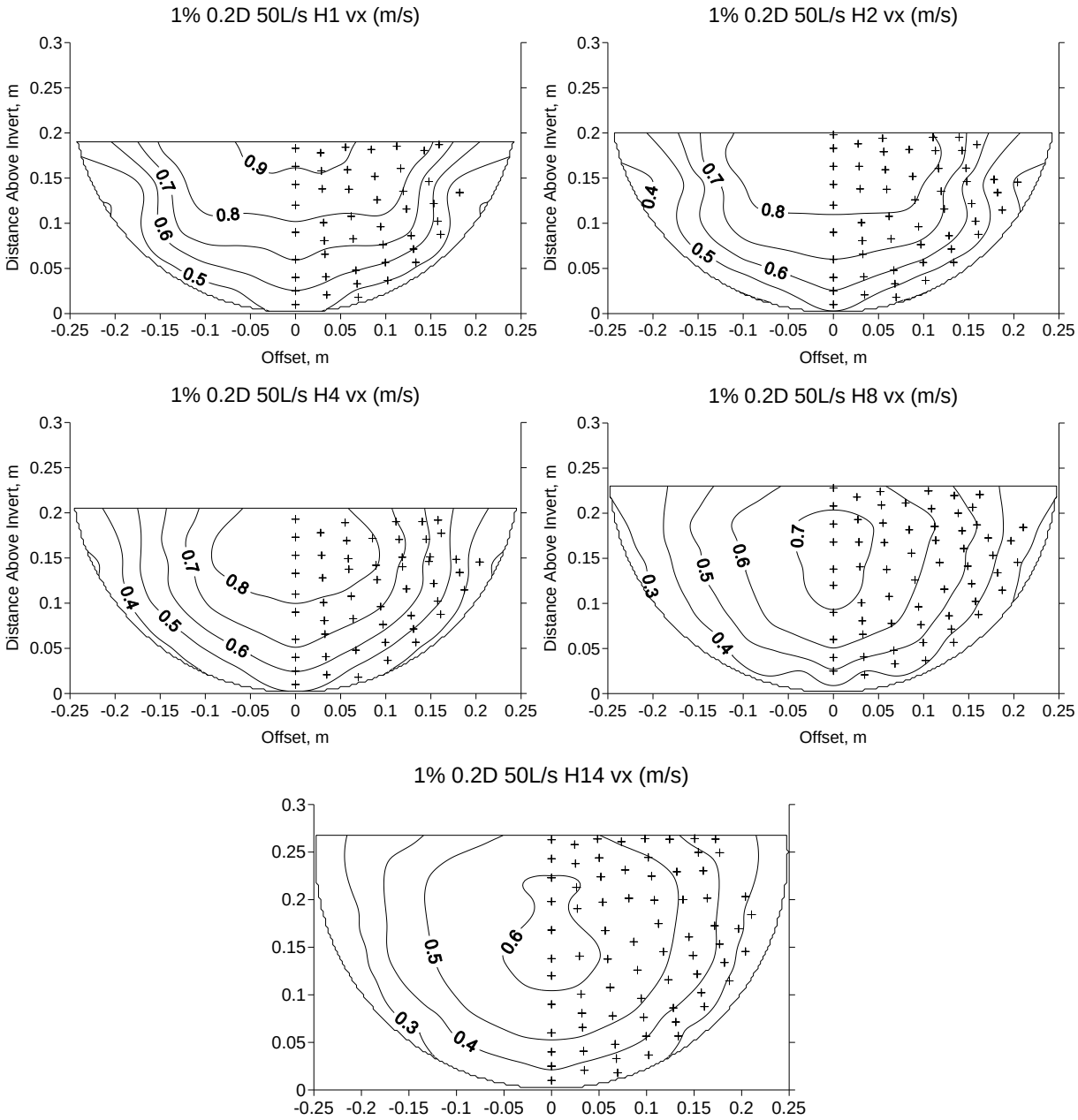

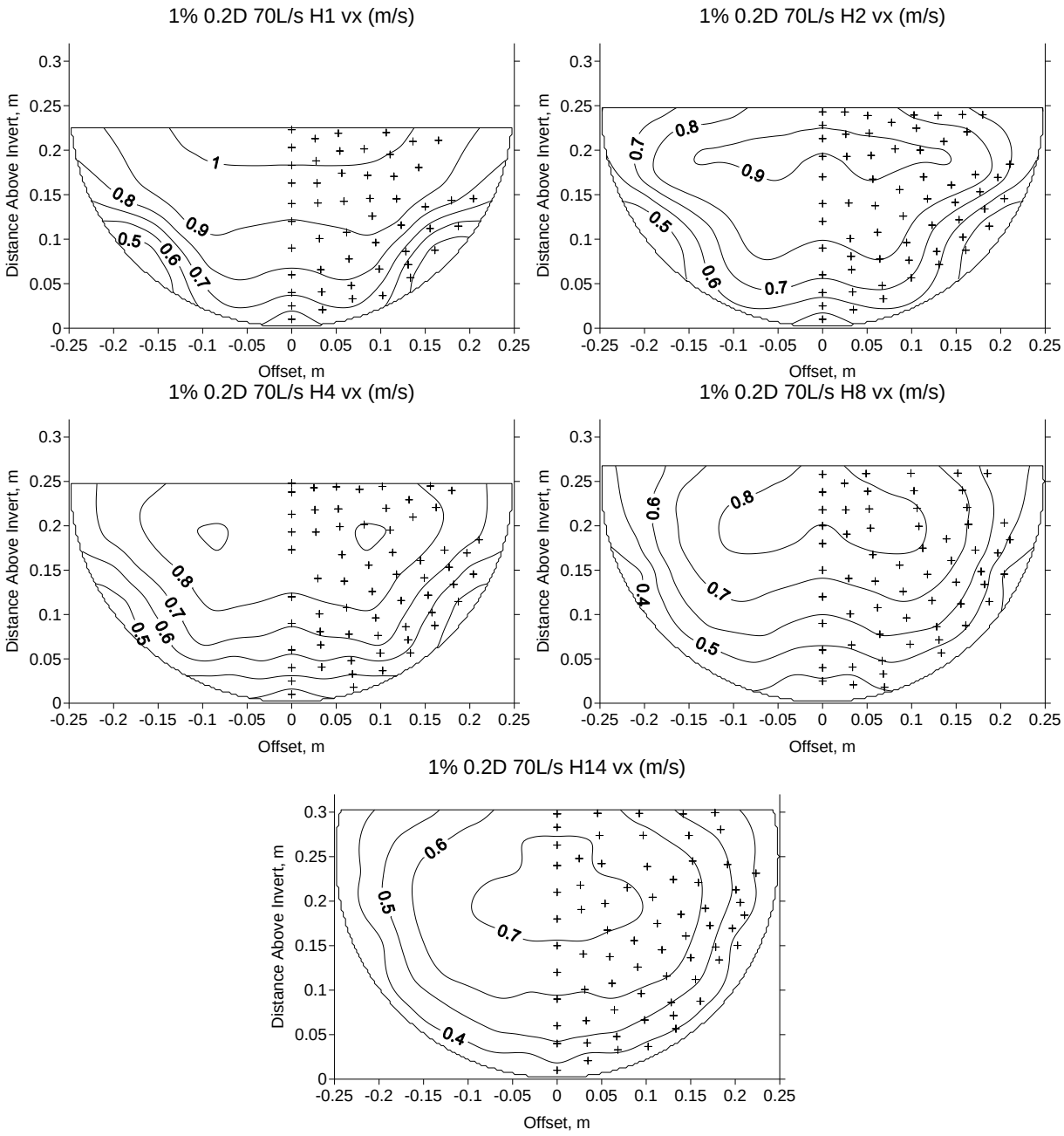
1% 0.2D 70L/s H1 vx (m/s)
1% 0.2D 70L/s H2 vx (m/s)
1% 0.2D 70L/s H4 vx (m/s)
1% 0.2D 70L/s H8 vx (m/s)
1% 0.2D 70L/s H14 vx (m/s)
Distance Above Invert, m
Offset, m

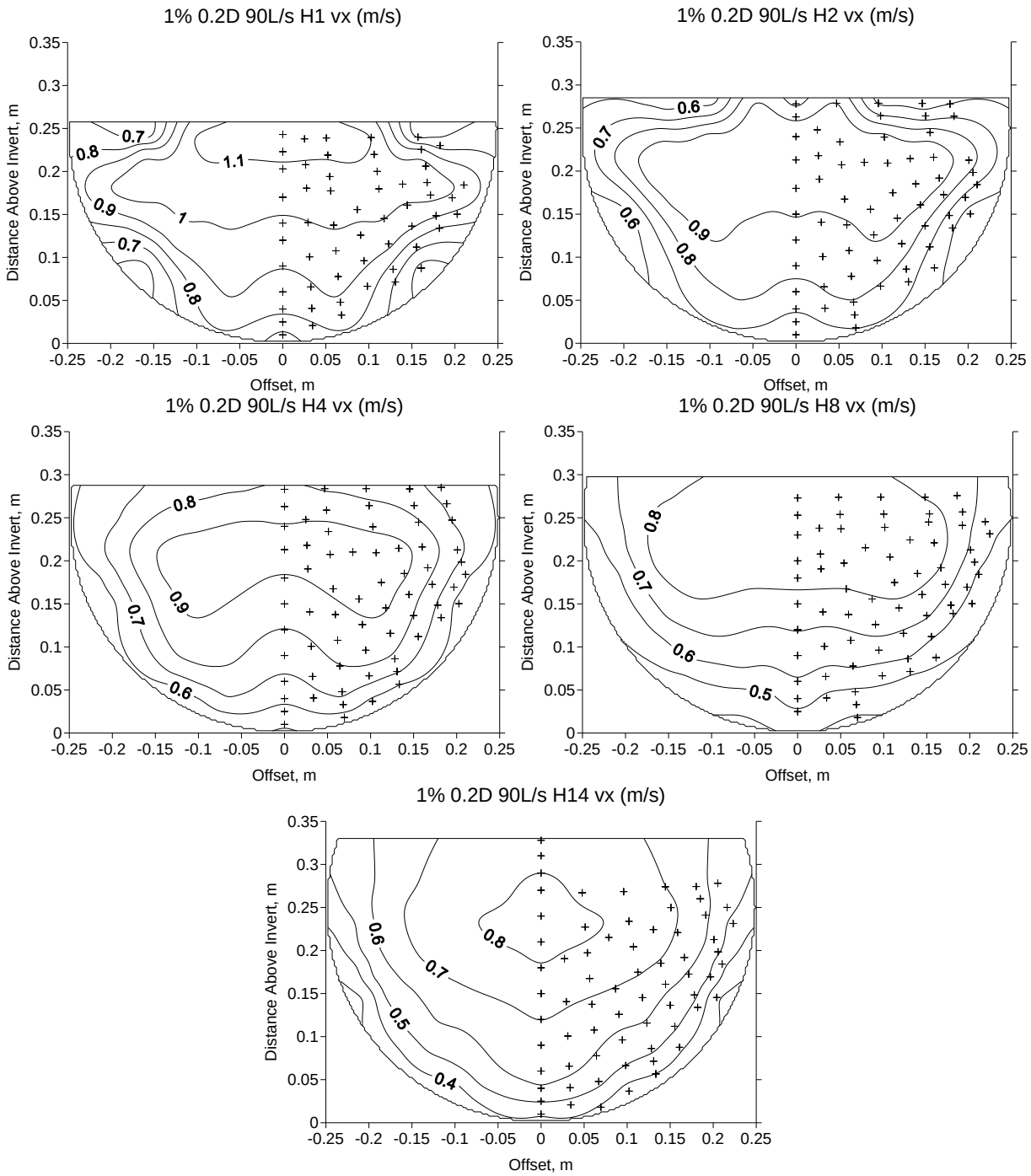
1% 0.2D 90L/s H1 vx (m/s)
1% 0.2D 90L/s H2 vx (m/s)
1% 0.2D 90L/s H4 vx (m/s)
1% 0.2D 90L/s H8 vx (m/s)
1% 0.2D 90L/s H14 vx (m/s)
Distance Above Invert, m
Offset, m

Appendix B: Details of Cross Sections and Data Quality

Table B1: Experimental results for 0.4% slope non-embedded

Run	X-Section	Y (m)	Area (m^2)	V_{ave} (m/s)	Q_{int} (L/s)	Error Q_{int} (%)
0.4% Slope Non-Embedded Q = 50.1 L/s V_{aveYn} = 0.62m/s	1	0.215	0.081	0.62	53.5	6.8
	2	0.217	0.082	0.61	52.4	4.5
	4	0.228	0.087	0.57	53.7	7.1
	8	0.225	0.086	0.58	53.0	5.8
	14	0.223	0.085	0.59	48.6	4.7
0.4% Slope Non Embedded Q = 70.0 L/s V_{aveYn} = 0.67 m/s	1	0.258	0.102	0.69	75.9	8.4
	2	0.269	0.108	0.65	74.5	6.5
	4	0.273	0.110	0.64	75.6	8.0
	8	0.271	0.109	0.64	75.1	7.3
	14	0.267	0.107	0.66	72.8	4.0
0.4% Slope Non Embedded Q = 89.8 L/s V_{aveYn}= 0.71 m/s	1	0.258	0.102	0.69	75.9	4.4
	2	0.269	0.108	0.65	74.5	6.5
	4	0.273	0.110	0.64	75.6	5.6
	8	0.271	0.109	0.64	75.1	7.2
	14	0.267	0.107	0.66	72.8	7.1

Table B2: Experimental results for 0.4 % slope 0.1 D embedded

Run	X-Section	Y (m)	Area (m^2)	V_{ave} (m/s)	Q_{int} (L/s)	Error Q_{int} (%)
0.4% Slope 0.1D Embedded Q =50.1 L/s V_{aveYn} = 0.62 m/s	1	0.253	0.099	0.50	55.4	10.5
	2	0.260	0.103	0.49	54.9	9.5
	4	0.261	0.104	0.48	53.6	6.9
	8	0.267	0.106	0.47	53.6	6.8
	14	0.271	0.108	0.46	51.7	3.2
0.4% Slope 0.1D Embedded Q = 70.0 L/s V_{aveYn}= 0.67 m/s	1	0.297	0.121	0.58	71.2	1.8
	2	0.301	0.124	0.57	70.9	1.4
	4	0.309	0.127	0.55	72.5	3.6
	8	0.315	0.130	0.54	74.1	5.9
	14	0.318	0.132	0.53	73.4	4.9
0.4% Slope 0.1D Embedded Q = 89.8 L/s V_{aveYn}= 0.71 m/s	1	0.341	0.142	0.63	90.3	0.5
	2	0.349	0.146	0.61	93.0	3.5
	4	0.359	0.151	0.60	92.1	2.5
	8	0.362	0.152	0.59	92.8	3.3
	14	0.363	0.153	0.59	93.0	3.5

Table B3: Experimental results for 0.4 % slope 0.2 D embedded

Run	X-Section	Y (m)	Area (m^2)	V_{ave} (m/s)	Q_{int} (L/s)	Error Q_{int} (%)
0.4% Slope 0.2D Embedded Q =50.1 L/s V_{aveYn}= 0.62 m/s	1	0.296	0.121	0.42	50.1	6.0
	2	0.300	0.123	0.41	52.7	5.2
	4	0.304	0.125	0.40	52.7	5.2
	8	0.313	0.130	0.39	54.0	7.8
	14	0.320	0.133	0.38	54.0	7.2
0.4% Slope 0.2D Embedded Q = 70.0 L/s V_{aveYn} = 0.67 m/s	1	0.344	0.144	0.49	72.8	4.0
	2	0.351	0.147	0.48	74.5	6.5
	4	0.354	0.148	0.47	72.8	4.1
	8	0.361	0.152	0.46	73.3	4.8
	14	0.367	0.154	0.45	72.8	4.1
0.4% Slope 0.2D Embedded Q = 89.8 L/s V_{aveYn} = 0.71 m/s	1	0.389	0.164	0.55	94.1	4.8
	2	0.397	0.167	0.54	93.6	4.1
	4	0.402	0.169	0.53	94.1	4.7
	8	0.407	0.171	0.53	93.6	4.2
	14	0.410	0.172	0.52	92.9	3.4

Table B4: Experimental results for 1.0 % slope non-embedded

Run	X-Section	Y (m)	Area (m^2)	V_{ave} (m/s)	Q_{int} (L/s)	Error Q_{int} (%)
1.0 % Slope Non-Embedded Q = 50.1 L/s V_{aveYn} = 0.86 m/s	1	0.155	0.052	0.97	51.4	2.5
	2	0.166	0.057	0.88	51.4	5.6
	4	0.166	0.057	0.88	49.4	-1.5
	8	0.167	0.058	0.87	44.5	-11.2
	14	0.176	0.062	0.81	52.2	4.2
1.0 % Slope Non Embedded Q = 70.0 L/s V_{aveYn} = 0.94 m/s	1	0.191	0.069	1.02	75.1	7.3
	2	0.180	0.064	1.10	66.9	-4.4
	4	0.194	0.070	1.00	73.5	5.0
	8	0.202	0.074	0.94	69.9	-0.1
	14	0.208	0.077	0.91	72.7	3.9
1.0 % Slope Non Embedded Q = 89.8 L/s V_{aveYn} = 1.01 m/s	1	0.219	0.083	1.09	96.8	7.8
	2	0.196	0.071	1.26	80.1	-10.9
	4	0.231	0.088	1.02	93.4	4.0
	8	0.228	0.087	1.03	86.0	-4.3
	14	0.237	0.092	0.98	89.8	-0.1

Table B5: Experimental results for 1.0 % slope 0.1 D embedded

Run	X-Section	Y (m)	Area (m^2)	V_{ave} (m/s)	Q_{int} (L/s)	Error Q_{int} (%)
1.0 % Slope 0.1D Embedded Q =50.1 L/s V_{aveYn} = 0.86 m/s	1	0.159	0.054	0.94	47.1	-6.0
	2	0.188	0.068	0.74	51.7	3.2
	4	0.186	0.066	0.76	48.5	-3.2
	8	0.186	0.066	0.76	46.5	-7.3
	14	0.220	0.083	0.60	48.7	-2.8
1.0 % Slope 0.1D Embedded Q = 70.0 L/s V_{aveYn} = 0.94 m/s	1	0.199	0.073	0.96	73.8	5.4
	2	0.214	0.080	0.87	72.5	3.6
	4	0.218	0.082	0.85	68.9	-1.6
	8	0.227	0.087	0.81	63.8	-8.8
	14	0.253	0.100	0.70	67.3	-3.8
1.0 % Slope 0.1D Embedded Q = 89.8 L/s V_{aveYn} = 1.01 m/s	1	0.232	0.089	1.01	95.9	6.8
	2	0.248	0.097	0.93	94.7	5.4
	4	0.246	0.096	0.93	87.4	-2.7
	8	0.259	0.102	0.88	84.8	-5.6
	14	0.288	0.117	0.77	94.2	4.8

Table B6: Experimental results for 1.0 % slope 0.2 D embedded

Run	X-Section	Y (m)	Area (m^2)	V_{ave} (m/s)	Q_{int} (L/s)	Error Q_{int} (%)
1.0 % Slope 0.2D Embedded Q =50.1 L/s V_{aveYn} = 0.86 m/s	1	0.195	0.071	0.71	46.3	-7.6
	2	0.201	0.074	0.68	47.8	-4.7
	4	0.206	0.076	0.66	47.1	-6.1
	8	0.231	0.089	0.57	45.7	-8.8
	14	0.269	0.107	0.47	48.4	-3.4
1.0 % Slope 0.2D Embedded Q = 70.0 L/s V_{aveYn} = 0.94 m/s	1	0.226	0.086	0.81	71.4	2.1
	2	0.248	0.097	0.72	72.3	3.4
	4	0.249	0.098	0.72	70.1	0.1
	8	0.268	0.107	0.65	67.4	-3.7
	14	0.303	0.124	0.56	69.2	-1.1
1.0 % Slope 0.2D Embedded Q = 89.8 L/s V_{aveYn} = 1.01 m/s	1	0.258	0.102	0.88	92.6	3.1
	2	0.285	0.115	0.78	92.6	3.1
	4	0.289	0.118	0.76	90.0	0.2
	8	0.298	0.122	0.74	85.1	-5.3
	14	0.332	0.138	0.65	85.7	-4.6

Table B7: Experimental results for 1.0% slope with baffled invert at various embedments

Run	X-Section	Y (m)	Area (m^2)	V_{ave} (m/s)	Q_{int} (L/s)	Error Q_{int} (%)
1.0 % Slope Non-Embedded Q = 89.8 L/s V_{aveYn} = 1.01 m/s	0.25L U/S	0.282	0.114	0.79	86.8	-3.4
	At Baffle	0.284	0.105	0.86	90.5	0.8
	0.25L D/S	0.277	0.112	0.81	86.4	-3.8
	0.5L D/S	0.273	0.110	0.82	86.9	-3.2
1.0 % Slope 0.1D Embedded Q = 89.8 L/s V_{aveYn} = 1.01 m/s	0.25L U/S	0.292	0.119	0.76	87.6	-2.5
	At Baffle	0.288	0.107	0.84	88.4	-5.0
	0.25L D/S	0.292	0.119	0.76	87.5	-4.8
	0.5L D/S	0.294	0.120	0.75	86.5	-3.7
1.0 % Slope 0.2D Embedded Q = 89.8 L/s V_{aveYn} = 1.01 m/s	0.25L U/S	0.325	0.135	0.67	85.4	-4.9
	At Baffle	0.325	0.125	0.72	89.1	-0.9
	0.25L D/S	0.322	0.134	0.67	86.8	-3.4
	0.5L D/S	0.325	0.135	0.66	87.7	-2.3

Appendix C: Water Surface Profiles

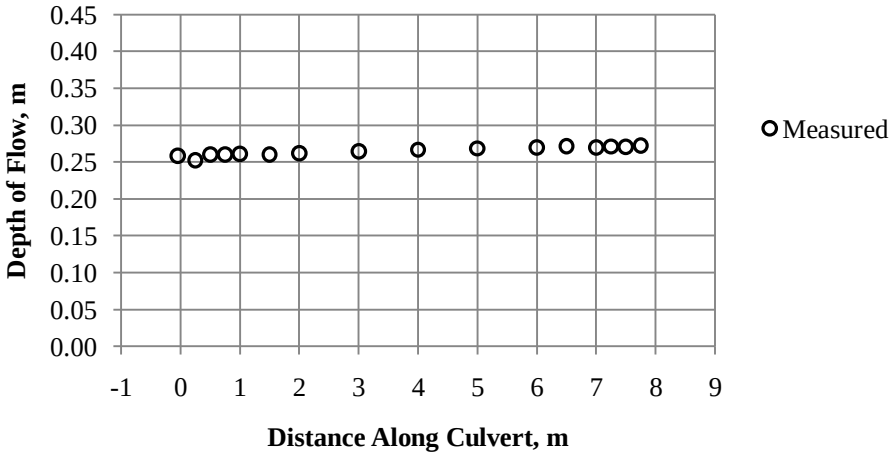

Figure C1: Water surface profile for 0.4% culvert slope, non-embedded, 50 L/s discharge.

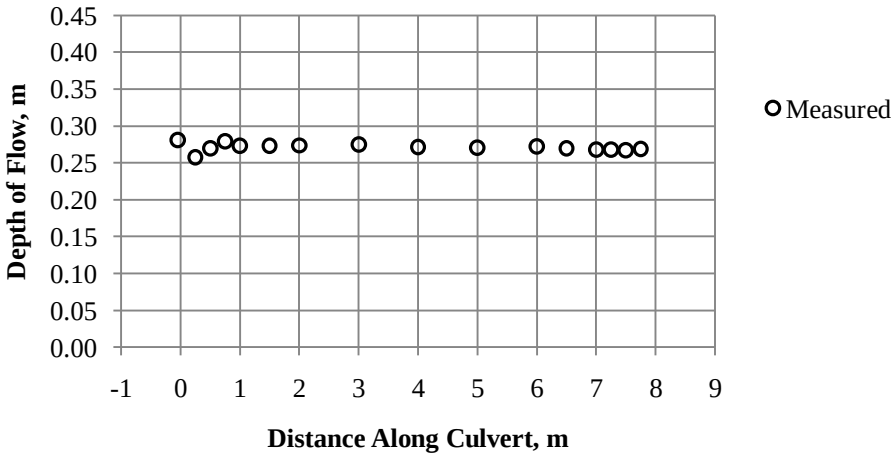

Figure C2: Water surface profile for 0.4% culvert slope, non-embedded, 70 L/s discharge.

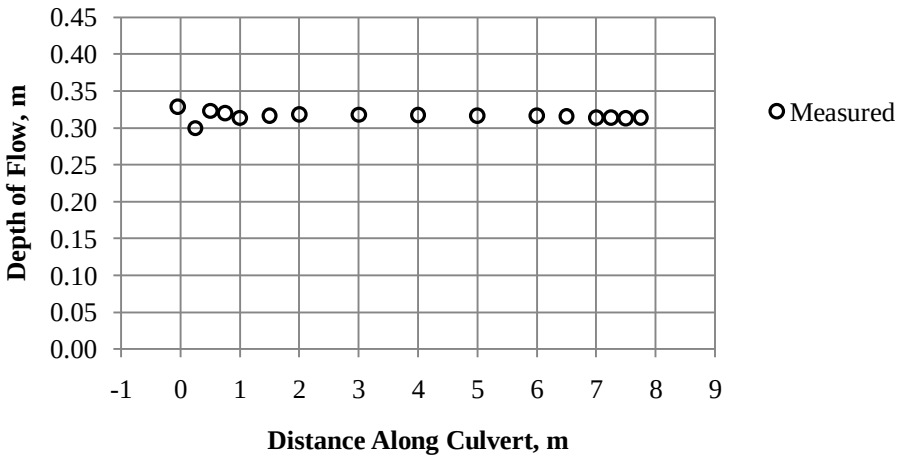

Figure C3: Water surface profile for 0.4% culvert slope, non-embedded, 90 L/s discharge.

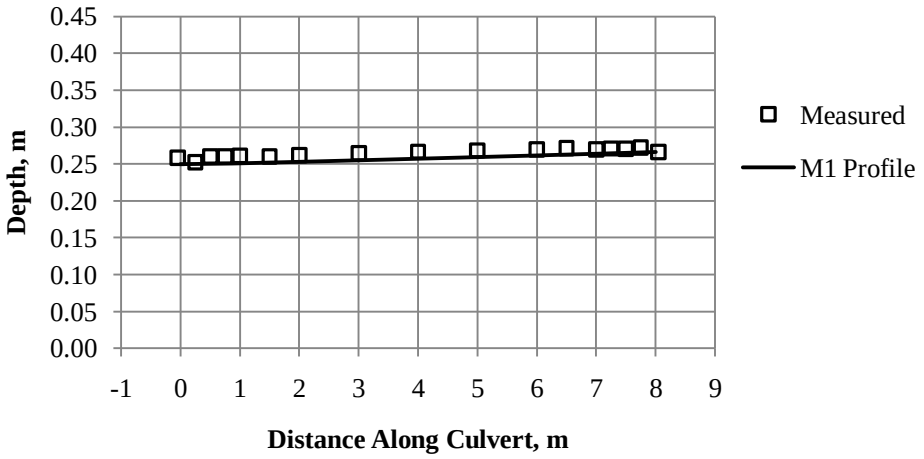

Figure C4: Water surface profile for 0.4% culvert slope, 0.1D embedded, 50 L/s discharge.

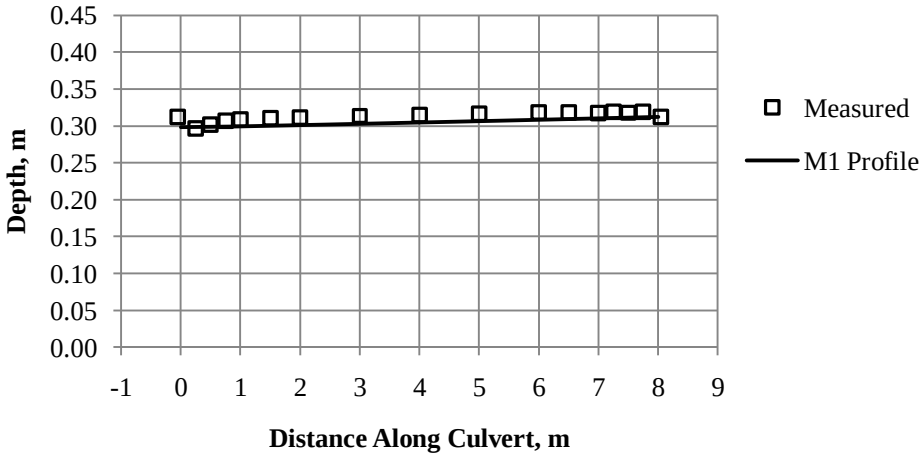

Figure C5: Water surface profile for 0.4% culvert slope, 0.1D embedded, 70 L/s discharge.

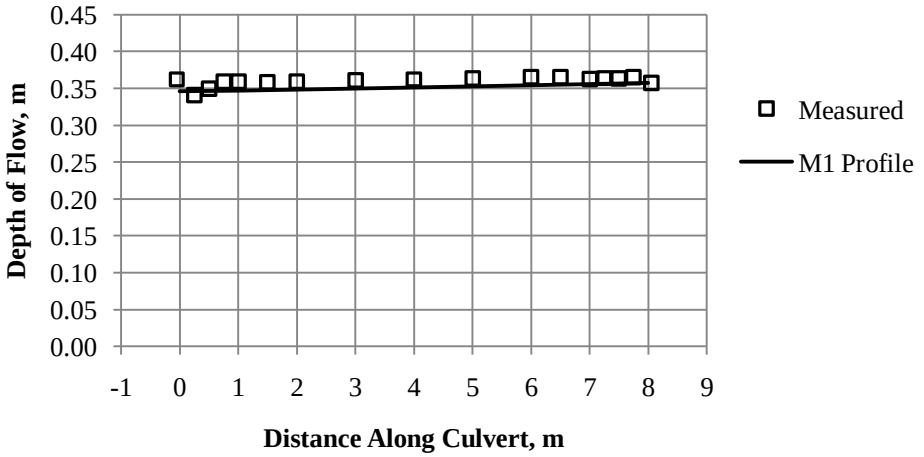

Figure C6: Water surface profile for 0.4% culvert slope, 0.1D embedded, 90 L/s discharge.

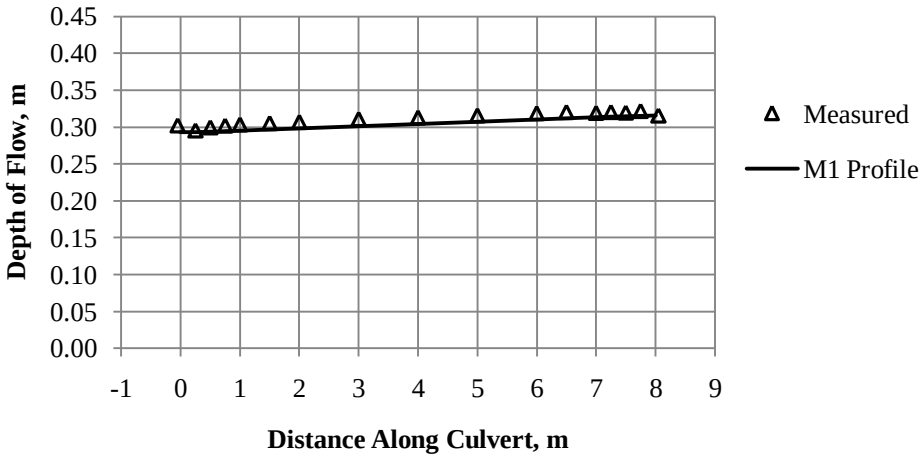

Figure C7: Water surface profile for 0.4% culvert slope, 0.2D embedded, 50 L/s discharge.

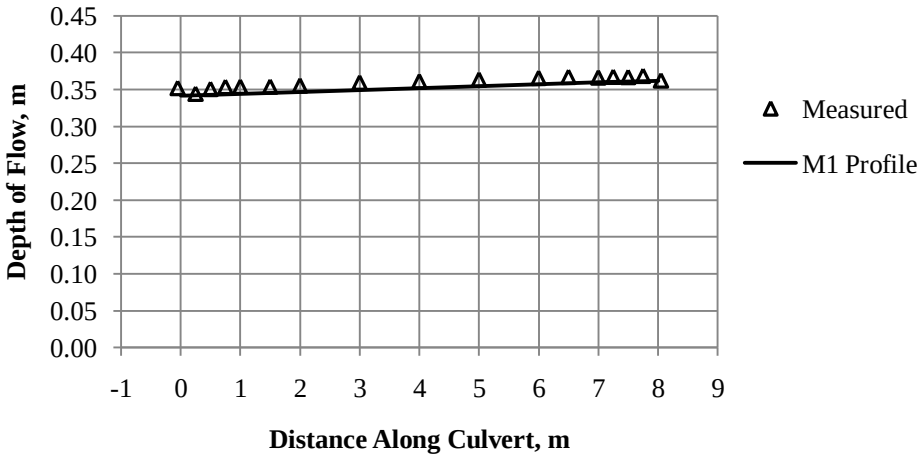

Figure C8: Water surface profile for 0.4% culvert slope, 0.2D embedded, 70 L/s discharge.

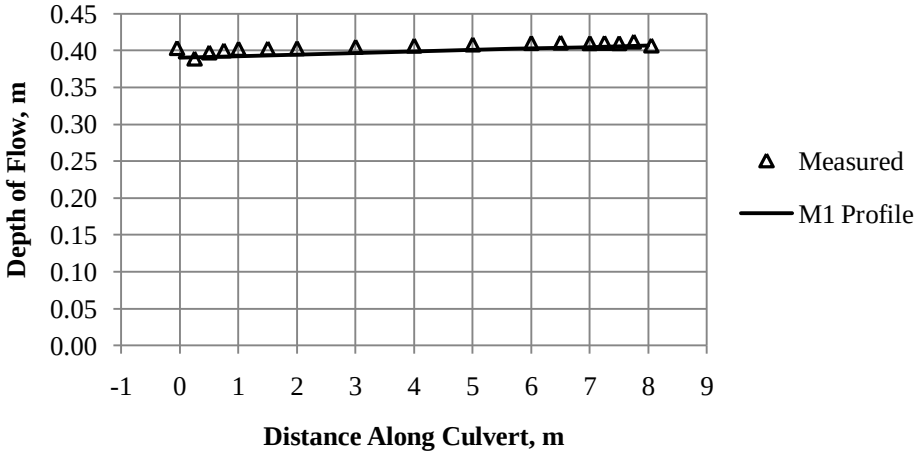

Figure C9: Water surface profile for 0.4% culvert slope, 0.2D embedded, 90 L/s discharge.

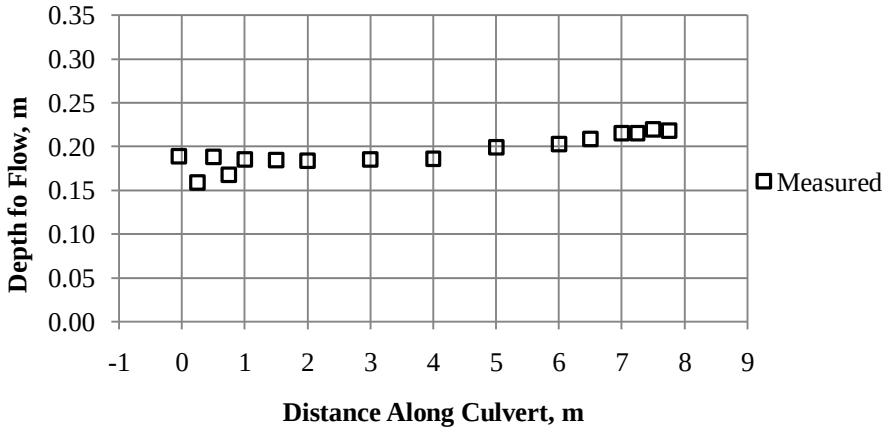

Figure C10: Water surface profile for 1.0% culvert slope, non-embedded, 50 L/s discharge.

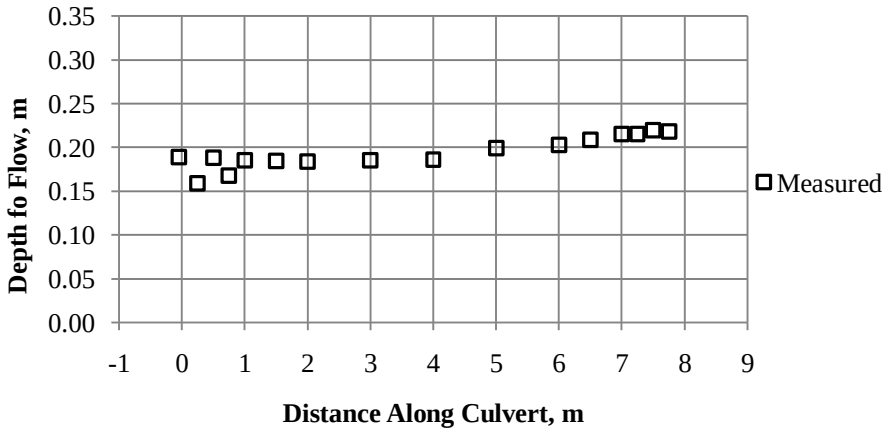

Figure C11: Water surface profile for 1.0% culvert slope, non-embedded, 70 L/s discharge.

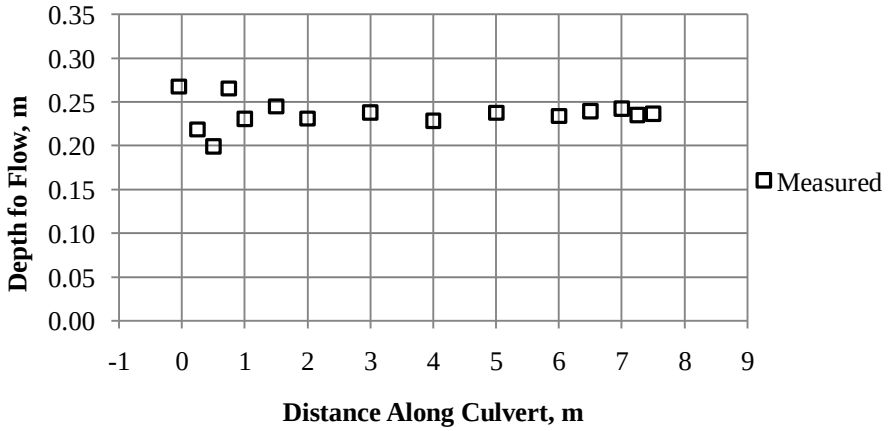

Figure C12: Water surface profile for 1.0% culvert slope, non-embedded, 90 L/s discharge.

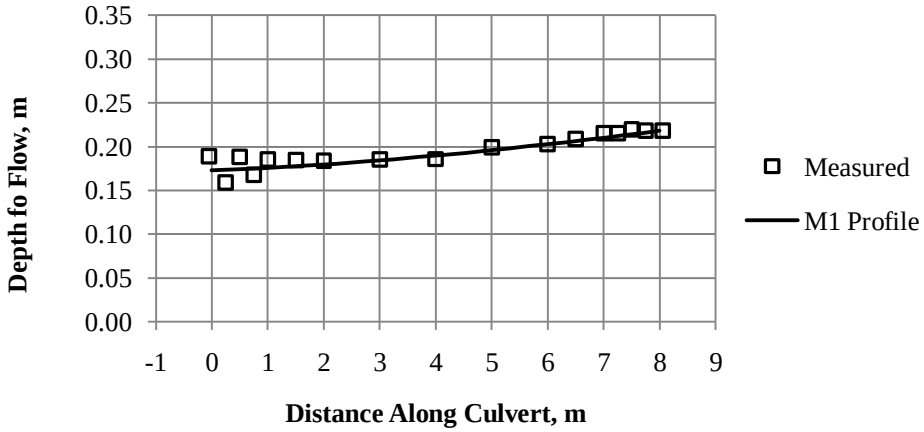

Figure C13: Water surface profile for 1.0% culvert slope, 0.1D embedded, 50 L/s discharge.

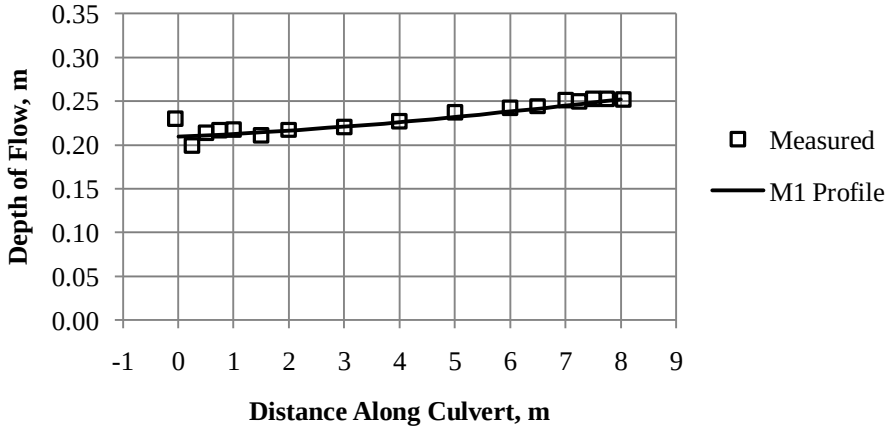

Figure C14: Water surface profile for 1.0% culvert slope, 0.1D embedded, 70 L/s discharge.

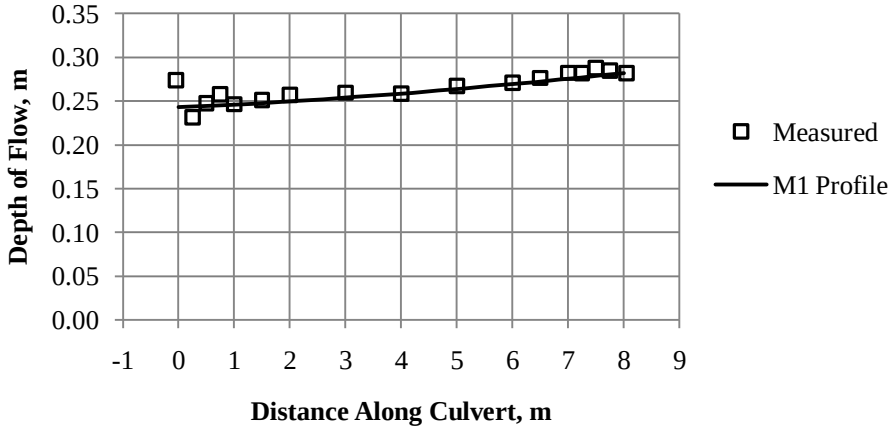

Figure C15: Water surface profile for 1.0% culvert slope, 0.1D embedded, 90 L/s discharge.

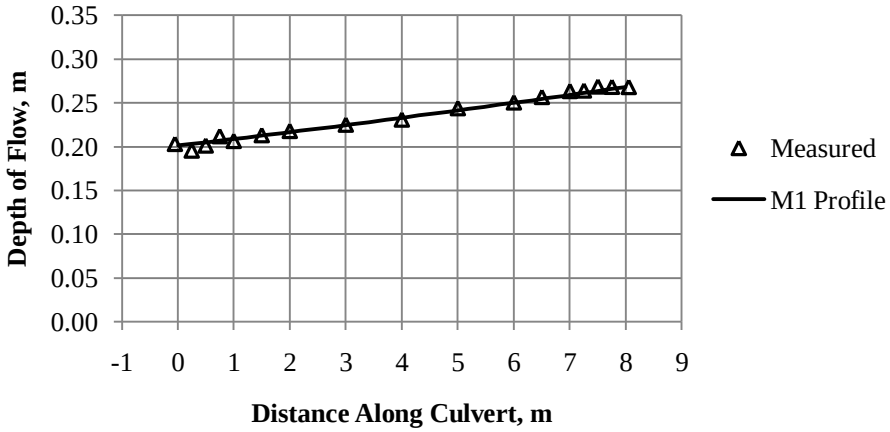

Figure C16: Water surface profile for 1.0% culvert slope, 0.2D embedded, 50 L/s discharge.

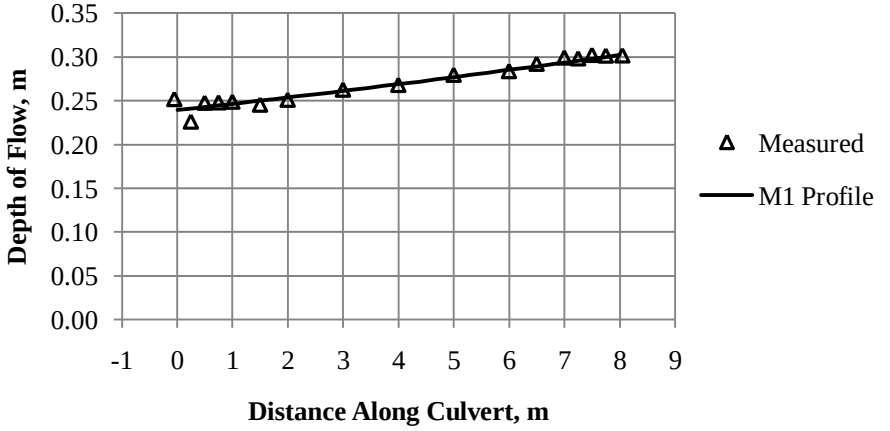

Figure C17: Water surface profile for 1.0% culvert slope, 0.2D embedded, 70 L/s discharge.

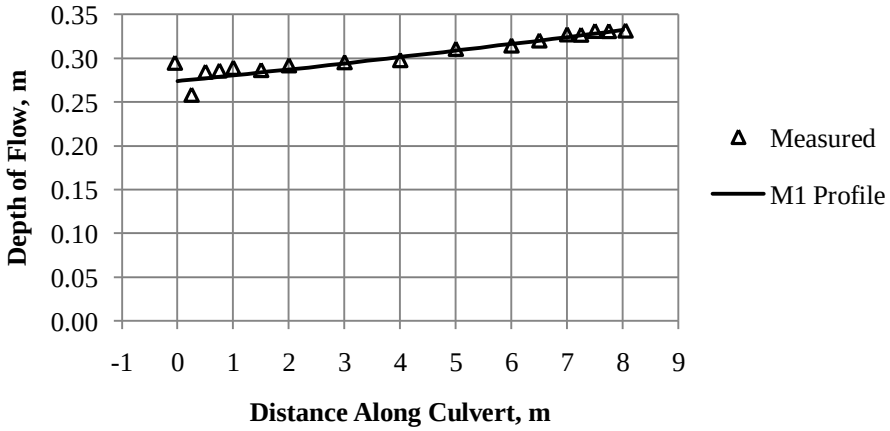

Figure C18: Water surface profile for 1.0% culvert slope, 0.2D embedded, 90 L/s discharge.

Appendix D: Centreline Vertical Velocity Profiles

0.4% Culvert Slope Non-Embedded

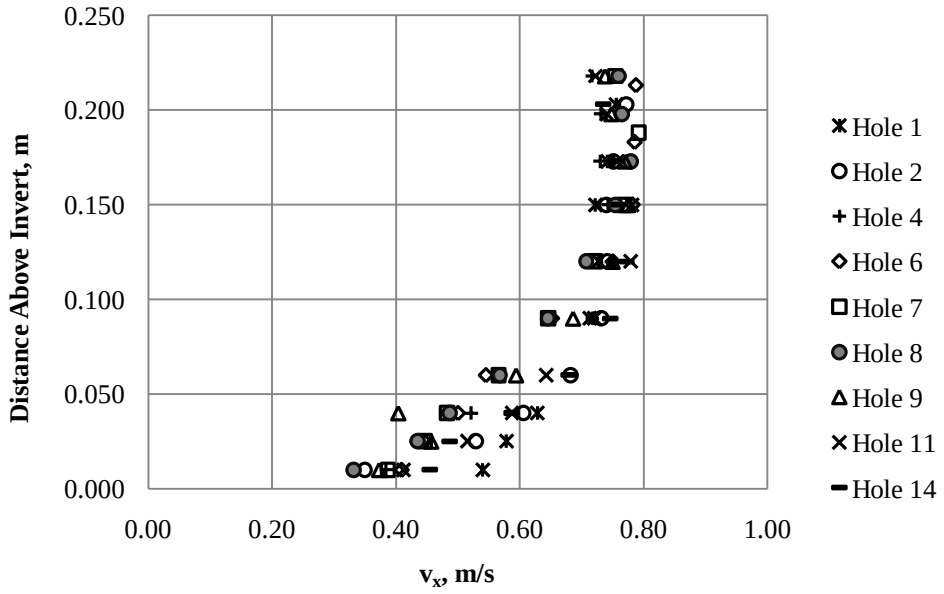

Figure D1: 0.4% Culvert Slope, Non-Embedded, 50 L/s

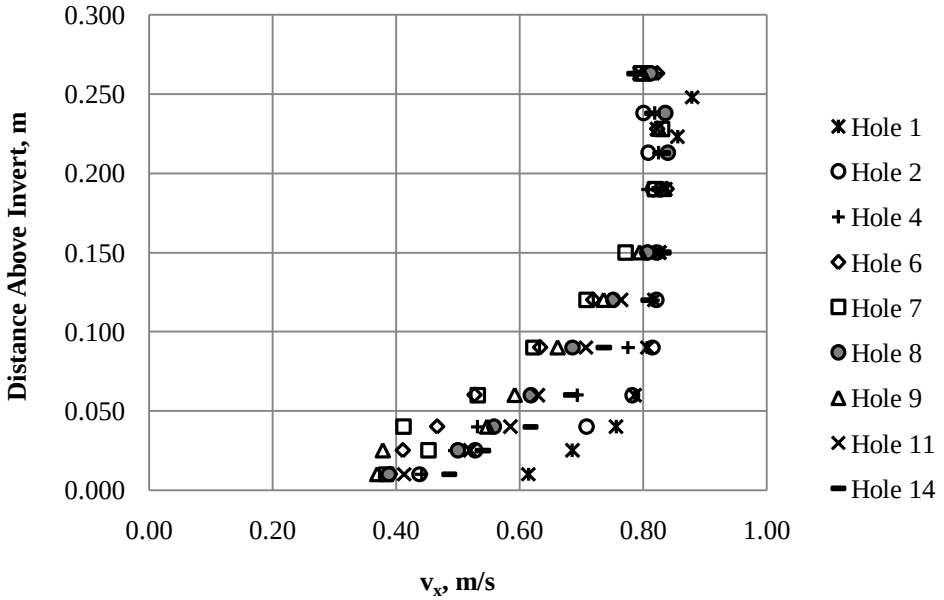

Figure D2: 0.4% Culvert Slope, Non-Embedded, 70 L/s

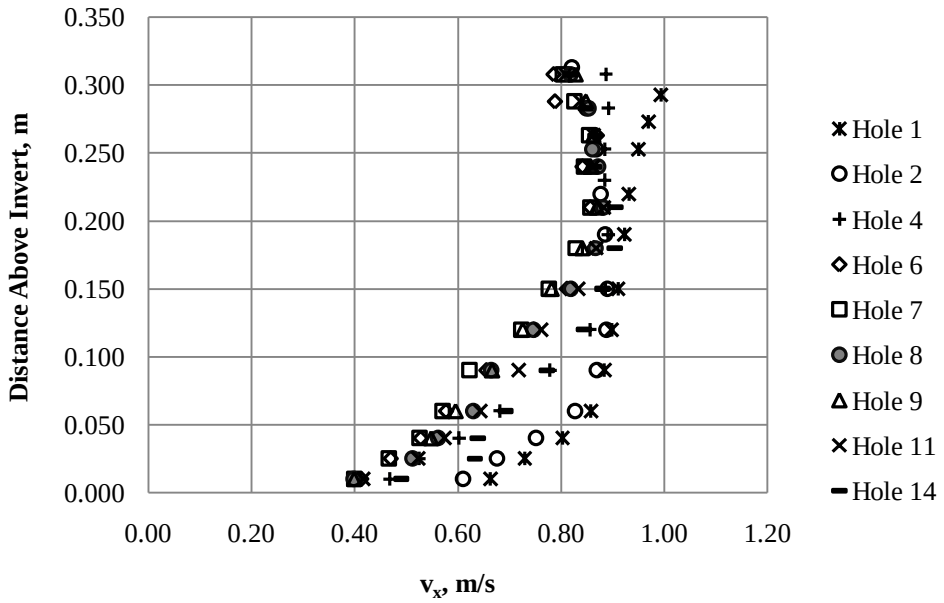

Figure D3: 0.4% Culvert Slope, Non-Embedded, 90 L/s

1.0% Culvert Slope Non-Embedded

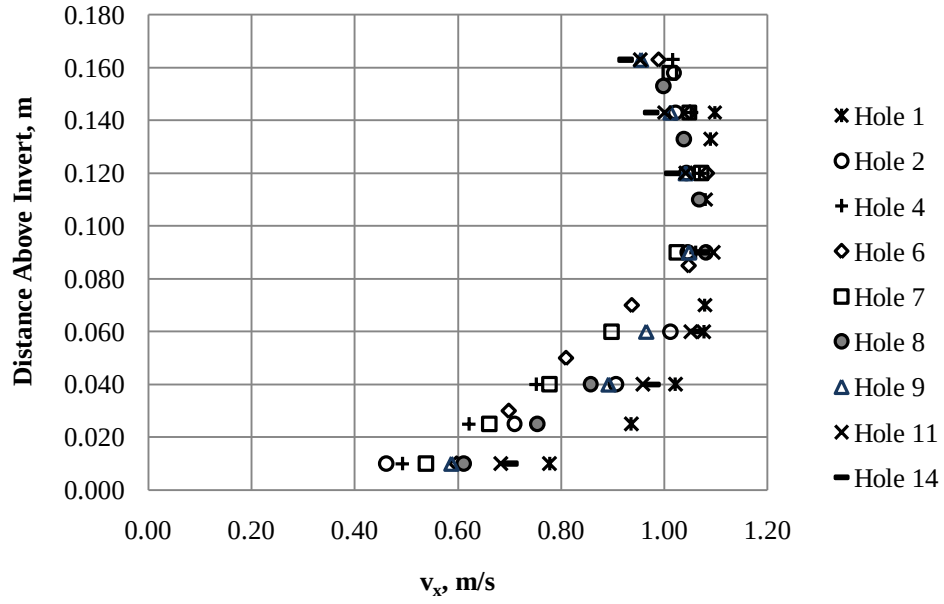

Figure D4: 1.0% Culvert Slope, Non-Embedded, 50 L/s

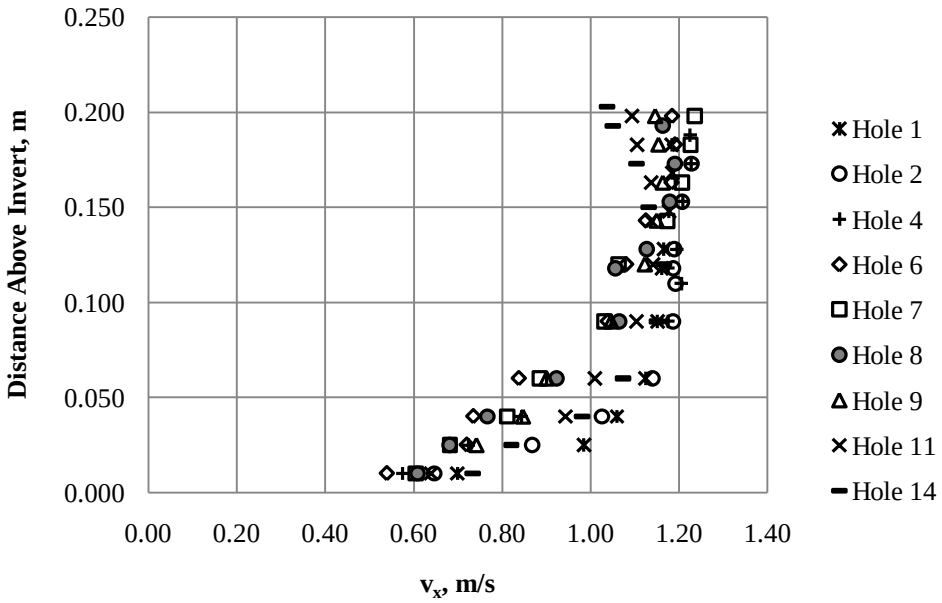

Figure D5: 1.0% Culvert Slope, Non-Embedded, 70 L/s

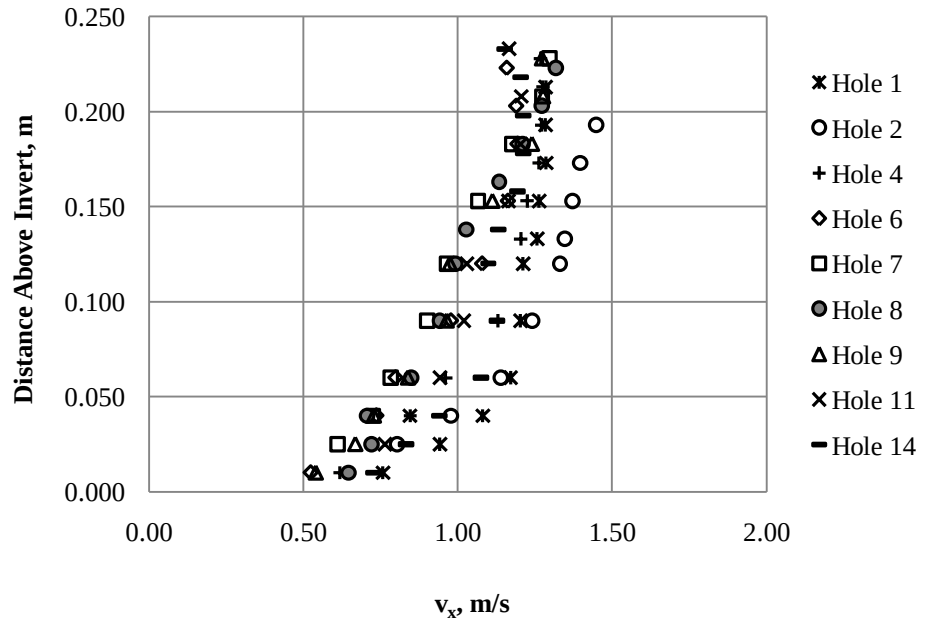

Figure D6: 1.0% Culvert Slope, Non-Embedded, 90 L/s

0.4% Culvert Slope 0.1D Embedded

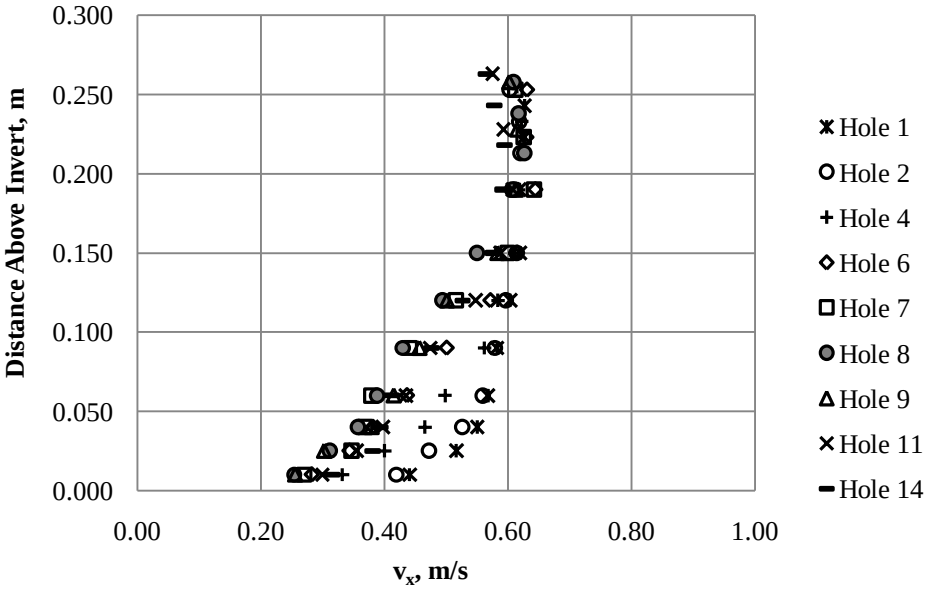

Figure D7: 0.4% Culvert Slope 0.1D, 50 L/s

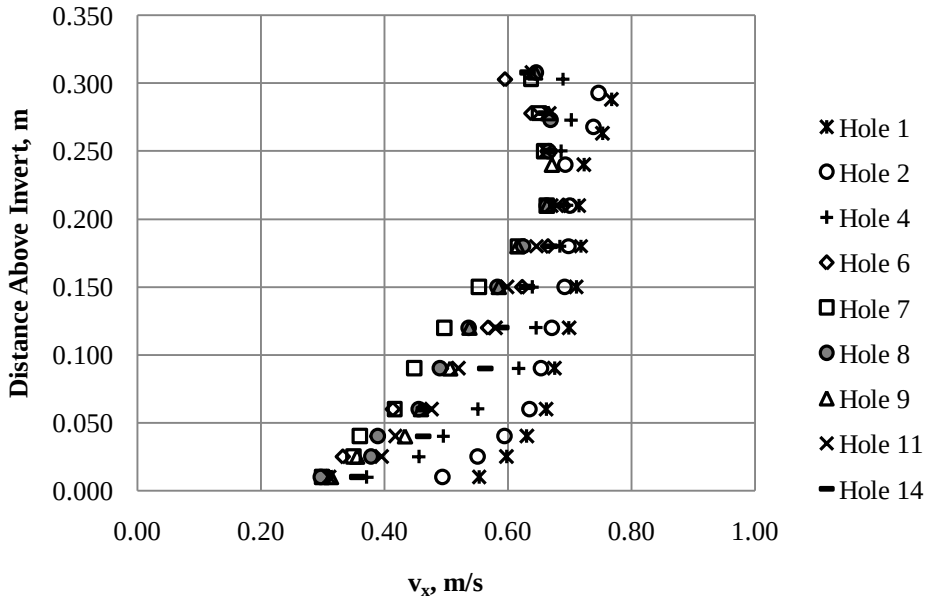

Figure D8: 0.4% Culvert Slope 0.1D, 70 L/s

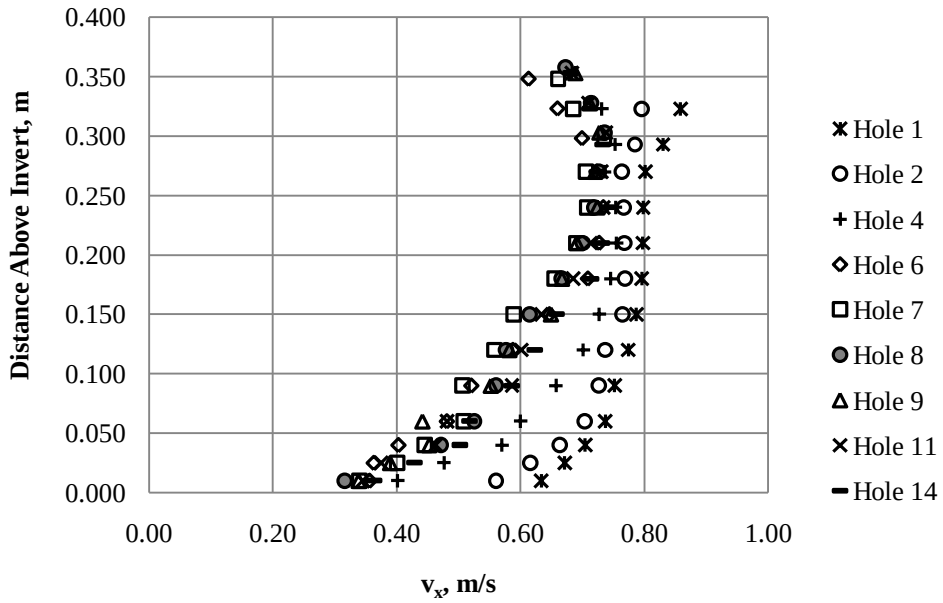

Figure D9: 0.4% Culvert Slope 0.1D, 90 L/s

1.0% Culvert Slope 0.1D Embedded

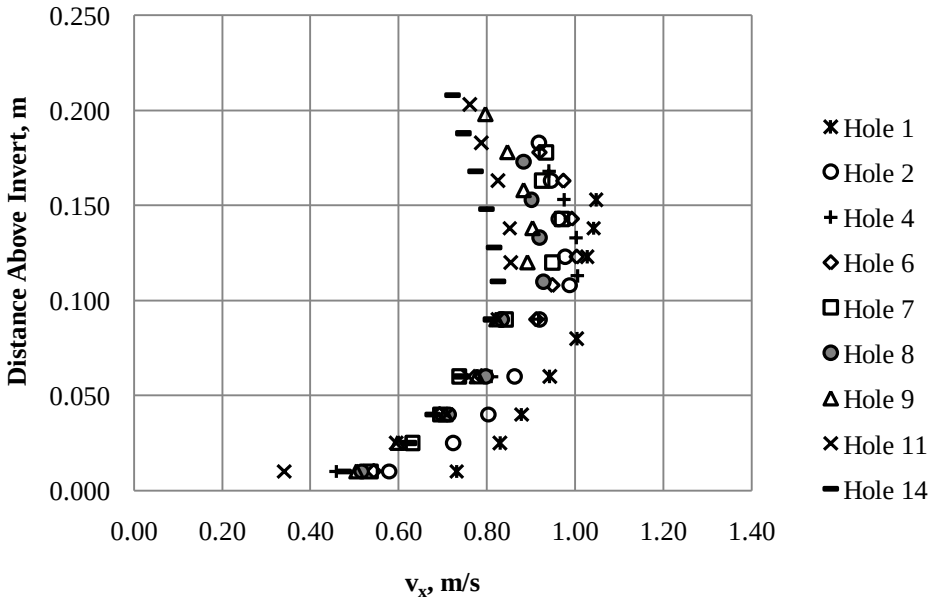

Figure D10: 1.0% Culvert Slope 0.1D, 50 L/s

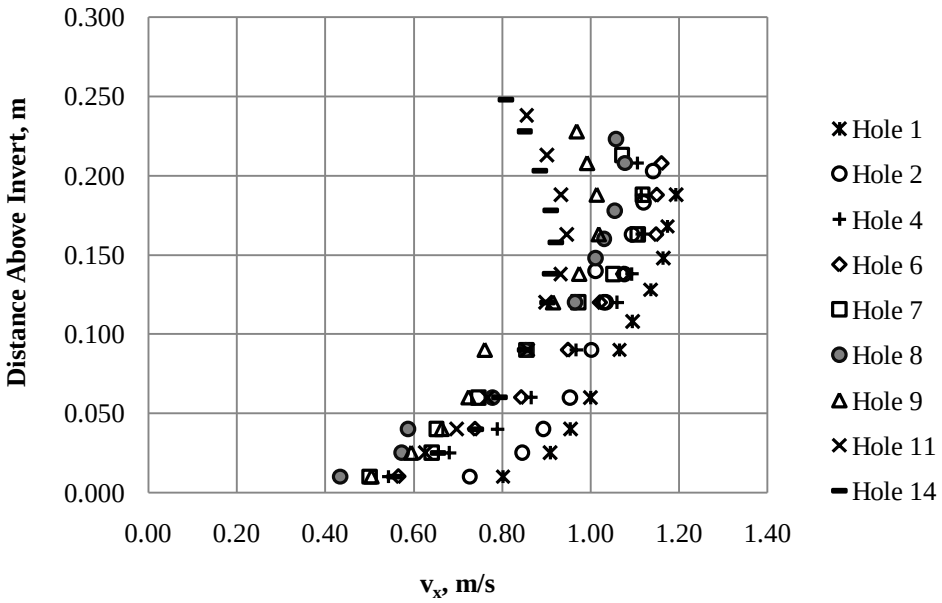

Figure D11: 1.0% Culvert Slope 0.1D, 70 L/s

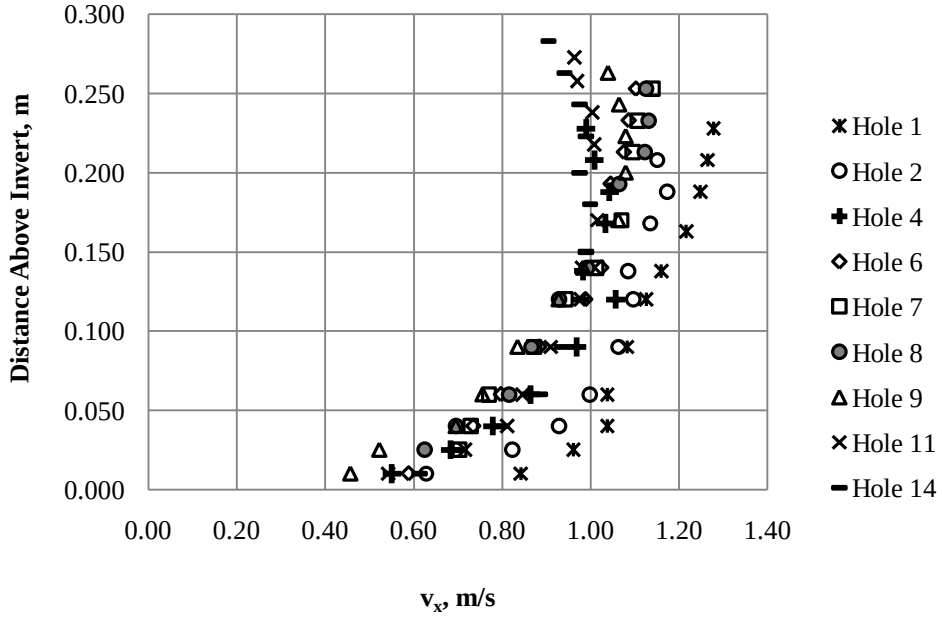

Figure D12: 1.0% Culvert Slope 0.1D, 90 L/s

0.4% Culvert Slope 0.2D Embedded

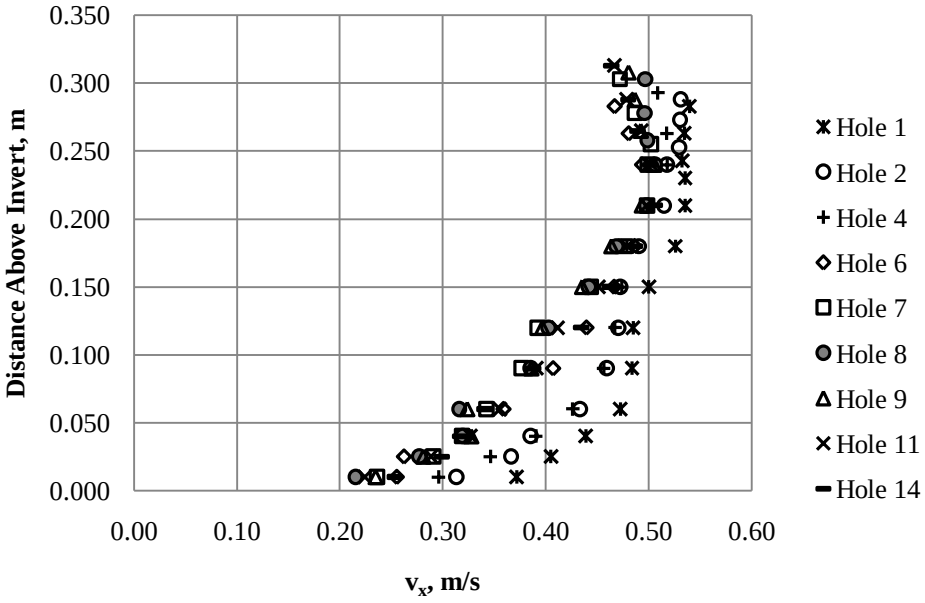

Figure D13: 0.4% Culvert Slope 0.2D, 50 L/s

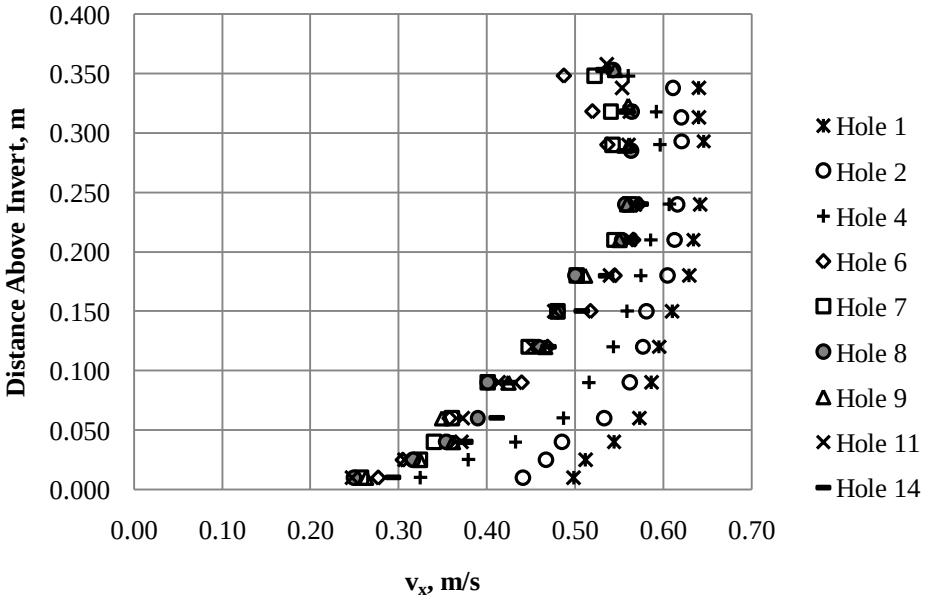

Figure D14: 0.4% Culvert Slope 0.2D, 70 L/s

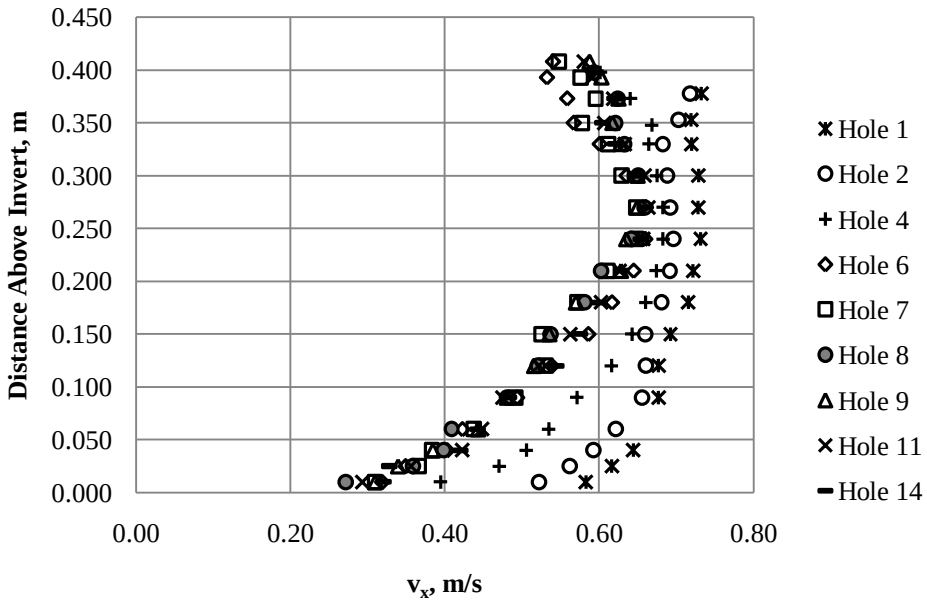

Figure D15: 0.4% Culvert Slope 0.2D, 90 L/s

1.0% Culvert Slope 0.2D Embedded

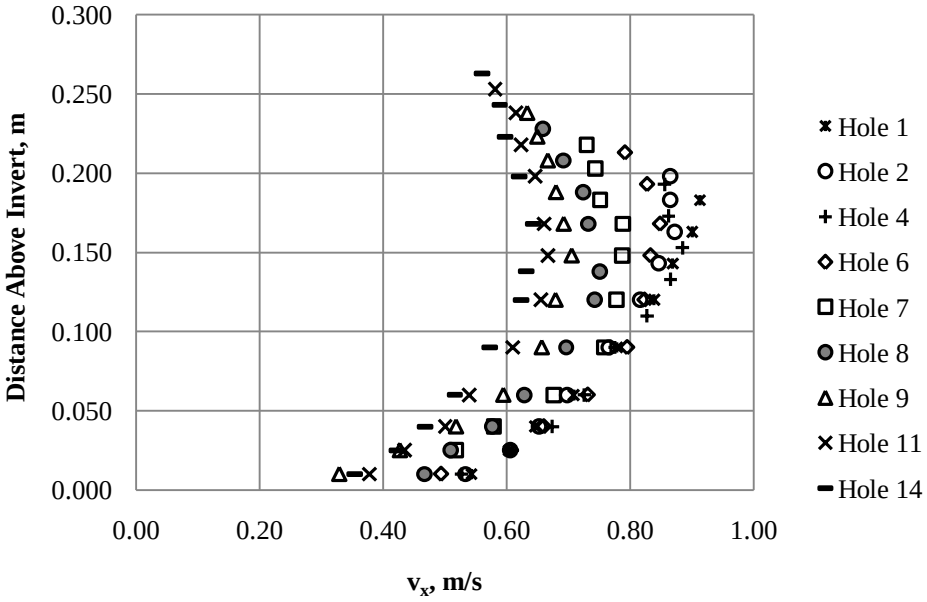

Figure D16: 1.0% Culvert Slope 0.2D, 50 L/s

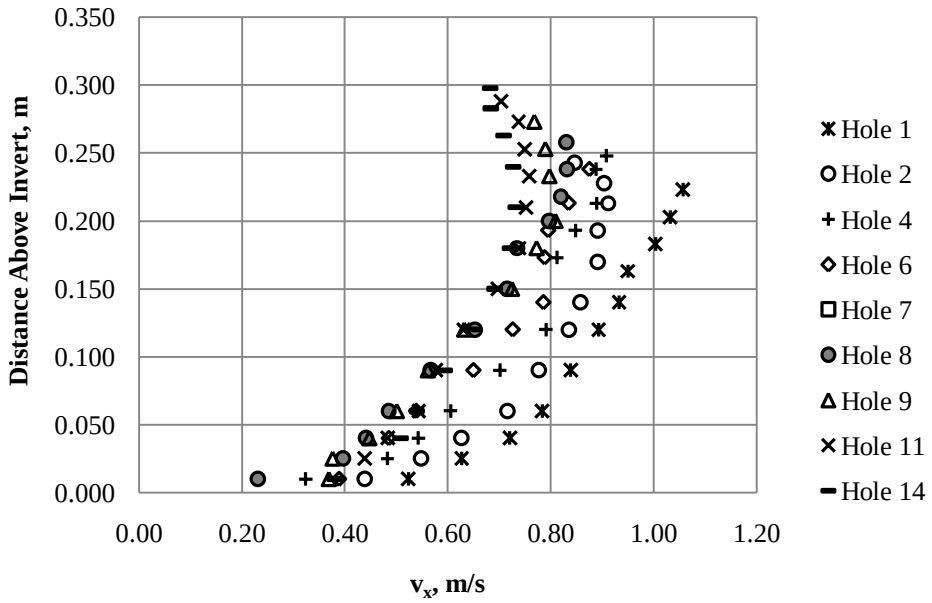

Figure D17: 1.0% Culvert Slope 0.2D, 70 L/s

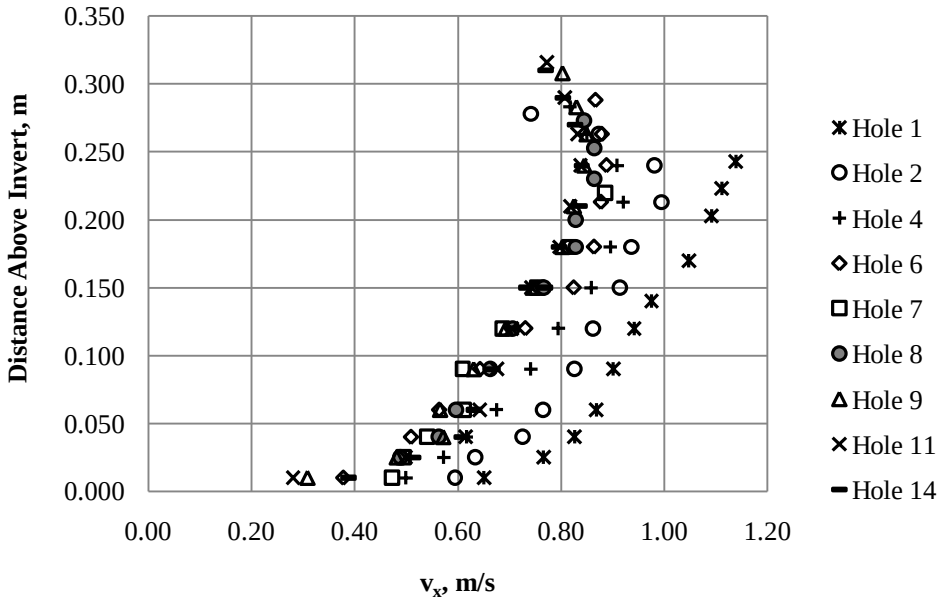

Figure D18: 1.0% Culvert Slope 0.2D, 90 L/s

Appendix E: Calculation of Shear Velocity at Various Offsets from Centreline

Table E1: 0.4% Culvert Slope

	Offset (z/r)	u_*/U^*		
		Datum		
		Corrugation Trough	Corrugation Midpoint	Corrugation Crest
0D 50 Hole 8	0.0	1.28	1.16	0.99
	0.2	1.21	1.05	0.83
	0.4	1.22	1.08	0.90
	0.6	0.94	0.89	0.67
	0.8	0.53	0.47	0.41
0D 50 Hole 14	0.0	1.21	1.05	0.87
	0.2	1.09	0.98	0.84
	0.4	0.99	0.86	0.71
	0.6	0.66	0.56	0.46
	0.8	0.42	0.37	0.32
0D 70 Hole 8	0.0	1.17	1.03	0.89
	0.2	1.12	0.97	0.78
	0.4	1.15	1.02	0.87
	0.6	0.95	0.84	0.73
	0.8	0.39	0.57	0.57
0D 70 Hole 14	0.0	1.06	0.93	0.79
	0.2	1.05	0.91	0.72
	0.4	1.01	0.89	0.74
	0.6	0.80	0.70	0.59
	0.8	0.53	0.4	0.43
0D 90 Hole 8	0.0	1.17	1.05	0.91
	0.2	1.17	1.03	0.84
	0.4	1.18	1.05	0.89
	0.6	1.02	0.91	0.77
	0.8	0.74	0.67	0.6
0D 90 Hole 14	0.0	1.04	0.93	0.80
	0.2	1.07	0.93	0.75
	0.4	1.09	0.96	0.82
	0.6	0.86	0.76	0.65
	0.8	0.80	0.74	0.66

Table E2: 1.0% Culvert Slope

	Offset (z/r)	u_*/U^*		
		Datum		
		Corrugation Trough	Corrugation Midpoint	Corrugation Crest
0D 50 Hole 8	0.0	1.29	1.13	0.90
	0.2	1.24	1.01	0.74
	0.4	0.95	0.79	0.61
	0.6	0.42	0.34	0.26
	0.8	-	-	-
0D 50 Hole 14	0.0	1.13	0.96	0.77
	0.2	0.87	0.70	0.51
	0.4	0.83	0.68	0.52
	0.6	0.4	0.32	0.15
	0.8	-	-	-
0D 70 Hole 8	0.0	1.26	1.12	0.95
	0.2	1.14	0.98	0.78
	0.4	1.11	0.94	0.76
	0.6	0.87	0.70	0.57
	0.8	0.16	0.13	0.09
0D 70 Hole 14	0.0	1.08	0.93	0.77
	0.2	0.87	0.73	0.55
	0.4	0.83	0.70	0.54
	0.6	0.50	0.42	0.32
	0.8	-	-	-
0D 90 Hole 8	0.0	1.14	1.03	0.89
	0.2	1.07	0.94	0.76
	0.4	0.80	0.69	0.59
	0.6	0.66	0.52	0.44
	0.8	0.47	0.45	0.37
0D 90 Hole 14	0.0	0.83	0.74	0.65
	0.2	0.76	0.65	0.52
	0.4	0.94	0.81	0.66
	0.6	0.93	0.80	0.66
	0.8	0.47	0.40	0.31

Appendix F: Comparison of the Percent of Cross Section Area Less than V_{aveYn}

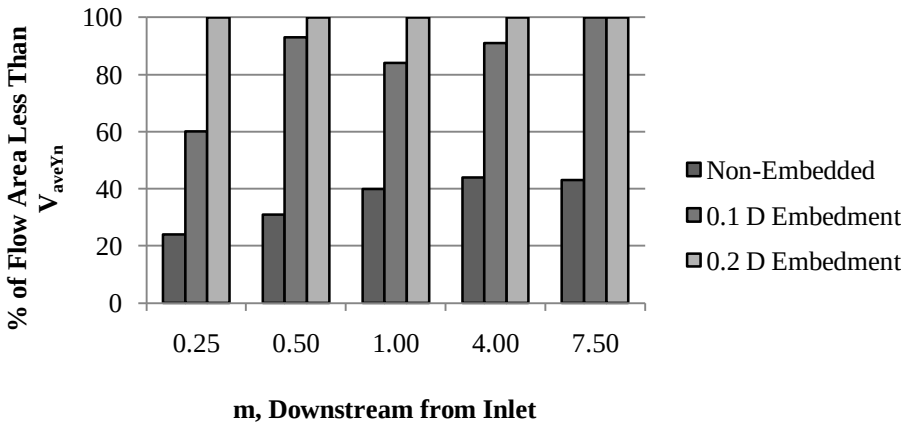

(a)

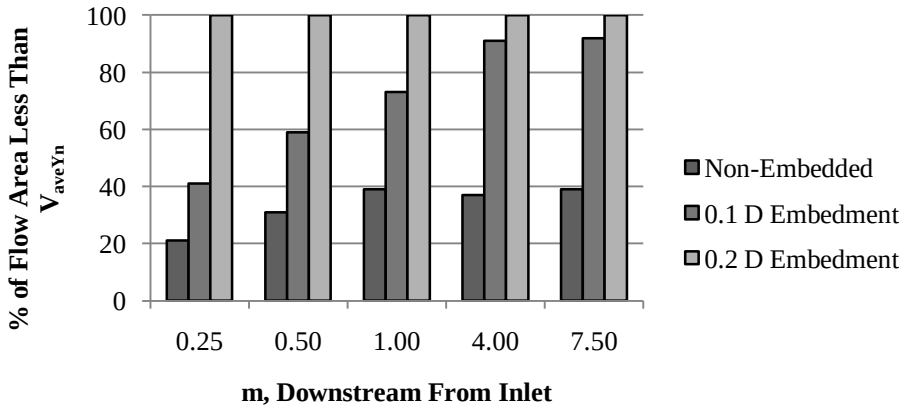

(b)

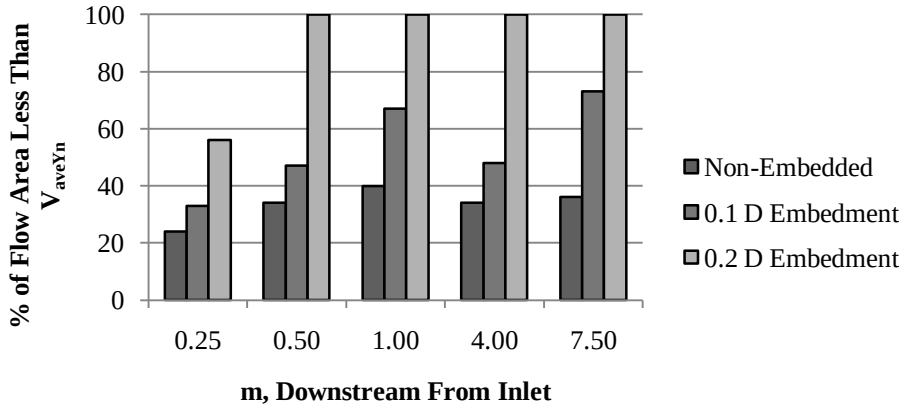

(c)

Figure F1: Percent of the flow area less than V_{ave} for 0.4% culvert slope a) 50 L/s, b) 70 L/s and c) 90 L/s

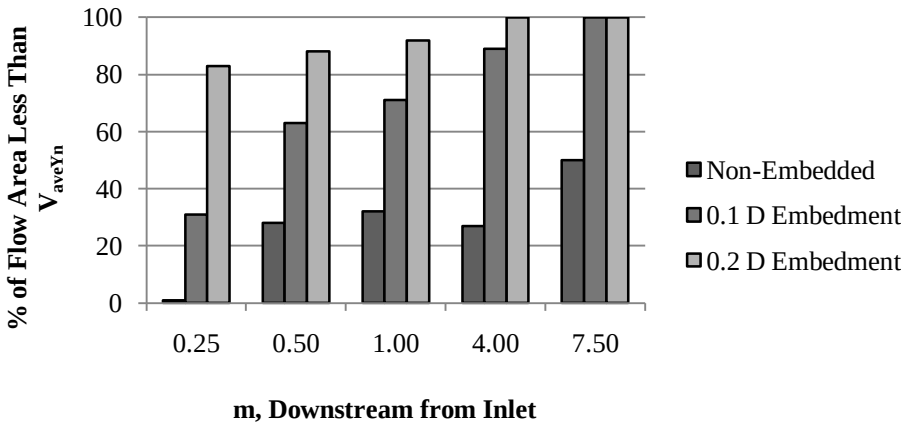

(a)

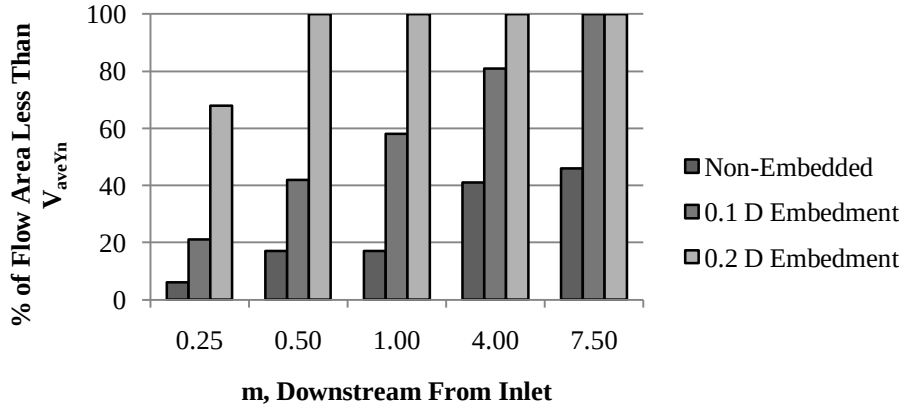

(b)

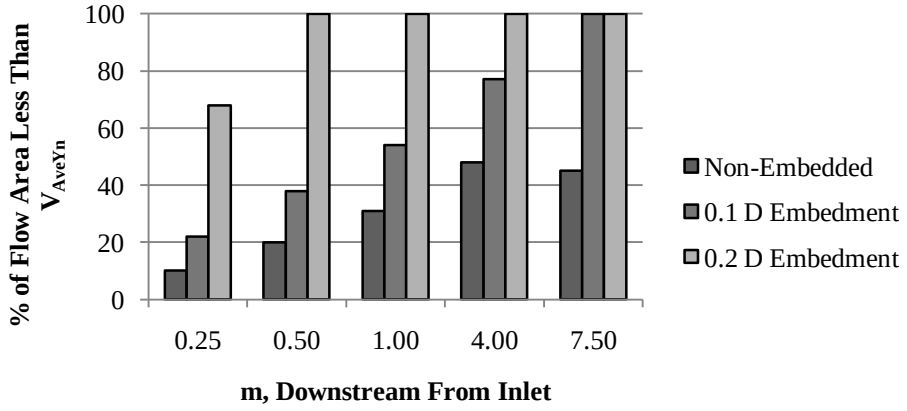

(c)

Figure F2: Percent of the flow area less than V_{ave} for 1.0% culvert slope a) 50 L/s, b) 70 L/s and c) 90 L/s

Appendix G: v_x/V_{aveYn} Contour Plots

Naming convention for contour plots

The title in each contour plot conveys the following information (in order):

- Culvert Slope (%)
- Embedment Depth (0D (non-embedded), 0.1D or 0.2D, where D=culvert diameter)
- Discharge (L/s)
- Cross Section Location (H1=hole 1, H2=hole 2 etc.)
- Measurement that is being represented by the contours.

For example: 0.4% 0D 50 L/s H1 v_x/V_{aveYn} indicates that the cross section is for the 0.4% culvert slope, non-embedded trial, at the 50 L/s discharge, the location is hole 1 and the contour plot is of the streamwise (x) direction velocity non-dimensionalized by the average cross section velocity.

Negative velocities have been indicated as white areas within the cross section.

0.4% Culvert Slope Non-Embedded Cross Sections

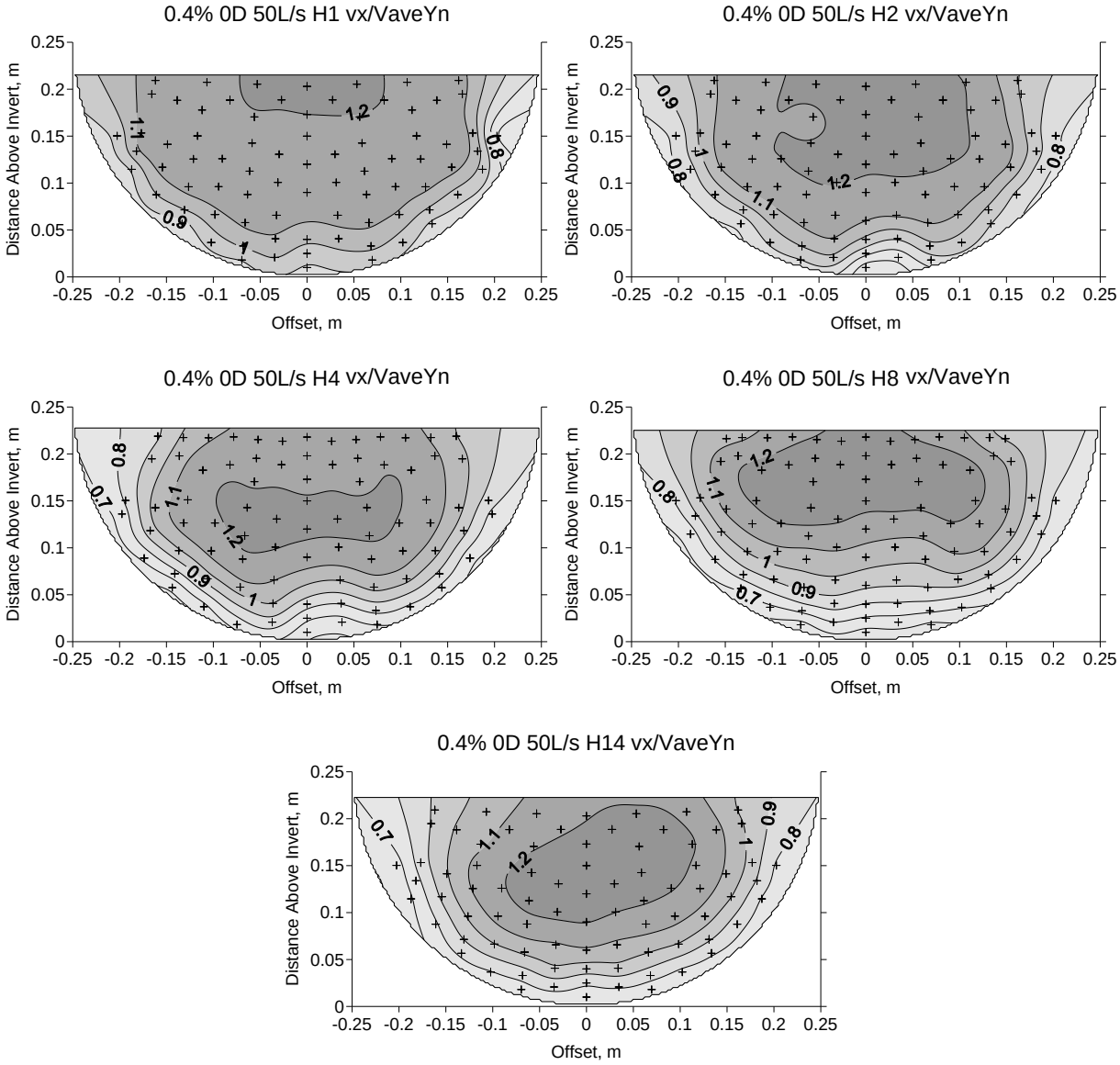

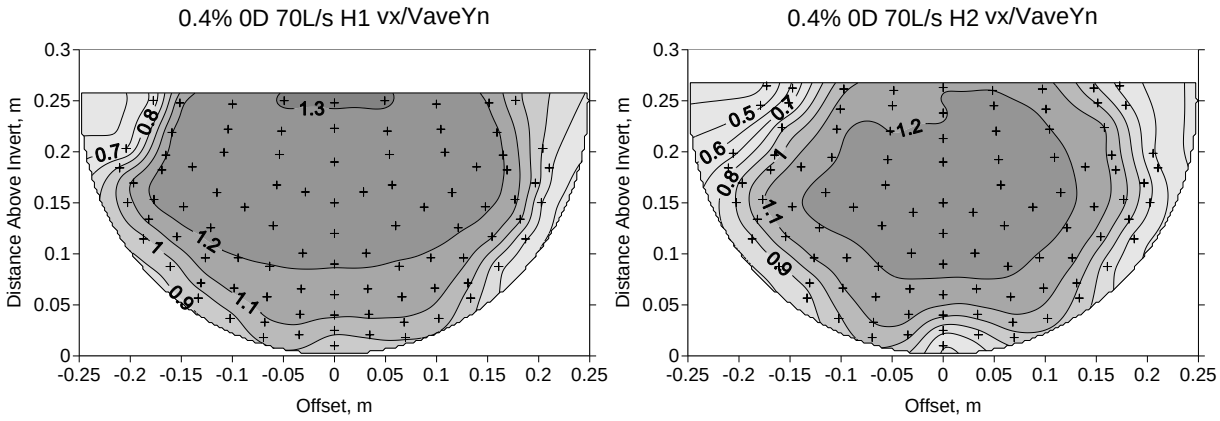
0.4% 0D 70L/s H1 vx/VaveYn
Distance Above Invert, m
Offset, m
0.3
0.25
0.2
0.15
0.1
0.05
0
-0.25 -0.2 -0.15 -0.1 -0.05 0 0.05 0.1 0.15 0.2 0.25
0.7
0.8
0.9
1
1.1
1.2
1.3

0.4% 0D 70L/s H2 vx/VaveYn
Distance Above Invert, m
Offset, m
0.3
0.25
0.2
0.15
0.1
0.05
0
-0.25 -0.2 -0.15 -0.1 -0.05 0 0.05 0.1 0.15 0.2 0.25
0.5
0.6
0.7
0.8
0.9
1
1.1
1.2

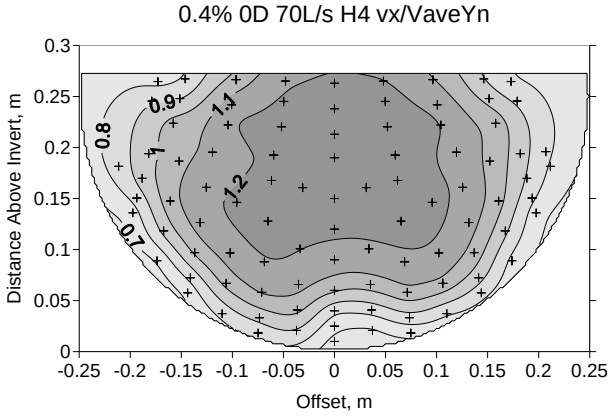
0.4% 0D 70L/s H4 vx/VaveYn
Distance Above Invert, m
Offset, m
0.3
0.25
0.2
0.15
0.1
0.05
0
-0.25 -0.2 -0.15 -0.1 -0.05 0 0.05 0.1 0.15 0.2 0.25
0.7
0.8
0.9
1
1.1
1.2

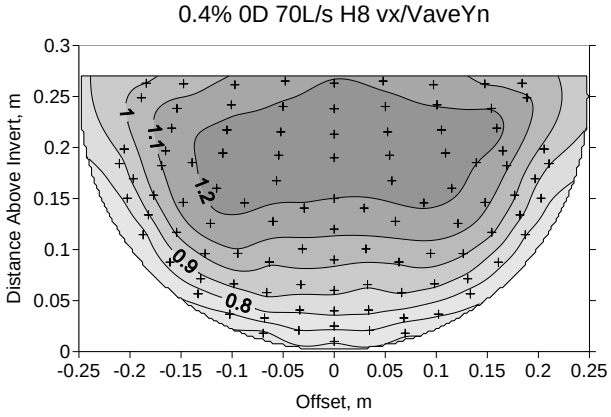
0.4% 0D 70L/s H8 vx/VaveYn
Distance Above Invert, m
Offset, m
0.3
0.25
0.2
0.15
0.1
0.05
0
-0.25 -0.2 -0.15 -0.1 -0.05 0 0.05 0.1 0.15 0.2 0.25
0.8
0.9
1
1.1
1.2

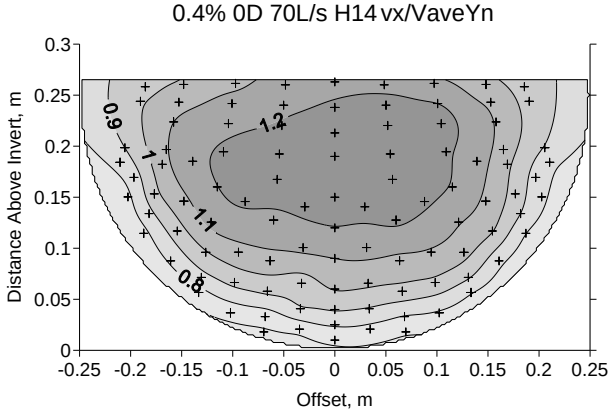
0.4% 0D 70L/s H14 vx/VaveYn
Distance Above Invert, m
Offset, m
0.3
0.25
0.2
0.15
0.1
0.05
0
-0.25 -0.2 -0.15 -0.1 -0.05 0 0.05 0.1 0.15 0.2 0.25
0.8
0.9
1
1.1
1.2

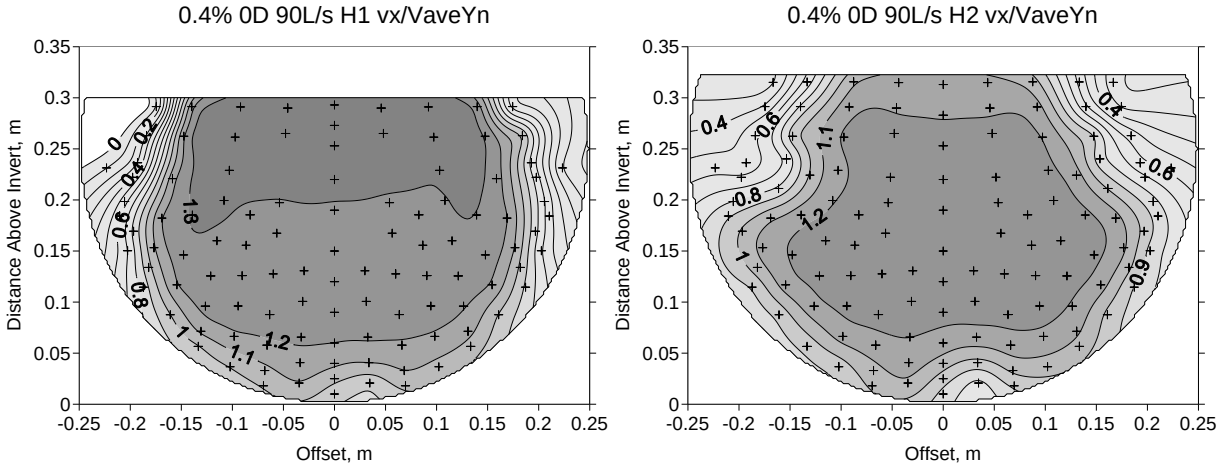
0.4% 0D 90L/s H1 vx/VaveYn
Distance Above Invert, m
Offset, m
0.4% 0D 90L/s H2 vx/VaveYn
Distance Above Invert, m
Offset, m

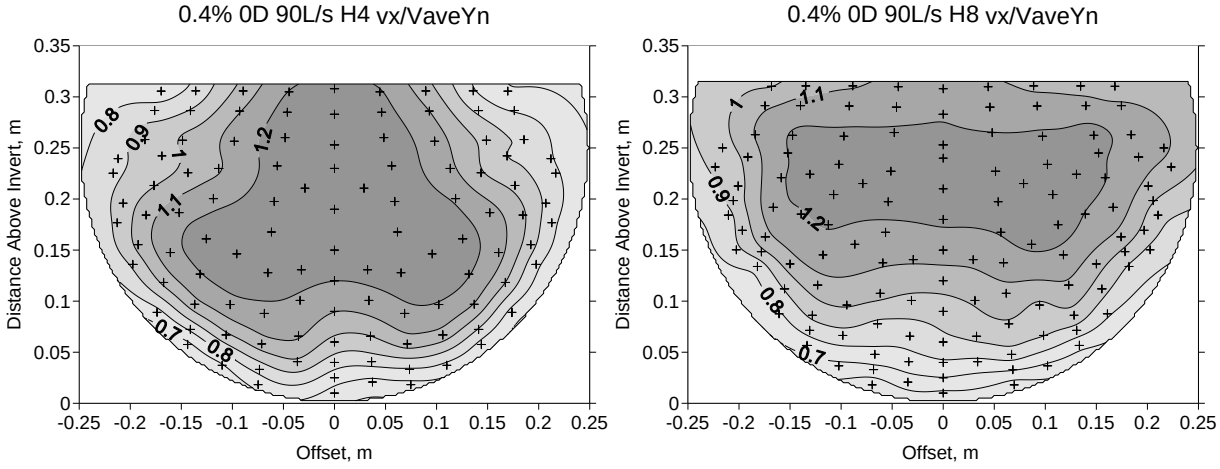
0.4% 0D 90L/s H4 vx/VaveYn
Distance Above Invert, m
Offset, m
0.4% 0D 90L/s H8 vx/VaveYn
Distance Above Invert, m
Offset, m

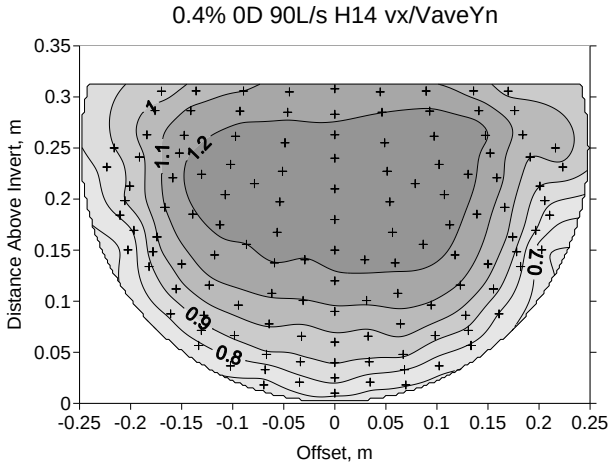
0.4% 0D 90L/s H14 vx/VaveYn
Distance Above Invert, m
Offset, m

1.0% Culvert Slope Non-Embedded Cross Sections

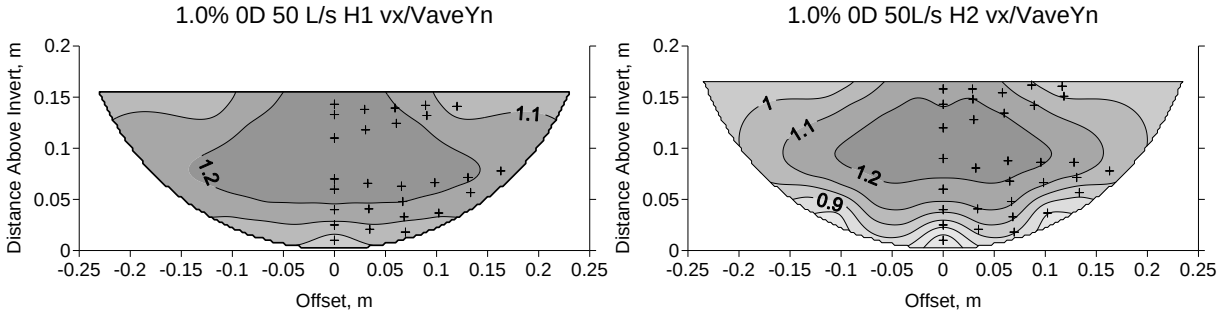

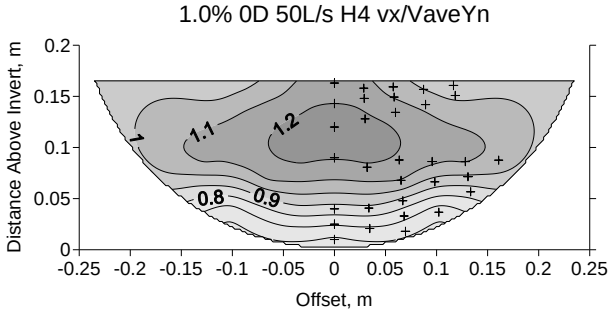

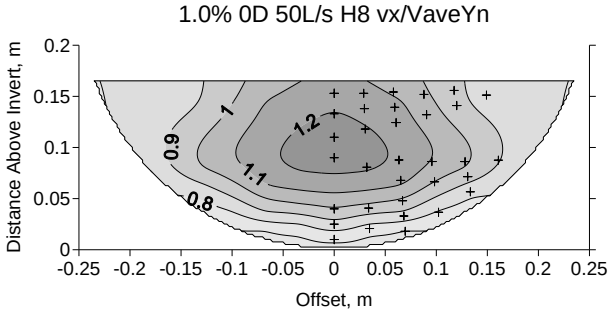

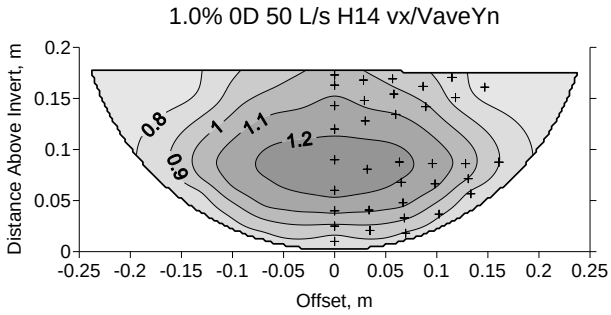

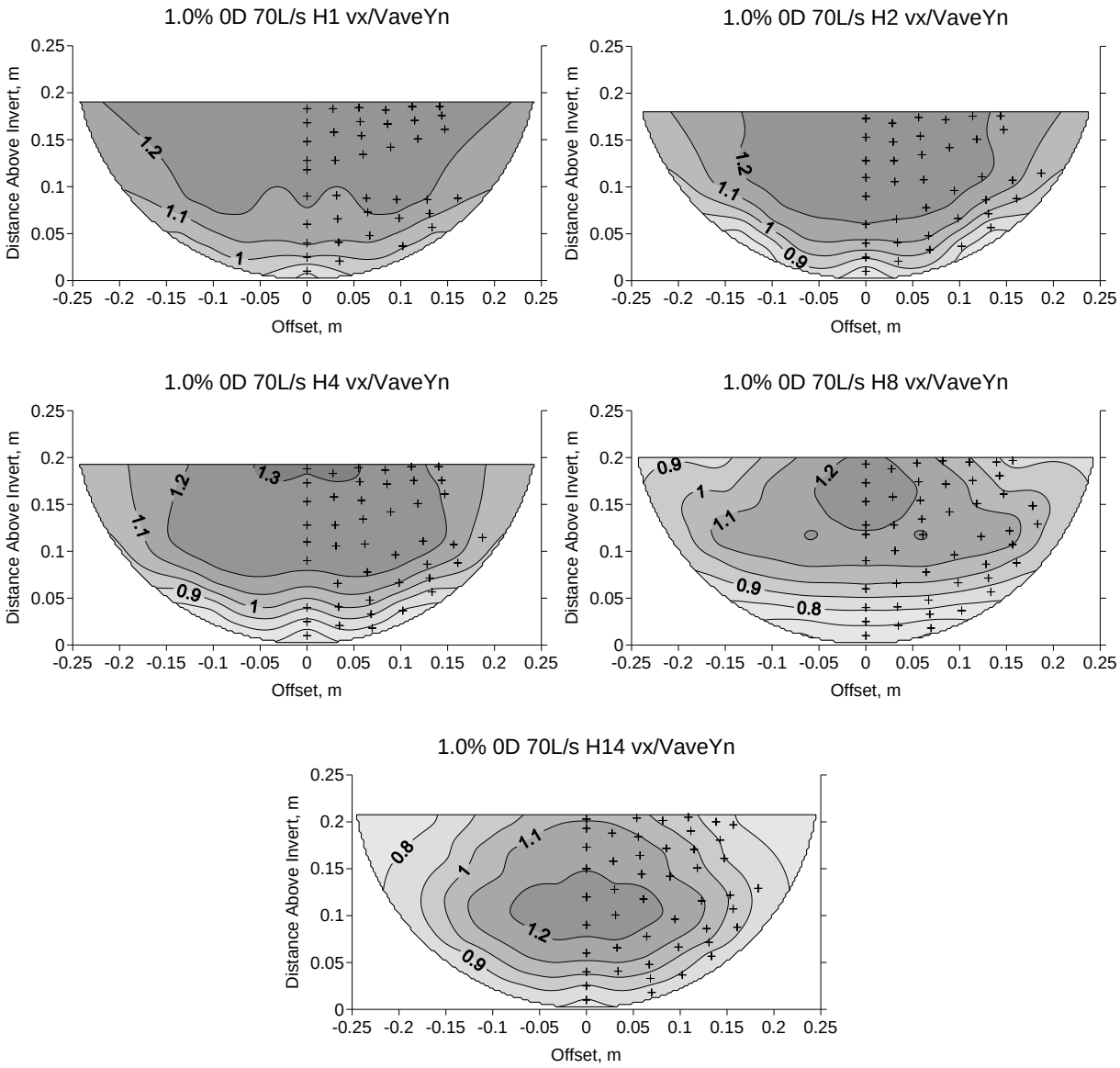
1.0% 0D 70L/s H1 vx/VaveYn
1.0% 0D 70L/s H2 vx/VaveYn
1.0% 0D 70L/s H4 vx/VaveYn
1.0% 0D 70L/s H8 vx/VaveYn
1.0% 0D 70L/s H14 vx/VaveYn
Distance Above Invert, m
Offset, m

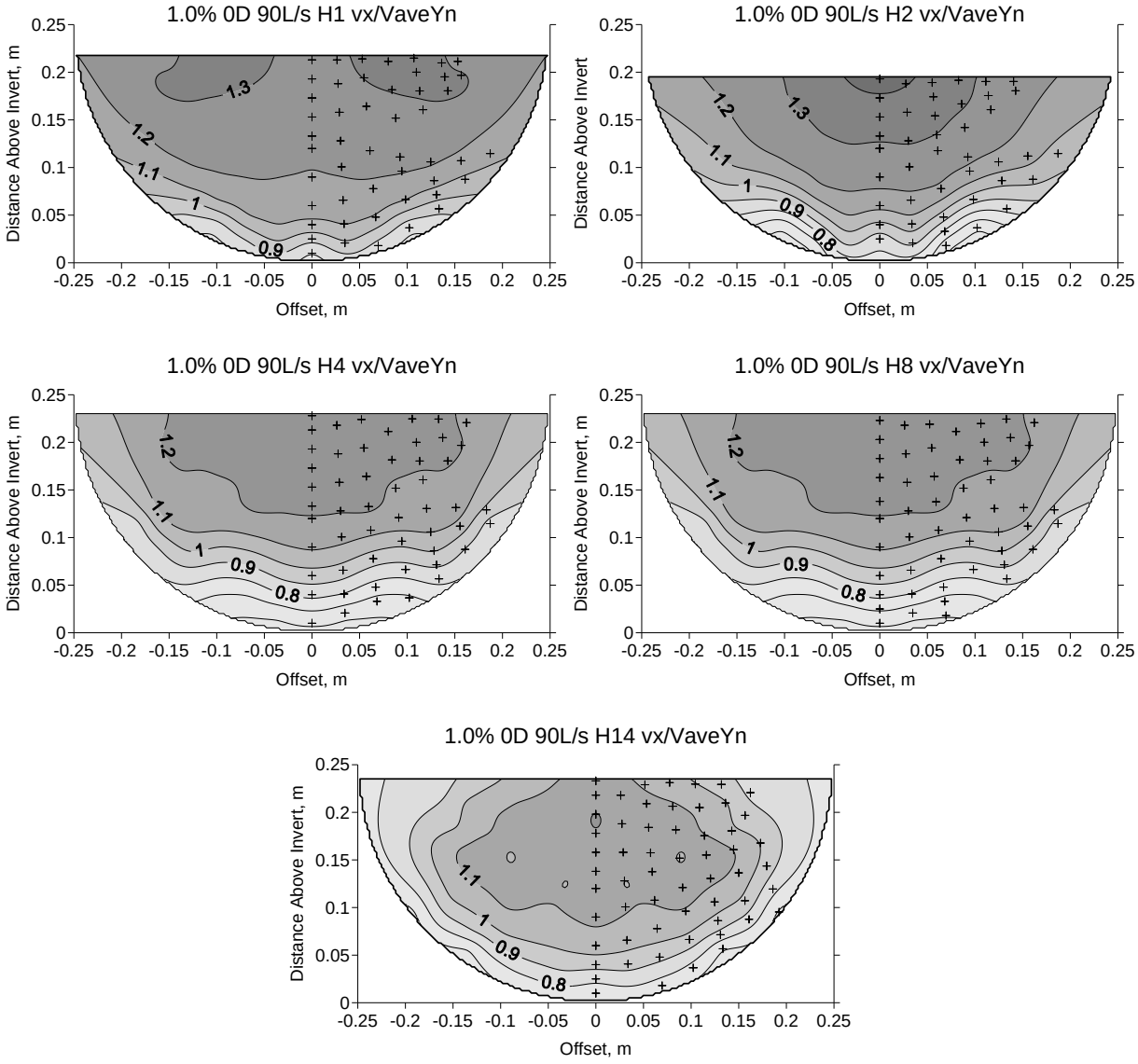
1.0% 0D 90L/s H1 vx/VaveYn
1.0% 0D 90L/s H2 vx/VaveYn
1.0% 0D 90L/s H4 vx/VaveYn
1.0% 0D 90L/s H8 vx/VaveYn
1.0% 0D 90L/s H14 vx/VaveYn
Distance Above Invert, m
Offset, m

0.4% Culvert Slope 0.1D Embedded Cross Sections

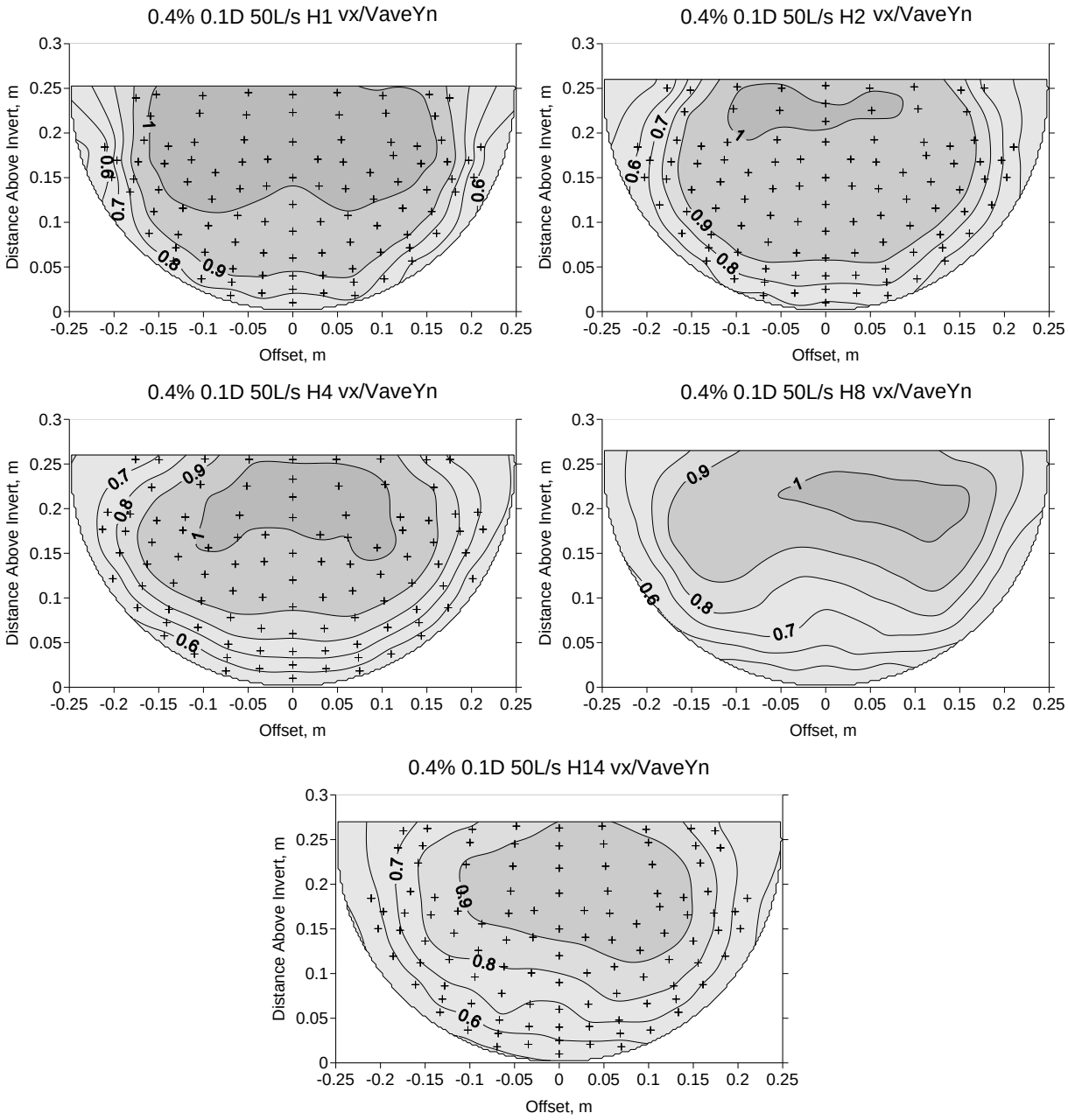

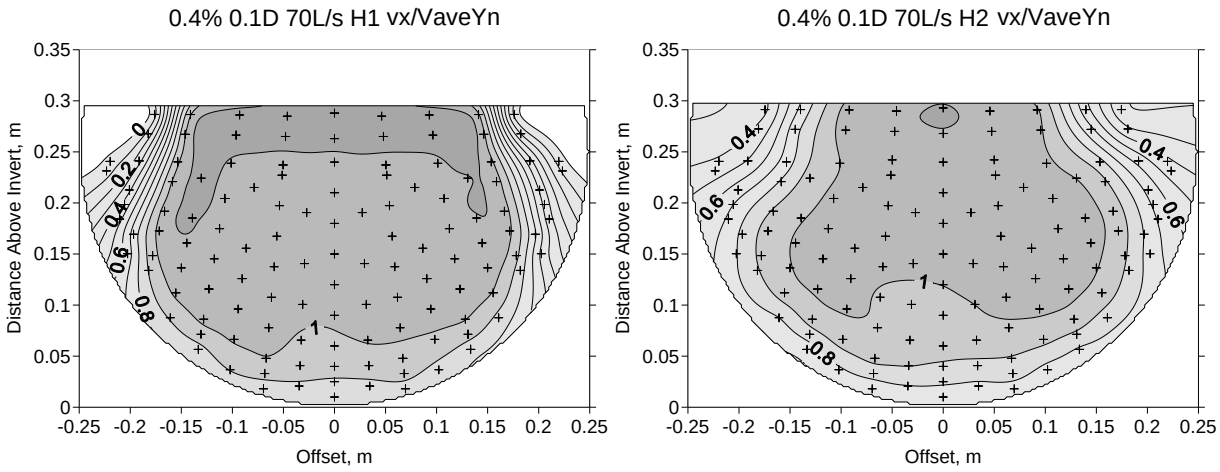
0.4% 0.1D 70L/s H1 vx/VaveYn
Distance Above Invert, m
Offset, m

0.4% 0.1D 70L/s H2 vx/VaveYn
Distance Above Invert, m
Offset, m

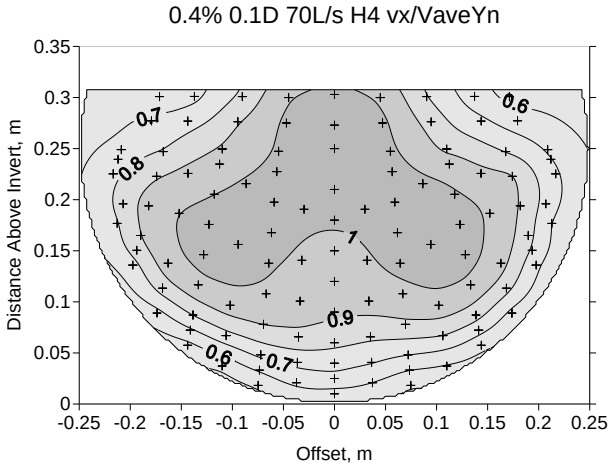
0.4% 0.1D 70L/s H4 vx/VaveYn
Distance Above Invert, m
Offset, m

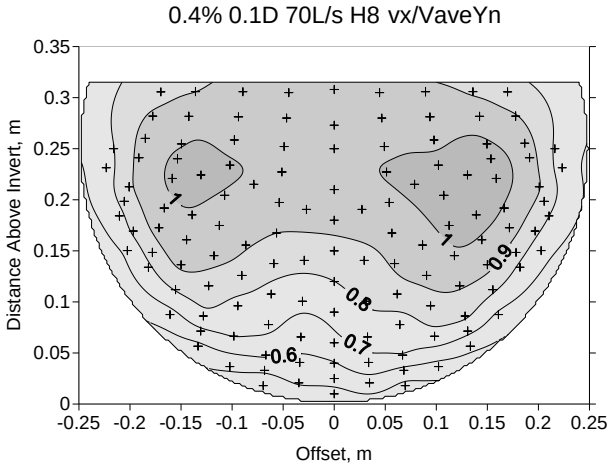
0.4% 0.1D 70L/s H8 vx/VaveYn
Distance Above Invert, m
Offset, m

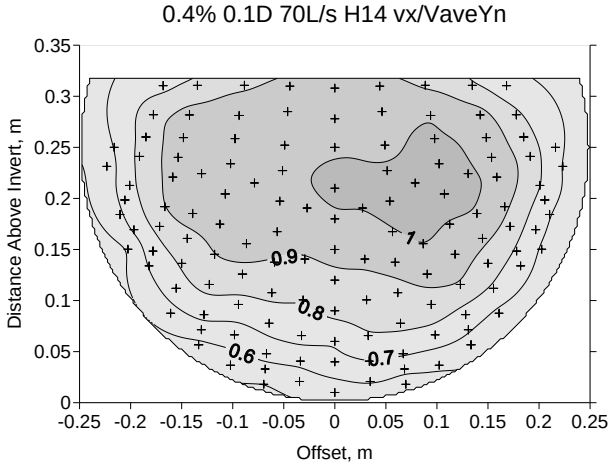
0.4% 0.1D 70L/s H14 vx/VaveYn
Distance Above Invert, m
Offset, m

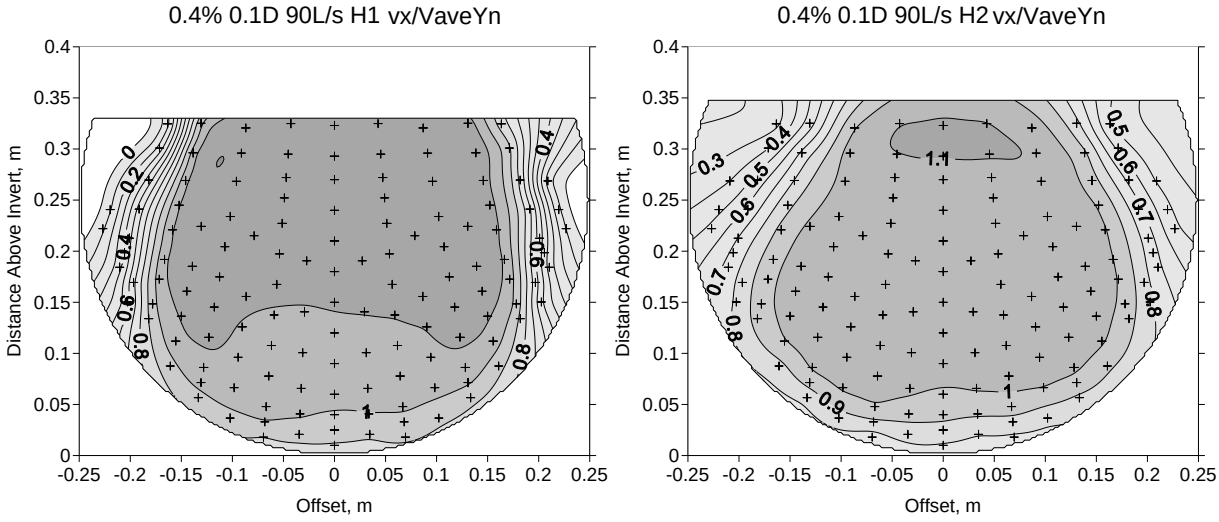
0.4% 0.1D 90L/s H1 vx/VaveYn
Distance Above Invert, m
Offset, m

0.4% 0.1D 90L/s H2 vx/VaveYn
Distance Above Invert, m
Offset, m

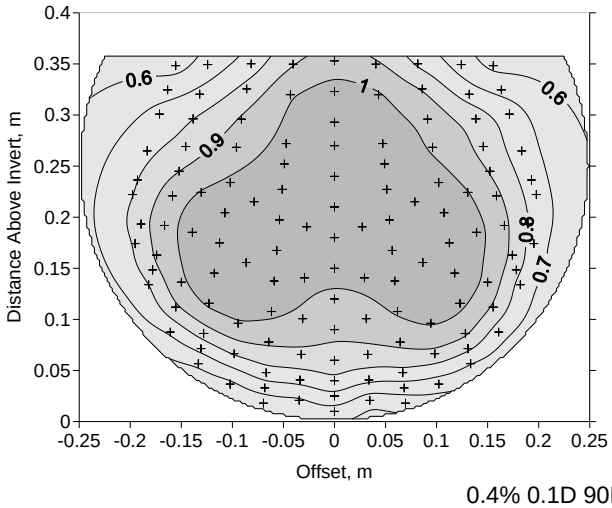
0.4% 0.1D 90L/s H4 vx/VaveYn
Distance Above Invert, m
Offset, m

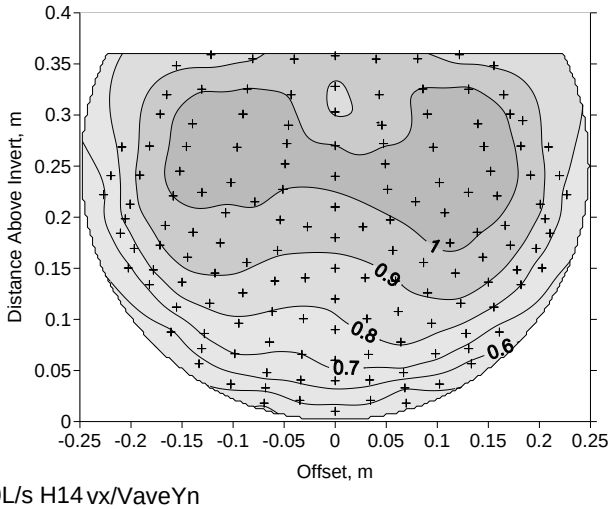
0.4% 0.1D 90L/s H8 vx/VaveYn
Distance Above Invert, m
Offset, m

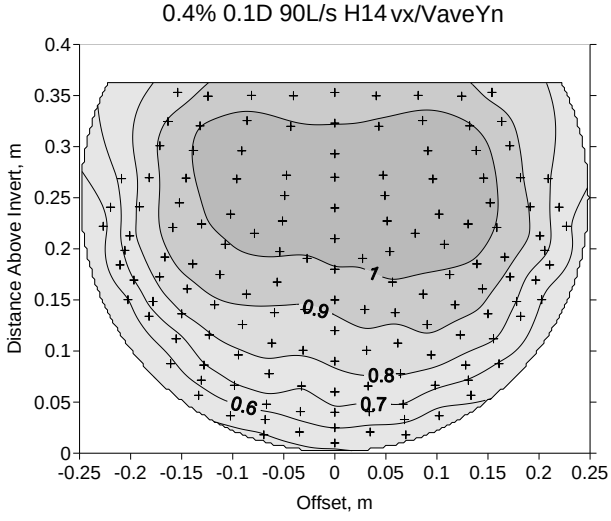
0.4% 0.1D 90L/s H14 vx/VaveYn
Distance Above Invert, m
Offset, m

1.0% Culvert Slope 0.1D Embedded Cross Sections

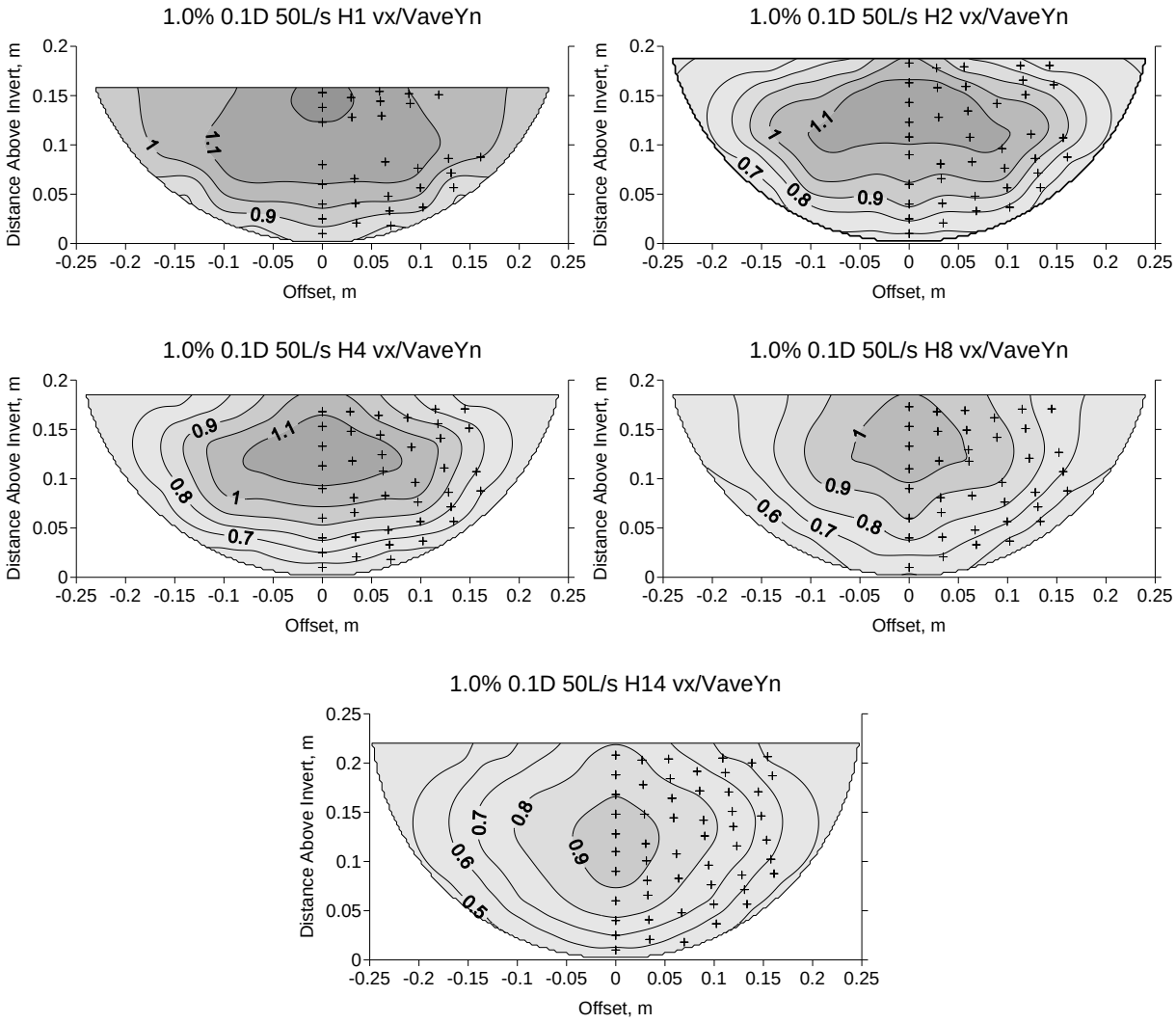

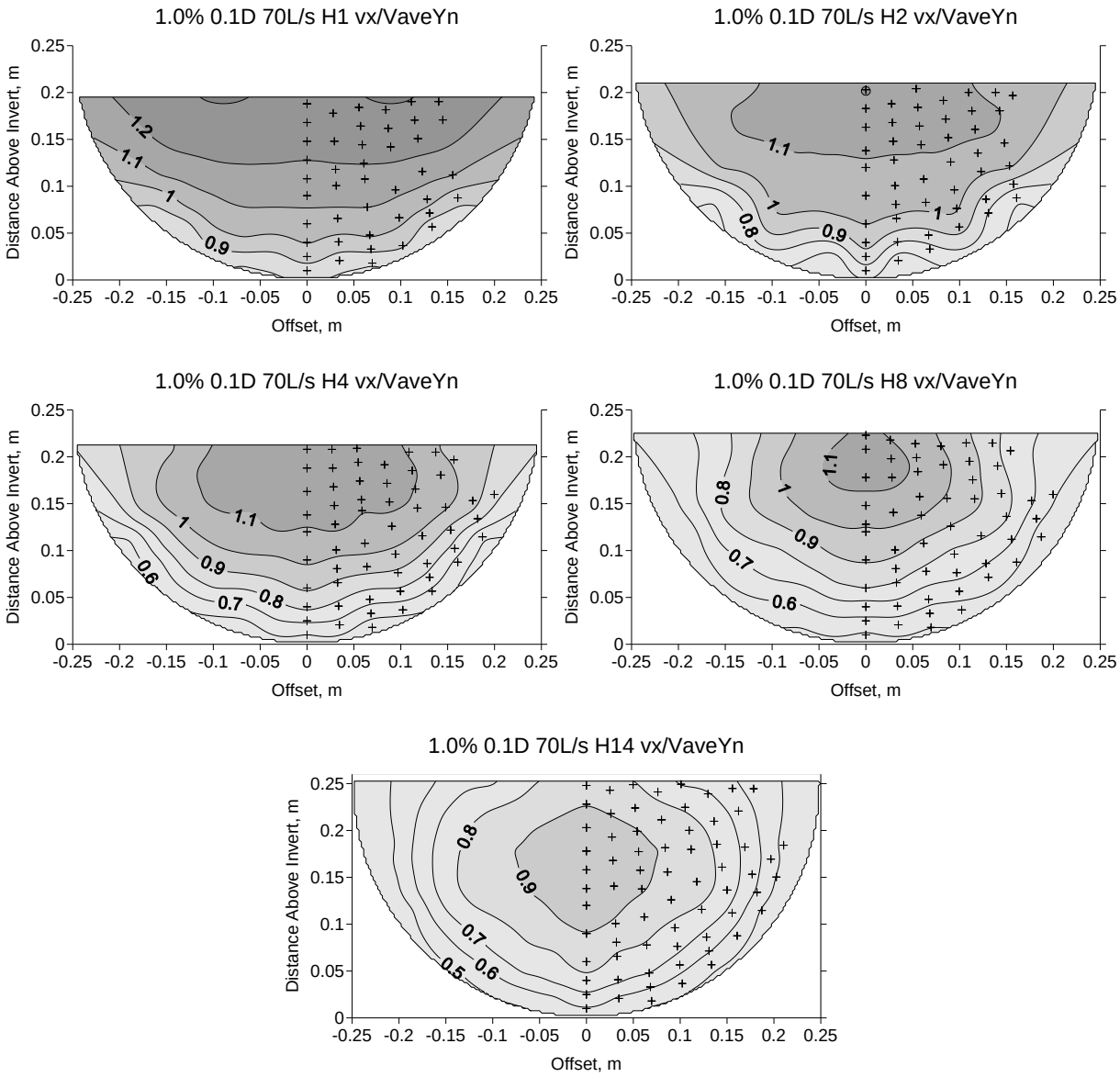
1.0% 0.1D 70L/s H1 vx/VaveYn
1.0% 0.1D 70L/s H2 vx/VaveYn
1.0% 0.1D 70L/s H4 vx/VaveYn
1.0% 0.1D 70L/s H8 vx/VaveYn
1.0% 0.1D 70L/s H14 vx/VaveYn
Distance Above Invert, m
Offset, m

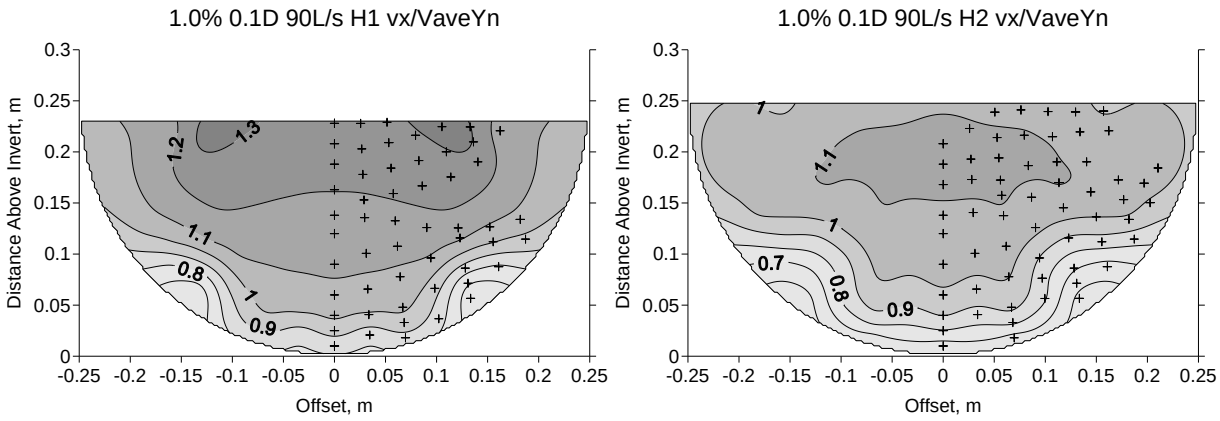
1.0% 0.1D 90L/s H1 vx/VaveYn
Distance Above Invert, m
Offset, m
1.2
1.3
1.1
0.8
1
0.9

1.0% 0.1D 90L/s H2 vx/VaveYn
Distance Above Invert, m
Offset, m
1
1.1
1
0.7
0.8
0.9

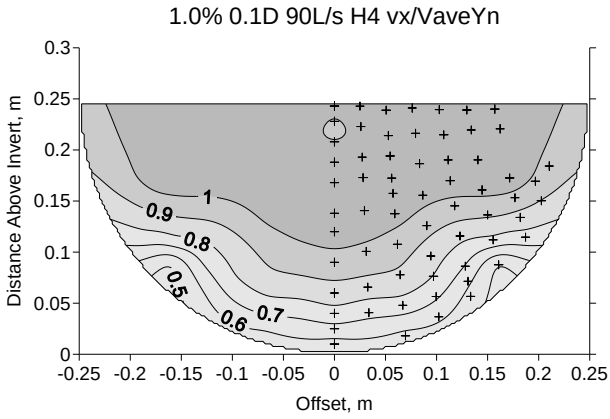
1.0% 0.1D 90L/s H4 vx/VaveYn
Distance Above Invert, m
Offset, m
1
0.9
0.8
0.5
0.6
0.7

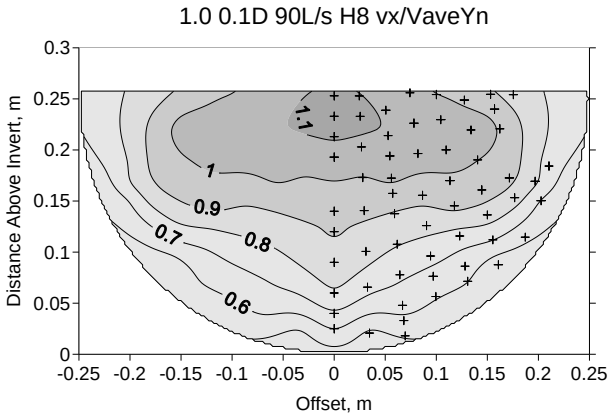
1.0 0.1D 90L/s H8 vx/VaveYn
Distance Above Invert, m
Offset, m
1.1
1
0.9
0.7
0.8
0.6

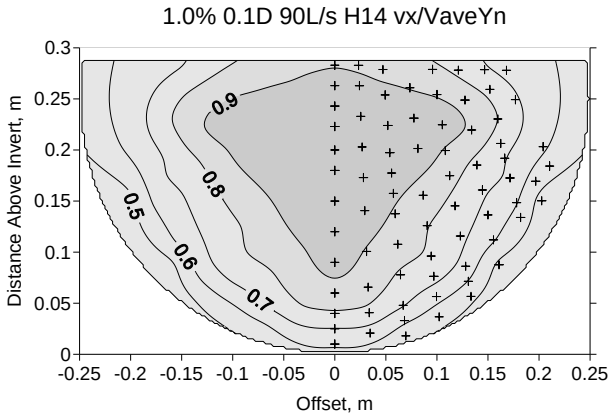
1.0% 0.1D 90L/s H14 vx/VaveYn
Distance Above Invert, m
Offset, m
0.9
0.8
0.5
0.6
0.7

0.4% Culvert Slope 0.2D Embedded Cross Sections

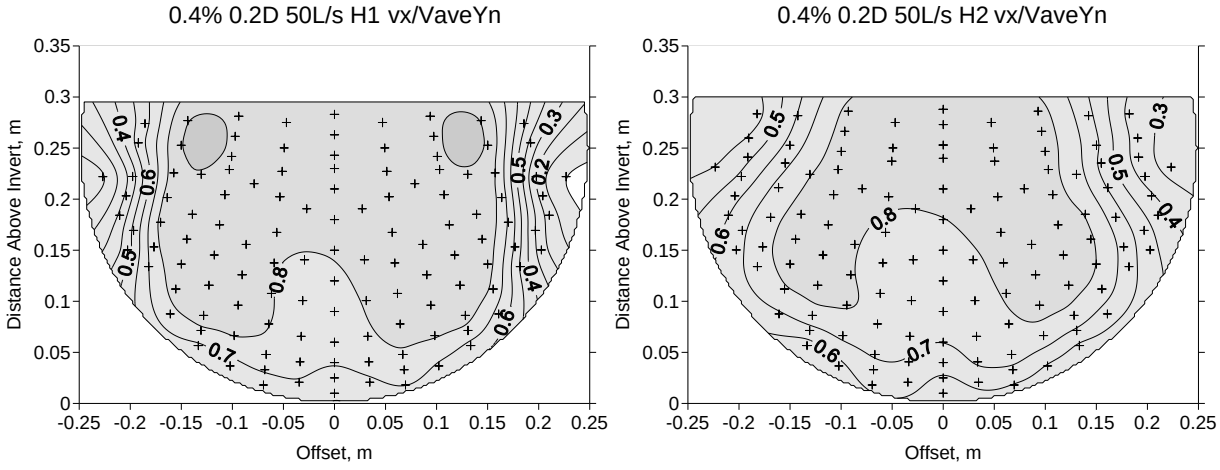

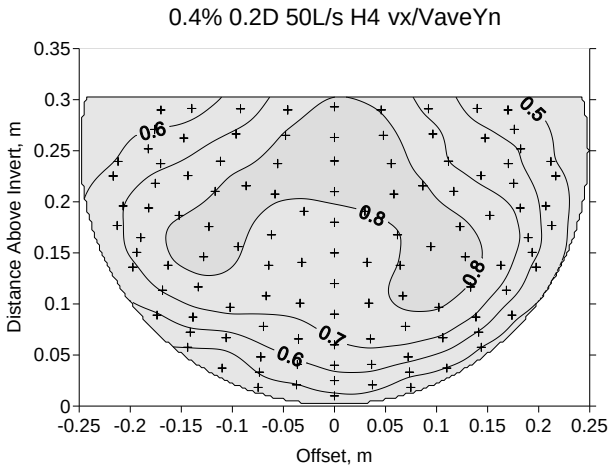

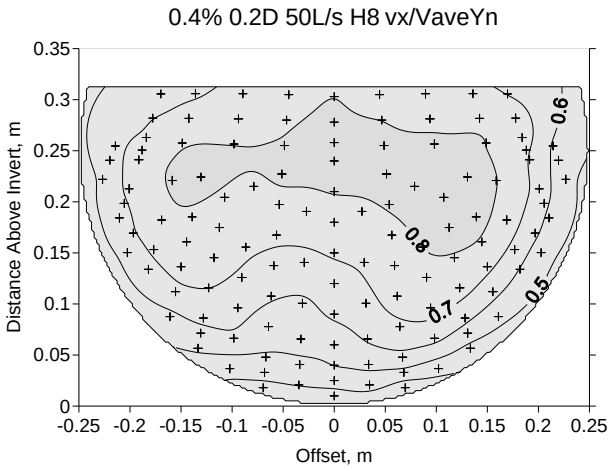

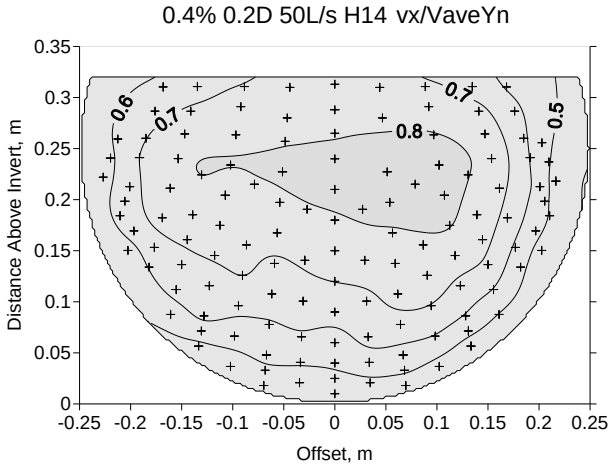

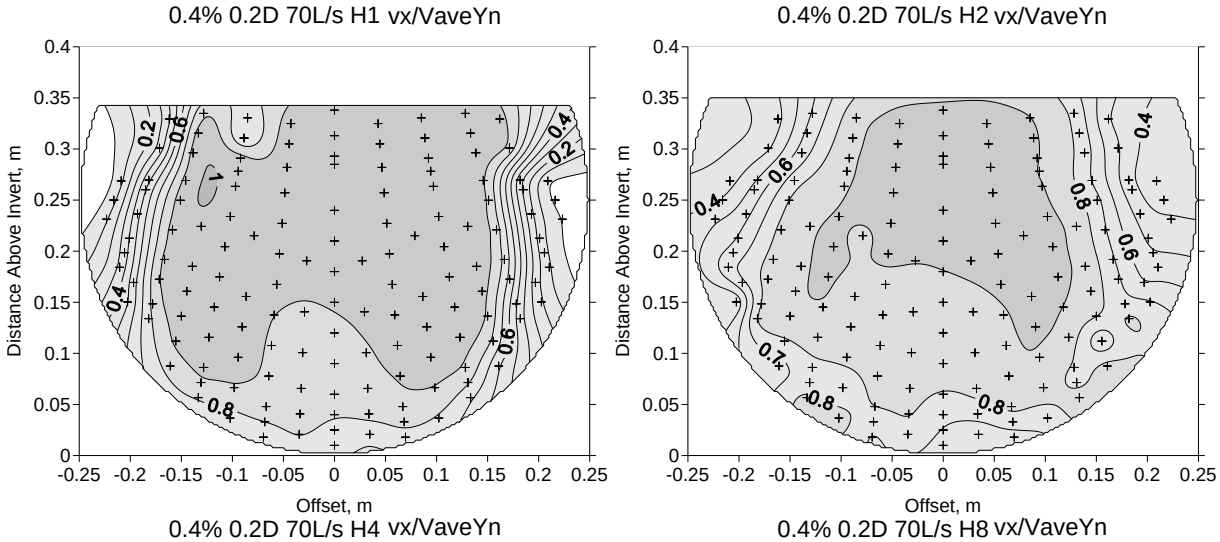
0.4% 0.2D 70L/s H1 vx/VaveYn
Distance Above Invert, m
Offset, m

0.4% 0.2D 70L/s H2 vx/VaveYn
Distance Above Invert, m
Offset, m

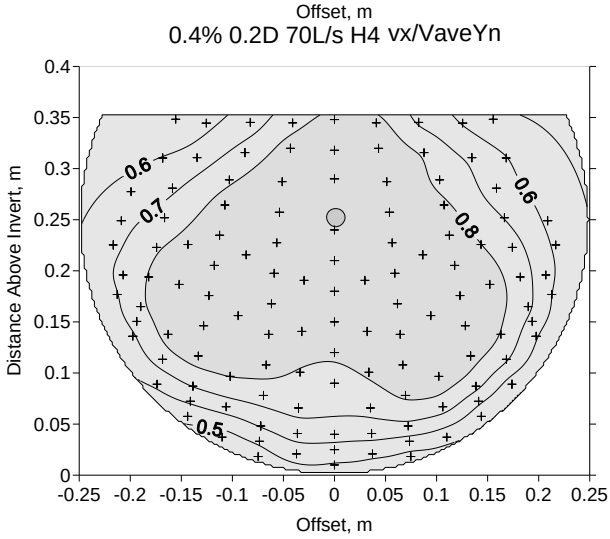
0.4% 0.2D 70L/s H4 vx/VaveYn
Distance Above Invert, m
Offset, m

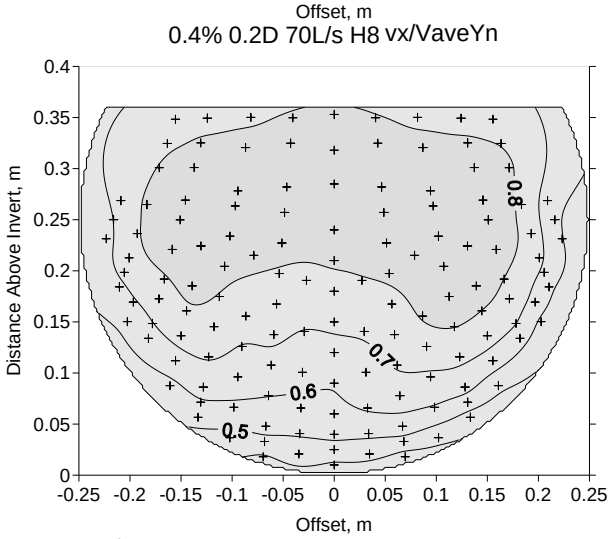
0.4% 0.2D 70L/s H8 vx/VaveYn
Distance Above Invert, m
Offset, m

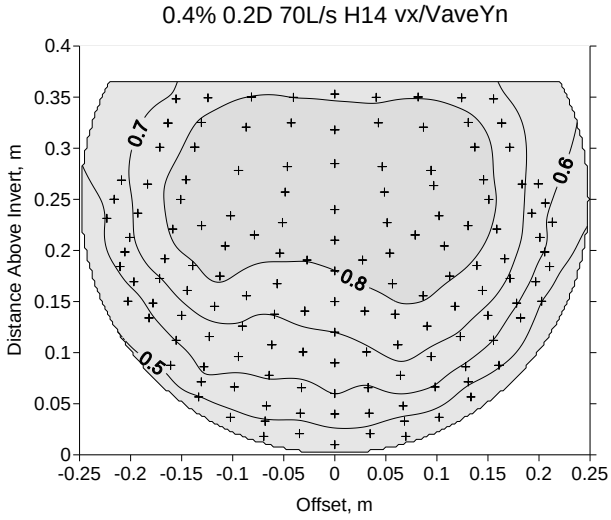
0.4% 0.2D 70L/s H14 vx/VaveYn
Distance Above Invert, m
Offset, m

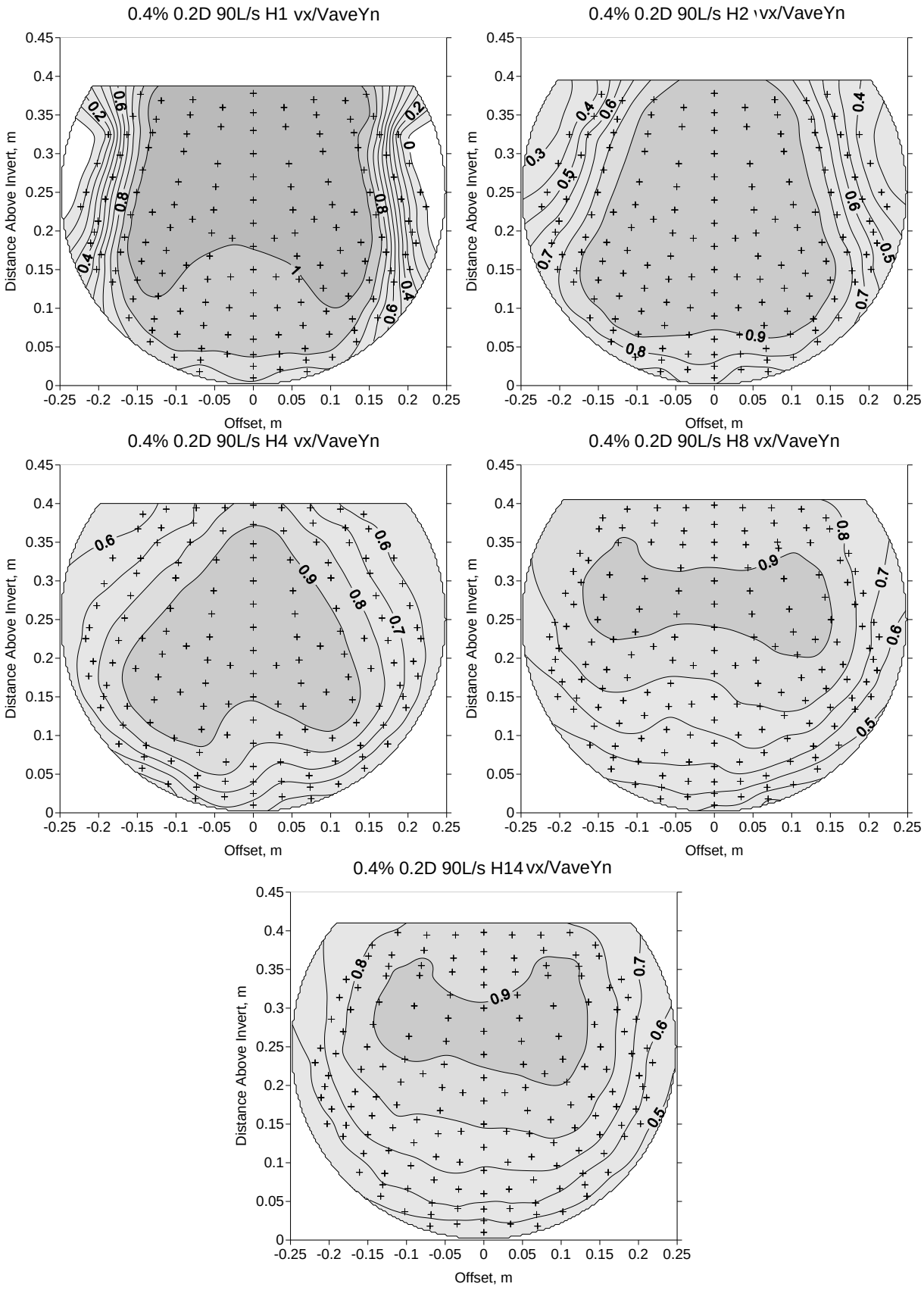
0.4% 0.2D 90L/s H1 vx/VaveYn
0.4% 0.2D 90L/s H2 vx/VaveYn
0.4% 0.2D 90L/s H4 vx/VaveYn
0.4% 0.2D 90L/s H8 vx/VaveYn
0.4% 0.2D 90L/s H14 vx/VaveYn
Distance Above Invert, m
Offset, m

1.0% Culvert Slope 0.2D Embedded Cross Sections

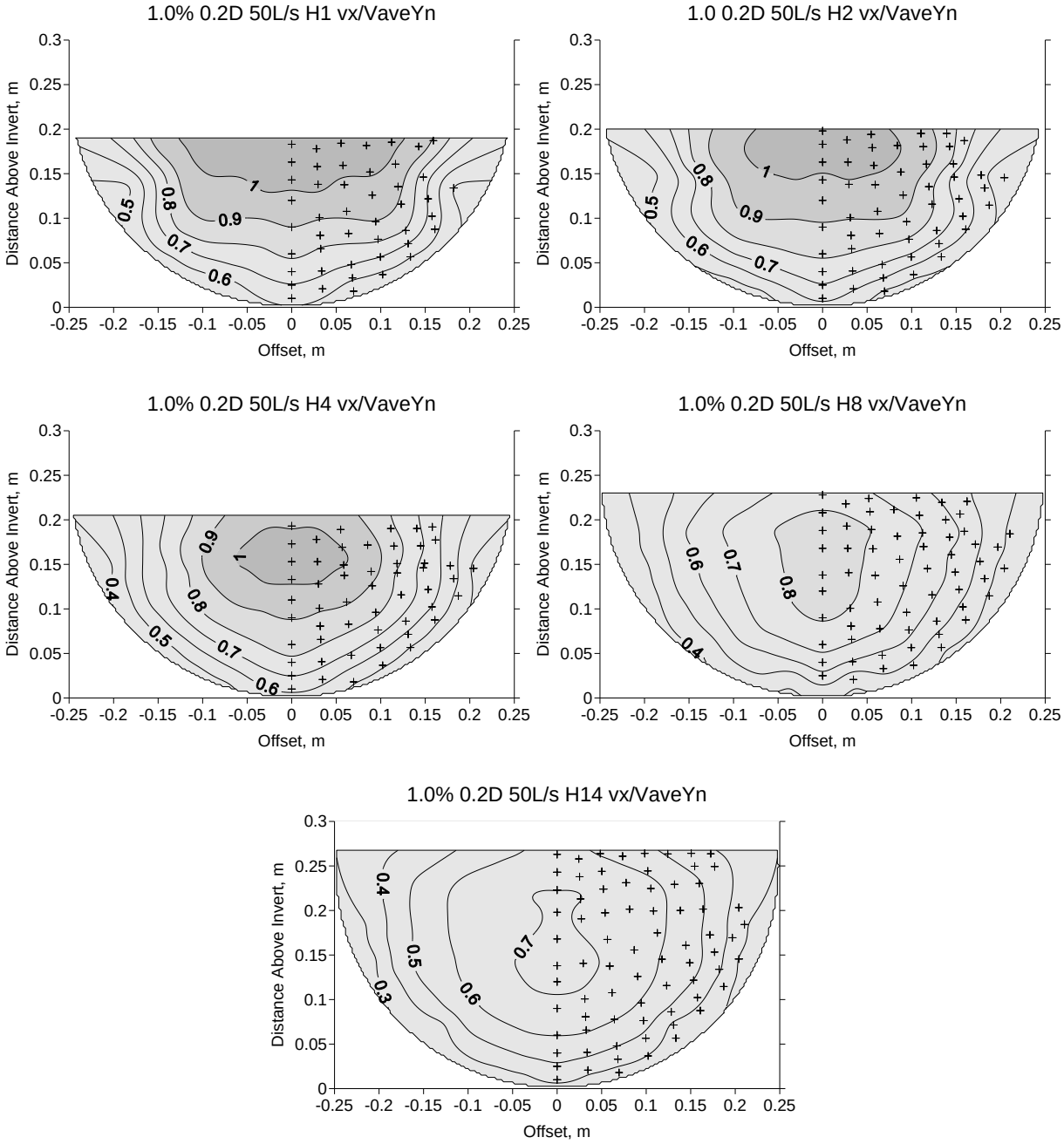

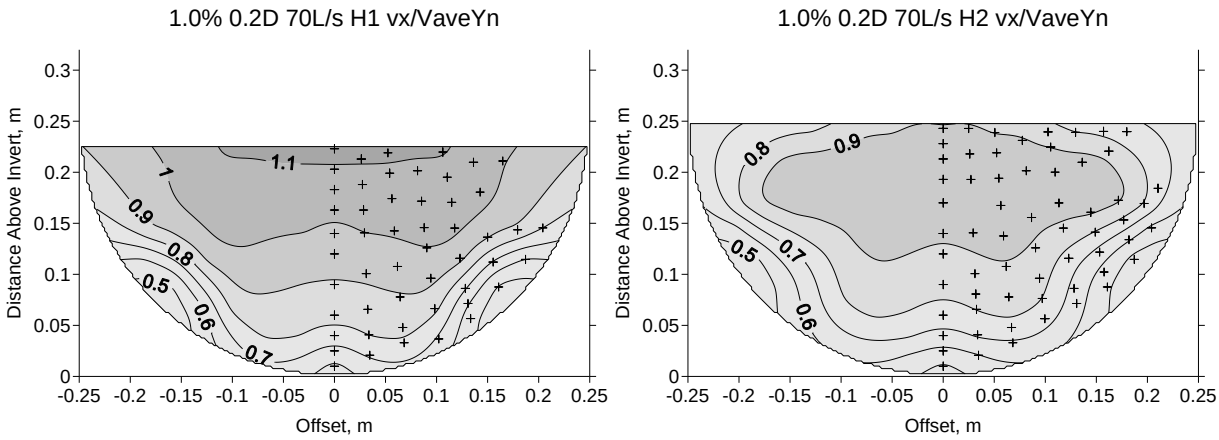
1.0% 0.2D 70L/s H1 vx/VaveYn
Distance Above Invert, m
Offset, m
1.1
1
0.9
0.8
0.5
0.6
0.7

1.0% 0.2D 70L/s H2 vx/VaveYn
Distance Above Invert, m
Offset, m
0.8
0.9
0.5
0.7
0.6

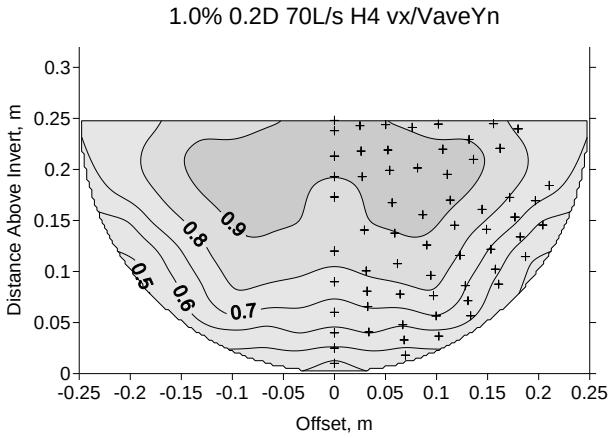
1.0% 0.2D 70L/s H4 vx/VaveYn
Distance Above Invert, m
Offset, m
0.9
0.8
0.5
0.6
0.7

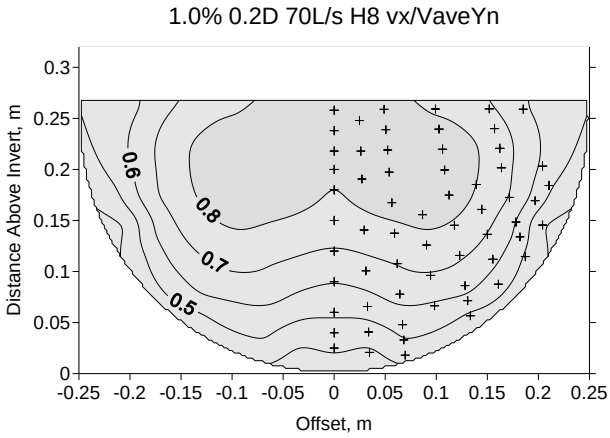
1.0% 0.2D 70L/s H8 vx/VaveYn
Distance Above Invert, m
Offset, m
0.6
0.8
0.7
0.5

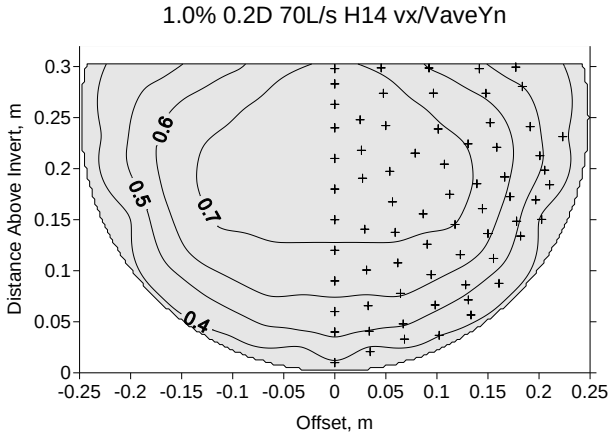
1.0% 0.2D 70L/s H14 vx/VaveYn
Distance Above Invert, m
Offset, m
0.6
0.5
0.7
0.4

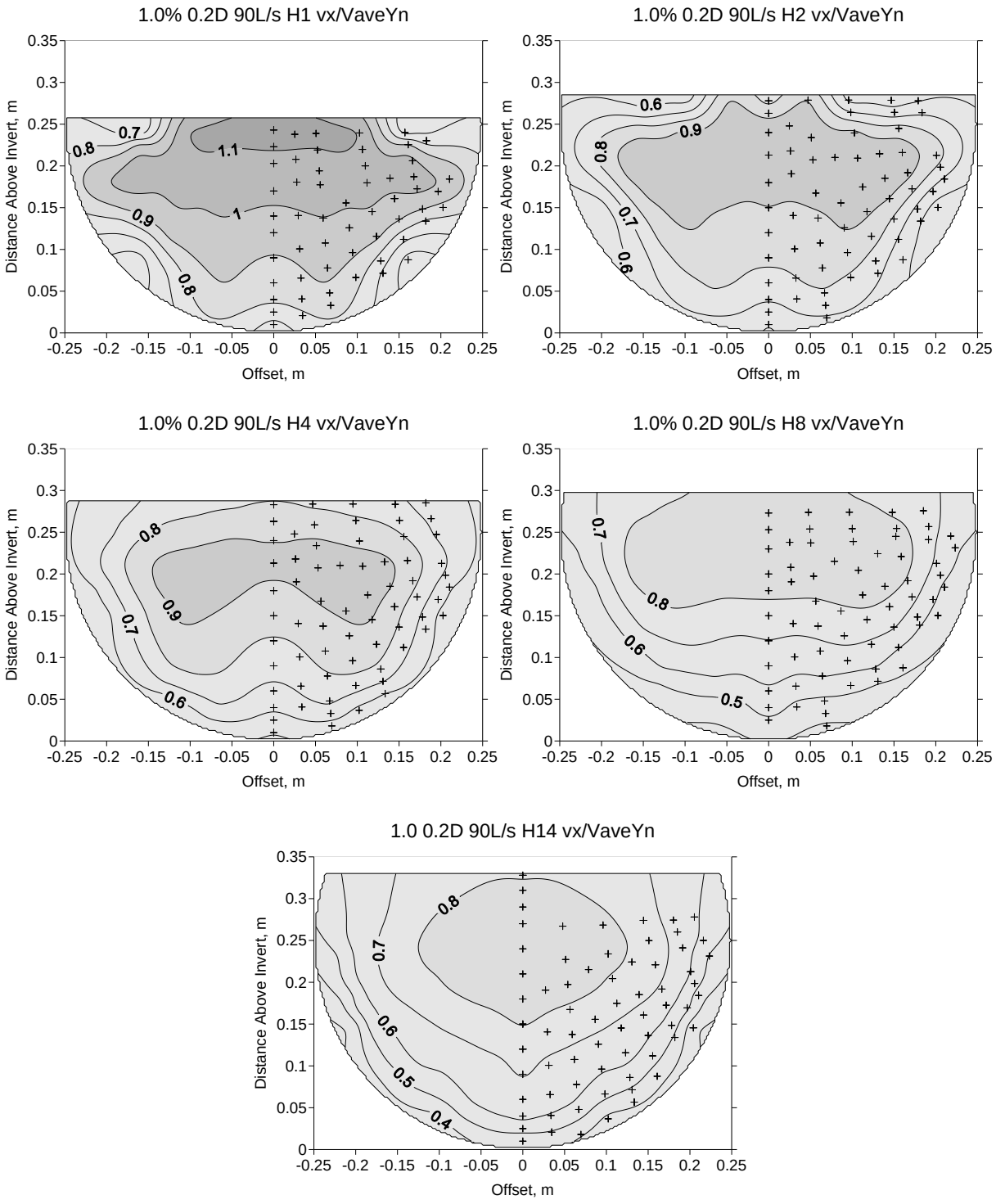
1.0% 0.2D 90L/s H1 vx/VaveYn
1.0% 0.2D 90L/s H2 vx/VaveYn
1.0% 0.2D 90L/s H4 vx/VaveYn
1.0% 0.2D 90L/s H8 vx/VaveYn
1.0 0.2D 90L/s H14 vx/VaveYn
Distance Above Invert, m
Offset, m

Appendix H: Percent of Flow Area with v_x less than V_{ave}

Culvert Slope		0.4%								
Embedment		0D			0.1D			0.2D		
Discharge (L/s)	Hole	50	70	90	50	70	90	50	70	90
% of Flow Area Less than V_{ave}	1	24.9	23.2	26.5	22.1	24.5	22.6	24.0	24.3	24.3
	2	30.9	28.1	28.8	28.3	31.6	29.9	31.2	27.6	29.1
	4	32.8	33.1	35.9	33.4	36.7	40.3	34.0	36.2	37.1
	8	29.8	30.5	28.6	33.5	33.2	32.9	29.8	32.0	32.0
	14	37.2	35.7	32.0	40.4	36.4	36.6	32.7	37.2	37.1
Culvert Slope		1.0%								
Embedment		0D			0.1D			0.2D		
Discharge (L/s)	Hole	50	70	90	50	70	90	50	70	90
% of Flow Area Less than V_{ave}	1	28.5	13.5	16.2	58.5	23.0	22.3	52.0	33.8	33.2
	2	31.3	47.1	61.9	41.6	26.5	25.1	50.7	36.2	37.9
	4	39.3	26.6	32.3	52.1	42.3	39.6	52.8	40.0	37.9
	8	55.4	40.8	52.3	65.4	60.9	53.4	57.1	49.7	51.3
	14	40.1	39.5	40.4	50.0	48.1	47.3	47.3	44.9	50.8

Appendix I: Sample of Ead et al. (2000) Calculations

Calculations for Ead et al. model for 0.4% culvert slope and 50 L/s discharge. This example shows calculation based on assuming a J value of 0.8 as discussed in Section 4.5.4 and a value of k_s equal to the corrugation height (0.013m). Equations for f_1, f_2 and f_3 are shown in Chapter 2 (Equations 2.13-2.16).

0.4% Slope, 50L/s

D=	0.513	m	**P=**	0.724	m
Q=	0.05	m3/s	**R=**	0.114	m
S=	0.004	m/m	**T=**	0.507	m
Y_n=	**0.216**	m	**z_o=**	**0.253**	m
Theta=	2.82	rad	**k_s=**	**0.013**	m
A=	0.083	m2	**g=**	9.81	m/s2
U*=	0.067		**J=**	**0.800**	
u^*_o=	0.054		**n=**	**0.024**	

$$\frac{v}{V_{ave}} = \left[\left(\frac{2.30}{\kappa}\right)\log\left(\frac{y_z}{k_s}\right) + 8.50\right]\sqrt{f_3\left(\frac{z}{z_0}\right)}\left(\frac{J\sqrt{g}n}{R^{1/6}}\right) \qquad \text{for } \frac{y_z}{k_s} < \frac{y_d}{k_s} \qquad [1]$$

(Eqn 2.11 from Chapter 2)

$$\frac{v}{V_{ave}} = \left[\left(\frac{2.30}{\kappa}\right)\log\left(\frac{y_z}{k_s}\right) + 8.50 - \frac{\frac{y_z}{k_s}f_1\left(\frac{z}{z_0}\right)}{\frac{y_z}{k_s}f_1\left(\frac{z}{z_0}\right)} \times f_2\left(\frac{z}{z_0}\right)\right]\sqrt{f_3\left(\frac{z}{z_0}\right)}\left(\frac{J\sqrt{g}n}{R^{1/6}}\right) \qquad [2]$$

$$\text{for } \frac{y_z}{k_s} > \frac{y_d}{k_s}$$

(Eqn 2.12 from Chapter 2)

Surfer Coordinates		Culvert							Eqn 1			
z, m	y, m	Elev, m	Y_z, m	z/z_o	$f_1(z/z_o)$	$f_2(z/z_o)$	$f_3(z/z_o)$	y_z/k_s	or 2?	Eqn 1	Eqn 2	v/V_{ave}
0.000	0.017	0.000	0.216	0.000	9.000	0.900	1.000	1.27	1	0.785	0.864	0.785
0.000	0.032	0.000	0.216	0.000	9.000	0.900	1.000	2.42	1	0.925	0.992	0.925
0.000	0.047	0.000	0.216	0.000	9.000	0.900	1.000	3.58	1	1.009	1.064	1.009
0.000	0.067	0.000	0.216	0.000	9.000	0.900	1.000	5.12	1	1.086	1.126	1.086
0.000	0.097	0.000	0.216	0.000	9.000	0.900	1.000	7.42	1	1.166	1.182	1.166
0.000	0.127	0.000	0.216	0.000	9.000	0.900	1.000	9.73	2	1.225	1.217	1.217
0.000	0.157	0.000	0.216	0.000	9.000	0.900	1.000	12.04	2	1.270	1.239	1.239
0.035	0.027	0.002	0.214	0.137	8.591	1.662	1.000	2.10	1	0.894	1.012	0.894
0.034	0.047	0.002	0.214	0.133	8.605	1.643	1.000	3.63	1	1.012	1.102	1.012
0.033	0.072	0.002	0.214	0.129	8.621	1.619	1.000	5.55	1	1.104	1.158	1.104
0.031	0.107	0.002	0.214	0.123	8.644	1.585	1.000	8.24	1	1.189	1.196	1.189
0.030	0.137	0.002	0.214	0.118	8.663	1.556	1.000	10.55	2	1.242	1.210	1.210
0.070	0.025	0.010	0.206	0.275	7.916	2.432	1.000	1.89	1	0.871	1.030	0.871

0.068	0.039	0.009	0.207	0.269	7.946	2.403	1.000	3.04	1	0.974	1.102	0.974
0.066	0.064	0.009	0.207	0.261	7.995	2.355	1.000	4.95	1	1.079	1.157	1.079
0.063	0.094	0.008	0.208	0.251	8.053	2.298	1.000	7.25	1	1.161	1.181	1.161
0.061	0.119	0.007	0.209	0.242	8.100	2.250	1.000	9.17	2	1.212	1.186	1.186
0.059	0.149	0.007	0.209	0.232	8.155	2.192	1.000	11.47	2	1.260	1.181	1.181
0.102	0.043	0.022	0.194	0.404	7.048	3.152	1.000	3.32	1	0.993	1.121	0.993
0.098	0.073	0.020	0.196	0.388	7.164	3.065	1.000	5.61	1	1.106	1.158	1.106
0.094	0.103	0.018	0.198	0.373	7.277	2.979	1.000	7.90	2	1.180	1.159	1.159
0.090	0.132	0.017	0.199	0.357	7.387	2.893	1.000	10.19	2	1.234	1.147	1.147
0.133	0.063	0.038	0.178	0.527	6.005	3.838	1.000	4.86	1	1.075	1.124	1.075
0.131	0.078	0.037	0.179	0.516	6.100	3.781	1.000	6.00	1	1.120	1.125	1.120
0.126	0.103	0.034	0.182	0.499	6.255	3.685	1.000	7.89	2	1.179	1.112	1.112
0.121	0.132	0.031	0.185	0.479	6.437	3.570	1.000	10.16	2	1.234	1.086	1.086
0.117	0.157	0.029	0.187	0.461	6.583	3.475	1.000	12.06	2	1.271	1.061	1.061
0.161	0.094	0.058	0.158	0.635	4.913	4.443	0.989	7.24	2	1.154	1.031	1.031
0.154	0.123	0.053	0.163	0.609	5.186	4.300	0.997	9.49	2	1.217	1.000	1.000
0.149	0.148	0.049	0.167	0.588	5.406	4.181	1.000	11.37	2	1.258	0.969	0.969
0.187	0.121	0.084	0.132	0.739	3.714	5.023	0.944	9.32	2	1.181	0.816	0.816
0.182	0.140	0.078	0.138	0.718	3.961	4.908	0.958	10.80	2	1.221	0.795	0.795
0.177	0.160	0.072	0.144	0.698	4.203	4.794	0.968	12.29	2	1.255	0.773	0.773
0.203	0.157	0.103	0.113	0.800	2.938	5.364	0.870	12.06	2	1.185	0.500	0.500
0.000	0.180	0.000	0.216	0.000	9.000	0.900	1.000	13.81	2	1.300	1.251	1.251
0.000	0.205	0.000	0.216	0.000	9.000	0.900	1.000	15.73	2	1.328	1.259	1.259
0.027	0.195	0.001	0.215	0.108	8.699	1.501	1.000	15.01	2	1.318	1.213	1.213
0.056	0.177	0.006	0.210	0.222	8.205	2.138	1.000	13.61	2	1.297	1.171	1.171
0.054	0.202	0.006	0.210	0.213	8.248	2.090	1.000	15.53	2	1.325	1.160	1.160
0.082	0.195	0.014	0.202	0.325	7.606	2.712	1.000	14.99	2	1.318	1.101	1.101
0.111	0.189	0.026	0.190	0.439	6.770	3.348	1.000	14.56	2	1.311	1.025	1.025
0.136	0.204	0.040	0.176	0.538	5.894	3.904	1.000	15.73	2	1.328	0.893	0.893
0.155	0.199	0.054	0.162	0.611	5.165	4.311	0.996	15.27	2	1.319	0.806	0.806

Appendix J: Ead et al. (2000) Model Analysis

Contour Plots of v_x/V_{ave} Produced with Ead et al. (2000) Model (using J value of 0.8)

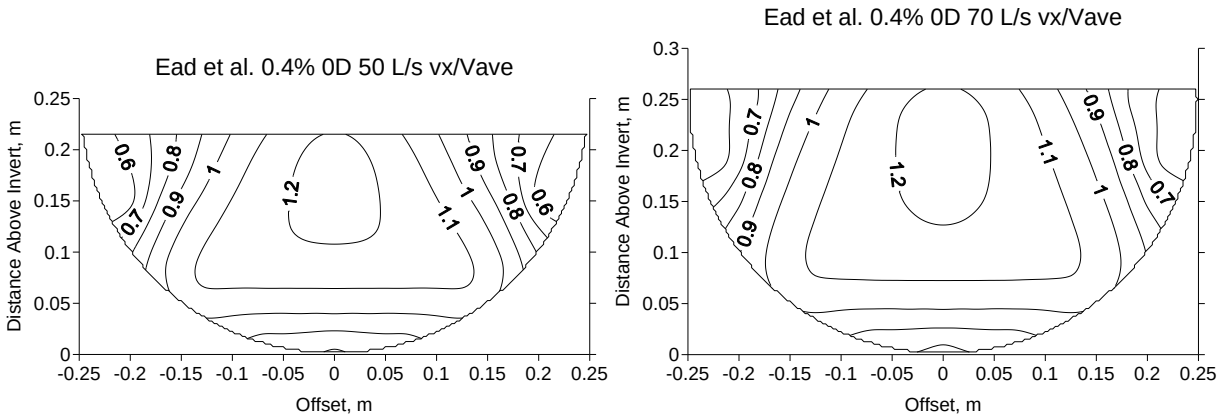

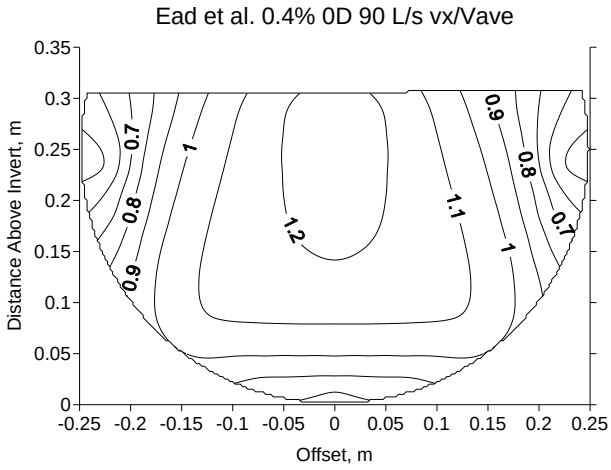

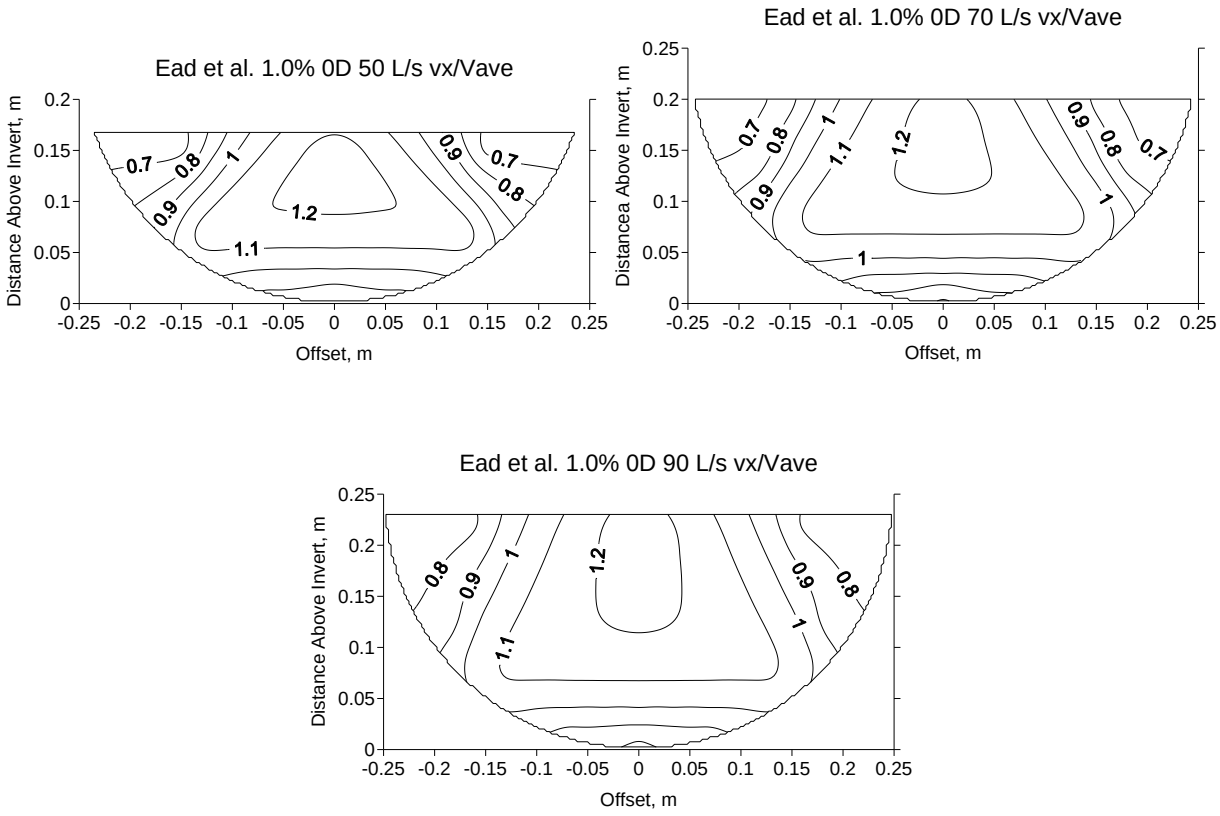
Ead et al. 1.0% 0D 50 L/s vx/Vave
Distance Above Invert, m
Offset, m
Ead et al. 1.0% 0D 70 L/s vx/Vave
Distancea Above Invert, m
Offset, m
Ead et al. 1.0% 0D 90 L/s vx/Vave
Distance Above Invert, m
Offset, m

Contour Plots of %Error of Point Velocity Calculated with Ead et al. (2000) Model (using J value of 0.8) Compared to Measured Data

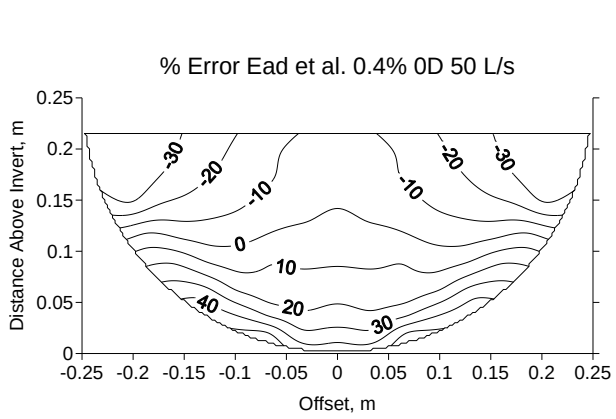

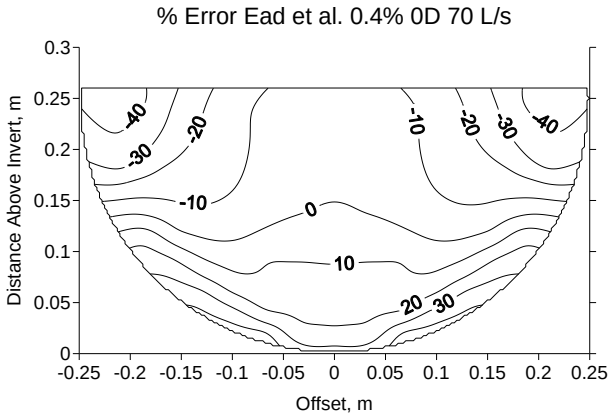

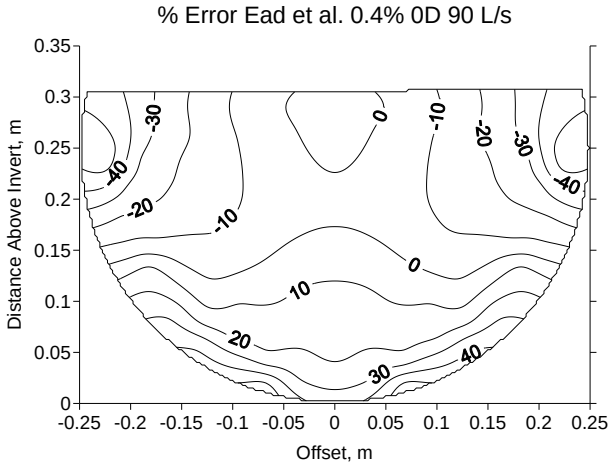

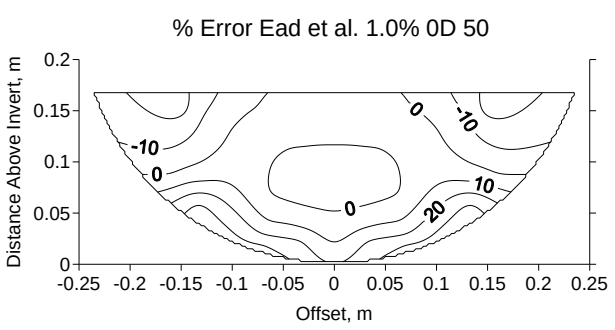
% Error Ead et al. 1.0% 0D 50
Distance Above Invert, m
Offset, m
0.2
0.15
0.1
0.05
0
-0.25 -0.2 -0.15 -0.1 -0.05 0 0.05 0.1 0.15 0.2 0.25
-10
0
0
-10
10
0
20

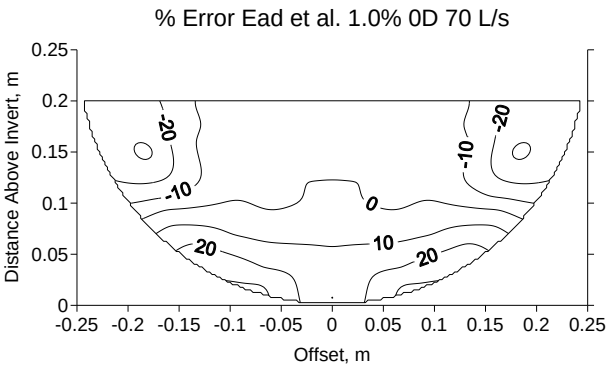
% Error Ead et al. 1.0% 0D 70 L/s
Distance Above Invert, m
Offset, m
0.25
0.2
0.15
0.1
0.05
0
-0.25 -0.2 -0.15 -0.1 -0.05 0 0.05 0.1 0.15 0.2 0.25
-20
-10
0
-20
-10
0
20
10
20

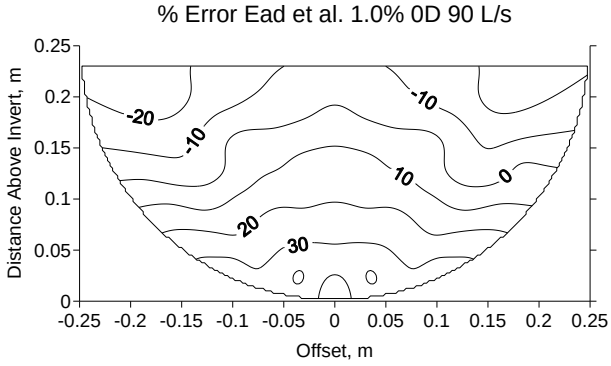
% Error Ead et al. 1.0% 0D 90 L/s
Distance Above Invert, m
Offset, m
0.25
0.2
0.15
0.1
0.05
0
-0.25 -0.2 -0.15 -0.1 -0.05 0 0.05 0.1 0.15 0.2 0.25
-20
-10
-10
10
0
20
30

Appendix K: Velocity Distribution Plots for Ead et al. (2000) Model (Using J Value of 0.8)

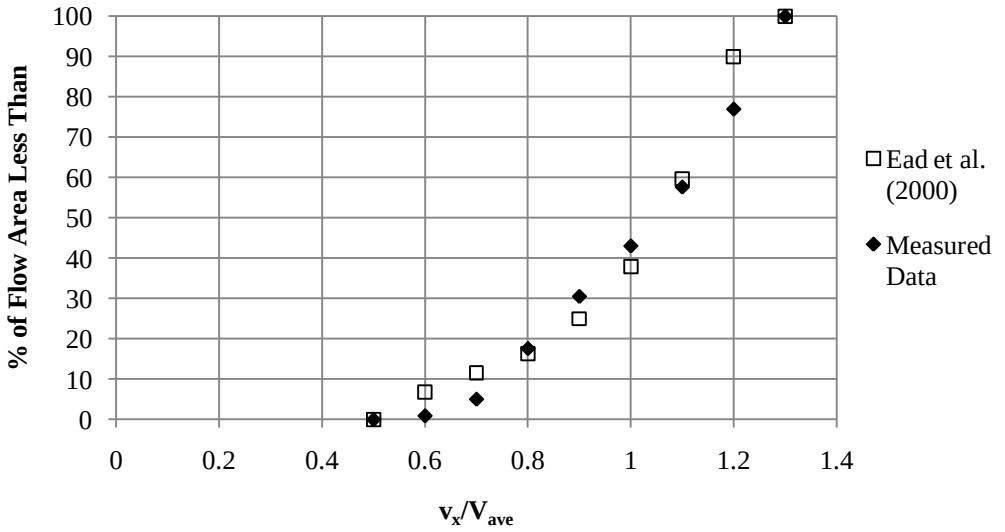

Figure K1: Velocity distribution for contour plots of Ead et al. Model and average of experimental data obtained at holes 8 and 14 for 0.4% culvert slope, 50 L/s discharge.

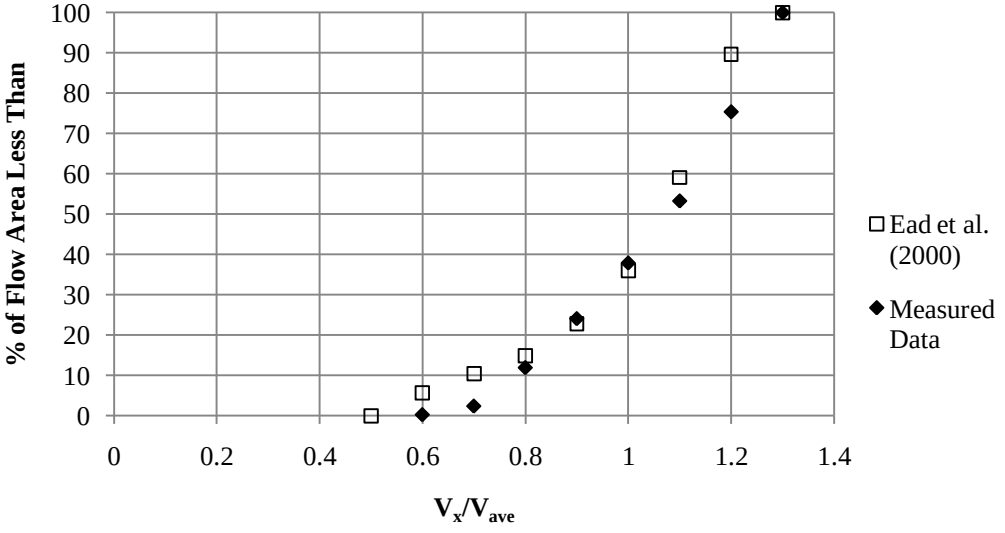

Figure K2: Velocity distribution for contour plots of Ead et al. Model and average of experimental data obtained at holes 8 and 14 for 0.4% culvert slope, 70 L/s discharge.

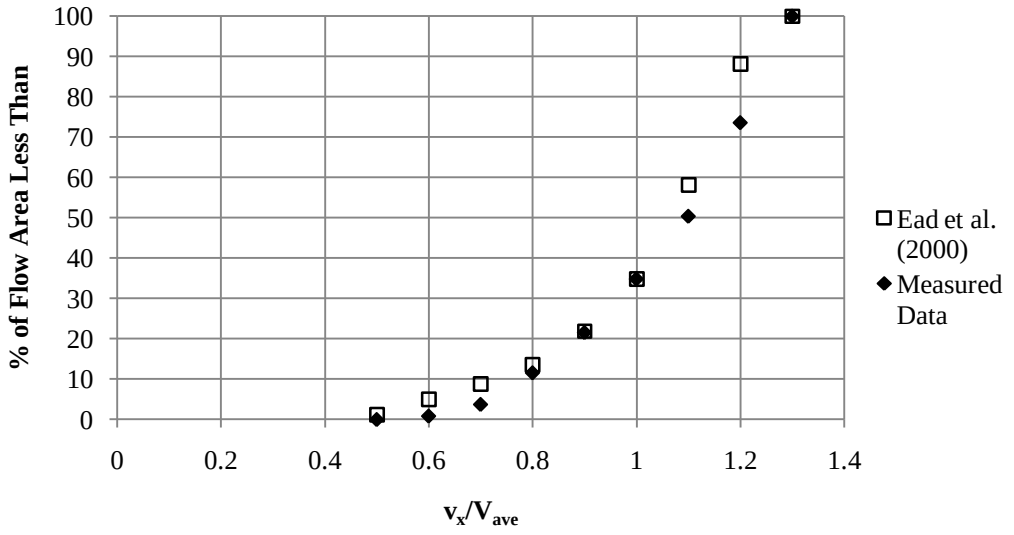

Figure K3: Velocity distribution for contour plots of Ead et al. Model and average of experimental data obtained at holes 8 and 14 for 0.4% culvert slope, 90 L/s discharge.

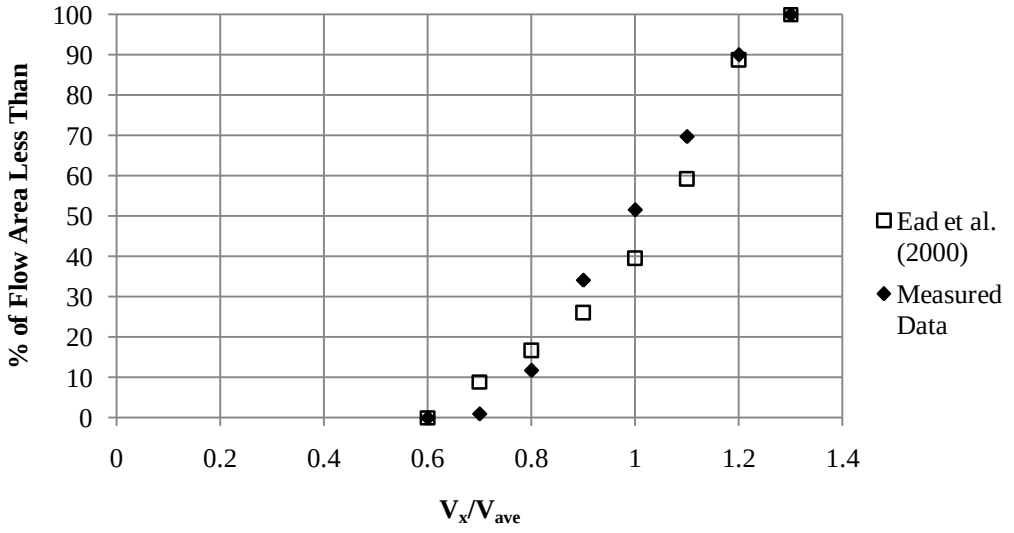

Figure K4: Velocity distribution for contour plots of Ead et al. Model and average of experimental data obtained at holes 8 and 14 for 1.0% culvert slope, 50 L/s discharge.

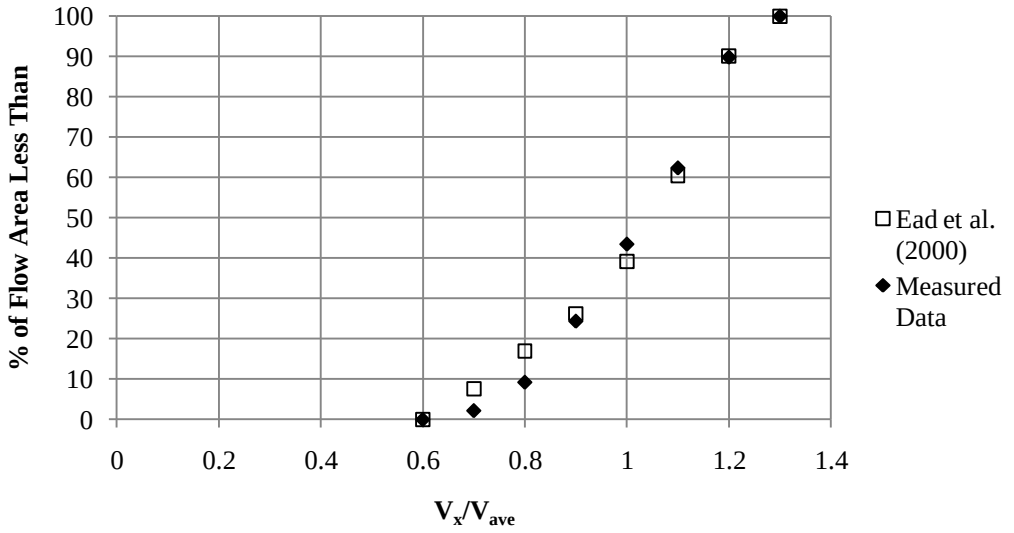

Figure K5: Velocity distribution for contour plots of Ead et al. Model and average of experimental data obtained at holes 8 and 14 for 1.0% culvert slope, 70 L/s discharge.

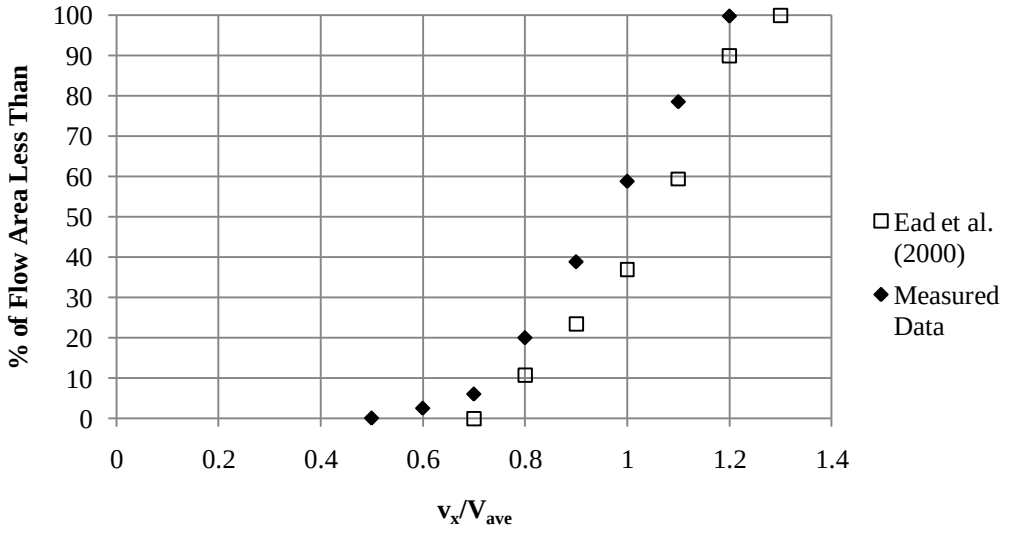

Figure K6: Velocity distribution for contour plots of Ead et al. Model and average of experimental data obtained at holes 8 and 14 for 1.0% culvert slope, 90 L/s discharge.

Appendix L: CentrelineTurbulence Intensity Profiles

0.4% Culvert Slope Non-Embedded

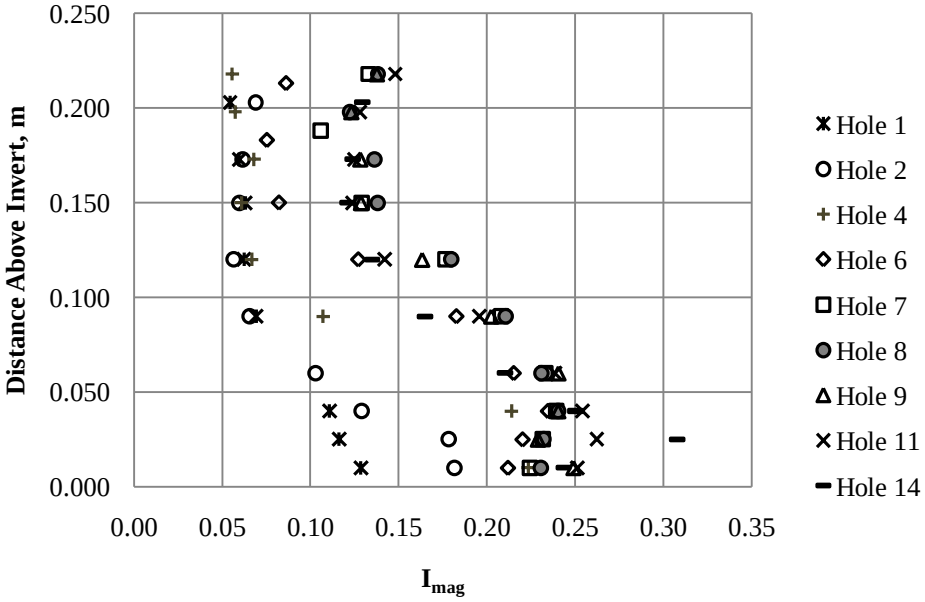

Figure L1: 0.4% Culvert Slope, Non-Embedded, 50 L/s

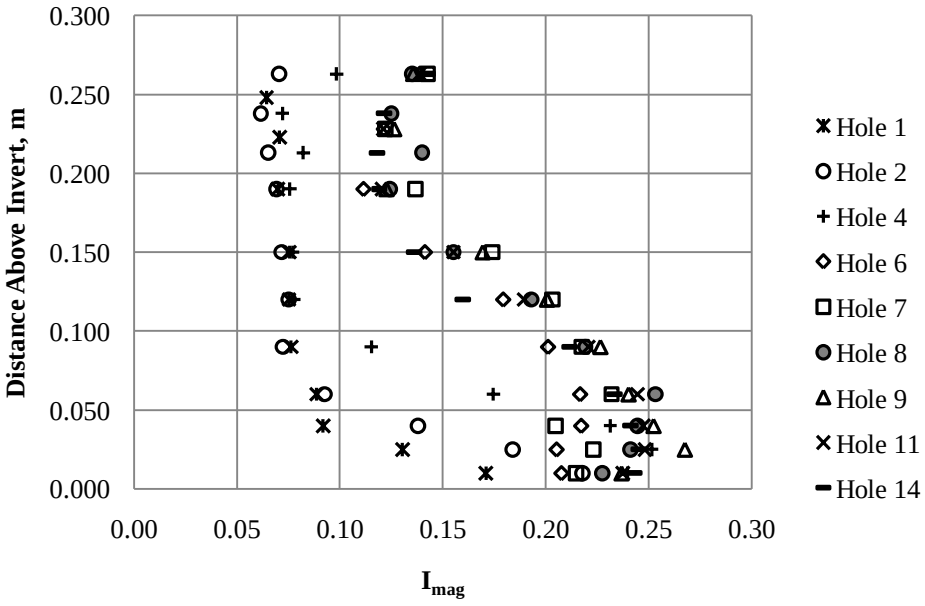

Figure L2: 0.4% Culvert Slope, Non-Embedded, 70 L/s

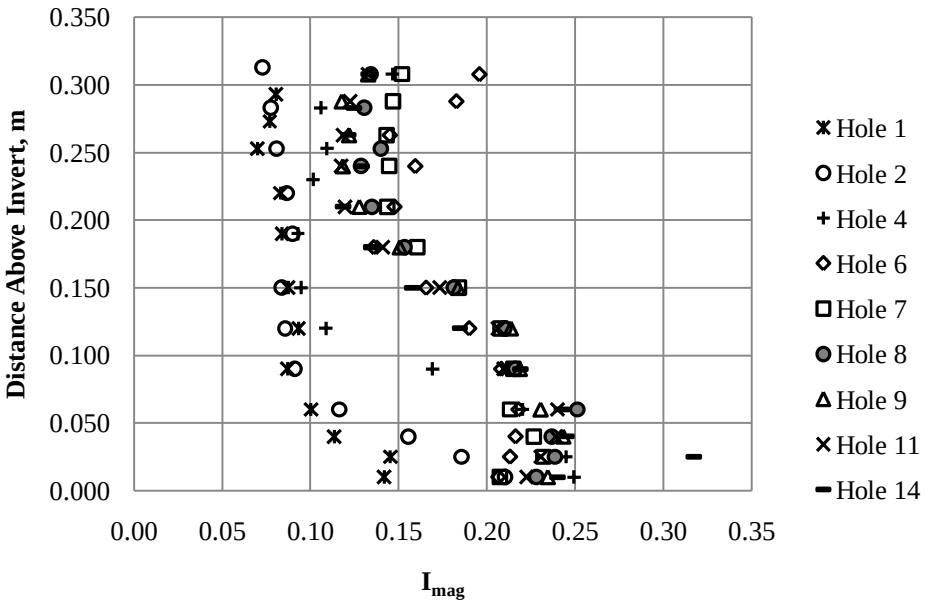

Figure L3: 0.4% Culvert Slope, Non-Embedded, 90 L/s

1.0% Culvert Slope Non-Embedded

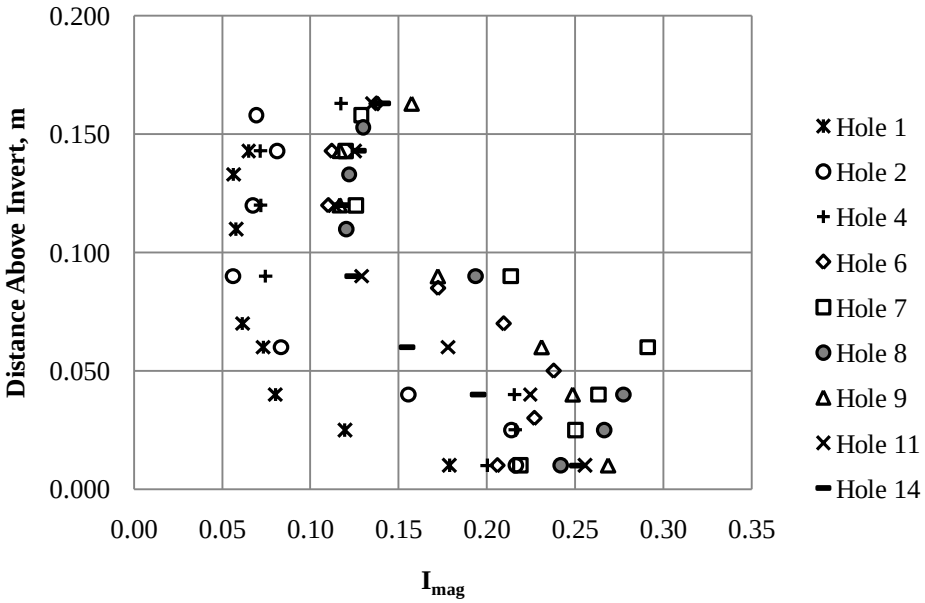

Figure L4: 1.0% Culvert Slope, Non- Embedded, 50 L/s

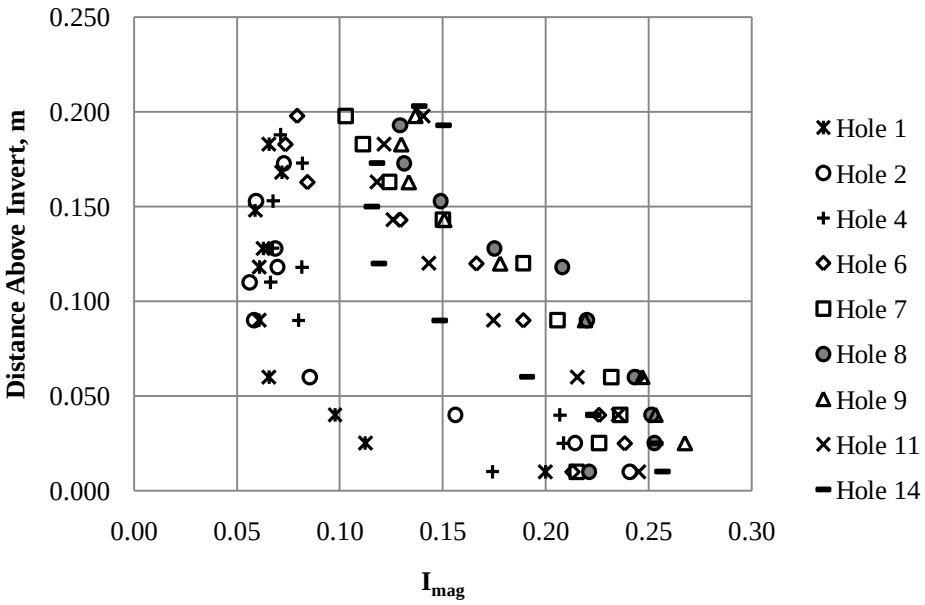

Figure L5: 1.0% Culvert Slope, Non- Embedded, 70 L/s

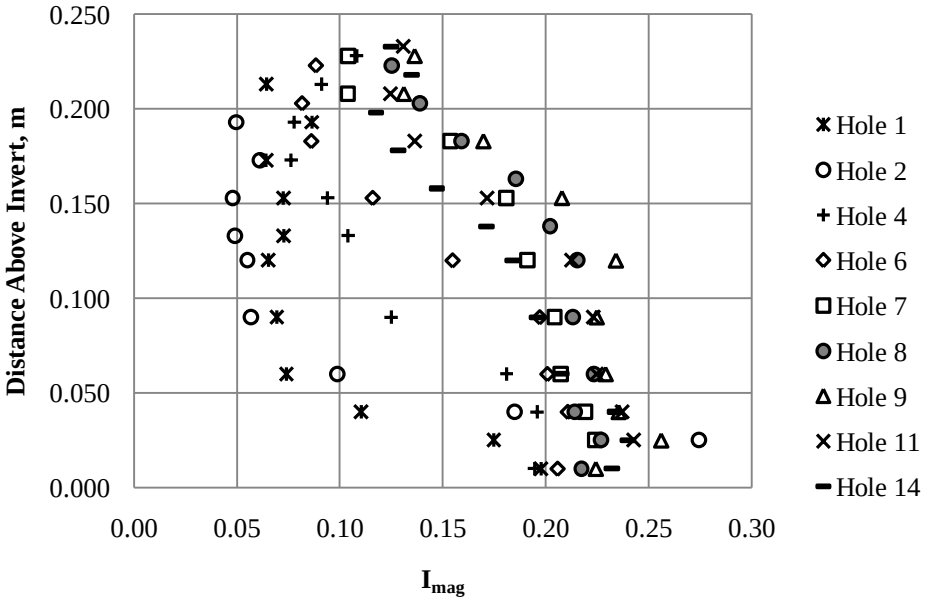

Figure L6: 1.0% Culvert Slope, Non- Embedded, 90 L/s

0.4% Culvert Slope 0.1D Embedded

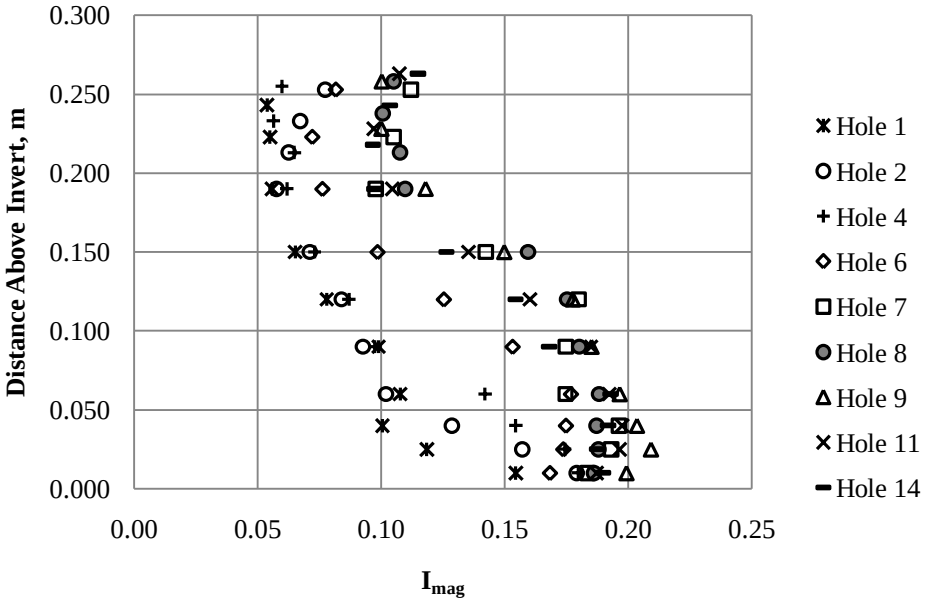

Figure L7: 0.4% Culvert Slope, 0.1D Embedded, 50 L/s

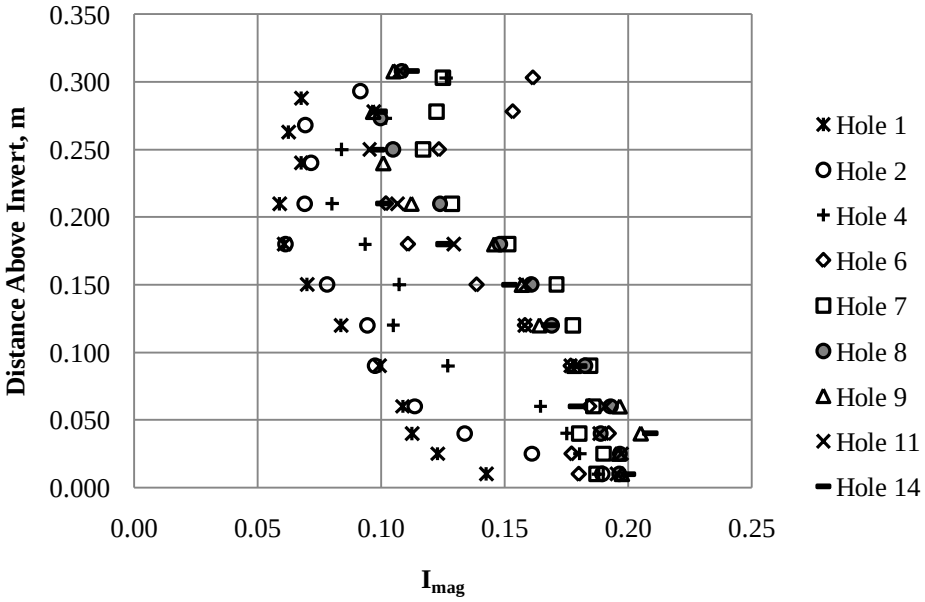

Figure L8: 0.4% Culvert Slope, 0.1D Embedded, 70 L/s

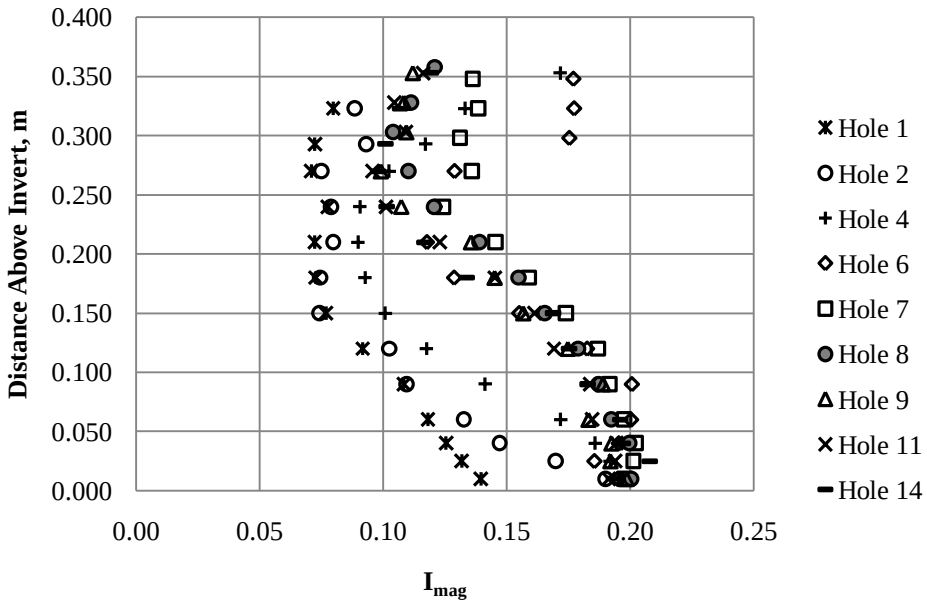

Figure L9: 0.4% Culvert Slope, 0.1D Embedded, 90 L/s

1.0% Culvert Slope 0.1D Embedded

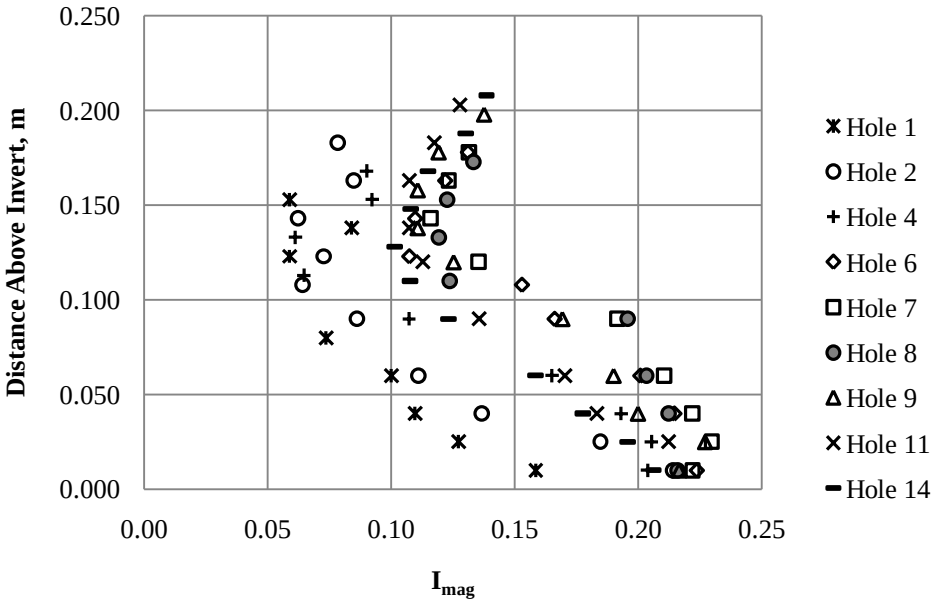

Figure L10: 1.0% Culvert Slope, 0.1D Embedded, 50 L/s

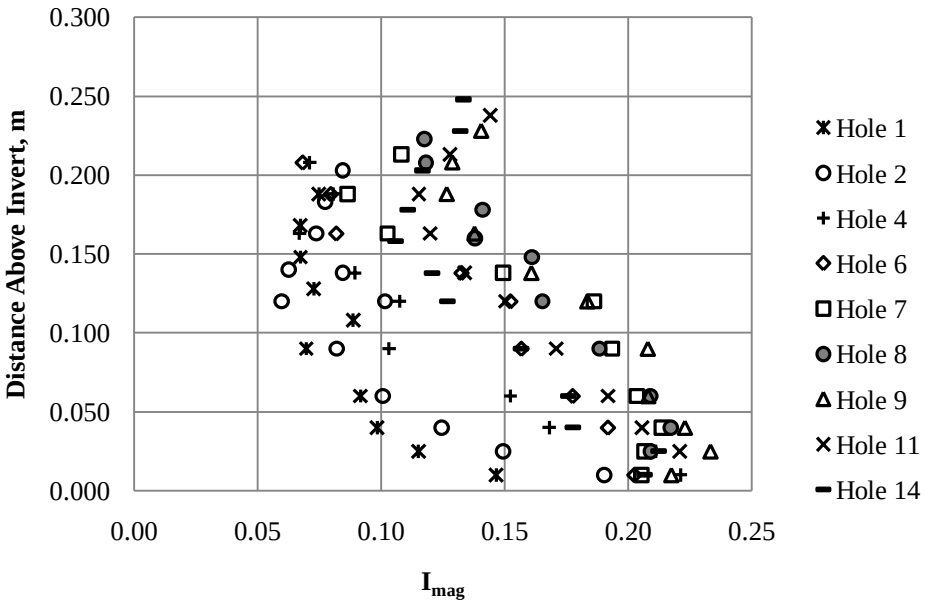

Figure L11: 1.0% Culvert Slope, 0.1D Embedded, 70 L/s

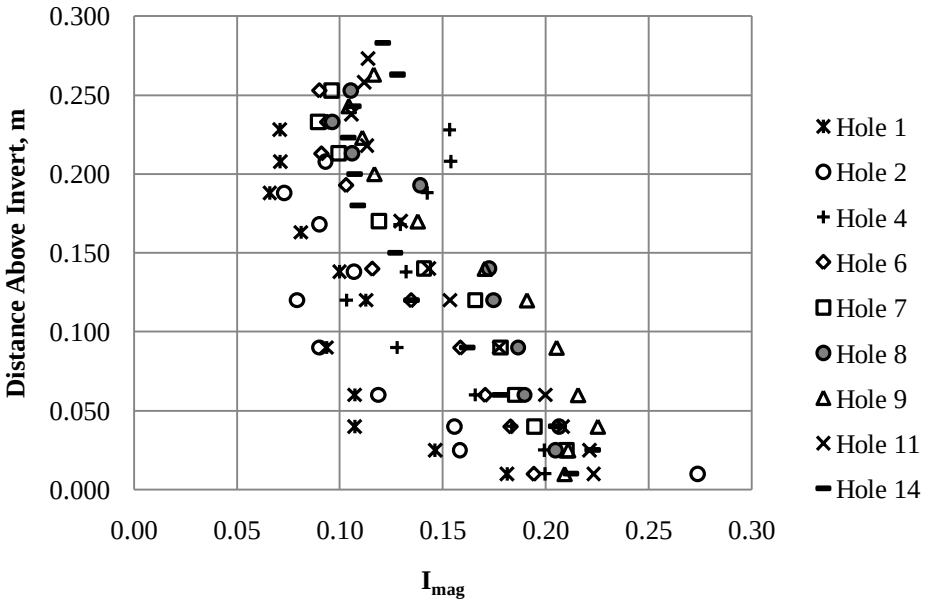

Figure L12: 1.0% Culvert Slope, 0.1D Embedded, 90 L/s

0.4% Culvert Slope 0.2D Embedded

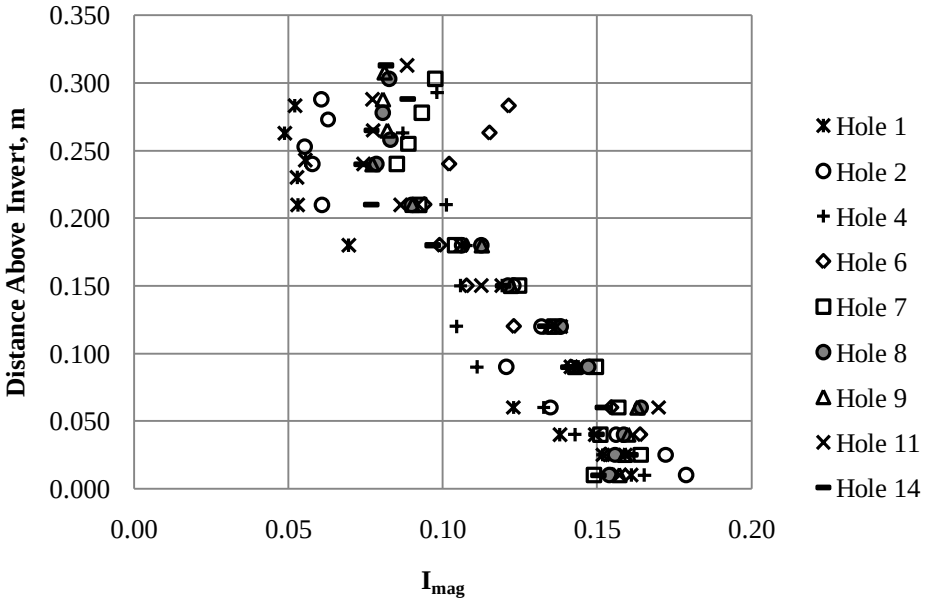

Figure L13: 0.4% Culvert Slope, 0.2D Embedded, 50 L/s

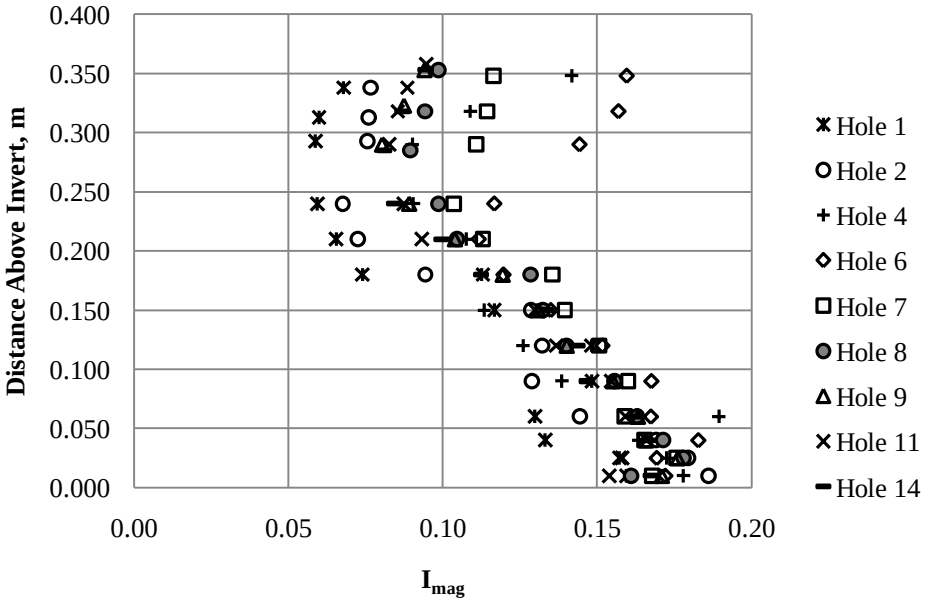

Figure L14: 0.4% Culvert Slope, 0.2D Embedded, 70 L/s

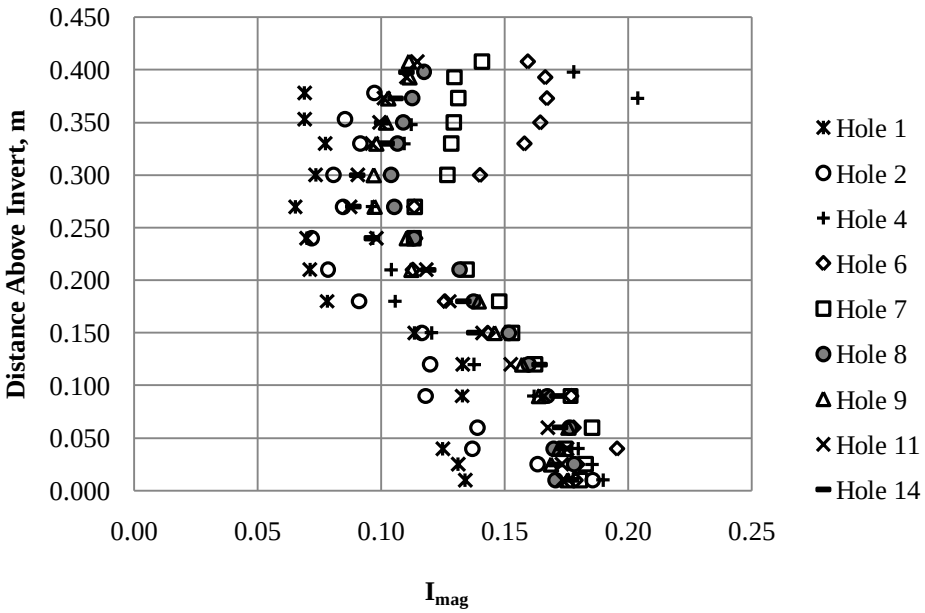

Figure L15: 0.4% Culvert Slope, 0.2D Embedded, 90 L/s

1.0% Culvert Slope 0.2D Embedded

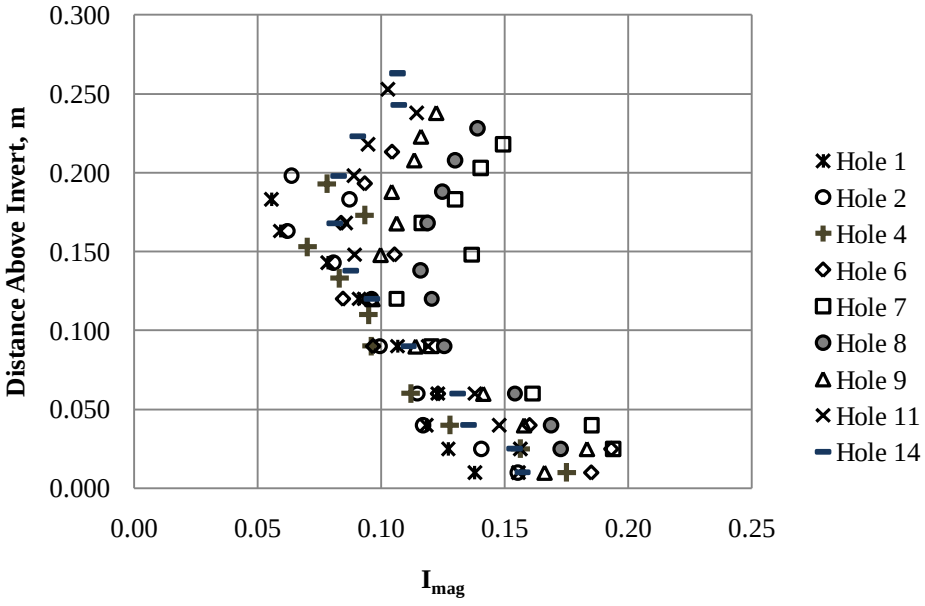

Figure L16: 1.0% Culvert Slope, 0.2D Embedded, 50 L/s

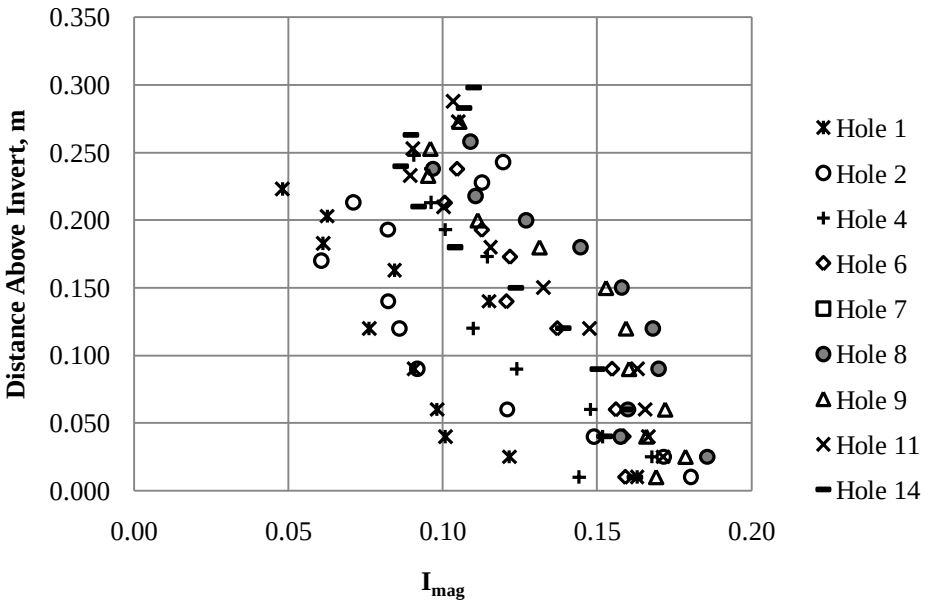

Figure L17: 1.0% Culvert Slope, 0.2D Embedded, 70 L/s

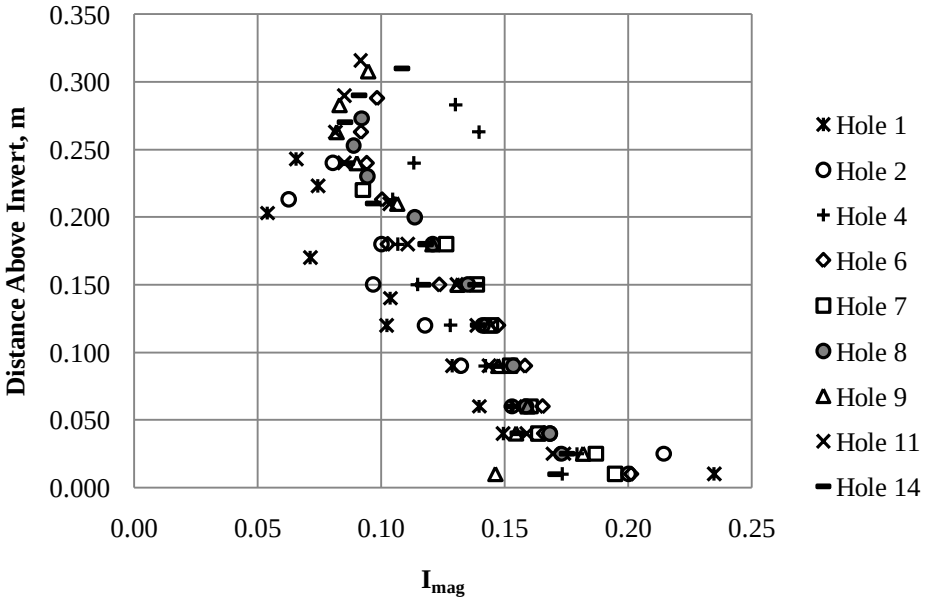

Figure L18: 1.0% Culvert Slope, 0.2D Embedded, 90 L/s

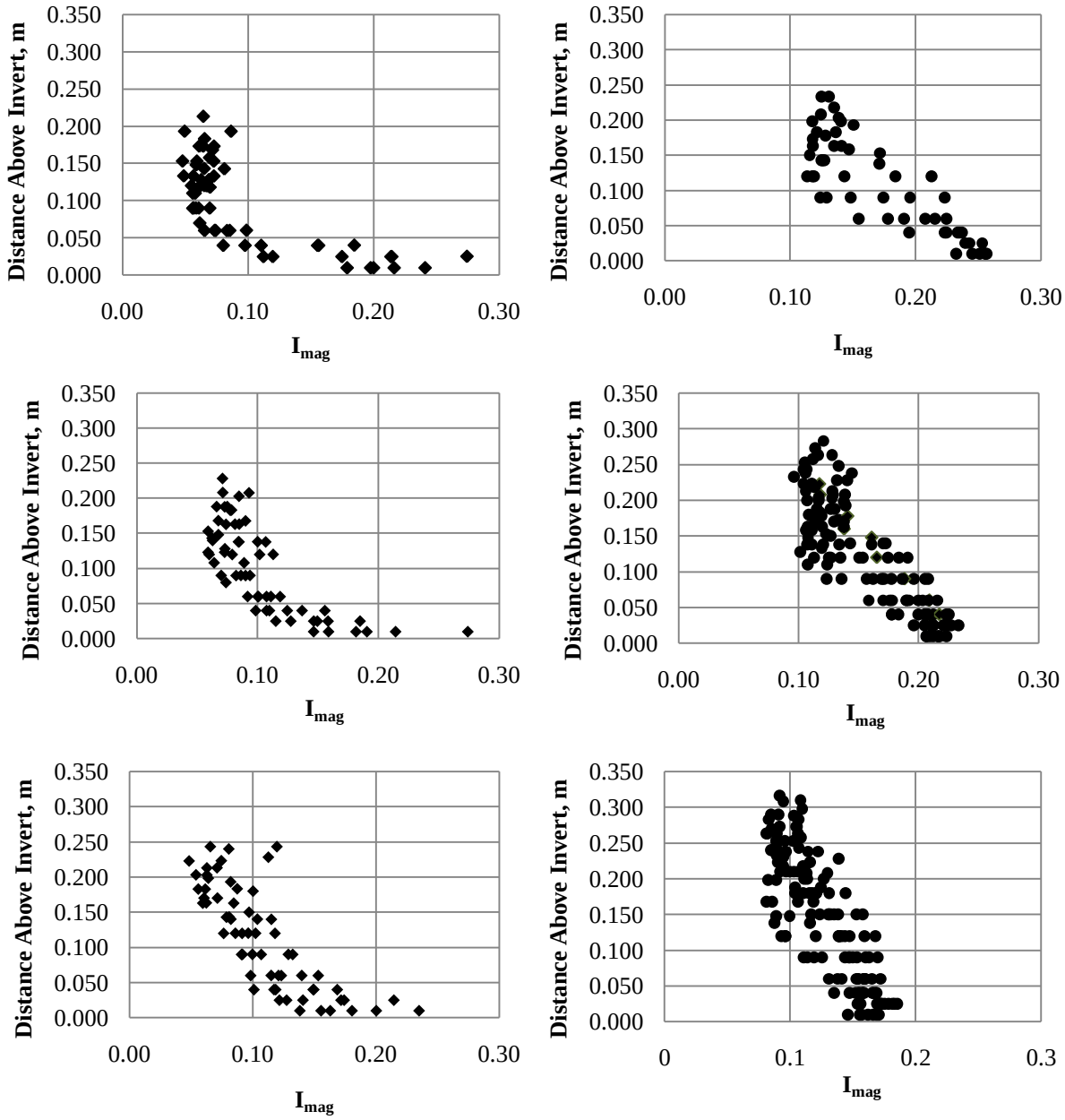

Figure L19: Combined centreline turbulence intensity profiles for the 1.0% culvert slope (50, 70, 90 L/s discharges) for Holes 1 and 2 (left column) and Holes 8-14 (right column). Top, middle and bottom rows are non-embedded, 0.1D embedded and 0.2D embedded test data, respectively.

Appendix M: Turbulence Intensity Contour Plots

Naming convention for contour plots

The title in each contour plot conveys the following information (in order):

- Culvert Slope (%)
- Embedment Depth (0D (non-embedded), 0.1D or 0.2D, where D=culvert diameter)
- Discharge (L/s)
- Cross Section Location (H1=hole 1, H2=hole 2 etc.)
- Measurement (and units if appropriate) that is being represented by the contours.

For example: 0.4% 0D 50 L/s H1 Imag indicates that the cross section is for the 0.4% culvert slope, non-embedded trial, at the 50 L/s discharge, the location is hole 1 and the contour plot is of turbulence intensity.

0.4% Culvert Slope Non-Embedded

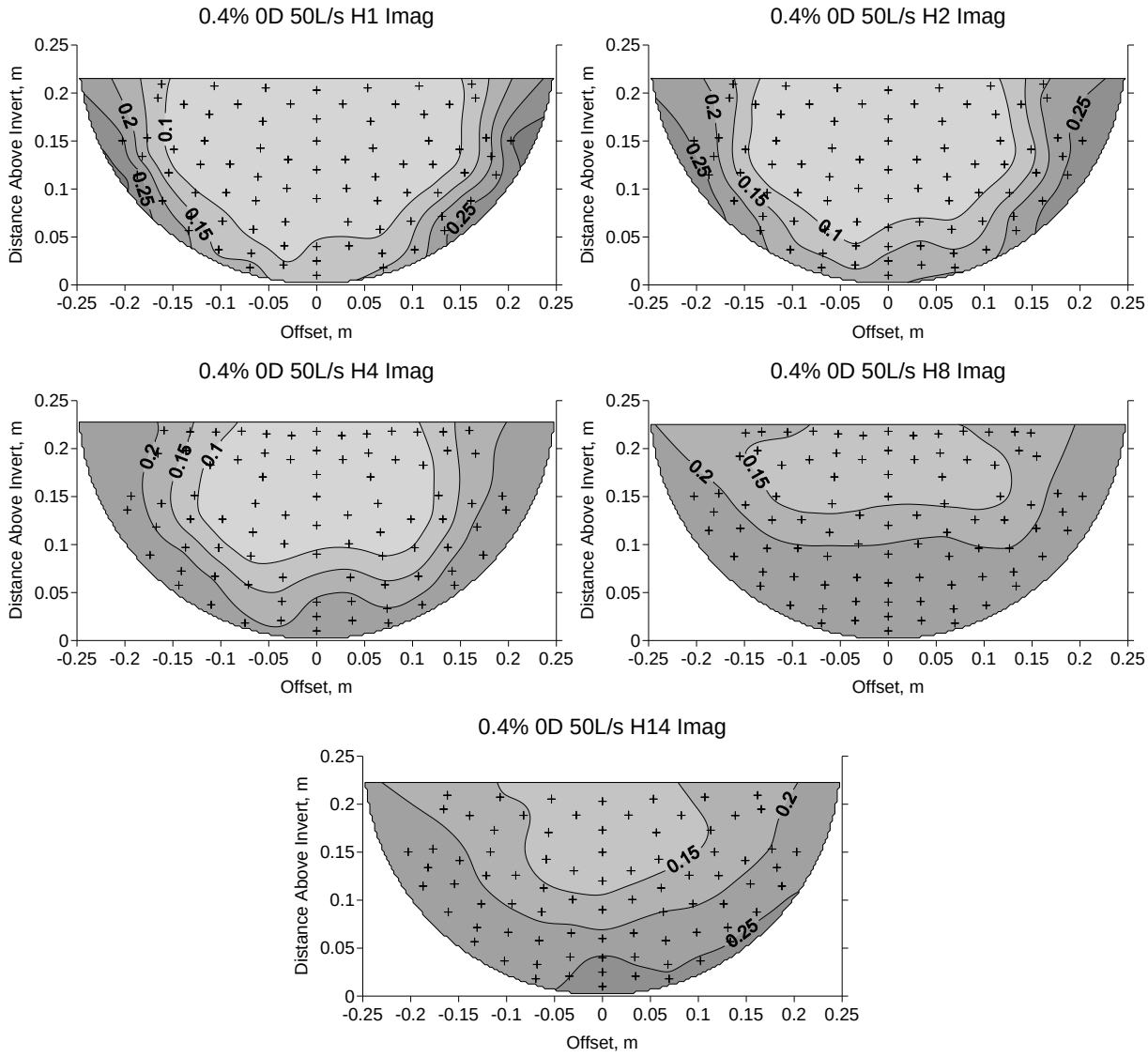

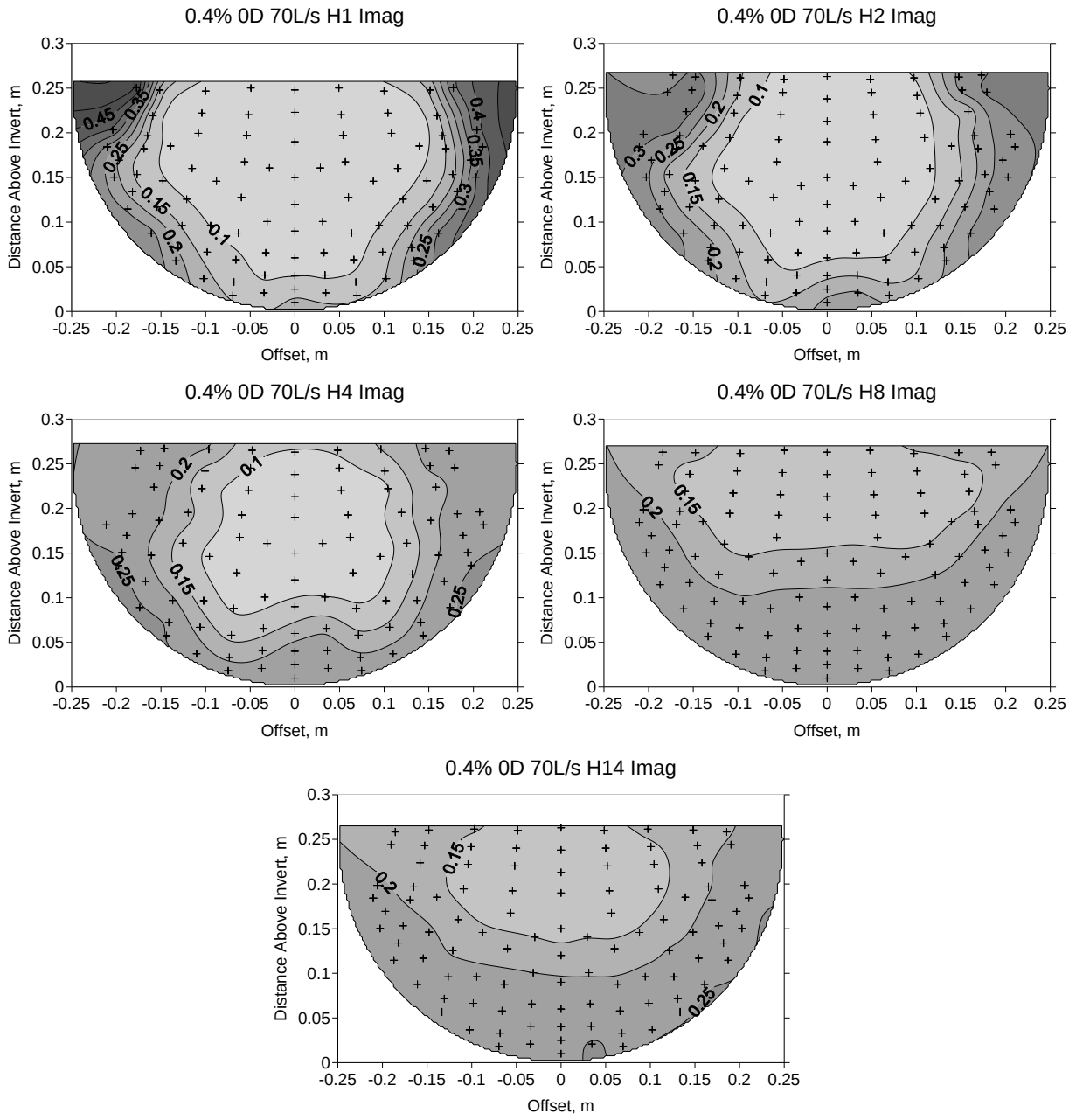
0.4% 0D 70L/s H1 Imag
0.4% 0D 70L/s H2 Imag
0.4% 0D 70L/s H4 Imag
0.4% 0D 70L/s H8 Imag
0.4% 0D 70L/s H14 Imag
Distance Above Invert, m
Offset, m

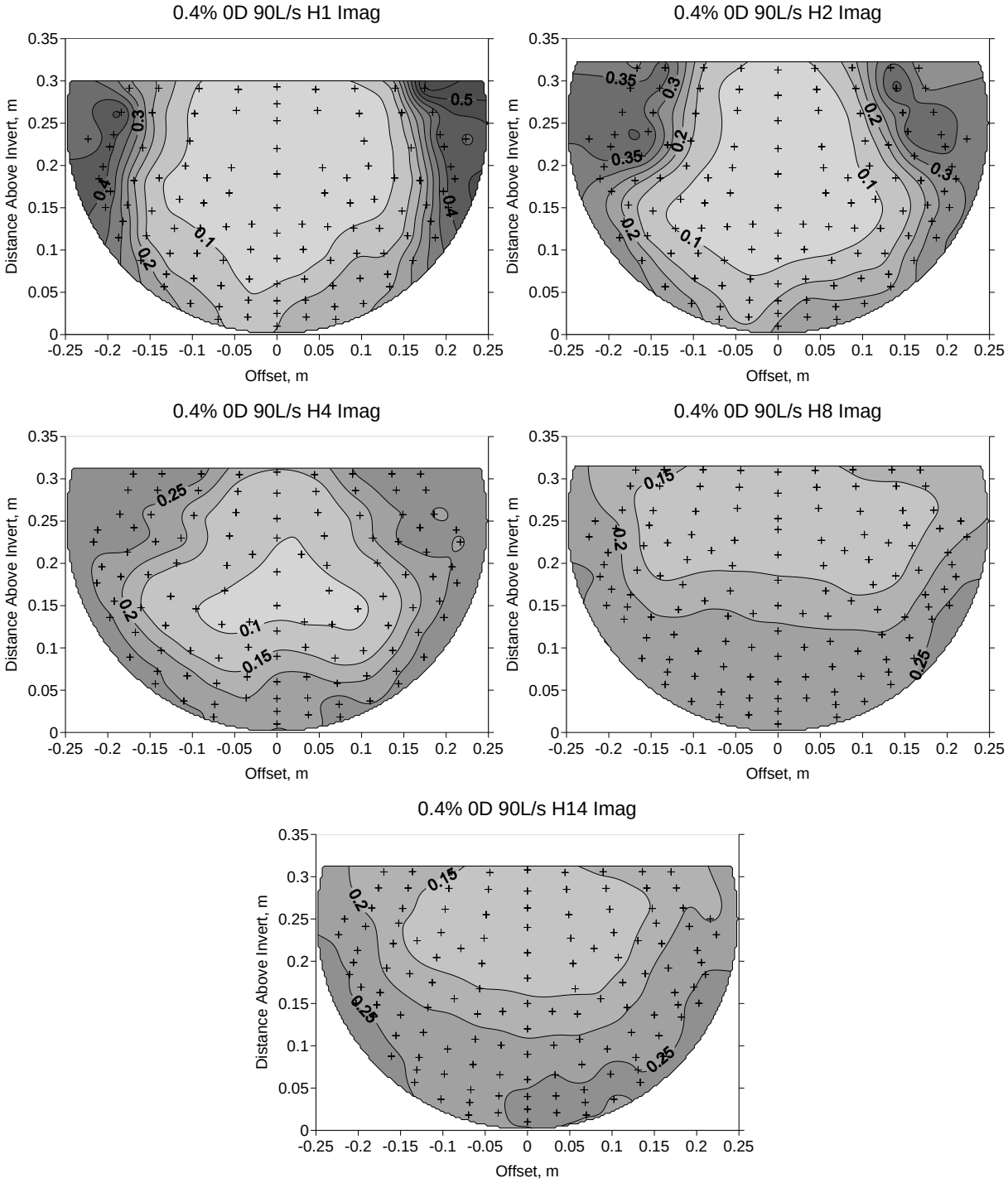
0.4% 0D 90L/s H1 Imag
0.4% 0D 90L/s H2 Imag
0.4% 0D 90L/s H4 Imag
0.4% 0D 90L/s H8 Imag
0.4% 0D 90L/s H14 Imag
Distance Above Invert, m
Offset, m

1.0% Culvert Slope Non-Embedded

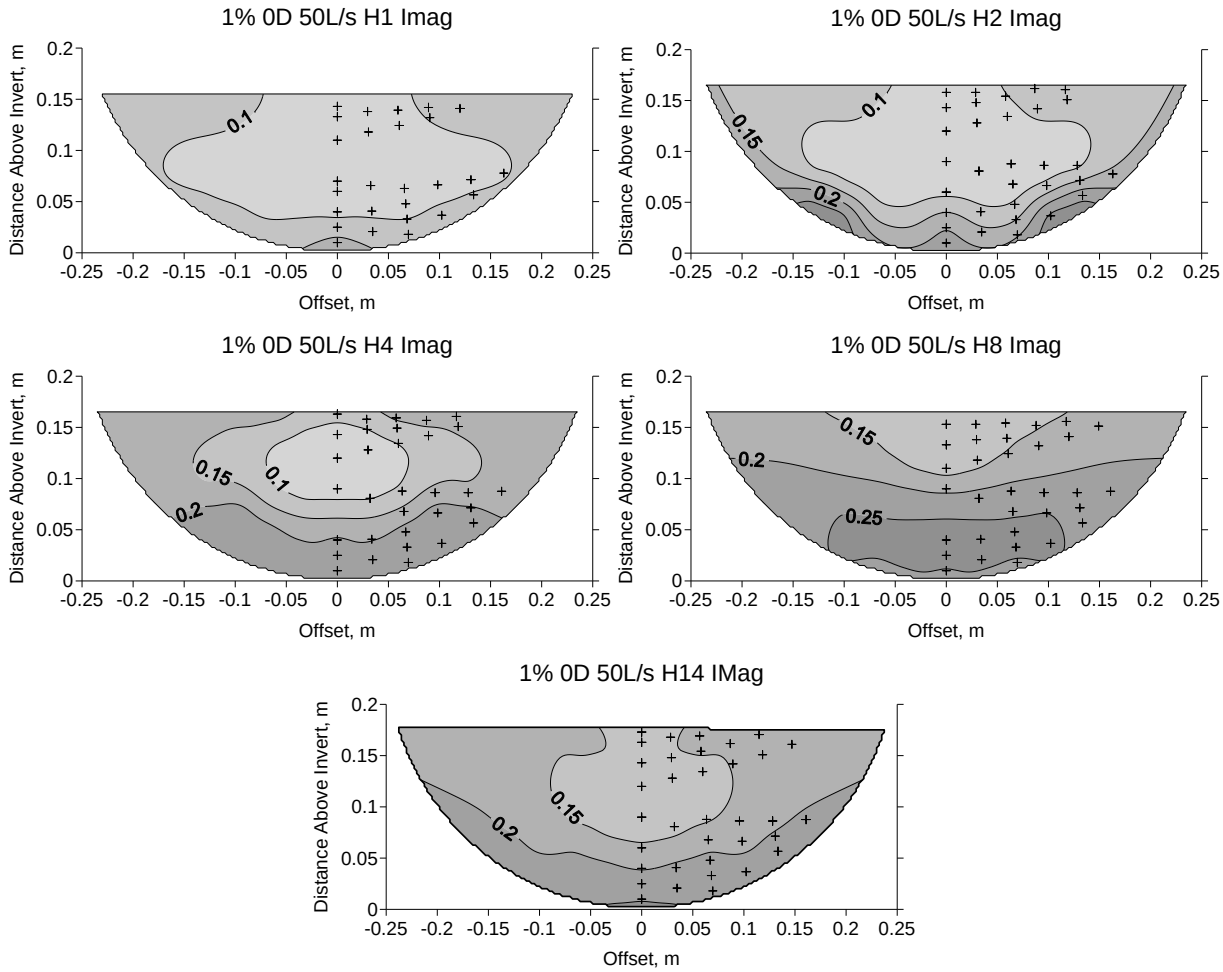

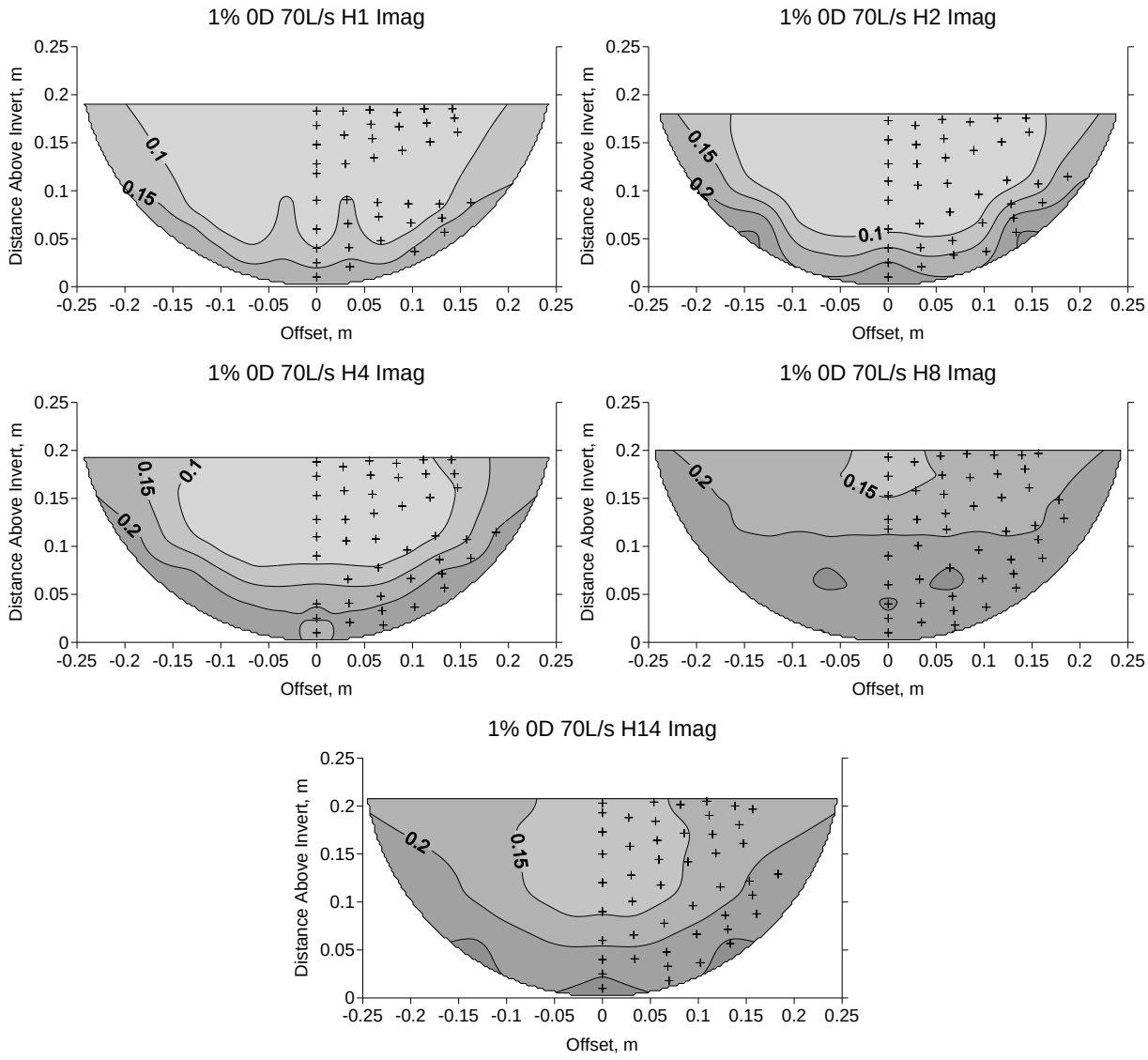
1% 0D 70L/s H1 Imag
1% 0D 70L/s H2 Imag
1% 0D 70L/s H4 Imag
1% 0D 70L/s H8 Imag
1% 0D 70L/s H14 Imag
Distance Above Invert, m
Offset, m
0.1
0.15
0.2

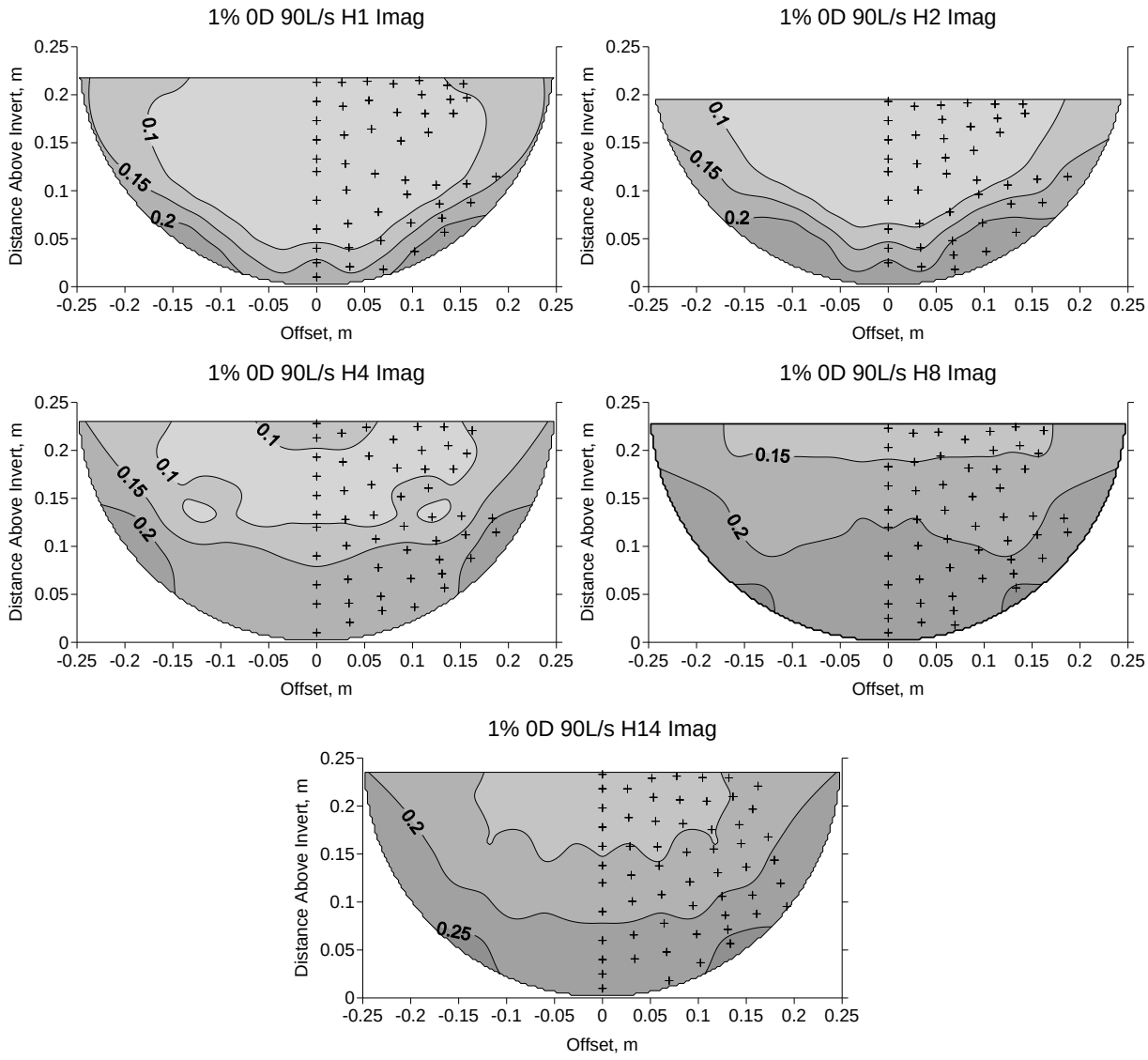
1% 0D 90L/s H1 Imag
1% 0D 90L/s H2 Imag
1% 0D 90L/s H4 Imag
1% 0D 90L/s H8 Imag
1% 0D 90L/s H14 Imag
Distance Above Invert, m
Offset, m
0.1
0.15
0.2
0.25

0.4% Culvert Slope 0.1D Embedded

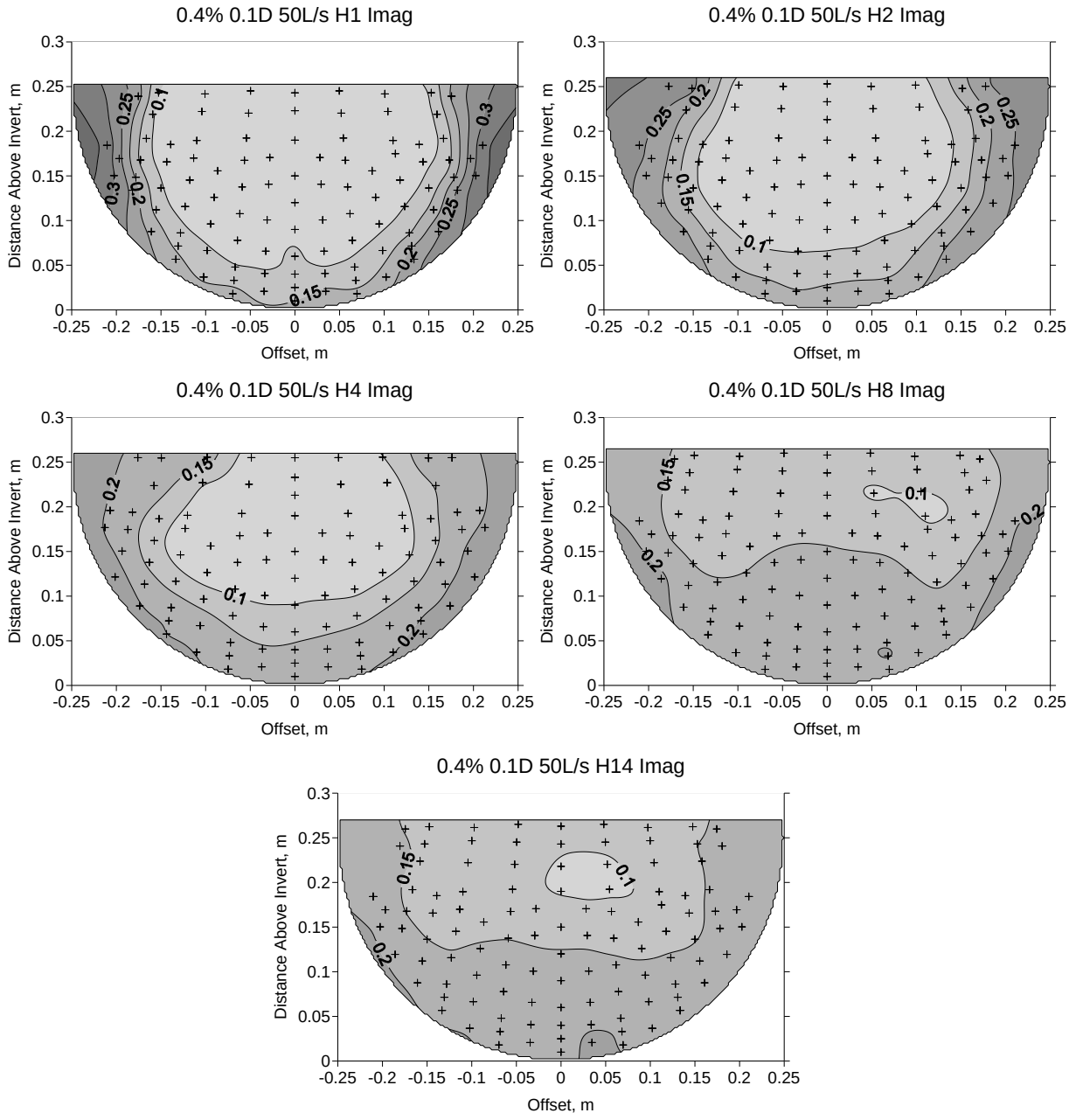

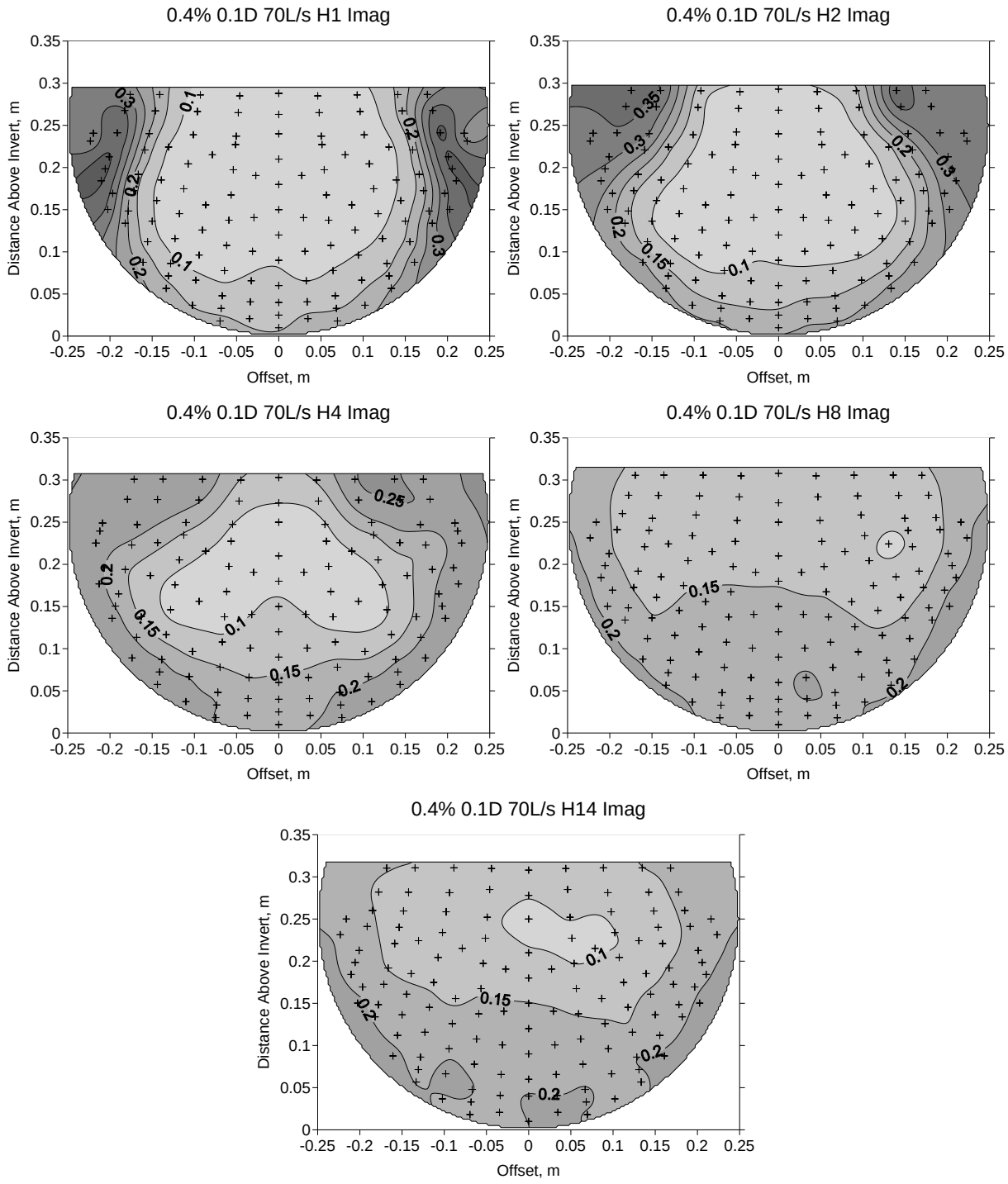
0.4% 0.1D 70L/s H1 Imag
0.4% 0.1D 70L/s H2 Imag
0.4% 0.1D 70L/s H4 Imag
0.4% 0.1D 70L/s H8 Imag
0.4% 0.1D 70L/s H14 Imag
Distance Above Invert, m
Offset, m

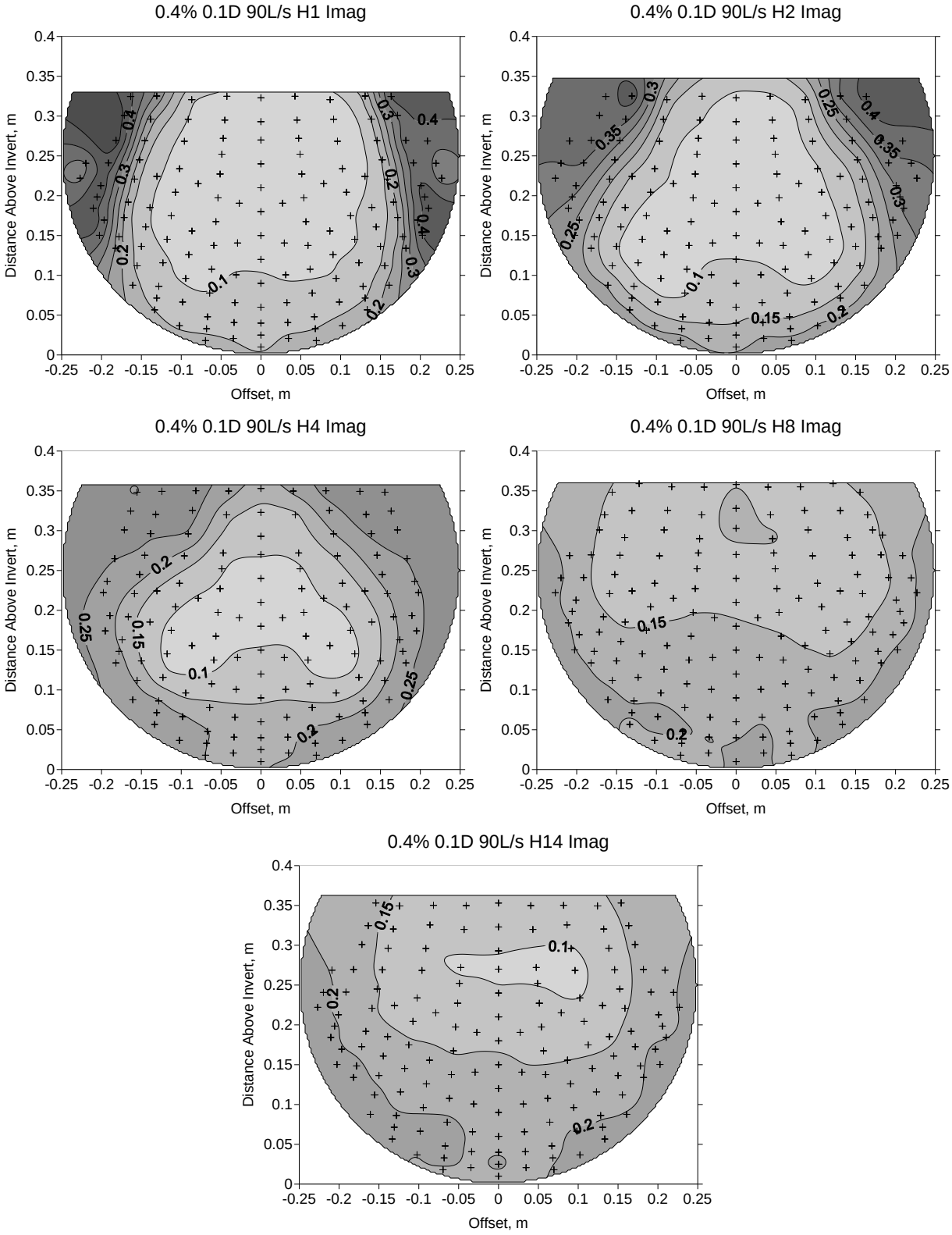
0.4% 0.1D 90L/s H1 Imag
0.4% 0.1D 90L/s H2 Imag
0.4% 0.1D 90L/s H4 Imag
0.4% 0.1D 90L/s H8 Imag
0.4% 0.1D 90L/s H14 Imag
Distance Above Invert, m
Offset, m

1.0% Culvert Slope 0.1D Embedded

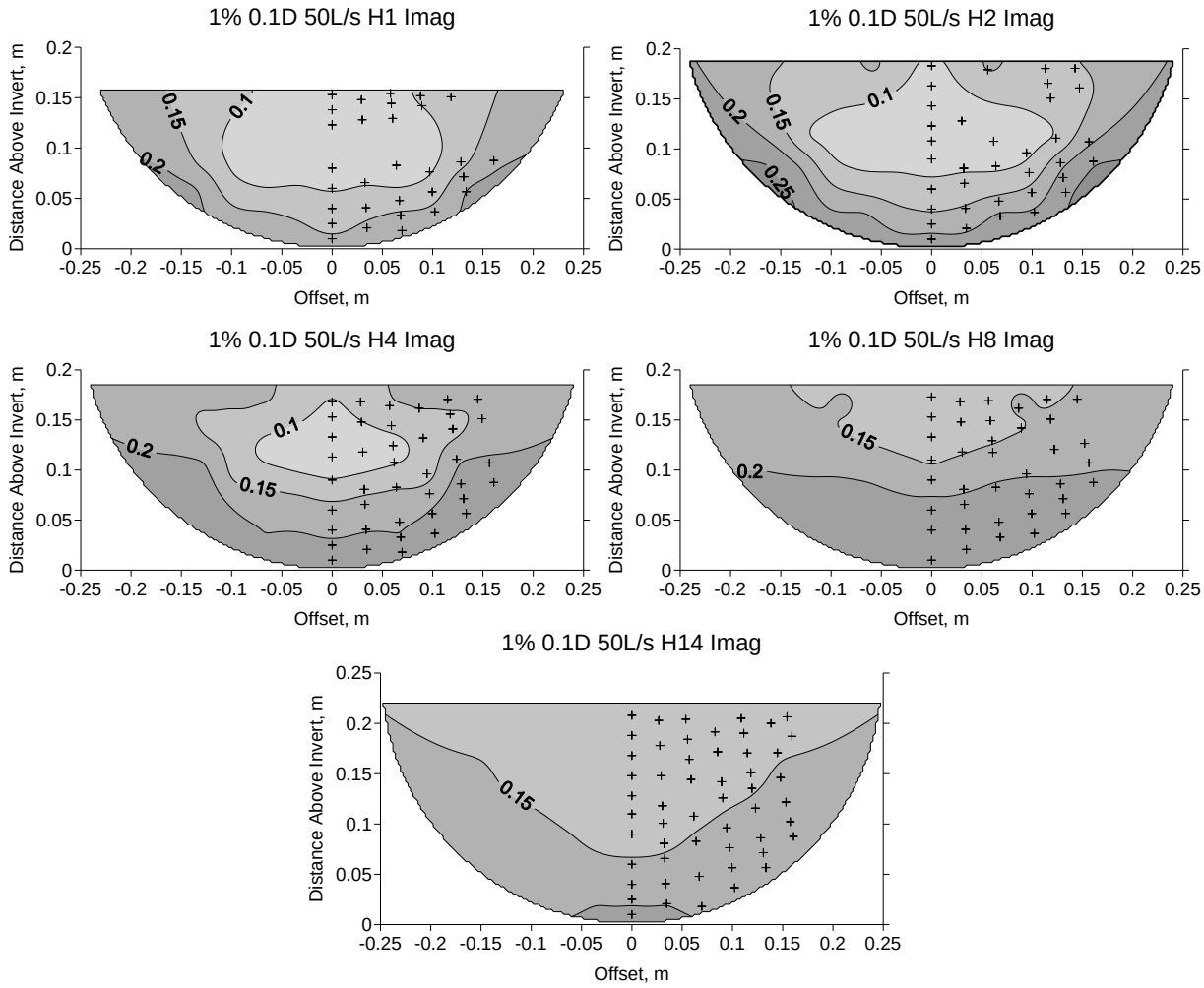

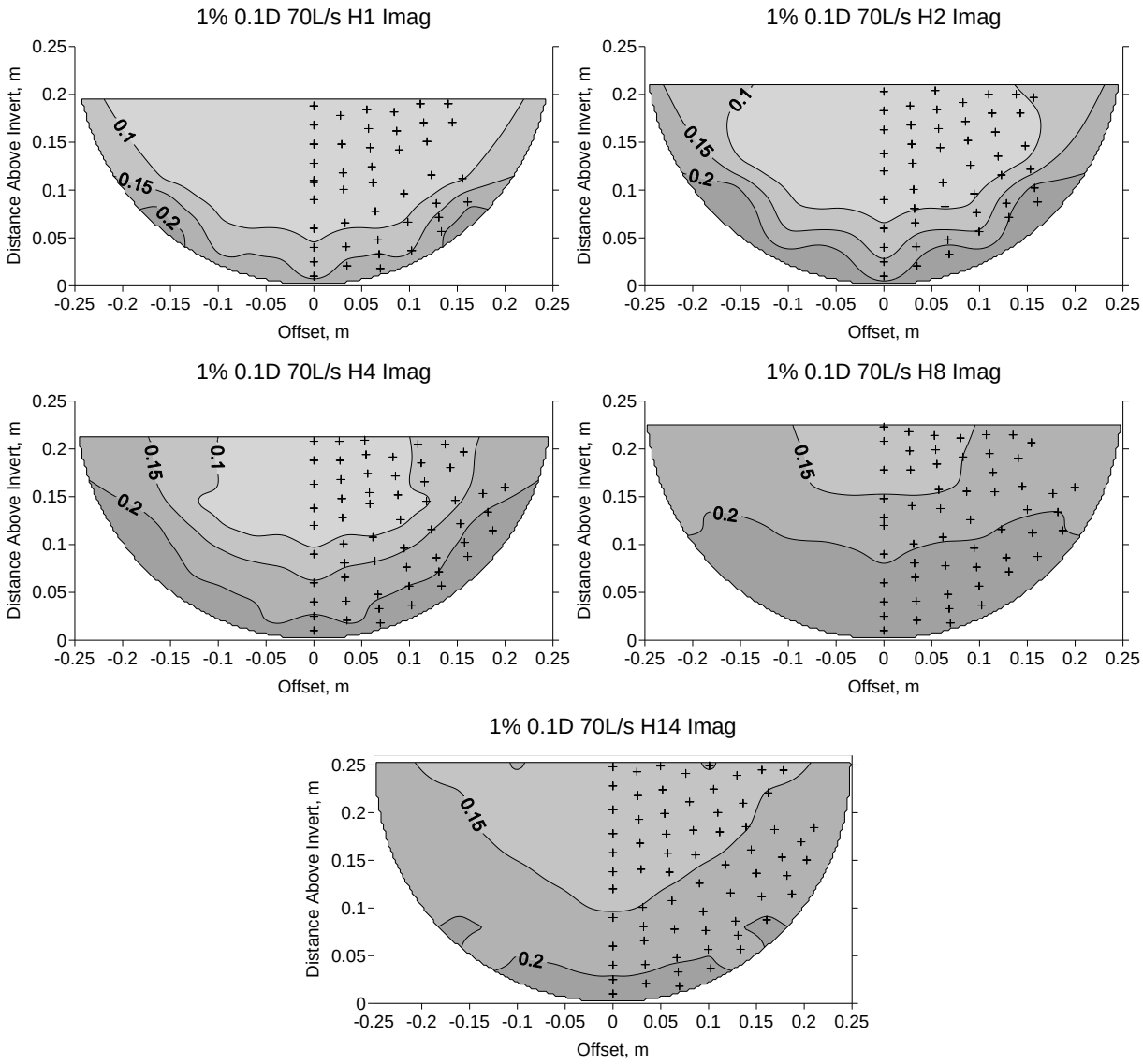
1% 0.1D 70L/s H1 Imag
1% 0.1D 70L/s H2 Imag
1% 0.1D 70L/s H4 Imag
1% 0.1D 70L/s H8 Imag
1% 0.1D 70L/s H14 Imag
Distance Above Invert, m
Offset, m
0.1
0.15
0.2

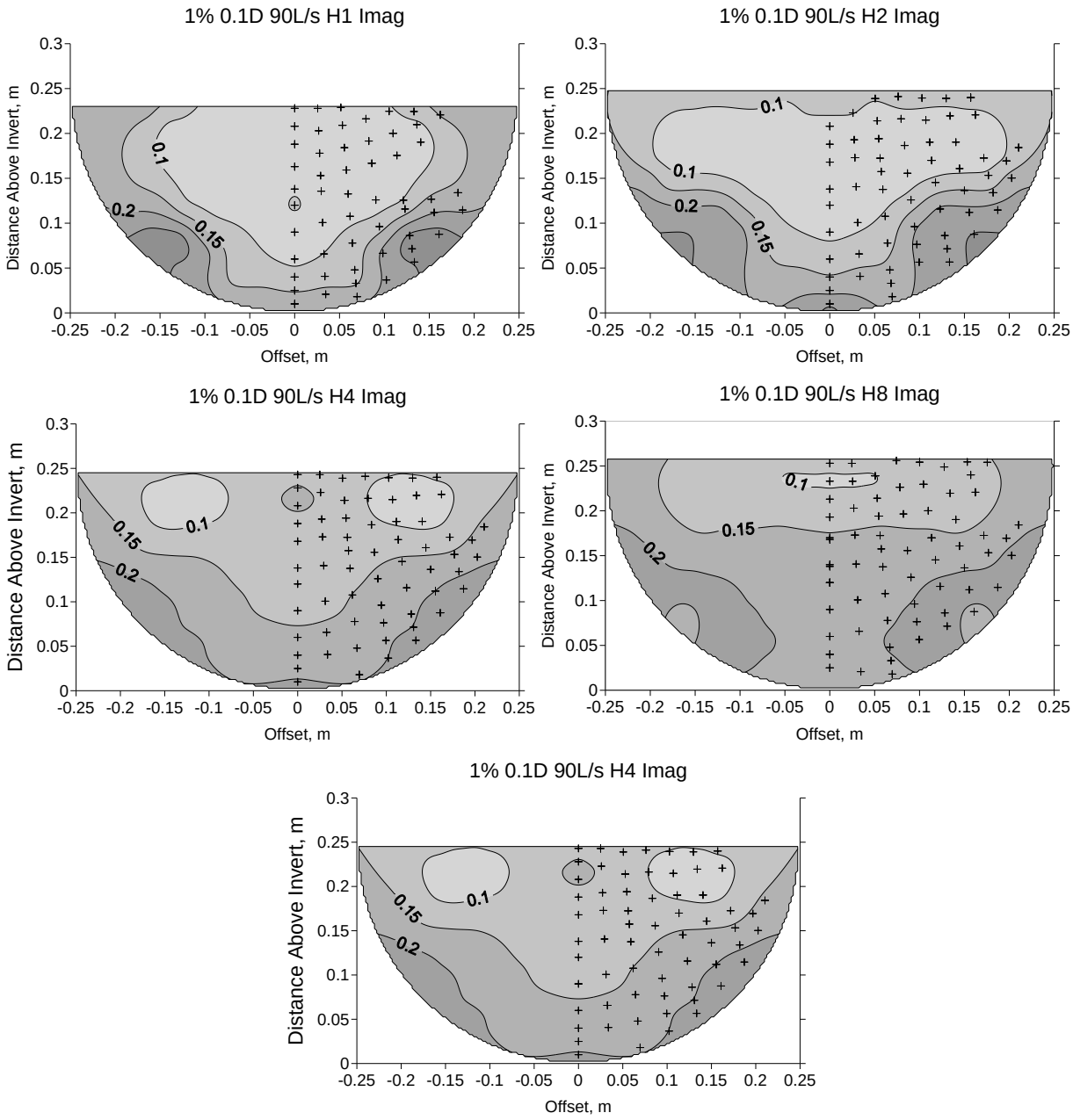
1% 0.1D 90L/s H1 Imag
1% 0.1D 90L/s H2 Imag
1% 0.1D 90L/s H4 Imag
1% 0.1D 90L/s H8 Imag
1% 0.1D 90L/s H4 Imag
Distance Above Invert, m
Offset, m
0.1
0.15
0.2

0.4% Culvert Slope 0.2D Embedded

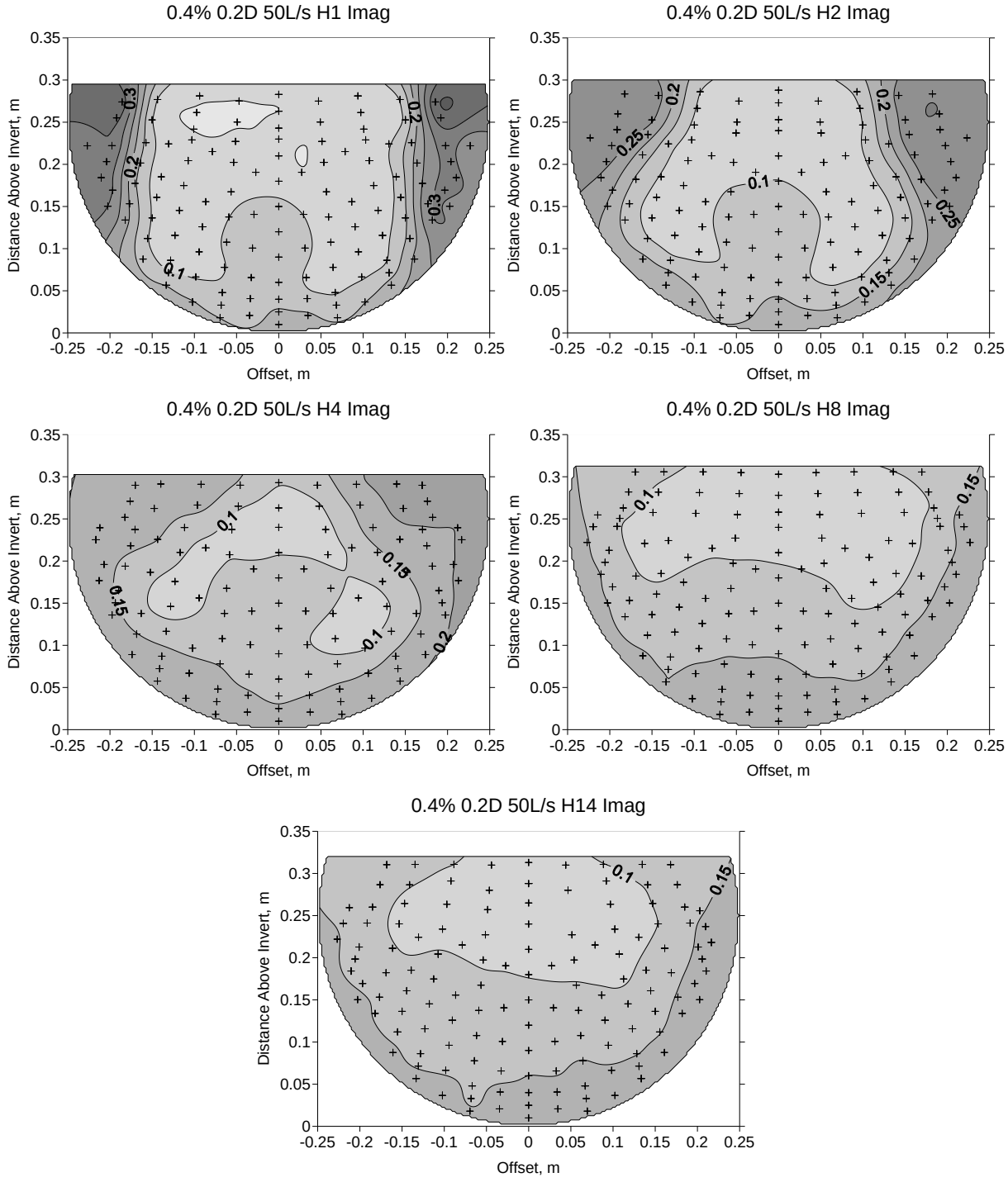

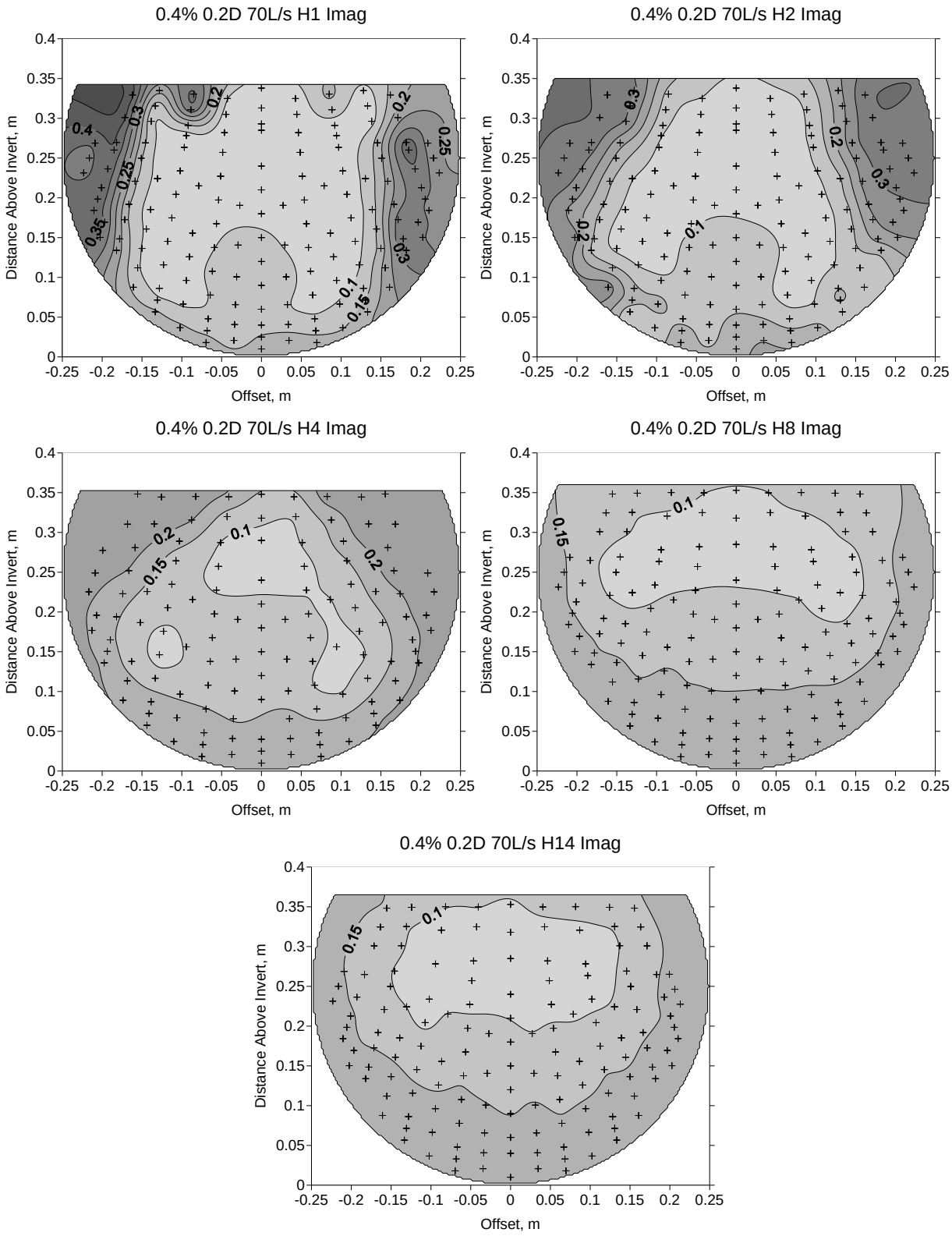
0.4% 0.2D 70L/s H1 Imag
0.4% 0.2D 70L/s H2 Imag
0.4% 0.2D 70L/s H4 Imag
0.4% 0.2D 70L/s H8 Imag
0.4% 0.2D 70L/s H14 Imag
Distance Above Invert, m
Offset, m

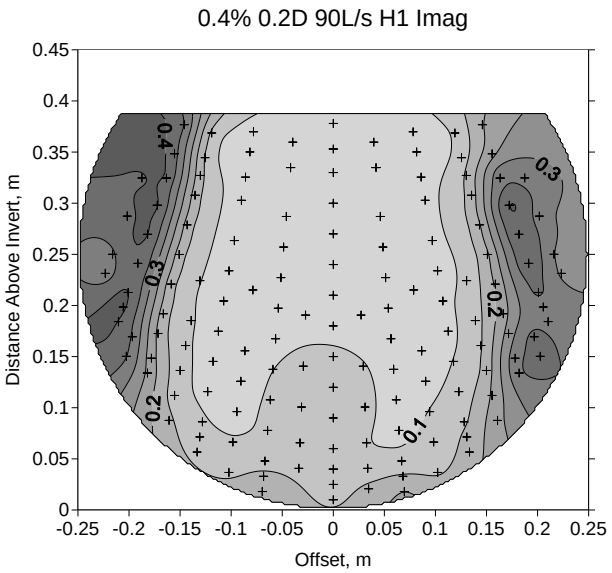
0.4% 0.2D 90L/s H1 Imag
Distance Above Invert, m
Offset, m
0.4
0.3
0.2
0.1

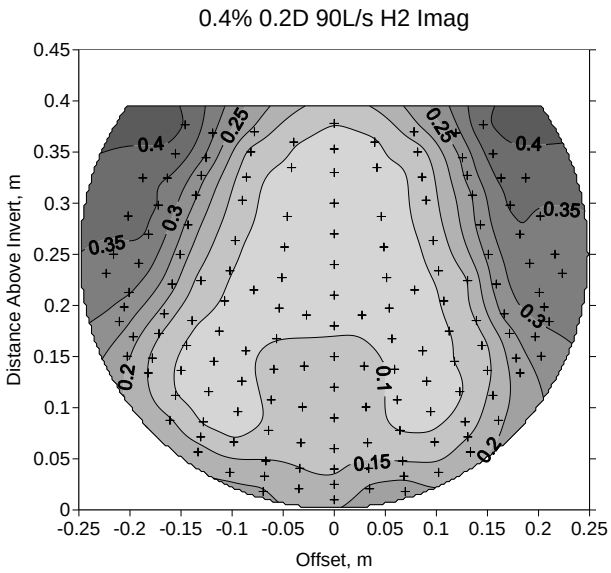
0.4% 0.2D 90L/s H2 Imag
Distance Above Invert, m
Offset, m
0.4
0.25
0.35
0.3
0.2
0.1
0.15

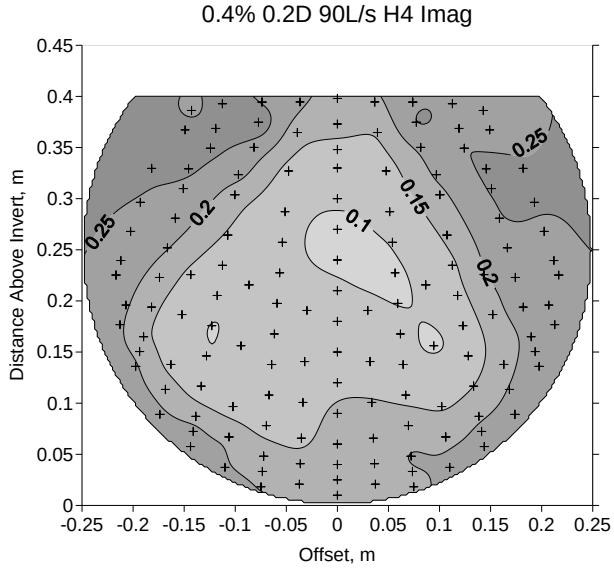
0.4% 0.2D 90L/s H4 Imag
Distance Above Invert, m
Offset, m
0.25
0.2
0.15
0.1

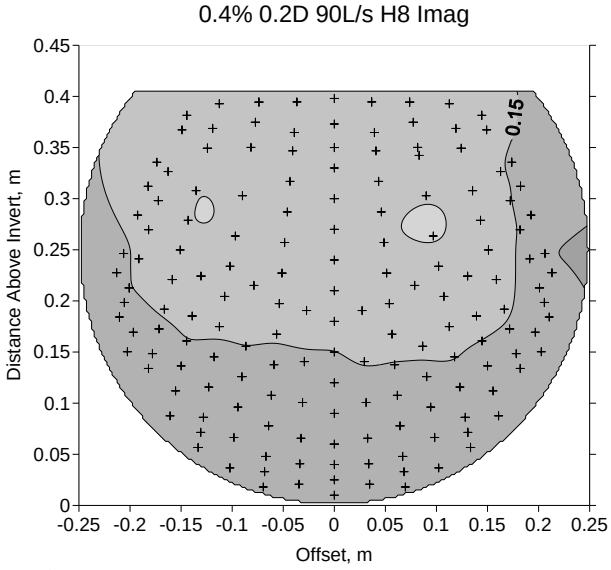
0.4% 0.2D 90L/s H8 Imag
Distance Above Invert, m
Offset, m
0.15

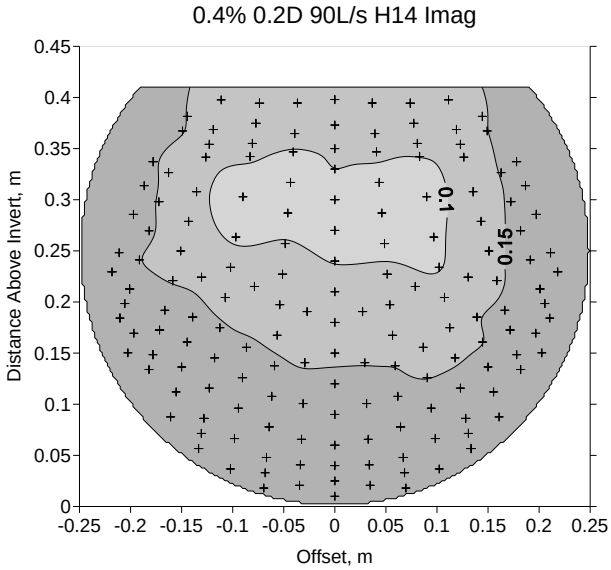
0.4% 0.2D 90L/s H14 Imag
Distance Above Invert, m
Offset, m
0.1
0.15

1.0% Culvert Slope 0.2D Embedded

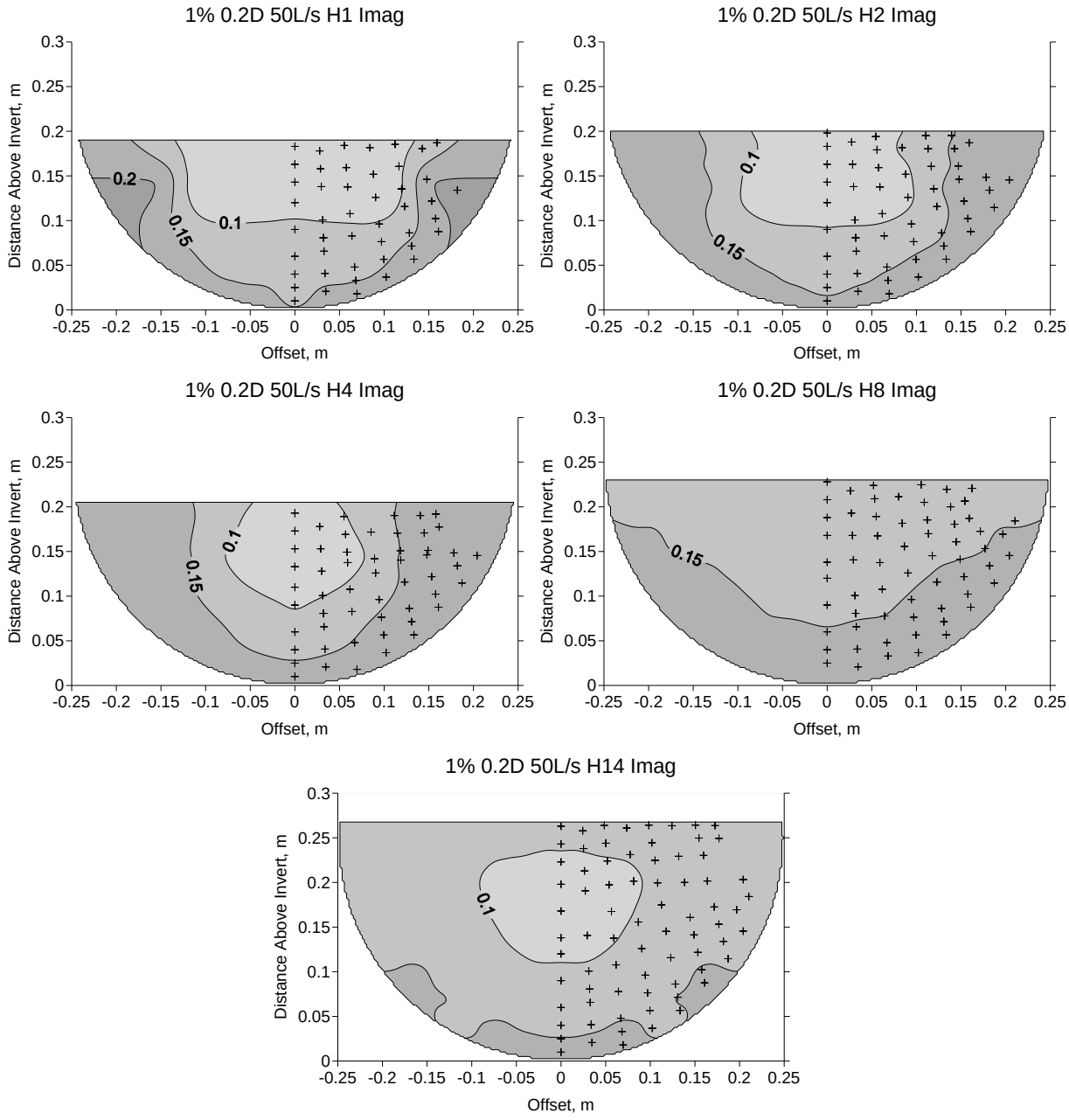

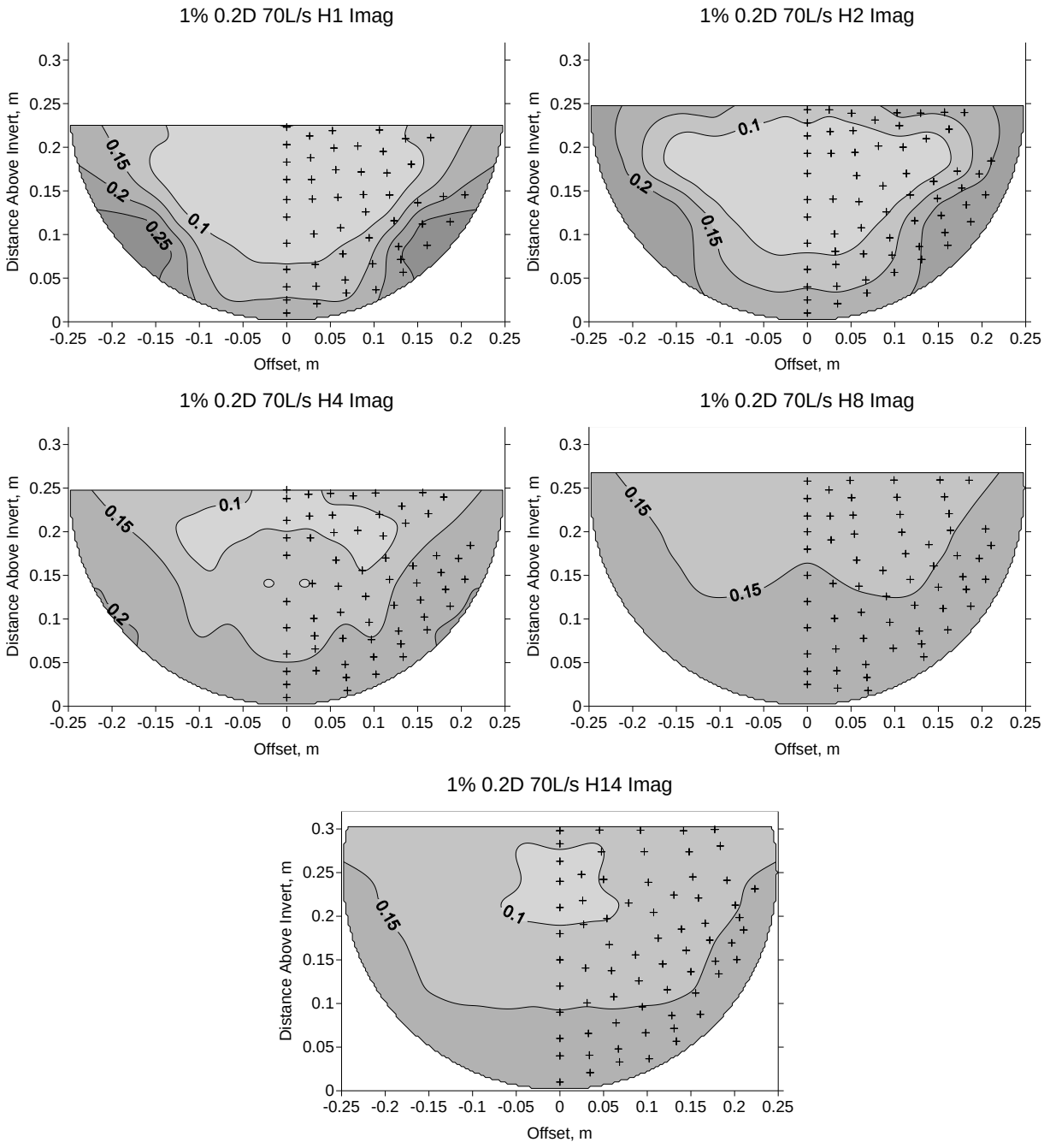
1% 0.2D 70L/s H1 Imag
1% 0.2D 70L/s H2 Imag
1% 0.2D 70L/s H4 Imag
1% 0.2D 70L/s H8 Imag
1% 0.2D 70L/s H14 Imag
Distance Above Invert, m
Offset, m
0.1
0.15
0.2
0.25

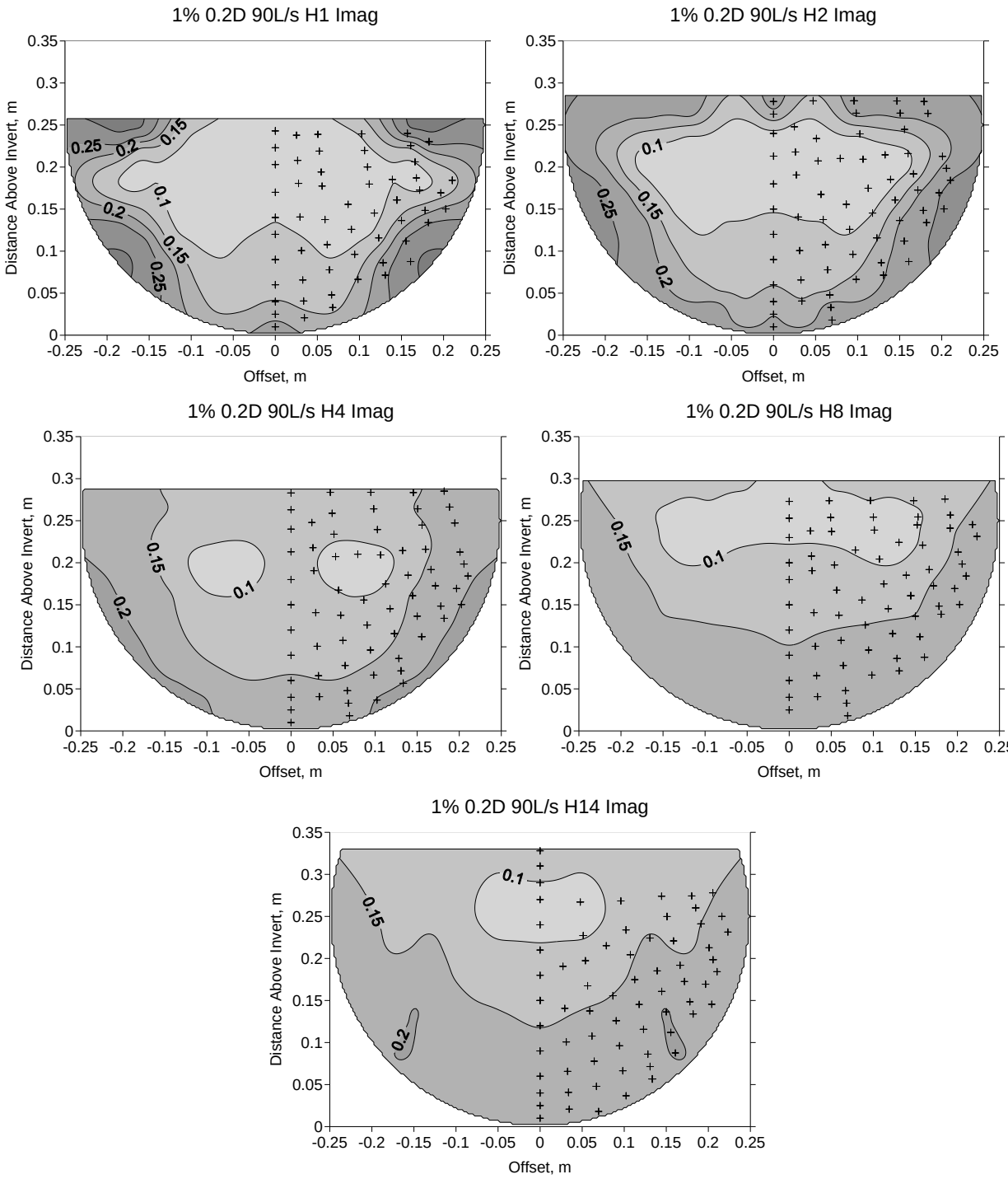
1% 0.2D 90L/s H1 Imag
1% 0.2D 90L/s H2 Imag
1% 0.2D 90L/s H4 Imag
1% 0.2D 90L/s H8 Imag
1% 0.2D 90L/s H14 Imag
Distance Above Invert, m
Offset, m
0.25
0.2
0.15
0.1
0.05
0
-0.25
-0.2
-0.15
-0.1
-0.05
0.05
0.1
0.15
0.2
0.25
0.3
0.35

Appendix N: Cross Section Average Turbulence Intensity Analysis

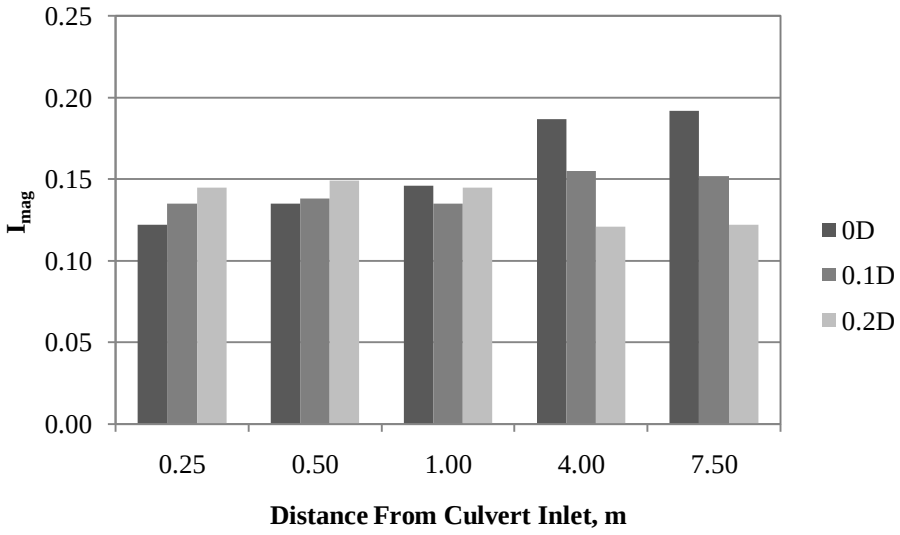

Figure N1: Average Turbulence Intensity for 0.4% Culvert Slope, 50L/s, Non-Embedded (0D), 0.1D and 0.2D Embedded

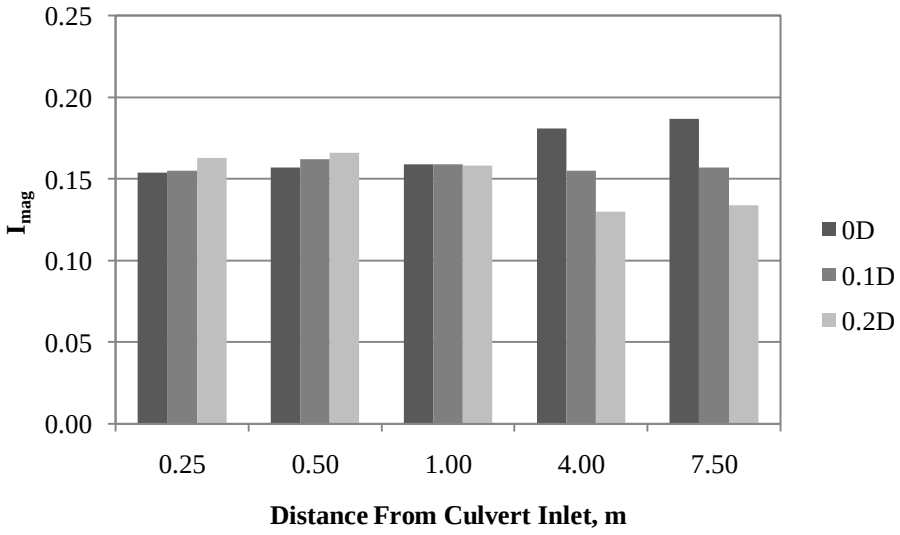

Figure N2: Average Turbulence Intensity for 0.4% Culvert Slope, 70L/s, Non-Embedded (0D), 0.1D and 0.2D Embedded

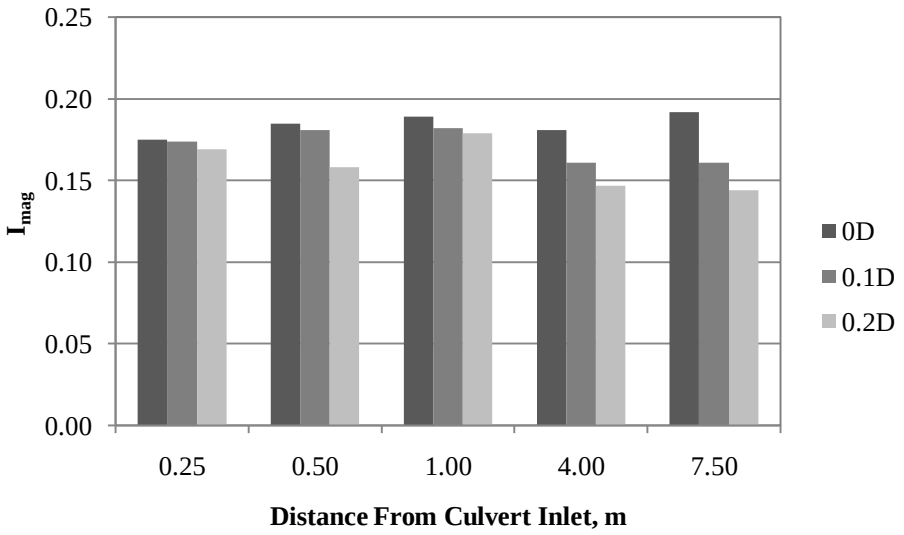

Figure N3: Average Turbulence Intensity for 0.4% Culvert Slope, 90L/s, Non-Embedded (0D), 0.1D and 0.2D Embedded

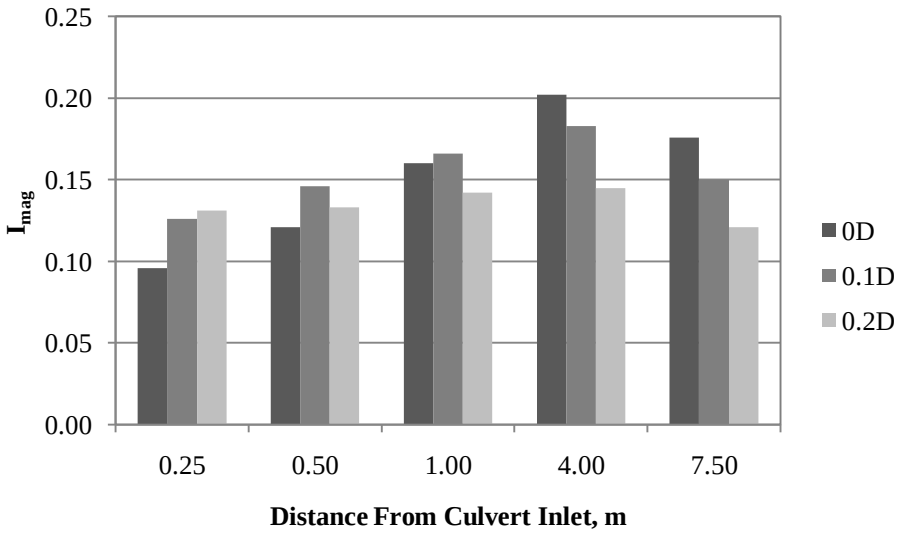

Figure N4: Average Turbulence Intensity for 1.0% Culvert Slope, 50L/s, Non-Embedded (0D), 0.1D and 0.2D Embedded

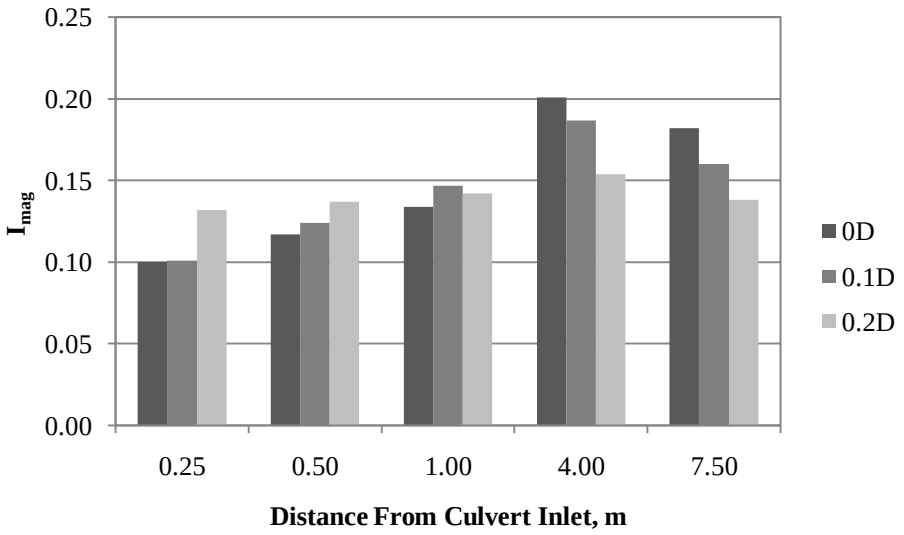

Figure N5: Average Turbulence Intensity for 1.0% Culvert Slope, 70L/s, Non-Embedded (0D), 0.1D and 0.2D Embedded

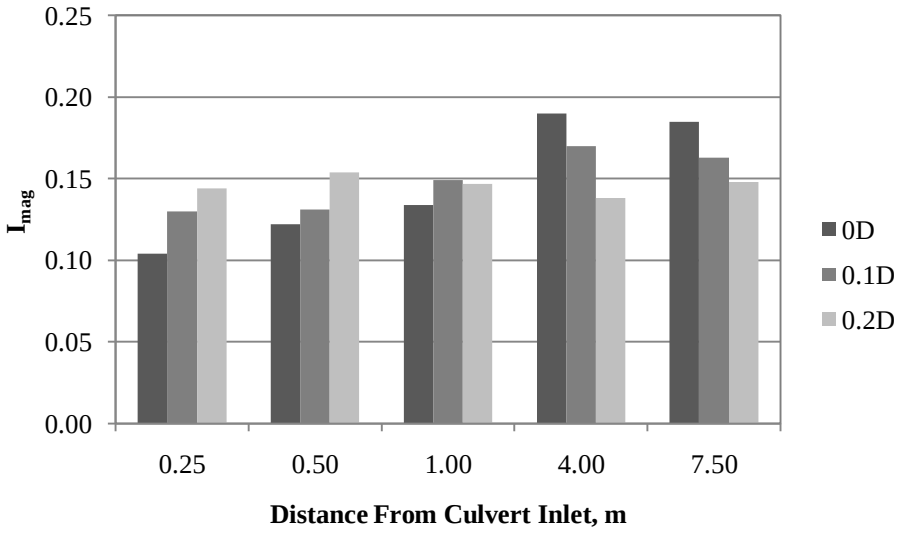

Figure N6: Average Turbulence Intensity for 1.0% Culvert Slope, 90L/s, Non-Embedded (0D), 0.1D and 0.2D Embedded

Appendix O: Data for Embedded Baffled Invert

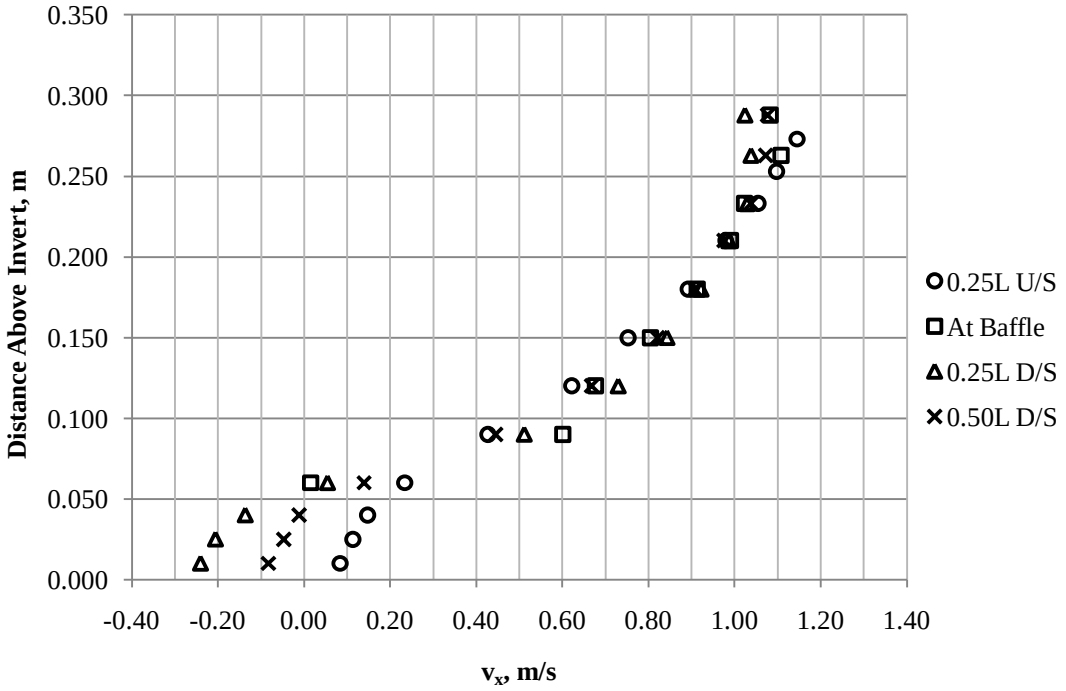

Figure O1: Centreline velocity profiles for 0.1D embedded baffled invert.

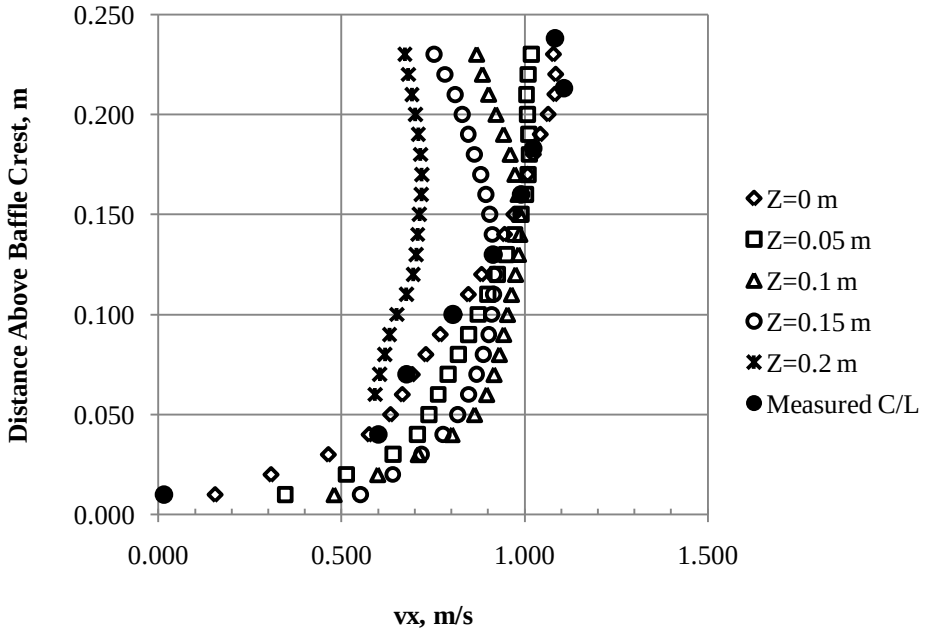

Figure O2: Velocity profiles at the baffle for various transverse offsets from the culvert centreline for the 0.1D embedded test.

Naming convention for contour plots

The title in each contour plot conveys the following information (in order):

- Culvert Slope (%)
- Embedment Depth (0D (non-embedded), 0.1D or 0.2D, where D=culvert diameter)
- Discharge (L/s)
- Cross Section Location (0.25L U/S, At Baffle, 0.25L D/S, 0.5L D/S, where L is the baffle spacing length and U/S and D/S mean upstream and downstream of the baffle location)
- Measurement (and units if appropriate) that is being represented by the contours (v_x or I_{mag}).

For example: Baffled Invert 1.0% 0.1D 90 L/s 0.25L U/S v_x (m/s) indicates that the cross section was measured at a 1.0% culvert slope, the culvert was embedded by 0.1 times the diameter, the discharge was 90 L/s, the location is 0.25L upstream from the baffle and the contour plot is of the streamwise (x) direction velocity in units of metres per second.

Negative velocities have been indicated as white areas within the cross section.

(Non-Embedded Cross Sections Contained in Main Body of Report)

0.1D Embedded Baffled Invert Velocity Cross Sections

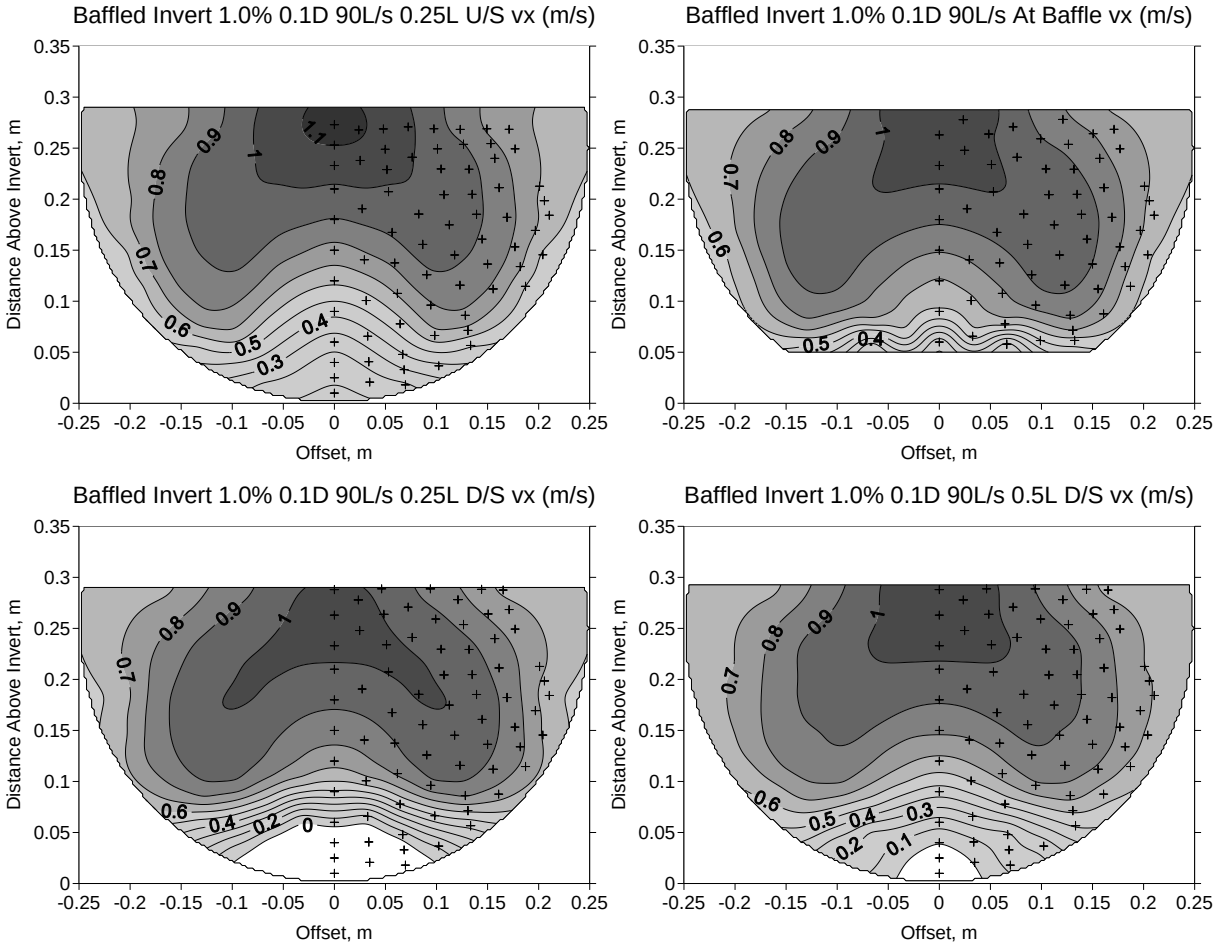

0.2D Embedded Baffled Invert Velocity Cross Sections

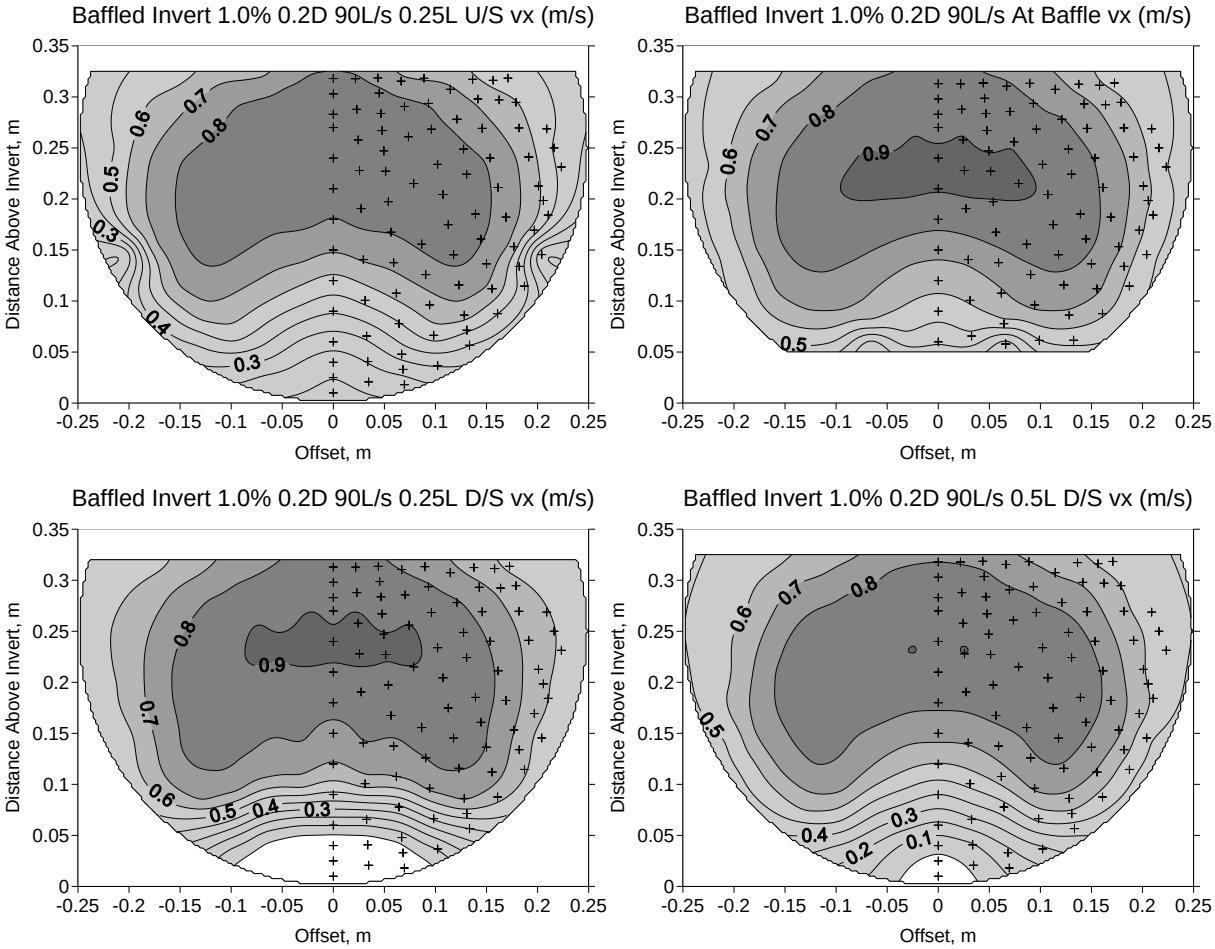

0.1D Embedded Baffled Invert I_{mag} Cross Sections

(Non-Embedded Cross Sections Contained in Main Body of Report)

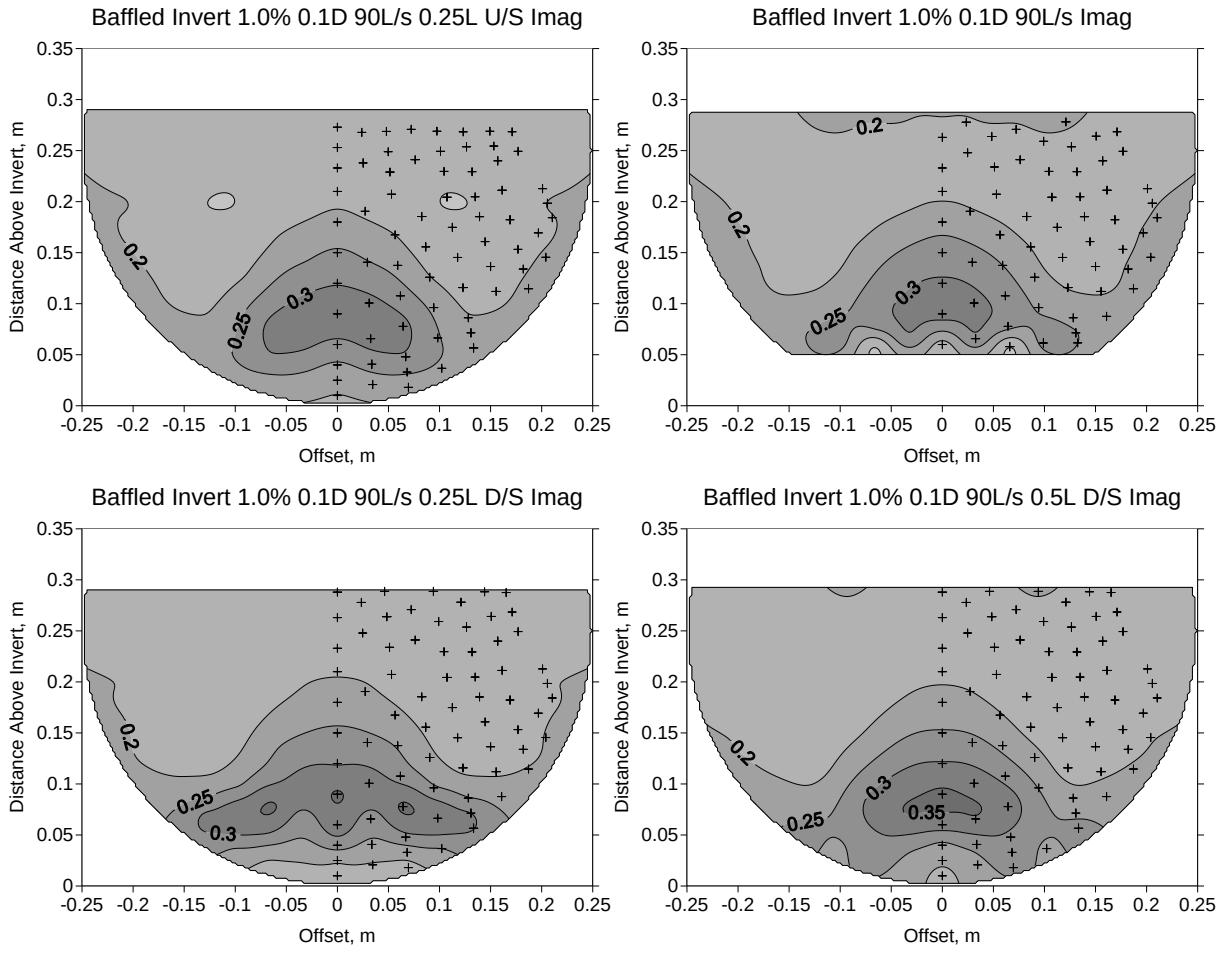

0.2D Embedded Baffled Invert I_{mag} Cross Sections